

Organic geochemical study on the Jurassic to Quaternary sediments of onshore and
offshore basins, Western Sri Lanka

スリランカ西部の陸域および海域堆積盆地におけるジュラ系～第四系堆積物に関する有機地球化学的研究

*A research report submitted to the
Department of Geoscience, Faculty of Science and Engineering, Shimane University*

In partial fulfillment for the Doctor of Philosophy Degree

By Amila Sandaruwan Ratnayake

Under supervision of
Prof. Yoshikazu Sampei

Department of Geoscience,
Faculty of Science and Engineering,
Shimane University, Nishikawatsu-cho 1060,
Matsue 690, Japan.

July 2015

Acknowledgements

I express my gratitude to my supervisors Prof. Yoshikazu Sampei, Senior Professor, Department of Geoscience, Faculty of Science and Engineering, Shimane University, Japan for his constant guidance, valuable advice and the enthusiastic support given throughout this work without concerning his demanding time. It has been an honor and a privilege working under his tutelage, and I look forward to continuing our work for the good of society and the world.

I extend my heartfelt thanks to Dr. Nalin Ratnayake, Senior Lecturer, Department of Earth Resources Engineering, Faculty of Engineering, University of Moratuwa, who helped me to perform research field works in the Bolgoda Lake and given permission to carry out initial laboratory works at University of Moratuwa, Sri Lanka.

I gratefully acknowledge the Director General Mr. Saliya Wickramasuriya of Petroleum Resources Development Secretariat (PRDS), Sri Lanka for access to the cuttings samples from the Mannar Basin and necessary permission to publish articles. Also, I would like to thank Mr. C. W. Kularathne and Mr. C. Senevirathne from PRDS for necessary field arrangements and guides.

I extend my sincere gratitude to Prof. A. Pitawala, Department of Geology, University of Peradeniya, Sri Lanka who advised me and encouraged to accomplish a good research works. I would have never found my place here without his supports.

I express my thanks to the members of the academic staff of Department of Geoscience, Shimane University and technical staff who helped me in many ways. Last but not least, I wish to extend my heartfelt appreciation to my family, and all colleagues of Shimane University for their friendship, and encouragement given to me all time.

Abstract

Sri Lanka records on of the longest and complete tectonic evolution from the mid-latitude in the southern hemisphere (during the Jurassic) to the equatorial northern hemisphere. Therefore, onshore and offshore sedimentary basins in Sri Lanka provide the natural laboratory to reconstruct paleoenvironmental and paleoclimatic during its northward voyage from Gondwana to Asia. The Jurassic Gondwana sediments were collected from the onshore Andigama and the Tabbowa Basins. The drillcore cutting samples from the Late Cretaceous to Miocene were obtained from the two exploration wells (the Barracuda and Dorado North) in the offshore Mannar Basin. The Late Quaternary sediment samples were collected from the coastal Bolgoda Lake in the southwest of Sri Lanka. CHNS elemental analysis ($n = 1279$) and gas chromatography and mass spectrometer (GC-MS) analysis ($n = 177$) were performed for sediment samples. The standard burial history, thermal maturity, and kinetic models were prepared for the Mannar Basin using petroleum system modeling software (BasinMod 1-D). The ^{14}C radiometric dating was carried out using accelerated mass spectrometry for the Late Quaternary Bolgoda Lake samples.

The Jurassic Andigama and Tabbowa Basins: Total organic carbon (TOC) contents are high (3.05-5.10%) in the Jurassic Andigama Basin, while the sandy sediments in the Jurassic Tabbowa Basin have very low TOC (0.04-0.17%). The Andigama mudstones are thermally immature, and the Tabbowa sediments are moderately matured in the oil generation stage based on sterane and hopane isomers proxies. The Jurassic Andigama Basin indicates a large proportion of middle-chain *n*-alkanes ($n\text{C}_{21}\text{-C}_{25}$), enriched C_{29} steranes, high C/N ratios (16.3-37.8), very low total sulfur (TS <0.001%) and higher pristane/phytane ratios (Pr/Ph = 2.1-3.0). These results suggest that terrestrial organic

matter (OM) were deposited in the freshwater swamp under oxic condition. Abundant retene, simonellite, perylene, 1- methylphenanthrenes, 1, 7- dimethylphenanthrene and 1, 2, 7- + 1, 2, 9- trimethylphenanthrenes in the Andigama mudstones indicate that the OMs were mainly originated from gymnosperm with fungi. In contrast, sandy sediments in the Tabbowa Basin have predominant nC_{16} - C_{21} alkanes with a minor peak of waxy n -alkanes (n - C_{29} , n - C_{31} , and n - C_{33}), very low TS (<0.001 %), abundant C_{27} steranes and higher Ts/(Ts + Tm) [Ts: 17 α (H)-22, 29, 30-trisnorhopane, Tm: 18 α (H)-22, 29, 30-trisnorhopane] triterpane ratios, which suggesting the OMs from algal origin with a significant terrestrial higher plants.

The pericratonic Mannar Basin (lithology): The Late Cretaceous to Late Paleocene lithology of the Barracuda well recorded mud dominant sediments and interbedded sandstone with volcanogenic materials, and the Dorado North well recorded sand dominant sediments and interbedded mudstone. At the end of the Late Paleocene, sedimentary facies were drastically changed from calcareous mudstone to argillaceous marl/ marlstone in the both wells. These facies variations have an apparent relation with the sedimentation rates in the basin. This shift is interpreted as the continuous subsidence of the basin and changes of an arid climate into warm and humid tropical conditions. The lowest sedimentation rate was recorded during the Eocene suggesting that the timing of collision between Indian and Asian plates. Burial history by 1D modeling indicates rapid subsidence from the Late Cretaceous to the Paleocene during the rift transition stage. Subsidence rate was decreased during the Eocene.

(Carbonate burial): The Late Cretaceous $CaCO_3$ rich (average of Dorado North = 24.7 ± 9.4 and Barracuda = 32.5 ± 9.4) sediments could indicate high-productive stage under warm climate. The Deccan-Reunion basalt could be acted as a significant

contributor to the mass extinction of coccolithophores/ foraminifera followed by reduction of CaCO₃ and organic carbon burial of the basin. The deposition of CaCO₃ rich sediments (average of Dorado North = 29.3 ± 11.4 and Barracuda = 40.2 ± 12.1) could indicate movement of Indian plate into northward warmer tropical latitudes since the Late Paleocene. It is correlated with the Cenozoic global cooling towards the present glaciated Earth.

(Organic carbon burial/ source rock beds): TOC contents are relatively low ($< 1\%$) in the lower most Early Campanian sediments of the Dorado North (average = $0.45 \pm 0.22 \%$) and Barracuda ($0.97 \pm 0.23 \%$) wells. However, the Early Campanian to Late Maastrichtian sediments (3320-3060 m) of the Dorado North ($1.64 \pm 0.57\%$), the Late Campanian to Late Maastrichtian sediments (4540-4270 m) of the Barracuda ($1.34 \pm 0.36\%$) and Middle Oligocene to Early Miocene sediments (2520-2139 m) of the Barracuda ($2.51 \pm 1.2 \%$) can be recognized as OM rich source rock beds in this basin. This Middle Oligocene to Early Miocene OM rich bed contains black carbon and laminations suggesting that seasonal events in this area possibly due to development of monsoon activity.

(OM type): The higher C/N ratios of the OM rich the Late Cretaceous sediments of the Dorado North (27.13 ± 12.4) and the Barracuda (20.36 ± 7.6 and 23.5 ± 15.0) wells can probably indicate accumulation of terrestrial OMs from higher plants. The *n*-alkane compositions of these samples indicate abundant middle-chain (nC_{21} - nC_{25}) and long-chain (nC_{27} - nC_{31}) wax from vascular plants with a significant amount of short-chain (nC_{18} - nC_{19}) wax from plankton. Therefore, the OM rich bed can probably contain gas prone Type II-III kerogen. The tectonic activities (separation of Laxmi Ridge-Seychelles and Seychelles) from the Indian plate could be accompanied enhancement of

TOC and terrestrial OM_s during the Late Cretaceous.

(Thermal maturity and kinetic models): These OM rich beds are thermally mature based on maturity parameters of C₂₉ sterane 20S/(20S + 20R) ratio (0.27-0.56 in the Barracuda and 0.20-0.33 in the Dorado North) and C₃₁ hopane 22S/(22S + 22R) ratio (0.49-0.56 in the Barracuda and 0.41-0.53 in the Dorado North). These results suggest that sediments in the Barracuda are more thermally matured than the Dorado North. In addition, OM rich Oligocene-Miocene sediments could not deeply subsidence to natural gas stage based on relatively lower maturity (C₂₉ sterane 20S/(20S + 20R) ratio = 0.28-0.37 and C₃₁ hopane 22S/(22S + 22 R) ratio = 0.45-0.48). Biomarker proxies are consistence with the maturity models. In detail, the standard rifting heat flows can be extrapolated with observed thermal maturity and gas deposit in the Mannar Basin. The kinetic model of the representative Cretaceous sediments (4260-4470 m) in the Barracuda well can indicate in-situ gas generation (mainly) since the Early Eocene. The in-situ gas generation was gradually increased and reached peak conditions during the Miocene (ca. 20 Ma). However, the Cretaceous sediments of the Dorado North and the Tertiary sediments of the both wells indicate poor cumulative hydrocarbon generation.

(Depositional environments): The OM rich sediments from Campanian–Maastrichtian and Oligocene–Miocene could be formed by the abundant input of terrestrial OM with nutrients for enhanced primary production in the marine area. The relatively higher C/S values in these beds could indicate weaker microbial activities (sulfate reduction) in terrestrial OM_s rich sediments. In contrast, C/S values of the Early-Late Paleocene sediments (average of Dorado North = 32.07 ± 20.21 and Barracuda = 16.21 ± 20.14) suggest oxic depositional environment due to regression of relative sea-level.

The coastal Bolgoda Lake: The history of the Bolgoda Lake can be divided into two major chronostratigraphic divisions that are quasi-steady state (from ~7.5 ky B.P. to ~2.5 ky B.P.) and non-steady state (from ~2.5 ky B.P. to the Recent). The moderate productive lower sediment sequence was mainly deposited in marine-terrestrial influence, oxygen-poor and anoxic conditions during mid-Holocene highstands. The major environmental change was characterized by enhancement of TOC (%) and accumulation of reworking terrestrial OM in the semi-closed aquatic system after the sea-level regression (~2.5 ky B.P.). The mid-Holocene regression has changed geomorphology of the study area from part of the bay of larger paleoriver system to semi-closed and separate fluvial dominant estuary of local streams. The *n*-alkanes ratios of $n\text{-C}_{29}/n\text{-C}_{\text{all}}$ and $n\text{-C}_{37}/n\text{-C}_{\text{all}}$ suggested a gradual climatic transition from wetter to dryer since middle Holocene. Accumulations of petroleum residues and pyrogenic polycyclic aromatic hydrocarbons (PAHs) in modern sediments identified anthropogenic activity after the European settlement (15th century).

TABLE OF CONTENTS	PAGE
Acknowledgements	ii
Abstract	iii
Table of Contents	viii
List of Figures	xiii
List of Tables	xviii
CHAPTER 1 INTRODUCTION	1
1.1 General introduction	1
1.2 Applications of organic geochemistry	2
1.3 Significance	2
1.4 Objectives	3
CHAPTER 2 STUDY AREA	5
2.1 The onshore sedimentary basins	5
2.2 The offshore Mannar Basin	7
2.2.1 Regional tectonic setting	7
2.2.2 Exploration history of Sri Lanka	9
2.3 The coastal Bolgoda Lake	11
CHAPTER 3 MATERIALS AND METHOEDS	13
3.1 Materials	13
3.1.1 The onshore sediment samples	13
3.1.2 The offshore sediment samples	13
3.1.3 The coastal sediment samples	13
3.2 Methods	14

3.2.1 Geochemical analysis and age dating	14
3.2.2 Cleaning of offshore cutting samples	15
3.2.3 Stratigraphy and basin modeling in the offshore Mannar Basin	16
CHAPTER 4 RESULTS	19
4.1 The onshore sedimentary basins	19
4.1.1 Bulk measurements	19
4.1.2 Molecular compositions	20
4.2 The offshore Mannar Basin	27
4.2.1 Stratigraphy	27
4.2.1.1 Sandstones	27
4.2.1.2 Interbedded red mudstones and black mudstones	27
4.2.1.3 Volcanogenic sediments	28
4.2.1.4 Calcareous mudstone-argillaceous marlstone boundary	28
4.2.2 Sedimentation rates and burial modeling	28
4.2.3 Bulk sedimentary organic matter	35
4.2.4 Molecular compositions of sedimentary organic matter	40
4.3 The coastal Bolgoda Lake	46
4.3.1 Field observations	46
4.3.2 Bulk sedimentary organic matter	46
4.3.3 Living organic source materials	51
4.3.4 Molecular sedimentary organic matter	52
4.3.5 ¹⁴ C age dating	53
CHAPTER 5 DISCUSSION	61
5.1 The onshore sedimentary basins	61

5.1.1 Thermal maturity	61
5.1.2 Origin of organic matter	62
5.1.3 Depositional environment	65
5.1.4 PAHs distribution in the Andigama mudstones	66
5.1.5 Alkylated phenanthrenes in the Andigama mudstones	67
5.2 The offshore Mannar Basin	68
5.2.1 Stratigraphy and lithology	68
5.2.1.1 Sandstones	68
5.2.1.2 Interbedded red mudstones	69
5.2.1.3 Black mudstones	69
5.2.1.4 Volcanogenic sediments	70
5.2.1.5 Calcareous mudstone-argillaceous marlstone boundary	70
5.2.1.6 Turbidites	71
5.2.2 History of sedimentation rates	71
5.2.3 Burial history	73
5.2.4 Sedimentary organic matter	74
5.2.4.1 Variations of carbonate deposition	74
5.2.4.2 Variations of organic matter delivery	76
5.2.4.3 Variations of organic matter type delivery	77
5.2.4.4 Depositional environments	80
5.2.5 Thermal maturity	82
5.2.5.1 Sterane distribution	82
5.2.5.2 Hopane distribution	83
5.2.5.3 Prediction of paleogeothermal regime	84

5.2.5.4 Kinetic model of the Mannar Basin	86
5.2.6 Paleoenvironment and paleoclimate	88
5.3 The coastal Bolgoda Lake	91
5.3.1 Present lake environments	91
5.3.1.1 Variations of organic matter delivery	91
5.3.1.2 Origin of organic matter in surface sediments	92
5.3.1.3 Depositional environments of the surface sediments	92
5.3.1.4 Mangrove mud cores	93
5.3.2 Environmental and climatic changes from middle Holocene	94
5.3.2.1 Age and sedimentation rates	94
5.3.2.2 Changes in organic matter contents	95
5.3.2.3 Changes in origin of organic matter type	95
5.3.2.4 Changes in depositional environments	97
5.3.2.5 PAHs as artificial marker	98
5.3.3 The Holocene sea-level changes and coastal landforms evolution	99
5.3.4 Paleoecological and chemotaxonomical significant	103
5.3.5 Early stage diagenesis in the tropical brackish sediments	110
5.3.5.1 Total hopane distribution in surface and mangrove sediments	110
5.3.5.2 Total hopane distribution in the lake core sediments	110
5.3.5.3 Effects of reworking geohopanoids in the recent sediments	112
5.3.6 Paleoclimate and environment	114
5.3.7 Future environmental implications	115
CHAPTER 6 CONCLUSION	117
6.1 The onshore sedimentary basins	117

6.2 The offshore Mannar Basin	117
6.2.1 Stratigraphy and lithology	117
6.2.2 Geochemical evaluations	119
6.3 The coastal Bolgoda Lake	121
6.4 General overview	124
REFERENCES	127
APPENDIX	153

LIST OF FIGURES

Figure	Captions	Pages
2.1	(a) Generalized map showing major geological units and sedimentary basins in Sri Lanka, inserted regional map shows the Mannar Basin, Cauvery Basin, Southern Basin, Krishna-Godavari Basin, Kerala-Konkan Basin, Mumbai Basin, Kutch Basin, Bengal Fan and Indus Fan. (b) field section and samples photographs of the Miocene – Quaternary Aruwakkalu profile, (c) field section, samples photographs and simplified structure of the Jurassic Andigama Basin, and (d) stratigraphic successions of the Jurassic Tabbowa Basin	6
2.2	Map shows exploration and stratigraphic wells of the Mannar and the Cauvery Basins	10
2.3	Map of Sri Lanka showing (a) the Bolgoda Lake and (b) core locations	12
4.1	Mass chromatograms ($m/z = 57$) showing distribution of <i>n</i> -alkanes in sediments of northwest onshore sedimentary units in Sri Lanka	22
4.2	Representative mass chromatograms of (a) steranes ($m/z = 217$) and (b) triterpanes ($m/z = 191$)	23
4.3	Representation total ion chromatograms (TIC) of aromatic fraction showing distribution of PAHs in the Andigama mudstones	24
4.4	Relative abundances of PAHs in the Andigama mudstones	24
4.5	Representative m/z 178, 192, 206 and 220 mass chromatograms for phenanthrene (P), methylphenanthrenes (MP), dimethylphenanthrenes (DMP) and trimethylphenanthrenes (TMP) in the Andigama mudstones	25
4.6	Stratigraphic successions of the Dorado North and the Barracuda exploration wells	29

4.7	Representative photomicrographs show surface mineral and maceral (organic) components in the Mannar Basin	32
4.8	Mud sedimentation rates of the Dorado North and the Barracuda exploration wells in m/Ma	33
4.9	Standard burial rates of the Dorado North and Barracuda exploration wells in m/Ma (a) total subsidence, (b) tectonic subsidence	33
4.10	Simplified standard burial history models of the Dorado North and the Barracuda exploration wells and stratigraphic correlations	34
4.11	Vertical distributions of TC (%), TOC (%), Carbonate-C (%), CaCO ₃ (%) of (a) the Dorado North (b) the Barracuda wells in the Mannar Basin	35
4.12	Vertical distributions of TOC (%), TN (%), TS (%), C/N ratio and C/S ratio of (a) the Dorado North (b) the Barracuda wells in the Mannar Basin	37
4.13	The correlation of (a) Carbonate-C (%) and (b) TOC (%) in the Dorado North and the Barracuda wells in the Mannar Basin	39
4.14	Mass chromatograms ($m/z = 57$) showing distribution of <i>n</i> -alkanes in bitumen of the Dorado North and Barracuda exploration wells	42
4.15	Mass chromatograms ($m/z = 57$) showing distribution of <i>n</i> -alkanes in kerogen of the Barracuda exploration well	43
4.16	Representative mass chromatograms of (a) steranes ($m/z = 217$) and (b) triterpanes ($m/z = 191$) in bitumen samples	44
4.17	Biomarker results of the Barracuda well	45
4.18	Surface distributions of TOC, C/N ratio and C/S ratio of the Bolgoda Lake surface sediments	48
4.19	Vertical distributions of TOC, TN, C/N ratio and C/S ratio of Core 1, Core 2,	

	and Core 3 in the Bolgoda Lake	49
4.20	Vertical distributions of TOC, C/N ratio and C/S ratio of the all very short mangrove mud core samples	50
4.21	Characteristics of <i>n</i> -alkanes mass chromatograms for OM type in the Bolgoda Lake and its watershed area	51
4.22	Individual concentration changes of algae, floating/ herbaceous plants, terrestrial plants and mangrove biomarkers in Core 1 and Core 2	52
4.23	Characteristic mass chromatograms patterns of before and after major environmental change	55
4.24	The characteristics of molecular proxies in Core 1 and Core 2	55
4.25	Depth profiles showing the distribution of (a) total hopane, (b) C ₃₁ hopane – 22S isomer, (c) C ₃₁ hopane – 22R isomers concentrations, (d) C ₃₁ hopane (22S/22R) ratio, (e) C ₃₁ hopane 22S/(22S + 22R) ratio and (f) Ts/(Ts + Tm) ratio in core samples	59
5.1	Relationship between hopane C ₃₁ 22S/(22S + 22R) and sterane C ₂₉ 20S/(20S + 20R)	62
5.2	Ternary diagram of C ₂₇ -C ₂₈ -C ₂₉ steranes showing OM sources and depositional environments	63
5.3	(a) Ts/(Ts + Tm) ratio versus 20S/(20S + 20R) of C ₂₉ sterane and (b) CPI versus 20S/(20S + 20R) of C ₂₉ sterane for onshore sediments	64
5.4	Relationship between C ₂₇ /(C ₂₇ + C ₂₉) sterane and Pr/Ph ratio showing OM sources and depositional conditions	65
5.5	Vertical distributions of hopane C ₃₁ 22S/(22S + 22R) and sterane C ₂₉ 20S/(20S + 20R) ratios in the Dorado North and Barracuda wells	84

5.6	Maturity models based on constant paleogeothermal gradients of (a) 23°C/km, (b) 70°C/km, and (c) standard rifting heat flow for the Dorado North and Barracuda exploration wells	87
5.7	Kinetic models based on standard rifting heat flow for (a) the Barracuda and (a) the Dorado North exploration wells	88
5.8	Stratigraphic correlations of representative cores in different coastal landforms on the west to southeast coast of Sri Lanka	103
5.9	The n -C ₂₇ , n -C ₂₉ and n -C ₃₁ n -alkanes ternary diagrams of the literature data separated into woody and non-woody plants	105
5.10	Temporal and spatial variations of n -C ₂₇ , n -C ₂₉ and n -C ₃₁ n -alkanes in (a) surface sediments, (b) mangrove mud cores, (c) Core 1, (d) Core 2 and (e) Core 3 of the Bolgoda Lake	108
5.11	Triangular diagram showing the abundance of n -C ₂₇ , n -C ₂₉ and n -C ₃₁ n -alkanes of (a) the Bolgoda Lake sediments and (b) a comparison with literature data elsewhere	109
5.12	Relationship between total hopane vs. algae OMs, macrophytes OMs, and terrestrial OMs in (a) the upper sedimentary succession and (b) the lower sedimentary succession of the Bolgoda Lake system	112
5.13	Cross plot between Ts/(Ts + Tm) ratio versus C ₃₁ hopane 22S/(22S + 22R) ratio in the Bolgoda Lake system	114
5.14	Model depicting the relation between sources of organic matter and deposition environment, and the successive stages in the evolution of environmental perturbation	116
6.1	Schematic cross-sections for paleoenvironmental and paleoclimate in onshore	

	and offshore sedimentary basins, western Sri Lanka	125
6.2	Distributions of TOC and bulk and molecular organic source indicators in all sedimentary basins	126
6.3	Correlations of TOC and bulk and molecular organic source indicators in all sedimentary basins	126

LIST OF TABLES

Table	Caption	Pages
3.1	Lithological characteristics of the sediments from northwest onshore sedimentary units in Sri Lanka	18
4.1	C, N, S elemental data of the sediment samples	19
4.2	Biomarker data of the sediment samples	21
4.3	Concentration and ratios of PAHs in the Andigama mudstones	26
4.4	Schematic stratigraphy of (a) the Dorado North and (b) the Barracuda exploration wells	30
4.5	The results of biomarker proxies in surface sediment samples	54
4.6	The results of biomarker proxies in mangrove mud core samples	56
4.7	The average concentration and proxies of PAHs in sedimentary units	56
4.8	Distribution of representative triterpanes biomarkers in m/z 191 mass chromatograms of surface sediments from the Bolgoda Lake	57
4.9	Distribution of representative triterpanes biomarkers in m/z 191 mass chromatograms of mangrove mud core samples	58
4.10	Results of ^{14}C radiometric dating and $\delta^{13}\text{C}$ stable isotopes analyses	60
5.1	Summary of the Holocene sea-level data in the Indian Ocean	101

INTRODUCTION

1.1 General introduction

Sri Lanka is geologically considered as metamorphic terrain of high-grade crystalline non-fossiliferous rocks belong to Precambrian age. Only one-tenth of landmass consists of sedimentary rocks of the limited ages including the Jurassic, Miocene and Quaternary (Cooray, 1984). Distribution of the Jurassic sediments are regulated in small basins exposed rarely and sporadically in the western land area, and the Miocene sediments are composed mainly of limestone narrowly exposed along the coastline of northwestern Sri Lanka (Figure 2.1(a)).

Recent offshore investigations in Sri Lanka have identified three paleoceanic sedimentary basins. Stagnant or semi-closed paleoceanic basins can act as major depositional sinks for organic matter (OM), and some of these basins develop as oil and/or gas generating systems. The Mannar Basin is the largest offshore sedimentary basin in Sri Lanka. It recorded thick sedimentary sequences of marine/ continent origins from the Late Jurassic to Recent in age.

Sri Lanka is presently located in the Lakadive region of the tropical central Indian Ocean locating about 800 km north of the equator. It is located at a sensitive geographical region of the Indian Ocean. High atmospheric winds of south Indian Ocean initially reach to the low atmospheric Indo-Asian continent through southwest of Sri Lanka. The coastal tract of Sri Lanka consists of the diverse Quaternary sedimentary deposits. The Bolgoda Lake can be recognized as the representative Quaternary basin in

southwest of Sri Lanka.

1.2 Applications of organic geochemistry

The Jurassic small onshore sedimentary basins have not been deeply subsided and are expected to have significant information of the original record of OM without over maturations. Therefore, a study of onshore sedimentary rocks on the northwest margin of Sri Lanka provides important organic geochemical information to understand the type of OM and depositional environments during the Jurassic age in Sri Lanka.

Organic geochemical investigations of the paleoceanic Mannar Basin provide fundamental guidelines to evaluate petroleum systems. Petroleum geoscience is the application of geochemical and geophysical principals to study of the origin, mitigation, accumulation, and alteration of petroleum. Since evaluation of source rock, its maturity and traps of reservoir rock are three key components for the occurrence of exploitable petroleum deposits (Tissot and Welte, 1978; Ryu, 2008; Petersen et al., 2009; Qiang et al., 2009; Hakimi et al., 2010). In addition, petroleum prospecting (Levenson, 1970) and modeling of petroleum formation (Tissot and Welte, 1978; Ryu, 2008; Qiang et al., 2009) can be considered as the main commercial applications of organic geochemistry.

In contrast, tropical coastal and marine systems have considerable value in the biogeochemical research on the global level. Therefore, sedimentary succession of the Late Quaternary Bolgoda Lake offers ideal opportunity to study paleoclimate, biogeochemical dynamics, and the geological processes in southwest of Sri Lanka.

1.3 Significance

Sri Lanka was positioned in the eastern Gondwanaland of mid-latitudes in the

southern hemisphere (67°S - 65°S and 34°E - 43°E) during the Jurassic period. Based on the geological frameworks of Sri Lanka, its separation from the eastern Gondwanaland and its northward motion have been extensively described by several authors (e.g., Molnar and Tapponnier, 1975; Cooray, 1984; Katz, 2000; Chatterjee et al., 2013). Sri Lanka had moved to the northern hemisphere during the Miocene (4°N - 8°N and 77°E - 79°E) and it presently locates about 800 km north of equator (5°N - 10°N and 79°E - 82°E). Therefore, Sri Lanka records one of the longest tectonic evolution from the mid-latitude in the southern hemisphere to the equatorial northern hemisphere. Secondly, the tectonic history of Sri Lanka record complete tectonic events such as continental breakup, sea-floor spreading, flood basalt volcanism, subduction and continental collision. Therefore, onshore and offshore sedimentary successions in Sri Lanka provide the natural laboratory to study evolution of environmental and climatic characteristics with respect to tectonic settings from the Jurassic to Recent in age.

The present day position of Sri Lanka is located sensitive geographical region due to transmission of inter-hemisphere mass and energy on the Earth. However, there is a paucity of literature data related to the late Quaternary biogeochemical characteristics in Sri Lanka. In many cases, the late Quaternary paleoclimatic proxies are applied to understand present scenarios and to project future climatic changes. Consequently, the comprehensive studies are essential to avoid lack of resolutions in the regional geographic scale. Therefore, organic geochemical characteristics of the Bolgoda Lake sediments would be used to understand past and present atmosphere-oceans-land surface interactions, and projecting future climatic changes.

1.4 Objectives

The general objectives of this study can be simply summarized as:

- (1) To investigate sources of organic matter and depositional environments,
- (2) To reconstruction paleoenvironmental and climatic characteristics, and
- (3) To estimate a significant of carbon burial in different sedimentary successions.

STUDY AREA

2.1 The onshore sedimentary basins

The Jurassic Gondwana Group sediments occur in Sri Lanka within a few onshore faulted small basins underlain by the Precambrian Wannai Complex (metamorphic rocks) (Figure 2.1(a)). The Jurassic sediments can be recognized as one of the oldest unmetamorphosed sedimentary units in the country (Cooray, 1984). The Jurassic sediments are not well exposed in Sri Lanka. These sedimentary beds are much less studied than the Precambrian metamorphic rocks, although several studies have examined their subsurface isostatic gravity anomalies (Tantrigoda and Geekiyanage, 1991) and plant fossil deposition (Edirisooriya and Dharmagunawardhane, 2013). The Jurassic Gondwana sediments examined in the present study were collected in the Andigama and the Tabbowa Basins (Figure 2.1(a)). The maximum depths to the basement of the Andigama and Tabbowa Basins are 1.2 and 1.5 km respectively, and a three-dimensional model indicates that approximately 65 km³ volume of the Gondwana sediments present in the Andigama Basin (Tantrigoda and Geekiyanage, 1991). In addition, thin coal seams were observed in well cuttings of the Andigama Basin (Cooray, 1984).

Several meters thick and widely extended limestone beds were deposited during the Miocene in the northwest (Puttalam-Jaffna) and the southeast (Minihagalkanda) of Sri Lanka (Cooray, 1984) (Figure 2.1(b)). The Quaternary period of northwest of Sri Lanka is characterized by deposition of thick (about 15-20 m) and elongated Red Earth beds (Cooray, 1984) (Figure 2.1(b)).

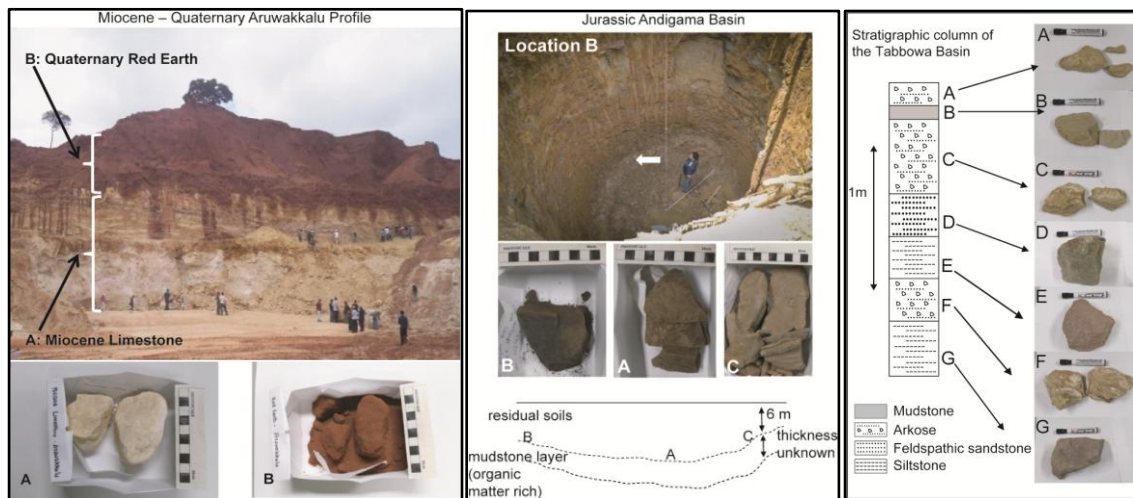
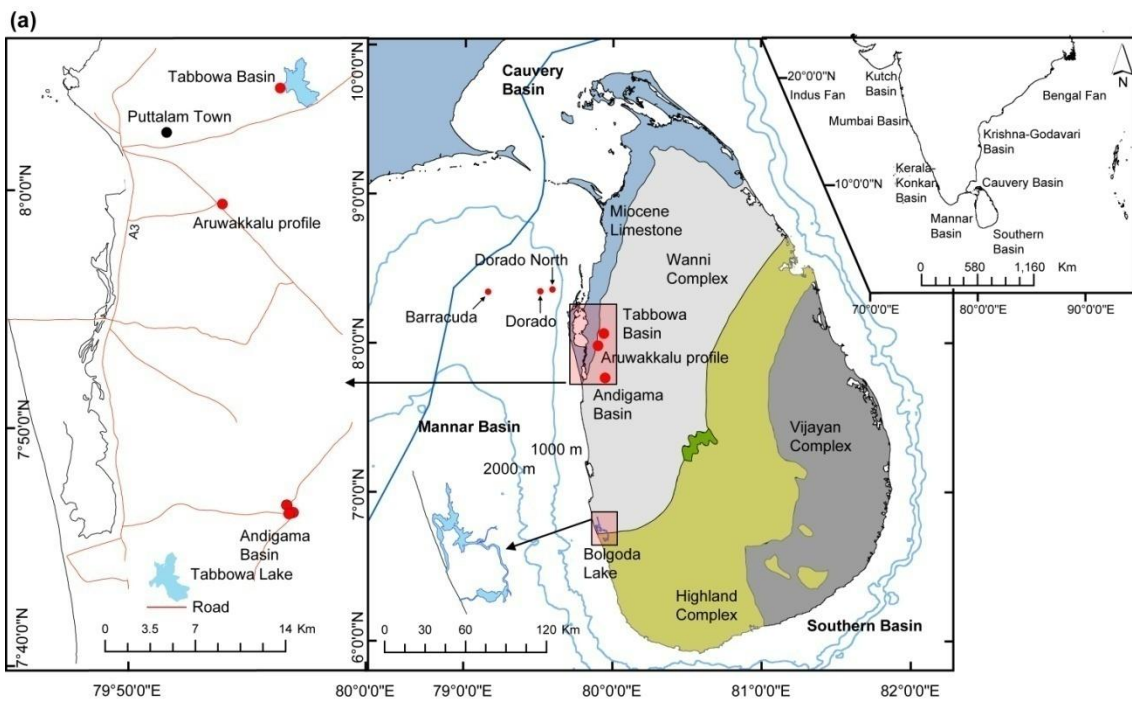


Figure 2.1: (a) Generalized map showing major geological units and sedimentary basins in Sri Lanka, inserted regional map shows the Mannar Basin, Cauvery Basin, Southern Basin, Krishna-Godavari Basin, Kerala-Konkan Basin, Mumbai Basin, Kutch Basin, Bengal Fan and Indus Fan. (b) field section and samples photographs of the Miocene – Quaternary Aruwakkalu profile, (c) field section, samples photographs and simplified structure of the Jurassic Andigama Basin, and (d) Stratigraphic successions of the Jurassic Tabbowa Basin.

2.2 The offshore Mannar Basin

The Mannar Basin is situated to the west to northwest of Sri Lanka (Figure 2.1(a)). The continental shelf of Sri Lanka is narrow (~30 km) and depicts steep slopes beyond the 500 m isobaths (Desa et al., 2006; Sreejith et al., 2008). Bathymetry of the basin ranges from 20 m to in over of 4,000 m. The area of the basin under the Sri Lankan jurisdiction is about 45,000 km² (Jayawardena, 2013). The Mannar Basin is filled with 6 s (seismic two-way travel time) thick succession of sediments (Desa et al., 2006). NNW-SSE trending Comorin Ridge, between 2-6° N latitudes and 77-79° E longitude, marks a significant crustal boundary in the basin (Sreejith et al., 2008). The Comorin Ridge has a relief of about 1,000 m from the surrounding bathymetry of ~3,500 m (Desa et al., 2006).

2.2.1 Regional tectonic setting

The basement of the Mannar Basin consists of Precambrian metamorphic rocks and continental to transitional crust (Cooray, 1984; Desa et al., 2006). The Precambrian rocks of Sri Lanka show a similarity to rocks of southeast India (e.g., Cooray, 1984; Dissanayake and Chandrajith, 1999; Cenki and Kriegsman, 2005; Tsunogae et al., 2008). Therefore, the basement can be divided into four areas based on the terrain age and composition. The gravity and magnetic anomalies of the southernmost part of the basin indicated highly attenuated and intruded continental to transitional crust (Sreejith et al., 2008). Consequently, continental to oceanic boundary of the basin lies about 250 km off southwest of Sri Lanka. Evolution of the N-S trending Mannar Basin consisted of four main phases including a syn-rift phase, rift transition phase, thermal sag phase and a passive margin stage.

The Indian Ocean floor is characterized by a system of active spreading ridges that now separate into four major fragments of the former supercontinent, Gondwana: Africa, India, Australia and Antarctica (Molnar et al., 1988; Katz, 2000; Kent et al., 2002; Subrahmanyam and Chand, 2006; Chatterjee et al., 2013). The breakup of Eastern Gondwanaland and the successive rifting, drifting, collision, and subduction in space and time are responsible for the present day configuration (Molnar and Tapponnier, 1975; Norton and Sclater, 1979; Molnar et al., 1988; Radhakrishna and Mathew, 1996; Acharyya, 2000; Katz, 2000; Kent et al., 2002; Desa et al., 2006; Gaina et al., 2007;

Chatterjee et al., 2013). Gravity models have determined relatively thin (~21 km thick) continental crust on the western margin of the basin, which may have evolved due to the crustal stretching during the rift process (Sreejith et al., 2008). The oldest formations could deposit during the syn-rift phase. The 2D seismic data in the Mannar Basin shows evidence of the oldest sedimentary sequence below the Lower Cretaceous (Rao et al., 2010). Also, the Late Jurassic sediments are documented in the drill core samples from the adjacent Cauvery Basin and outcrops in faulted basins (Tabbowa and Andigama) within Wannu Complex of Sri Lanka (Figure 2.1(a)).

Strong gravity and magnetic anomalies in the southern part of the Mannar Basin is interpreted as evidence of a lateral migrating tip of a seafloor spreading ridge flanked on either side by a highly attenuated crust. The seafloor created during the Early Cretaceous is estimated to have evolved with variable half-spreading rates (5.5 cm/yr-131 Ma, ~5.25 cm/yr-126.7 Ma and 1.53 cm/yr-121 Ma). Also, the Middle Cretaceous crust is evolved with comparability slower half spreading rate (0.6 cm/yr-84 Ma). Further, changes of fracture systems from the Early Cretaceous crust (~NNW-SSE) to the Tertiary crust (N-S) indicate a changes in the spreading direction of Sri Lanka (Desa et al., 2006). The stretching process were eventually led to continental splitting and also it contributed to the evolution of the rifted offshore sedimentary basins on western and eastern margin of the India (Sreejith et al., 2008).

The thermal sag phase of the Mannar Basin can be probably affected by separation of Madagascar/ Seychelles from India (Storey et al., 1995; Torsvik et al., 1998; Ali and Aitchison et al., 2008). Petroleum Resources Development Secretariat (PRDS) data reveal that the youngest age of K^{40}/Ar^{40} whole rock dating of penetrated igneous layers in the Pearl-1 exploration well is 76.8 Ma. Similarly, the mean Ar^{40}/Ar^{39} age determination of volcanic rocks and dikes (n = 17) from the timing of hotspot related volcanism during the breakup of Madagascar and India recorded 87.6 ± 0.6 Ma (Storey et al., 1995).

The northward movement was drastically reduced after the subduction of the Indian plate beneath the Asian Plate (ca. 50 Ma) and their continued convergence (Molnar and Tapponnier, 1975; Powell et al., 1988; Métivier et al., 1999; Ali and Aitchison et al., 2008; Chatterjee et al., 2013). Erosions of the Himalaya and adjacent terrain have formed the world's two largest submarine sediment masses, the Indus and Bengal fans,

around the Indian subcontinent (Davies et al., 1995; Métivier et al., 1999; Clift, 2006; Harris, 2006). The Mannar Basin draws special regional and global interest because of its tectonic settings and relation to the Indus and Bengal submarine fans (Figure 2.1(a)).

2.2.2 Exploration history of Sri Lanka

The offshore geophysical investigations have shown three oceanic basins in Sri Lanka namely the Cauvery Basin, the Mannar Basin and the Southern Basin (Figure 2.1(a)).

History of oil exploration in Sri Lanka began in 1957. The onshore and shallow-water previous petroleum explorations have been mainly performed in the Cauvery Basin. Three onshore exploration wells (Pesalai-1, 2, 3) were drilled by Soviets on the Mannar Island during 1972-1975. Also, four offshore shallow-water exploration wells (Palk Bay-1 and Delef-1 in 1976 and Pedro-1 and Pearl-1 in 1981) were drilled for covering approximately 12,600 km² in the Cauvery Basin and upper flank of the Mannar Basin within Sri Lankan waters (Figure 2.2). Penetrated reservoirs had failed to produce commercial hydrocarbons. However, exploration wells of the Indian side the Cauvery Basin, e.g., PH-9-1-located 30 km to the north of Pedro-1 (Figure 2.2), confirmed the presence of active petroleum system. Pearl-1 is the closest exploration well located to present study area of the Mannar Basin. This well penetrated at a total depth of 3050 m with no significant accumulation of oil or gas. The lack of top seal above breakup unconformity and faulting within the section are important reasons for an absence of hydrocarbons in Pearl-1. Geochemical investigations were carried out for cutting samples from exploration wells at University of New South Wales (Shaw, 2002). Results can be summarized as;

1. The Lower Cretaceous and probably underlying the Jurassic sections appear to contain the best potential hydrocarbon source rocks (e.g., the Lower Cretaceous rocks of Pesalai wells are very organic rich, averaging around 3.48% organic content and values as high as 6%).
2. The dominant kerogen type in most of the samples analyzed is humic. Gas or gas-distillate should be the primary products of catagenesis. The analyzed samples were located on structural higher planks. Therefore, depositional environments of these samples were near-shore and/or shallow water.

3. The samples analyzed were either thermally immature or only moderately mature.
4. The average present day geothermal gradient from the exploration wells in the Cauvery Basin is 23°C/ 1000 m. The reported vitrinite reflectance and burial history modeling describes that lower possibility of hydrocarbon generations from Tertiary sediments of the Cauvery Basin.

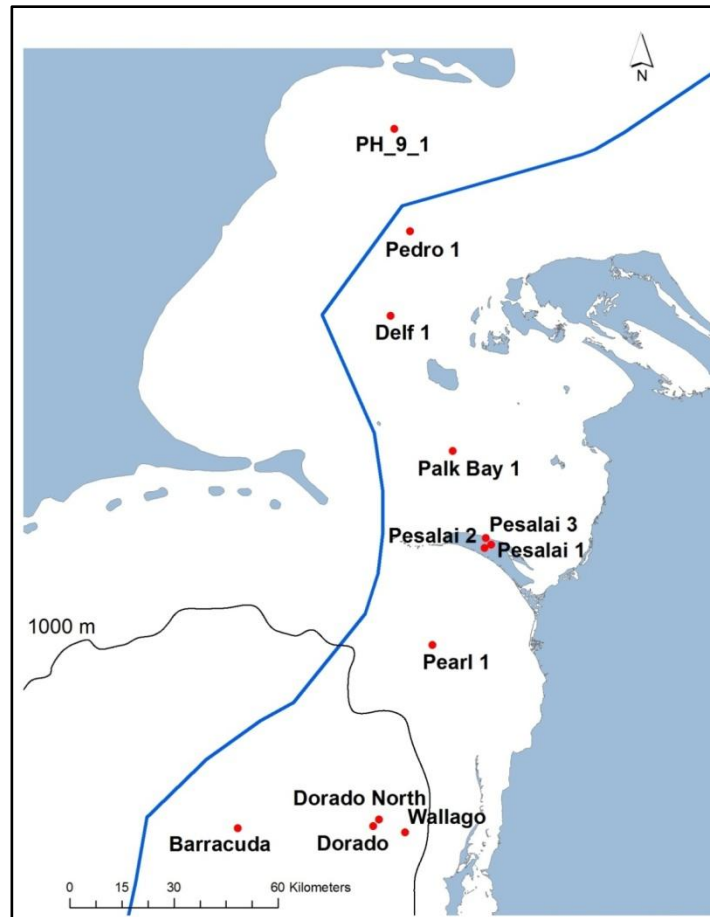


Figure 2.2: Map shows exploration and stratigraphic wells of the Mannar and the Cauvery Basins.

The initial seismic reflection surveys were carried out by different consortia such as 420 km of onshore and 75 km of offshore seismic data by Compaigne General de Geophysique in 1967-1968, some onshore data and 4837 km of offshore seismic data by Soviets in 1972-1975, 1947 km of seismic data around the Sri Lanka by Western Geophysical in 1976, 2829 km of seismic data in the Palk Strait and the Mannar Basin by Western Geophysical and Pexamin Pacific in 1976, 1556 km of seismic data in the

Palk Strait and the Mannar Basin by Cities Services in 1978-1981 and 980 km of offshore data by Petro Canada International Assistance Corporation in 1984.

Petroleum exploration works in Sri Lanka has remained without any further investigation since 1984. During 2001, the Norwegian geophysical company (TGS-NOPEC) acquires 1100 km of two dimensional (2D) seismic data in the poorly explored deep water regions of the Mannar Basin. Sri Lanka government offered offshore exploration license to Cairn Lanka Private Limited (Cairn) in 2008 for the exploration block SL 2007-01-001. Cairn drilled three exploration wells (Dorado, Dorado North and Barracuda) in 2011 one exploration well (Wallago) in 2013.

2.3 The coastal Bolgoda Lake

The Bolgoda Lake system is situated in the low country wet zone of Sri Lanka (Figure 2.3). The study area is mainly fed by regular tidal flushing and freshwater from surrounding streams and southwest monsoon (northern hemisphere summer monsoon/ Indian monsoon). The lake is not naturally connected to the Indian Ocean throughout the year due to growth of sand bars during the dry seasons. The tidal amplitude of the shallow Bolgoda Lake (the maximum depth = 2 m) varies from 0.75 cm to 1 cm. Also, the average daily variations of tidal amplitude change from 1 cm to 6.2 cm close to the estuary mouth (Siriwardena and Perera, 1986). The mean annual rainfall of the study area is about 2500 mm and the mean annual temperature is around 27 °C. The vegetation of the study area is dominated by mangroves and marshy species.

The Bolgoda Basin is separated from surrounding larger river basins by low elevated ridge systems that have opening in many places. Wickramagamage (2011) demonstrated that geomorphology and stratigraphy of the Bolgoda Lake flood plain can probably indicate a larger paleoriver system. The author considers main facts of (1) relative area of the estuary (lake) and freshwater inflows compared to the total area of the Bolgoda Basin and (2) the existence of a larger offshore canyon at the outfall of the basin. The sedimentary succession of the faulted Bolgoda Basin underlies weathered metamorphic rocks of the Precambrian age. Units are described in the geological map (GSMB, 1996) as lagoonal/ estuarine and stiff brown/ blue-grey organic-rich sediments in the watershed area can be probably deposited during the sea-level highstands.

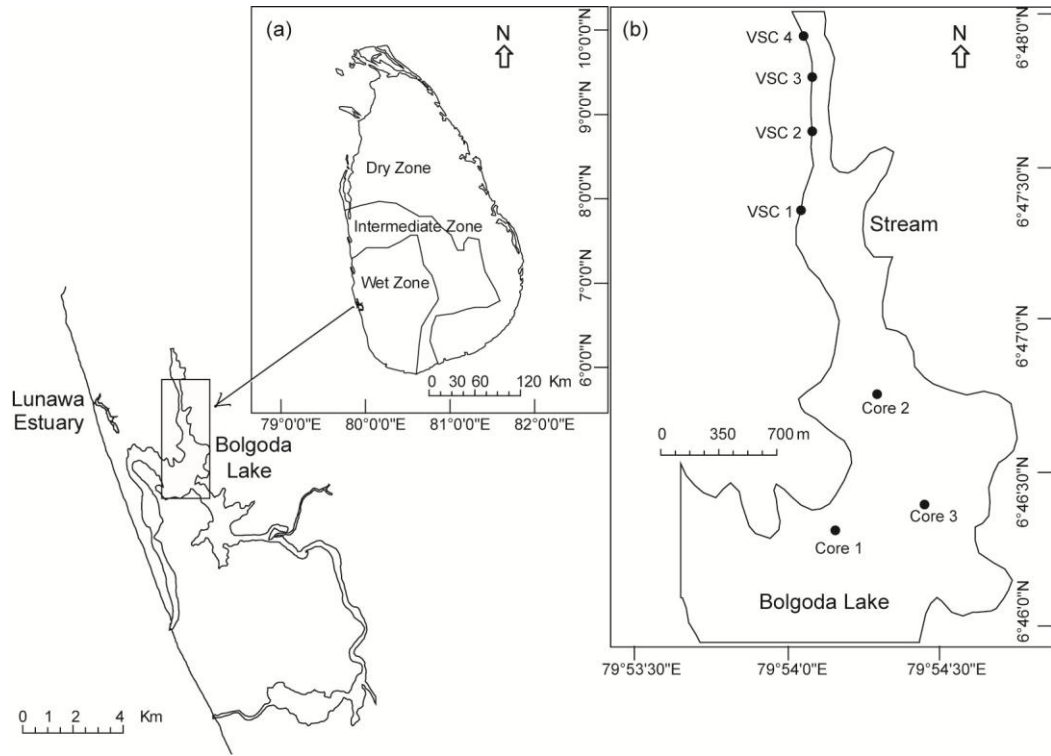


Figure 2.3: Map of Sri Lanka showing (a) the Bolgoda Lake and (b) core locations

MATERIALS AND METHODS

3.1 Materials

3.1.1 The onshore sediment samples

The Andigama beds are completely covered with over 5 m thick recent soils (Figure 2.1 (c)). Four unweathered hard Andigama mudstone samples (three mudstones and one sandy mudstone) were collected from wells sections ($7^{\circ} 46' N$ and $79^{\circ} 56' E$, 50 m above sea level; Figure 2.1(c)). The best exposures of the Jurassic rocks in the Tabbowa Basin were found close to the Tabbowa irrigation tank ($8^{\circ} 04' N$ and $79^{\circ} 55' E$, 20 m above sea level; Figure 2.1(a)). However, the outcrops have been subjected to a significant recent weathering process due to fluvial activities in the area. Therefore, outer parts of the samples (about 10-20 cm) were carefully removed to separate weathered surface. Seven samples were collected from the Tabbowa beds (Figure 2.1(d)) that contain siltstone, arkose sandstone and mudstones (Table 3.1). In addition, representative samples of the Miocene limestone and Quaternary Red Earth were collected from the Aruwakkalu profile ($7^{\circ} 59' N$ and $79^{\circ} 54' E$, 40 m above sea level; Figure 2.1(b)).

3.1.2 The offshore sediment samples

PRDS of Sri Lanka recently carried out a drilling program in the Mannar Basin using the deepwater drillship *Chikyu*. The 403 drillcore cutting samples were taken at 10 m intervals from two exploration wells, namely Dorado North (sampling depth range from 2200 m to 3622 m) and Barracuda (sampling depth range from 2139 m to 4741 m). The Dorado North well was drilled in a water depth of 1346.4 m and the Barracuda well was drilled in a water depth of 1509 m. In the Barracuda exploration well, natural gasses were predominantly discovered in totally 24 m thick of three hydrocarbon bearing sandstones between the depths of 4067-4206 m.

3.1.3 The coastal sediment samples

Twenty-eight surface samples, the penetration depth is around 0-3 cm and about

300 g of wet samples, were collected at pre-decided locations using a Birge Ekman type grab sampler. Also, three core samples (Core 1-160 cm, Core 2-150 cm, and Core 3-110 cm) were collected using a gravity corer (Figure 2.3). In addition, four short mangrove mud core samples (VSC 1-15 cm, VSC 2-15 cm, VSC 3-15 cm, and VSC 4-11 cm) were collected on the embankment of freshwater inflow stream of the Bolgoda Lake (Figure 2.3). The maximum water depth of mangrove mud core sampling locations is around 10 cm. All sediment samples were placed in cool boxes and taken to the Ocean Resource Engineering laboratory at University of Moratuwa, Sri Lanka for initial laboratory works. Then samples were placed in oven at 60 °C for 24 hours.

In contrast, living OM of floating fern (genus-*Salvinia*), floating plant (water hyacinth, genus-*Eichhornia*), mangrove plants and herbaceous terrestrial wood fragments were collected from the lake and its watershed area for identifying characteristic nature of organic source matters in tropical environment.

3.2 Methods

3.2.1 Geochemical analysis and age dating

Total carbon (TC), TOC, TN, and TS percentages were determined using combustion method with a FISONs (Carlo Erba) 1180 elemental analyzer. TC contents were first determined. The samples were ground into fine powders before analysis then about 10 mg of samples were placed in a tin caps, which were crimp-sealed prior to analysis. TOC contents were determined using powdered samples (about 10 mg in weight) in a separate run for similar set of samples. Accurately weighed samples were placed in a silver film. After that, few drops of 1M HCl were added to remove inorganic carbon and then dried at 110°C for 45 min. The dried samples were sealed and placed within tin caps, which were also sealed. BBOT [2, 5-bis-(5-tert-butyl-2-benzoxazol-2-yl)-thiophene] standard were placed in a tin film and regression analysis was the method used for quantitative analysis.

Bitumen was extracted from the sediments using the soxhlet extraction technique, refluxing using dichloromethane: methanol 9:1 v/v solution (72 hours for onshore and offshore sediments and 24 hours for recent coastal sediments). Activated copper granules were added to remove elemental sulfur. The insoluble portions after extraction (kerogen) were ground into fine powder (see Vandenbroucke and Largeau, 2007).

Kerogen was again extracted using the soxhelt extraction technique, refluxing using dichloromethane: methanol 9:1 v/v solution. Activated copper granules were again added to remove elemental sulfur. Bitumen and kerogen were dried at room temperature. Aliphatic and aromatic fractionations in bitumen and kerogen were separated using UV light on a thin layer chromatography plate (silica gel 60 PF₂₅₄ containing gypsum) with hexane as a mobile phase. The *n*-alkanes and PAHs fractions were separated after washing with hexane. Bitumen and kerogen were directly used for gas chromatography (GC: Shimadzu 2010) coupled with a mass spectrometer (MS: Shimadzu GCMS-QP 2010). Identification of organic compounds was performed by comparison of GC retention times, mass spectra with published data and standard solution. The *n*C₂₄ tetracosane, cholestane and PAHs mix (Accu Standard Inc. Z-013-17) were used as the external standards.

A small three woods, two shells and two bulk organics were carefully selected from the Recent Bolgoda Lake sediments in order to avoid misleading age results. The ¹⁴C radiometric dating was carried out using accelerated mass spectrometry at the Beta Analytic Inc Laboratory, USA. The δ¹³C values were used as in aid to determine the origin of OM type.

3.2.2 Cleaning of offshore cutting samples

The Mannar Basin cutting samples can be contaminated by drilling mud, rock sloughing from above, or may be due to lost circulation and pulverization. All cutting samples were washed extensively using methods of manual and ultrasonic cleaning to remove drilling mud and oil. Samples were manually cleaned using 250 ml of dichloromethane: methanol 9:1 v/v solution in 500 ml beaker by stirring. The same volume was used for 10 samples. In this step, samples were stirred about 3 min and liquid part was removed. Next, it was again cleaned two times using 50 ml of dichloromethane: methanol 9:1 solution in same beaker by hand. Samples were dried under room temperature in Draft Chamber (Fume Hood) for 24 hours.

The dried samples were sieved using 1 mm sieve. The particle size less than 1 mm was separated and the solid cutting samples, larger than 1mm in size, were used for ultrasonic cleaning. Samples (about 25-35g) in a beaker with aluminum foil cap were subjected to ultrasonic cleaning using about 75 ml of dichloromethane: methanol 9:1 v/v

solution under the 90% instrumental power intensity of ultrasonic cleaner for 30 min. Finally samples were washed again using 25 ml of dichloromethane: methanol 9:1 v/v solution by hand for 3 minutes. Samples were dried under room temperature at in Draft Chamber (Fume Hood) for 24 hours.

3.2.3 Stratigraphy and basin modeling in the offshore Mannar Basin

Samples were described to examine mineralogy, color, texture, rounding, sorting, grain size and cementing materials at constant sampling rates in the Mannar Basin. Cutting samples are quite small about 0.5-3 cm, so large scale features such as fractures, bedding planes, and fossils often cannot be observed. Surface features of cutting samples were observed using the OLYMPUS CX 31-DP 21 magnifier.

Unpublished paleontological and geophysical reports from the PRDS allow dating the sedimentary succession in the Mannar Basin. In particular, sequence boundaries were identified based on amplitude variations on seismic and correlating with corresponding biostratigraphic studies to get age profiles in the Mannar Basin. Age profiles in the unpublished final report of the exploration wells were obtained from PRDS with the special permission. Lithostratigraphic successions described in this study were reconstructed using fitting of sedimentological observations into the age profiles. Also, sedimentation rates of the Dorado North and the Barracuda wells were calculated using approximate thickness of each mudstone beds.

Standard burial history of the Mannar Basin was modeled using petroleum system modeling software (BasinMod 1-D) based on the charter member of Platte River's Petroleum System Suit. Present thicknesses and the begin age of each facies were used for the model. Also, new lithologies such as argillaceous marl/ marlstone, calcareous mudstone/ mudstone, and calcareous mudstone/ mudstone/ volcanic sediments were defined by mixing the percentages of the default lithologies. Minor hiatuses can be recorded close to the Upper Maastrichtian, Upper Paleocene, middle part of the Middle Eocene in the Dorado North and Barracuda wells and middle part of the Upper Eocene, early part of the Middle Oligocene and early part of the Middle Miocene in the Barracuda well based on the previous interpretations of the Mannar Basin (Rao et al., 2010), Cauvery Basin (Shaw, 2002) and other rift-basins of the Indian subcontinent (e.g., Rao, 2001) and facies changes in the lithostratigraphic units of the exploration

wells. Eroded thicknesses of each unconformity were unknown but seemed small as discussed later. Therefore, around 10-20 m eroded thicknesses were used for the burial model. Consequently, uplifting was not described in the standard burial history model of the rifted Mannar Basin. Computer simulations automatically calculated initial lithological parameters of porosity, matrix density, matrix heat capacity, etc. The water and marine bottom depths were fixed throughout the sedimentary succession for the burial model.

The observations of present day geothermal gradients were performed to understand the regional thermal activity of the study area. The two extreme values of the thermal gradients, the low most 23°C/km and the upper most 70°C/km, were used as the limits of the search range of thermal gradients. The maturity and kinetic models were prepared using petroleum system modeling software (BasinMod 1-D). The several simulations of paleogeothermal gradients were examined to extrapolate the observed compositions of hydrocarbons with respect to geological conditions. Maturity modeling histories are functioned of time and geothermal gradients. In contrast, the kinetic models involve calculation of possible oil/gas generation. In this study, kerogen (organofacies) compositions were determined based on C₂₇, C₂₈ and C₂₉ sterane percentages. The average total organic carbon (TOC %) values of each sedimentary facies were input to the stratigraphic data table. The default value (0.20) was used as the most reasonable value for the saturation threshold after successive comparison with several possibilities. The surface temperature was entered as 20°C throughout the sedimentary successions. The pressure parameter was not considered for these kinetic models.

Table 3.1: Lithological characteristics of the sediments from northwest onshore sedimentary units in Sri Lanka

Sample	Description of lithological properties	Age
Andigama Basin		
Mudstone A	Brown to black color hard and dense mudstone with black carbonaceous matter	Jurassic
Mudstone B	Brown to black color hard and dense mudstone with larger black carbonaceous matter (ca. 0.1-1 cm)	Jurassic
Mudstone B2	Brown to black color mudstone with small black carbonaceous matter	Jurassic
Sandy mudstone C	Brown color silty mudstone with thin sandy bed	Jurassic
Tabbowa Basin		
Upper arkose bed A	Angular to sub-angular grains of quartz and feldspar associated with reddish color hematite	Jurassic
Mudstone bed B	Dark and/or light gray color mudstone in thin bedding plain	Jurassic
Middle arkose bed C	Quartz and feldspar associated with black fine fragments and thin beds	Jurassic
Feldspathic sandstone D	Medium to coarse grained light brown color sandstone.	Jurassic
Upper siltstone E	Brownish to reddish mudstone associated with fine quartz grains.	Jurassic
Lower arkose bed F	Quartz and feldspar associated with black fine fragments and thin beds	Jurassic
Lower siltstone G	Brownish to reddish mudstone associated with fine quartz grains.	Jurassic
Aruwakkalu Profile		
Aruwakkalu limestone	Hard, partly crystalline, compact rock associated with very fine sands and black organic matter	Miocene
Aruwakkalu Red Earth	Small, rounded quartz grains in earthy material composed of clay and iron oxide	Quaternary

RESULTS

4.1 The onshore sedimentary basins

4.1.1 Bulk measurements

The TC, TOC, TN and TS data are listed in Table 4.1. The Andigama Basin has high TOC content in brown to black color mudstone (A = 3.05, B = 5.10 and B2 = 3.34%), but sandy brown mudstone has low TOC content (0.49%). The Tabbowa beds have very low TOC content ranging from 0.04% to 0.17%. Also, no significant variation is evident in the different lithostratigraphic units of these beds. The Aruwakkalu limestone ($\text{CaCO}_3 = \text{ca. } 87\%$) and the Red Earth represent low TOC values of 0.06% and 0.41% respectively. The analyzed all samples have low to high TN content ranging from 0.01 to 0.20%. The TS values are very low ($<0.001\%$) in all samples of these basins.

Table 4.1: C, N, S elemental data of the sediment samples (n.d., not determined)

Sample	TN (%)	TOC (%)	TS (%)	C/N ratio	TC (%)	Carb-C (%)	CaCO_3 (%)
Andigama Basin							
Mudstone A	0.174	3.05	<0.001	17.5	3.44	0.39	3.25
Mudstone B	0.135	5.10	<0.001	37.8	6.12	1.02	8.58
Mudstone B2	0.205	3.34	<0.001	16.3	3.38	0.04	0.34
Sandy mudstone C	0.166	0.49	<0.001	2.9	0.57	0.08	0.71
Tabbowa Basin							
Upper arkose bed A	0.010	0.06	<0.001	5.6	0.08	0.02	0.21
Mudstone bed B	0.013	0.17	<0.001	13.1	0.18	0.01	0.08
Middle arkose bed C	0.010	0.09	<0.001	9.5	0.11	0.01	0.12
Feldspathic sandstone D	0.010	0.06	<0.001	6.3	0.06	0.00	0.00
Upper siltstone E	0.010	0.04	<0.001	4.3	0.10	0.06	0.49
Lower arkose bed F	0.009	0.08	<0.001	8.2	0.12	0.04	0.38
Lower siltstone G	0.011	0.05	<0.001	5.0	0.04	n.d	0.00
Aruwakkalu Profile							
Aruwakkalu limestone	0.072	0.06	<0.001	0.9	10.42	10.36	86.99
Aruwakkalu Red Earth	0.035	0.41	<0.001	11.7	0.36	n.d	0.00

4.1.2 Molecular compositions

The *n*-alkanes proxies are summarized in Table 4.2. The *n*-alkanes distribution is characterized by a unimodal distribution pattern with the middle-chain predominance in the Andigama and the Aruwakkalu limestone samples and the lower-chain predominance in the Tabbowa and the Aruwakkalu Red Earth samples (Figure 4.1). The *n*-alkanes distribution of the Andigama samples is characterized by an odd predominance after *n*-C₂₃ (Figure 4.1). Representative steranes ($m/z = 217$) and triterpanes ($m/z = 191$) distributions are shown in Figure 4.2. A variety of aromatic compounds is present only in brown to black color mudstones of the Andigama Basin (Figure 4.3; Table 4.3). Phenanthrene (P, $m/z = 178$), fluoranthene (Fla, $m/z = 202$), pyrene (Py, $m/z = 202$), benzo[*a*]anthracene (BaAn, $m/z = 228$), chrysene/triphenylene (Chry + Tpn, $m/z = 228$), benzo[*a*]fluoranthene (Bfla, $m/z = 252$), benzo[*e*]pyrene (BePy, $m/z = 252$), benzo[*a*]pyrene (BaPy, $m/z = 252$), perylene (Pery, $m/z = 252$), indeno[*cd*]pyrene (InPy, $m/z = 276$) and benzo[*ghi*]perylene (BghiP, $m/z = 276$) were detected as non-alkylated PAHs. Relative proportions of PAHs of representative mudstones in the Andigama Basin are shown in Figure 4.4. Cadalene (Cad, $m/z = 183$), methylphenanthrenes (MP, $m/z = 192$), dimethylphenanthrenes (DMP, $m/z = 206$) and trimethylphenanthrenes (TMP, $m/z = 220$), simonellite (Sim, $m/z = 237$) and retene (Ret, $m/z = 219$) were abundant alkylated PAHs in the Andigama mudstones (Figures 4.3 and 4.5).

Table 4.2: Biomarker data of the sediment samples

Sample	<i>n</i> -alkanes				Triterpanes $\frac{22S}{(22S+22R)}$ for C ₃₁	Steranes				
	$C_{20}</n>/nC_{all}$	P _{aq}	ACL	CPI		20R (%)			$\frac{C_{29}}{(C_{27}+C_{28}+C_{29})}$	$\frac{C_{29}}{20S/(20S+20R)}$
					C ₂₇	C ₂₈	C ₂₉			
Andigama Basin										
Mudstone A	0.21	0.58	26.9	1.85	0.46	21	11	68	0.68	0.18
Mudstone B	0.19	0.59	27.0	1.93	0.48	20	11	70	0.70	0.17
Mudstone B2	0.23	0.69	26.3	1.77	0.47	25	13	61	0.61	0.18
Sandy mudstone C	0.03	0.69	26.4	1.86	0.47	25	15	60	0.60	0.15
Tabbowa Basin										
Upper arkose bed A	0.39	0.66	26.5	2.15	0.53	38	16	46	0.46	0.32
Mudstone bed B	0.35	0.58	26.9	2.11	0.50	27	17	56	0.56	0.26
Middle arkose bed C	0.61	0.51	27.3	2.57	0.56	63	12	25	0.25	0.41
Feldspathic sandstone D	0.53	0.68	26.2	2.40	0.55	38	26	36	0.36	0.38
Lower arkose bed F	0.66	0.71	25.9	2.25	0.55	40	19	41	0.41	0.41
Lower siltstone G	0.35	0.63	26.4	3.07	0.61	37	23	40	0.40	0.45
Aruwakkalu Profile										
Aruwakkalu limestone	0.12	0.69	26.2	1.61	0.54	34	22	44	0.44	0.30
Aruwakkalu Red Earth	0.35	0.24	29.9	4.78	0.62	48	16	36	0.36	0.56

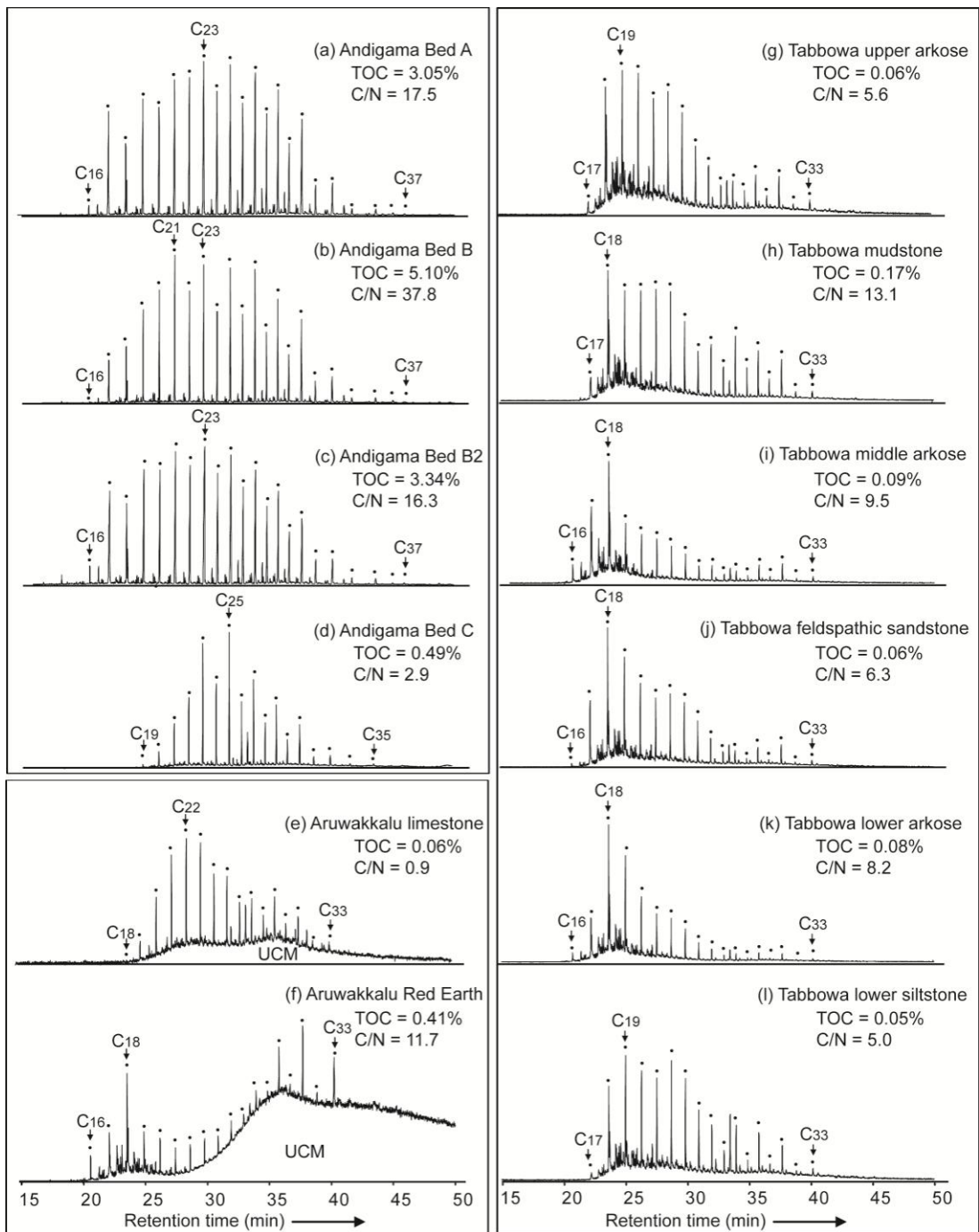


Figure 4.1: Mass chromatograms ($m/z = 57$) showing distribution of n -alkanes in sediments of northwest onshore sedimentary units in Sri Lanka (UCM: unresolved complex mixture).

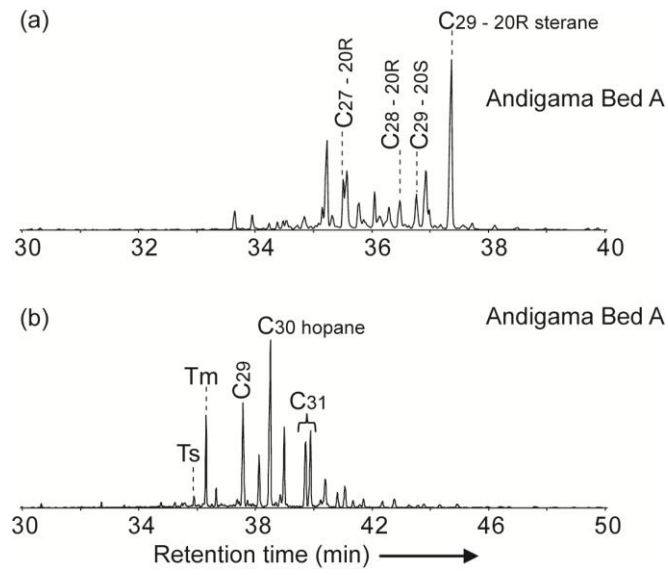


Figure 4.2: Representative mass chromatograms of (a) steranes ($m/z = 217$) and (b) triterpanes ($m/z = 191$).

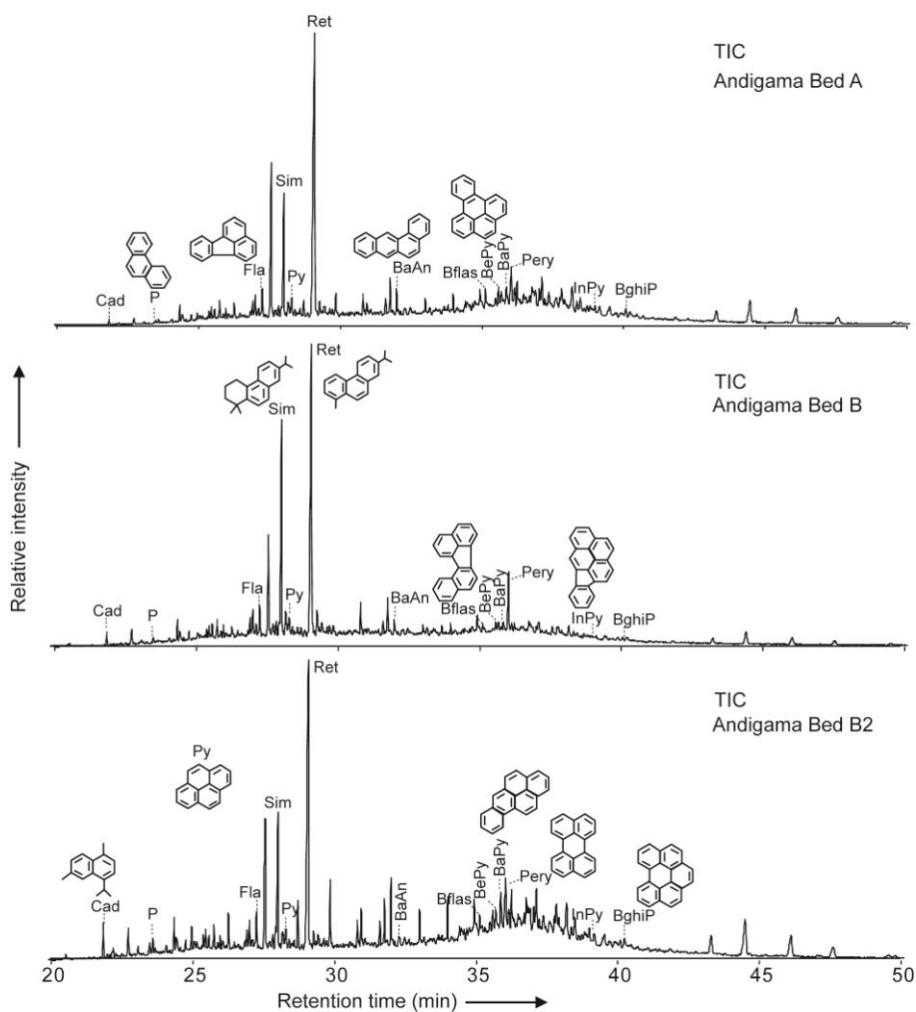


Figure 4.3: Representation total ion chromatograms (TIC) of aromatic fraction showing distribution of PAHs in the Andigama mudstones.

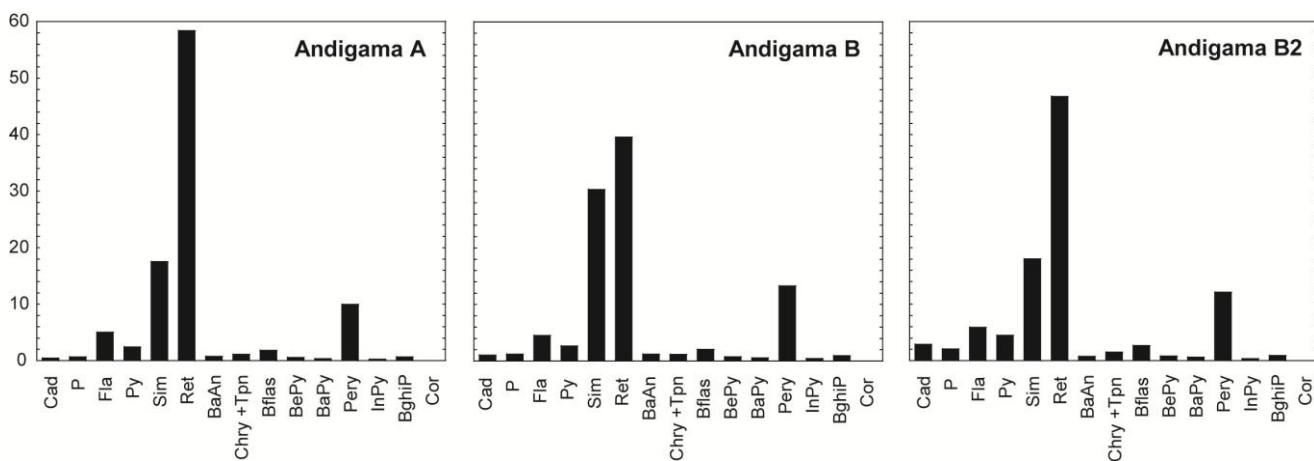


Figure 4.4: Relative abundances of PAHs in the Andigama mudstones.

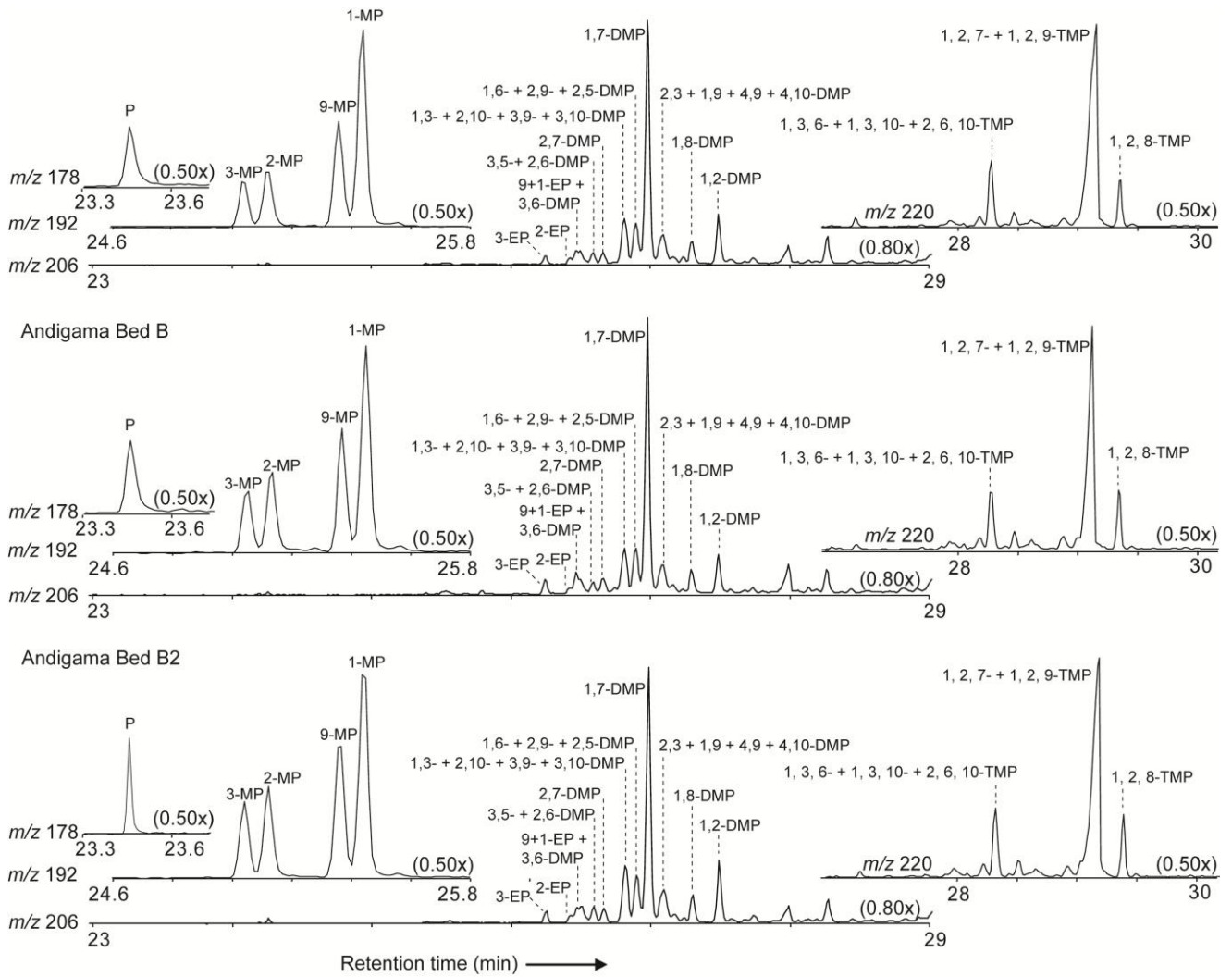


Figure 4.5: Representative m/z 178, 192, 206 and 220 mass chromatograms for phenanthrene (P), methylphenanthrenes (MP), dimethylphenanthrenes (DMP) and trimethylphenanthrenes (TMP) in the Andigama mudstones.

Table 4.3: Concentration and ratios of PAHs in the Andigama mudstones (b.d.l.: below detection limit, MPR: methylphenanthrene ratio and MPI 3: methylphenanthrene index 3).

^aNon-alkylated PAHs = (P + Fla + Py + BaAn + Chry + Tpn + Bfla + BePy + BaPy + Pery + InPy + BghiP + Cor)

^bAlkylated PAHs = (Cad + Sim + Ret)

MPR = [2-MP]/ [1-MP]

MPI 3 = ([2-MP] + [3-MP]) / ([1-MP] + [9-MP])

	Brown to black color Andigama mudstone		
	A	B	B2
Cad (µg/g TOC)	0.12	0.12	0.61
P (µg/g TOC)	0.17	0.14	0.44
Fla (µg/g TOC)	1.34	0.53	1.29
Py (µg/g TOC)	0.64	0.32	0.98
Sim (µg/g TOC)	4.49	3.44	3.82
Ret (µg/g TOC)	14.96	4.50	9.93
BaAn (µg/g TOC)	0.26	0.19	0.22
Chry + Tpn (µg/g TOC)	0.37	0.17	0.41
Bfla (µg/g TOC)	0.64	0.32	0.79
BePy (µg/g TOC)	0.29	0.18	0.36
BaPy (µg/g TOC)	0.20	0.13	0.26
Pery (µg/g TOC)	3.90	2.31	3.94
InPy (µg/g TOC)	0.07	0.05	0.08
BghiP (µg/g TOC)	0.26	0.16	0.29
Cor (µg/g TOC)	b.d.l	b.d.l	b.d.l
Non-alkylated PAHs ^a (µg/g TOC)	8.13	4.51	9.07
Alkylated PAHs ^b (µg/g TOC)	19.56	8.07	14.36
Total PAHs (µg/g TOC)	27.69	12.57	23.43
MP/P	5.75	3.07	2.91
Fla/Py	2.09	1.68	1.31
Fla/ (Fla + Py)	0.68	0.63	0.57
InPy/ (InPy + Bpery)	0.29	0.33	0.30
BaAn/228	0.40	0.52	0.34
MPR	0.30	0.41	0.40
MPI3	0.35	0.48	0.45

4.2 The offshore Mannar Basin

4.2.1 Stratigraphy

The stratigraphic succession of the Mannar Basin was described using the Dorado North and Barracuda cutting samples (Figure 4.6). The details descriptions are given in Appendix. Stratigraphic units are summarized in Table 4.4. Also, magnifying observations of representative lithology are shown in Figure 4.7.

4.2.1.1 Sandstones

The overall sandstones units of the two wells from the Mannar Basin are mainly composed of wacke, with detrital quartz and feldspar. Subangular to subrounded quartz grains are poorly to moderately sorted in an authigenic matrix. Also, rigid rock fragments, heavy minerals and marine bioclasts are recorded in minor quantities. No significant mineralogical differences were observed throughout sandstone sedimentary successions. Sandstones are texturally and mineralogical immature. The detrital mineralogy of the Dorado North well is dominated by quartz, with abundant feldspar. The detrital mineralogy of the Barracuda well is dominated by feldspar, with abundant quartz. The average authigenic cement and clay percentages of the Dorado North well are ~5% and ~15% respectively. In the Barracuda well, the average authigenic cement and clay percentages are ~10% and ~20% respectively.

4.2.1.2 Interbedded red mudstones and black mudstones

Well log analysis indicates the existence of thin red color centimeter scale mudstone layers in the Early to Late Campanian and Late Paleocene to Eocene sediments of the Mannar Basin (Table 4.4 and Figure 4.6). A little or no remaining

amorphous organic matter contains in red color mudstones (Figure 4.7(b)).

The uppermost Early Campanian sediments of the both wells predominantly contain black color mudstone in different thicknesses (Figure 4.6). Mudstone thicknesses are prominent in the Barracuda well (Table 4.4). Black mudstones comprise a large proportion of mixed a- and b-types amorphous organic matter (Figure 4.7(e)).

4.2.1.3 Volcanogenic sediments

The Late Maastrichtian sediments of the Barracuda well consist of medium gray to brownish black color volcanogenic tuffaceous sediments and interbedded mudstone/sandstone (Table 4.4 and Figure 4.6). Photomicrograph confirms the variation in grain size and color in volcanic rocks (Figure 4.7(f)). Olivine and plagioclase are typical phenocryst phase possibly suggesting of basaltic composition.

4.2.1.4 Calcareous mudstone-argillaceous marlstone boundary

Although both well samples show carbonate accumulation throughout the whole sedimentary successions, a clear boundary between calcareous mudstones/ mudstones/ interbedded sandstone in the lower portion of the wells and argillaceous marl/ marlstone in the upper portion of the wells is recognized at 2580 m in the Dorado North well and at 3060 m in the Barracuda well, respectively (Figure 4.6).

4.2.2 Sedimentation rates and burial modeling

Sedimentation rates of the Dorado North and the Barracuda wells are shown in Figure 4.8. Computer simulations of the tectonic and total subsidence of the basin are shown in Figures 4.9 and 4.10. The total subsidence is defined as the sum of subsidence

due to tectonics and subsidence due to sediment loading (load-induced subsidence).

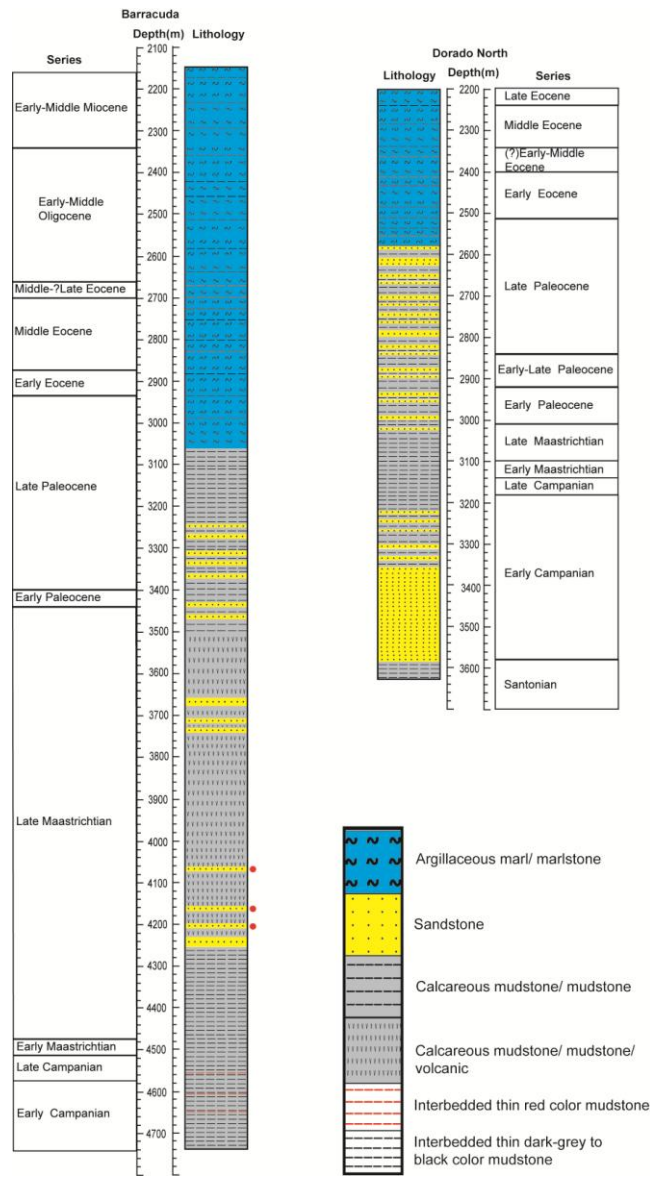


Figure 4.6: Stratigraphic successions of the Dorado North and the Barracuda exploration wells.

Table 4.4: Schematic stratigraphy of the (a) the Dorado North and (b) the Barracuda exploration wells

Table 4.4 (a)

Series	Depth/ m	Thickness/ m	Lithology	Special features
Late Paleocene to Eocene	2200-2580	380	Light gray to medium light gray color calcareous mudstone/ fine to medium grained, light gray to medium light gray	Red color mudstones (2350 m to 2580 m), black fine-scaled laminations (2200 m to 2370 m and 2430 m to 2580 m)
Early Paleocene to Late Paleocene	2580-3010	430	Fine to coarse grained, light gray to medium light gray color calcareous mudstone and interbedded sandstone layers	
Late Campanian to Maastrichtian	3010-3210	200	Fine grained, olive gray to brownish black color mudstone	Black color mudstone (3180 m to 3210 m)
Early Campanian	3210-3350	140	Interbedded fine to medium grained, light gray to olive gray color calcareous mudstone/ sandstone layers	Red color mudstones (3230 m to 3270 m), black color mudstone (3270 m to 3300 m)
Early Campanian	3350-3580	230	Medium to coarse grained, light gray color sandstone	

Table 4.4 (b)

Series	Depth/ m	Thickness/ m	Lithology	Special features
Late Paleocene to Early-Middle Miocene	2139-3060	920	Fine to medium grained, light gray to medium dark gray color marls/ calcareous mudstone	Red color mudstones (2660 m to 2720 m), black fine-scaled laminations (2440 m to 2660 m and 2750 m to 3060 m)
Early Paleocene to Late Paleocene	3060-3440	380	Fine to medium grained, very light gray to medium light gray color calcareous mudstone and interbedded sandstone	Black fine-scaled laminations (3060 m to 3200 m)
Late Maastrichtian	3440-4260	820	Medium to coarse grained, medium gray to brownish black color volcanogenic sediments/ interbedded mudstone/ sandstone	
Early Campanian to Late Maastrichtian	4260-4741	480	Fine to medium grained, greenish black to brownish black color mudstone	Red color mudstones (4550 m to 4660 m), black color mudstone (4510 m to 4550 m and 4660 m to 4741 m)

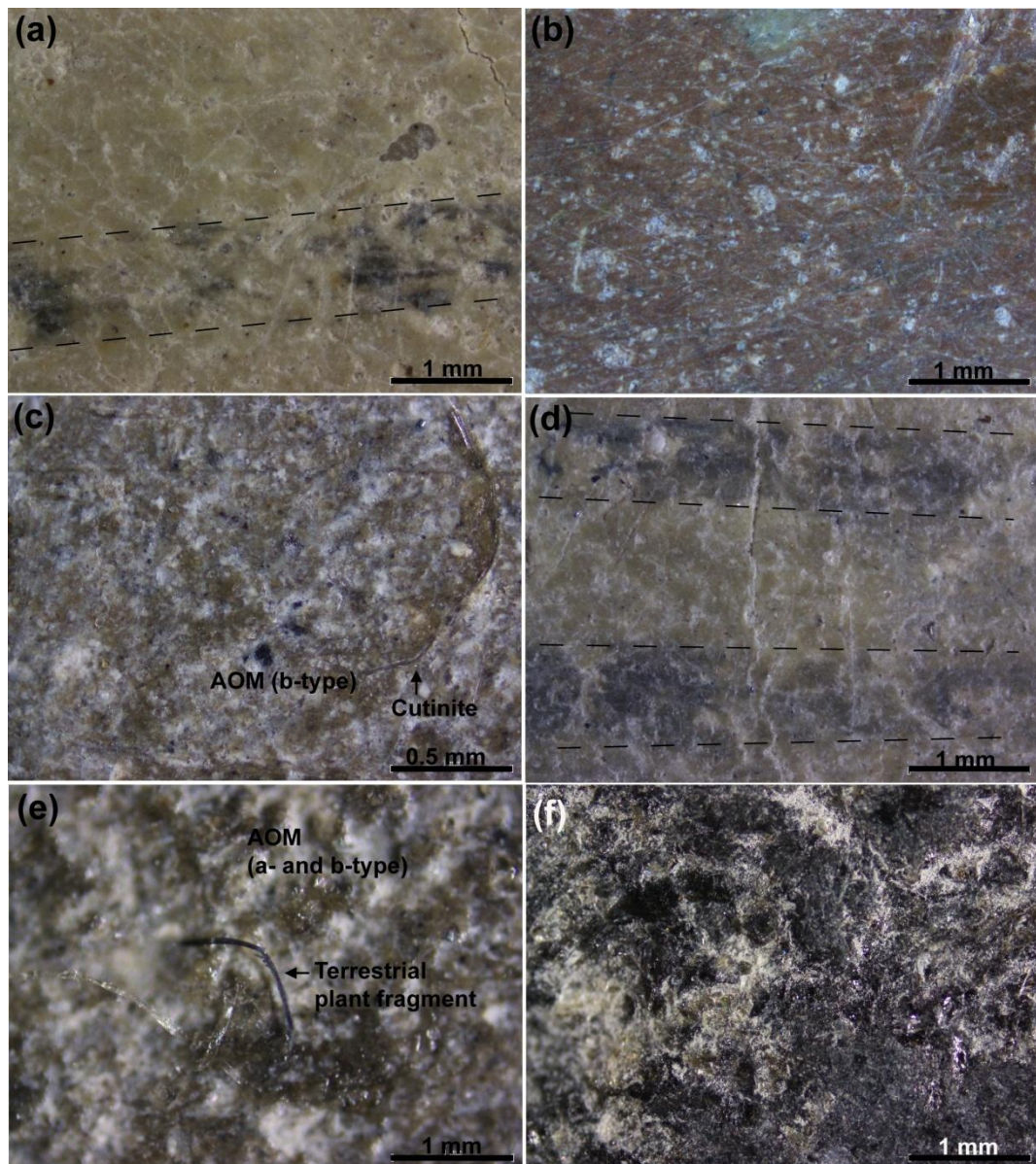


Figure 4.7: Representative photomicrographs show surface mineral and maceral (organic) components in the Mannar Basin. Images (a) and (b) were taken from the Dorado North well, (a) the Late Eocene marlstone (2230-2230 m), (b) the Early Eocene red color mudstone (2400-2410 m). Images (c) to (f) were taken from the Barracuda well, (c) the Middle Oligocene marlstone (2370-2380 m), (d) the Early Oligocene marlstone (2550-2560 m), (e) the Late Paleocene interbedded black color mudstone (3170-3180 m), and (f) the Late Maastrichtian volcanic rock (3870-3880 m).

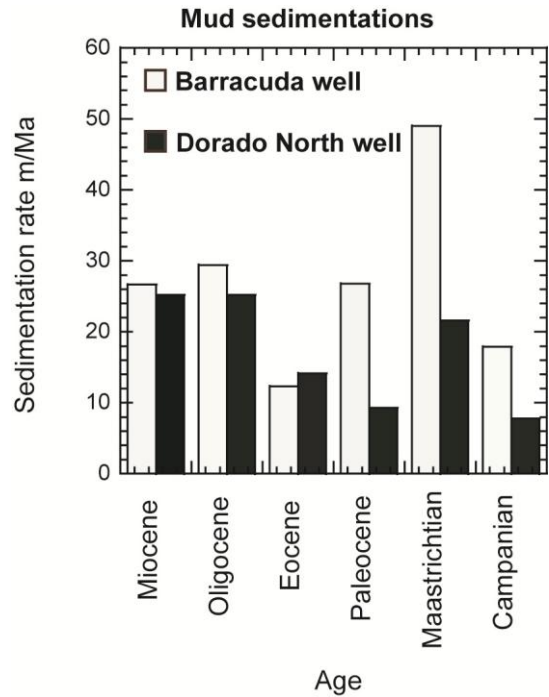


Figure 4.8: Mud sedimentation rates of the Dorado North and the Barracuda exploration wells in m/Ma.

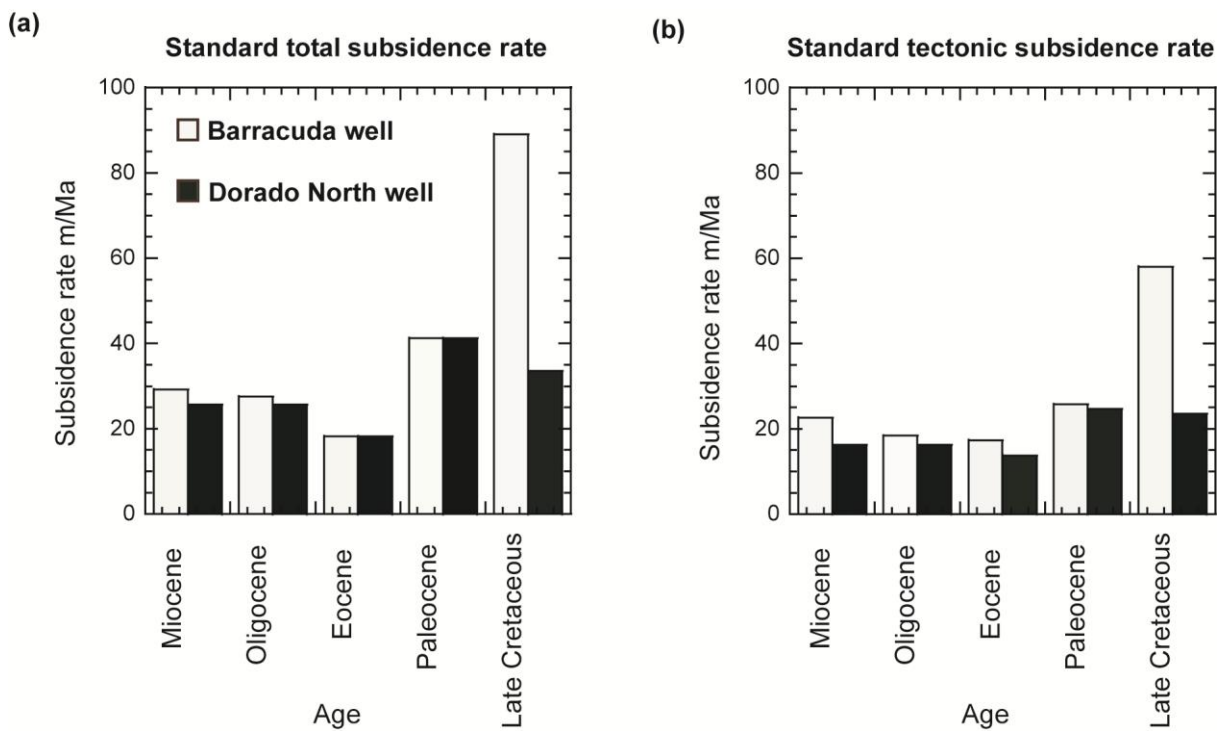


Figure 4.9: Standard burial rates of the Dorado North and Barracuda exploration wells in m/Ma (a) total subsidence, (b) tectonic subsidence.

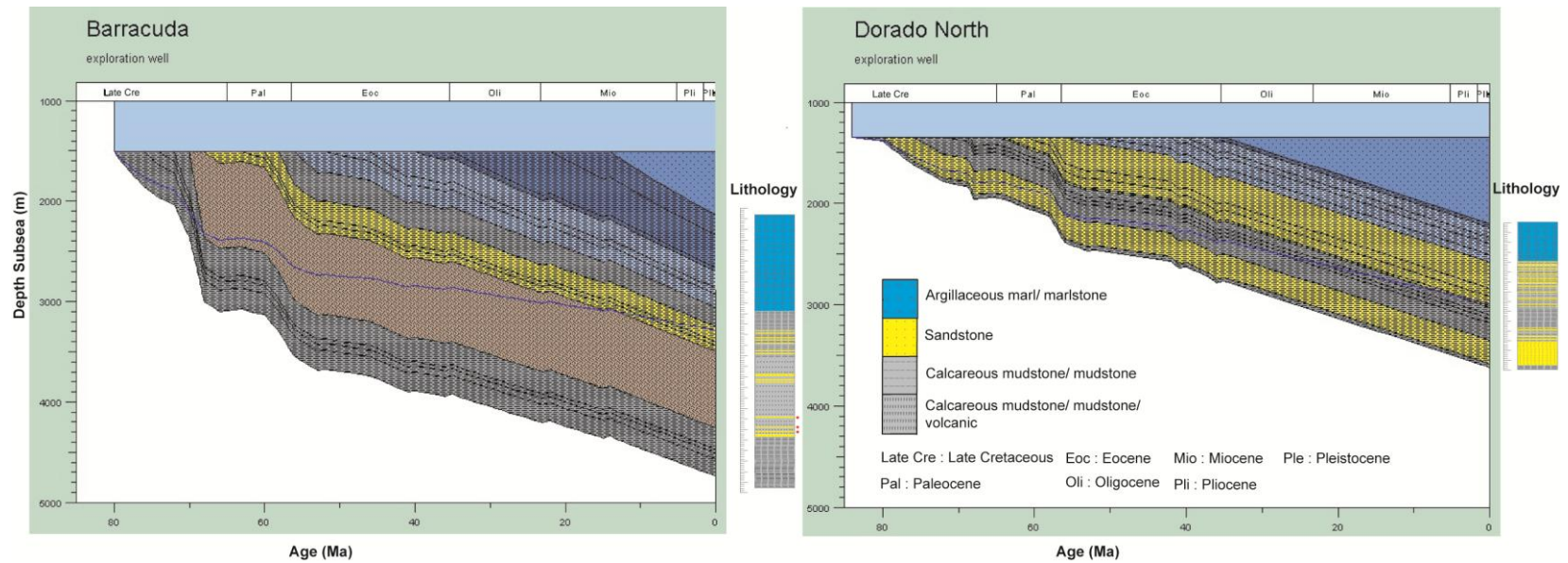


Figure 4.10: Simplified standard burial history models of the Dorado North and the Barracuda exploration wells and stratigraphic correlations. Blue color line shows the general trend of tectonic subsidence. The thicknesses of the eroded sections are unknown. Therefore, the flat intervals indicate no-subsidence or some minor uplifting.

4.2.3 Bulk sedimentary organic matter

The vertical distribution of TC (%), TOC (%), Carbonate-C (%), and CaCO₃ (%) of the Dorado North and the Barracuda exploration wells are shown in Figure 4.11 (a) and Figure 4.11 (b) respectively. TOC (%), TN (%), C/N ratios and C/S ratios of the Dorado North and the Barracuda exploration wells are shown in Figure 4.12 (a) and Figure 4.12 (b) respectively. Also, the correlation of Carbonate-C (%) and TOC (%) in the Dorado North and the Barracuda wells are shown in Figure 4.13 (a) and Figure 4.13 (b) respectively.

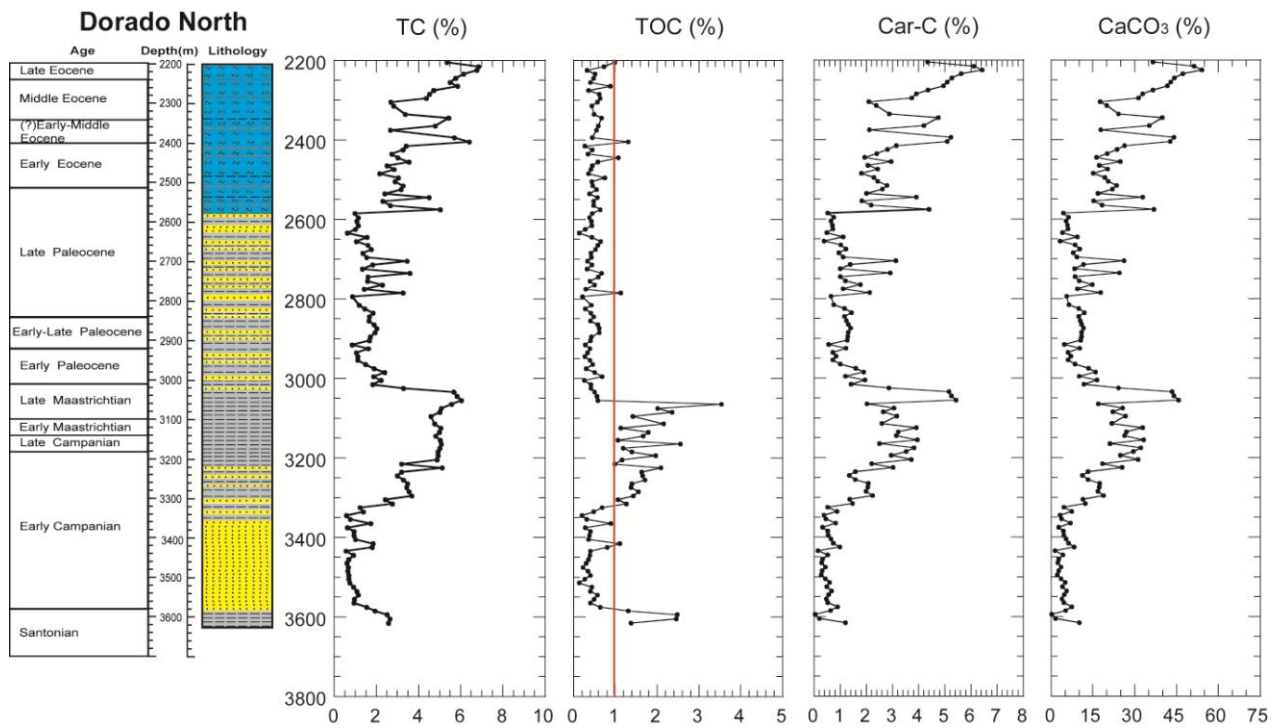


Figure 4.11 (a): Vertical distributions of TC (%), TOC (%), Carbonate-C (%), and CaCO₃ (%) of the Dorado North exploration well in the Mannar Basin.

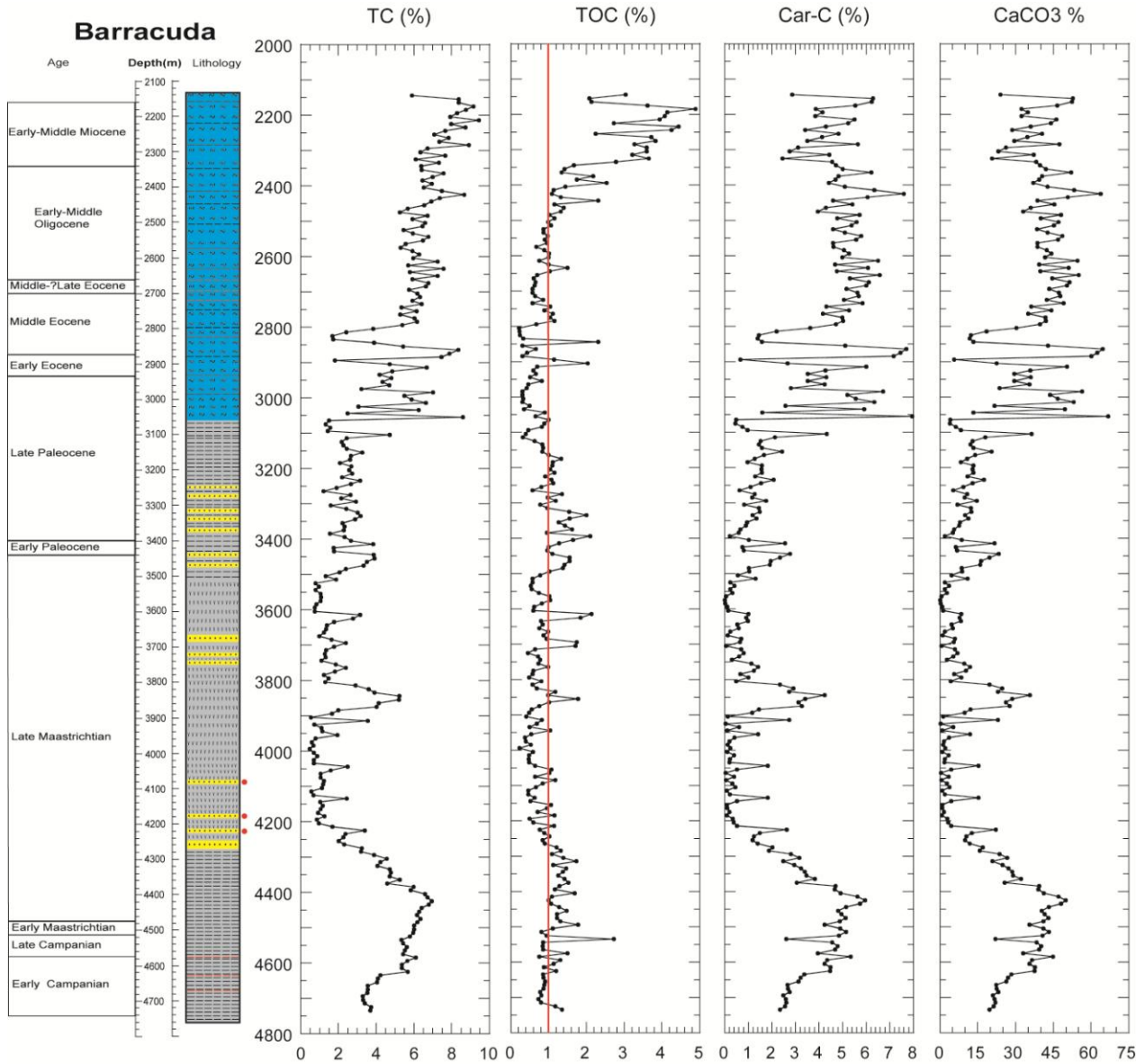


Figure 4.11 (b): Vertical distributions of TC (%), TOC (%), Carbonate-C (%), and CaCO₃ (%) of the Barracuda exploration well in the Mannar Basin.

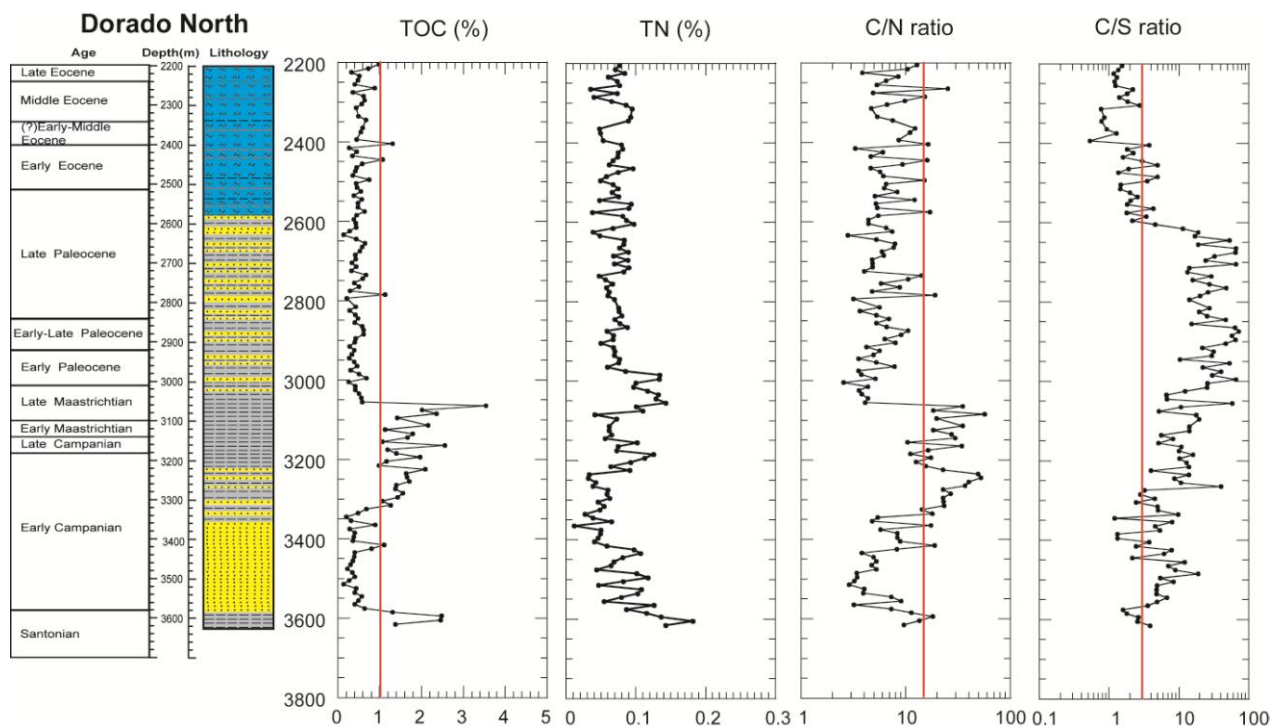


Figure 4.12 (a): Vertical distributions of TOC (%), TN (%), TS (%), C/N ratio and C/S ratio of the Dorado North exploration well in the Mannar Basin.

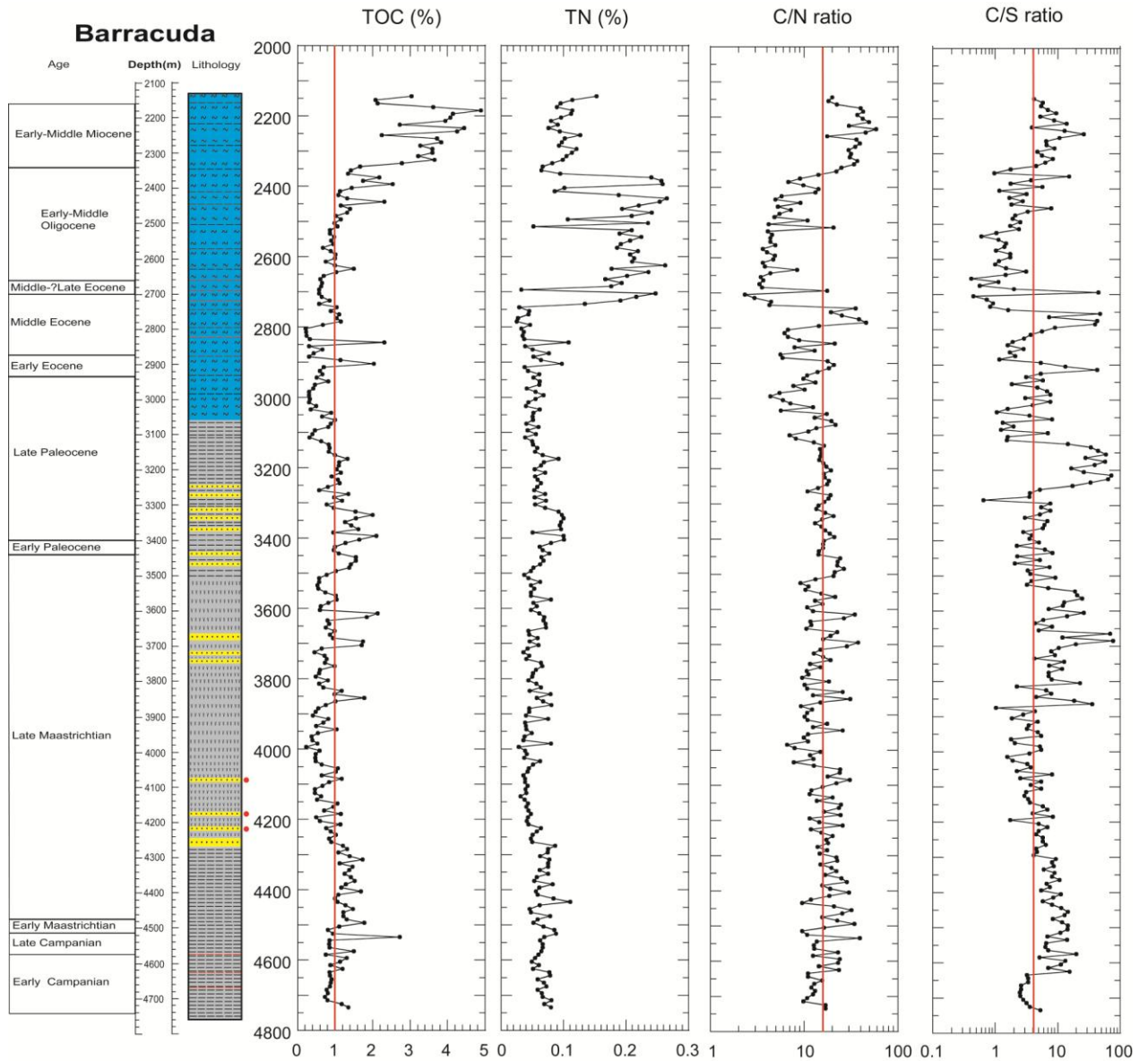


Figure 4.12 (b): Vertical distributions of TOC (%), TN (%), TS (%), C/N ratio and C/S ratio of the Barracuda exploration well in the Mannar Basin.

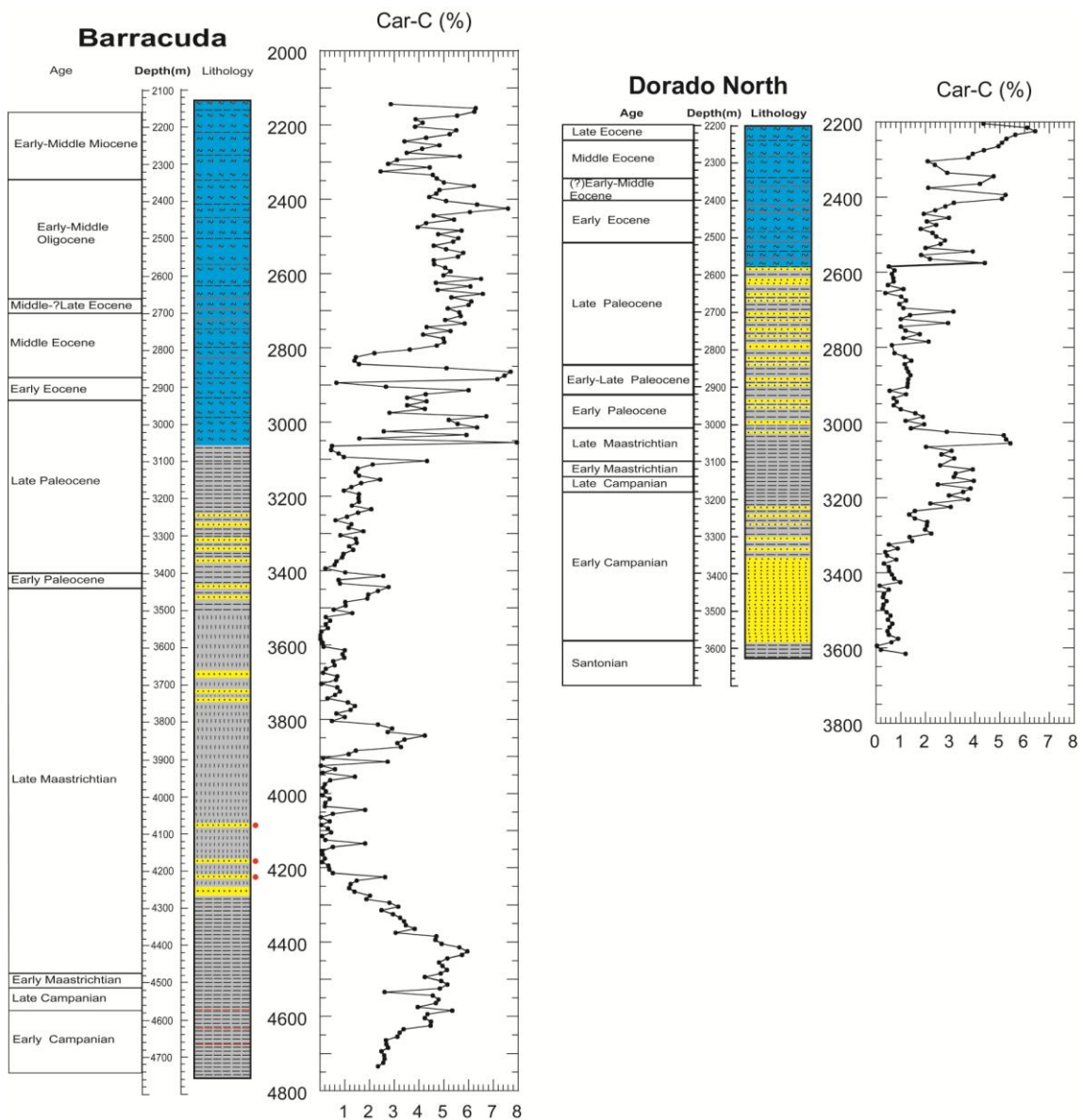


Figure 4.13 (a): The correlation of Carbonate-C (%) in the Dorado North and the Barracuda wells in the Mannar Basin.

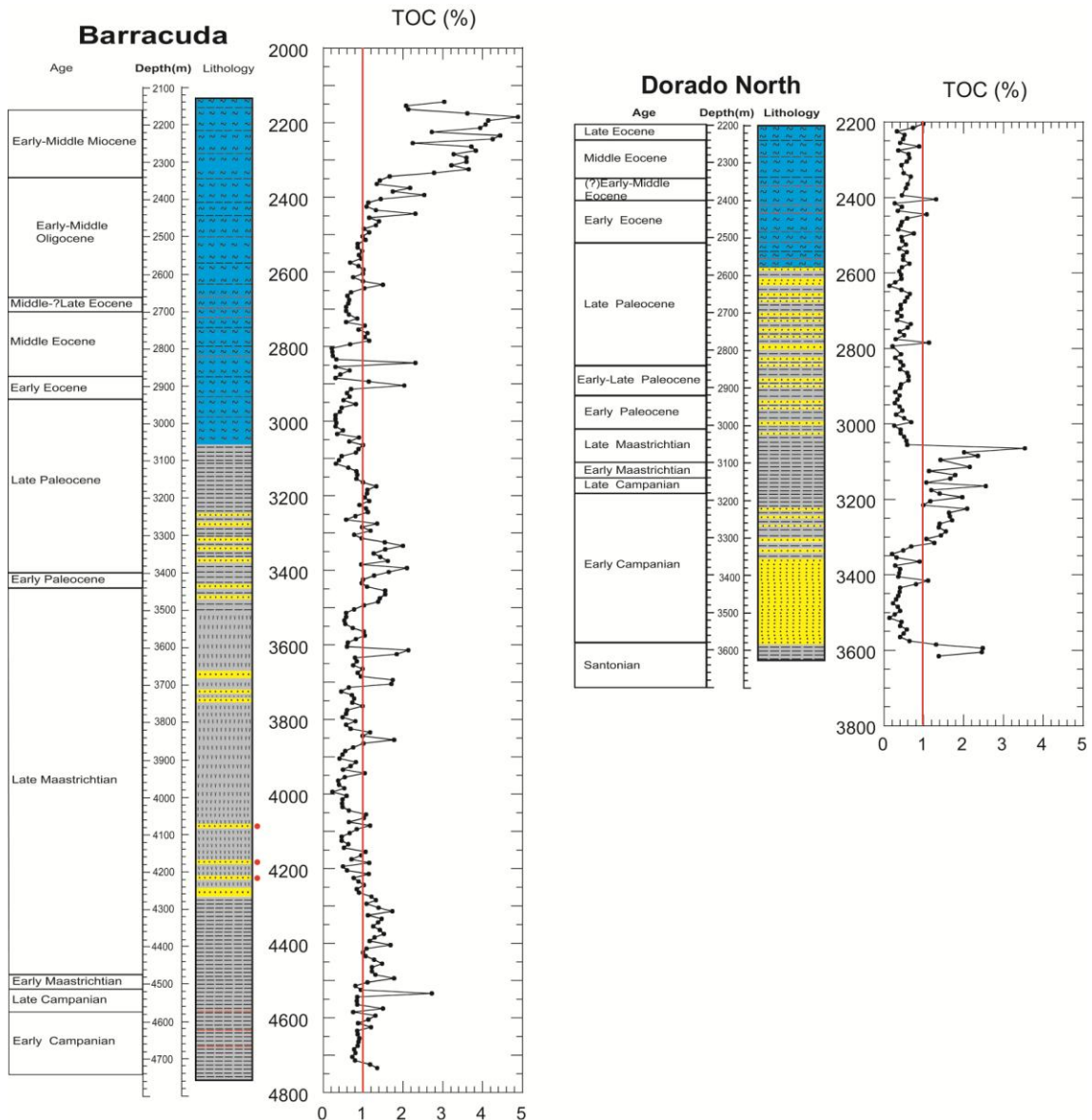


Figure 4.13 (b): The correlation of TOC (%) in Dorado North and Barracuda wells in the Mannar Basin.

4.2.4 Molecular compositions of sedimentary organic matter

The m/z 57 mass chromatograms of n -alkane behaviors in representative bitumen of the Dorado North and Barracuda wells are shown in Figure 4.14. The m/z 57 mass chromatograms of bitumen samples consist of abnormally high unresolved complex mixture (UCM). The UCM can probably indicate biodegradation or contamination of some amount of drill mud and oils during the drilling (e.g., Jones et al., 1983; Volkman

et al., 1992; Grice et al., 2000; Frysinger et al., 2003). The m/z 57 mass chromatograms of n -alkane behaviors in kerogen of the Barracuda wells samples are shown in Figure 4.15. Therefore, the author considers kerogen portions to calculate n -alkane proxies in the Mannar Basin.

However, bitumen was used to calculate m/z 191 and m/z 217 fractions due to negligible contamination as shown in absent of UCM (Figure 4.16). Therefore, biodegradation and contamination do not control variations in sterane and hopane compositions compared to n -alkanes (e.g., Volkman et al., 1992; Curiale and Bromley, 1996). Drill mud and oil can probably show fast moving nature along with n -alkanes in a thin layer chromatography plate (silica gel 60 PF₂₅₄ containing gypsum) with hexane as a mobile phase. Sterane and hopane concentrations were low to allow calculation of biomarker proxies in kerogen. The biomarker results of the Barracuda wells are summarized in Figure 4.17.

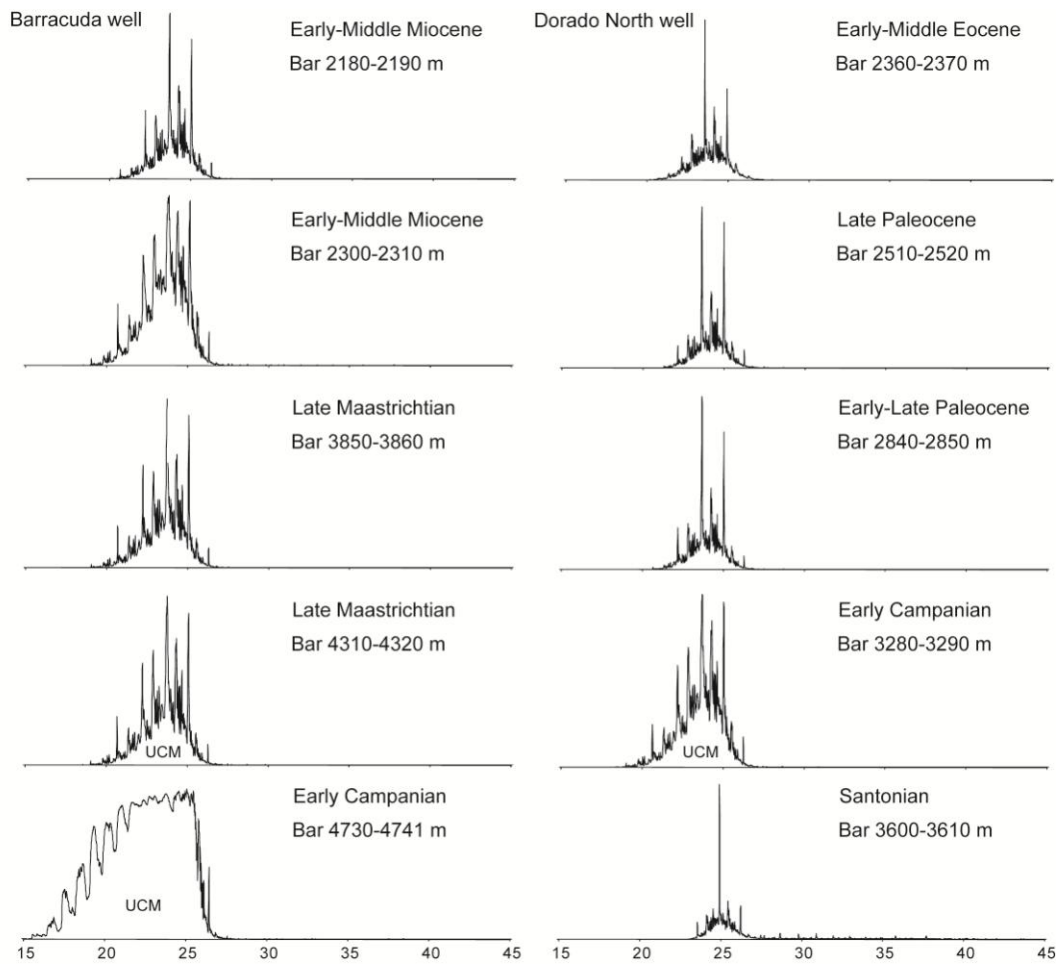


Figure 4.14: Mass chromatograms ($m/z = 57$) showing distribution of n -alkanes in bitumen of the Dorado North and Barracuda exploration wells (UCM: unresolved complex mixture).

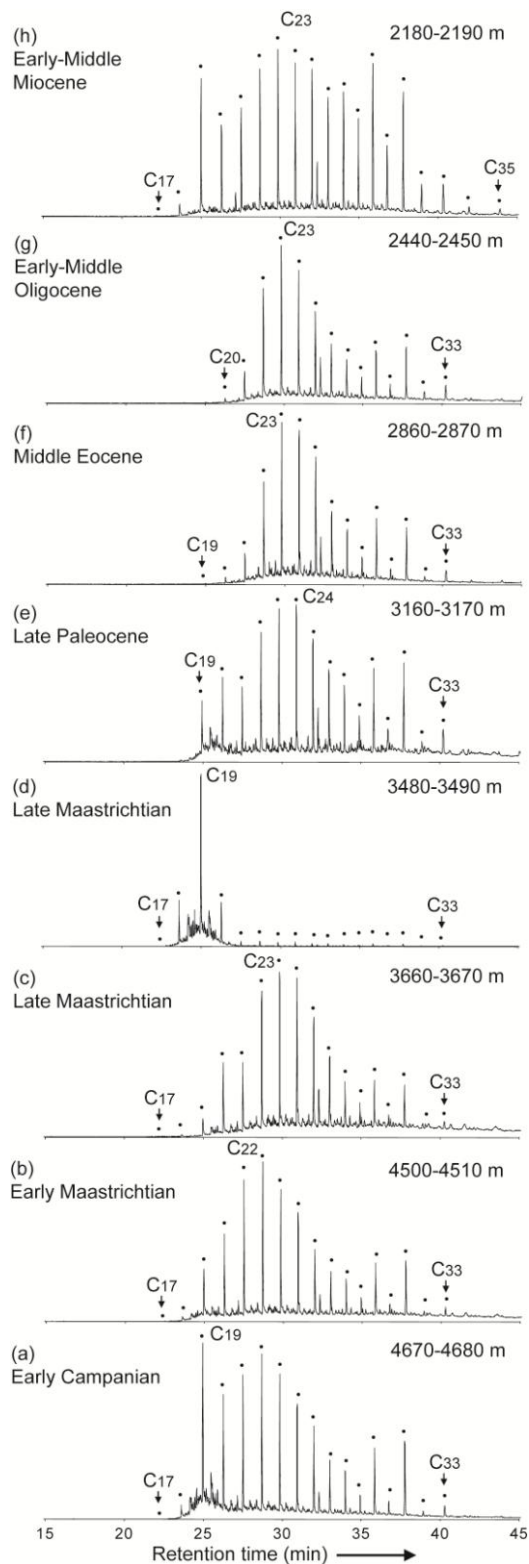


Figure 4.15: Mass chromatograms ($m/z = 57$) showing distribution of n -alkanes in kerogen of the Barracuda exploration well.

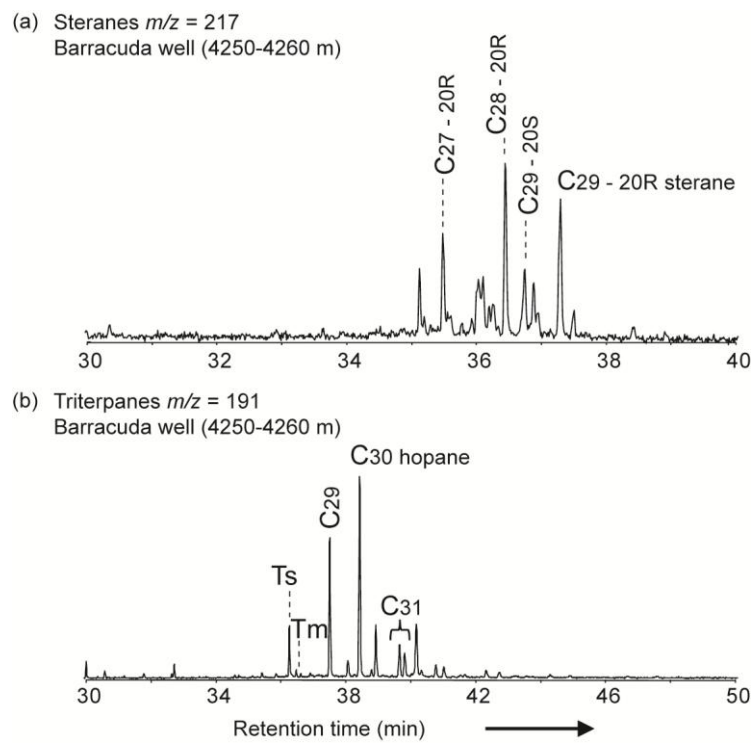


Figure 4.16: Representative mass chromatograms of (a) steranes ($m/z = 217$) and (b) triterpanes ($m/z = 191$) in bitumen samples.

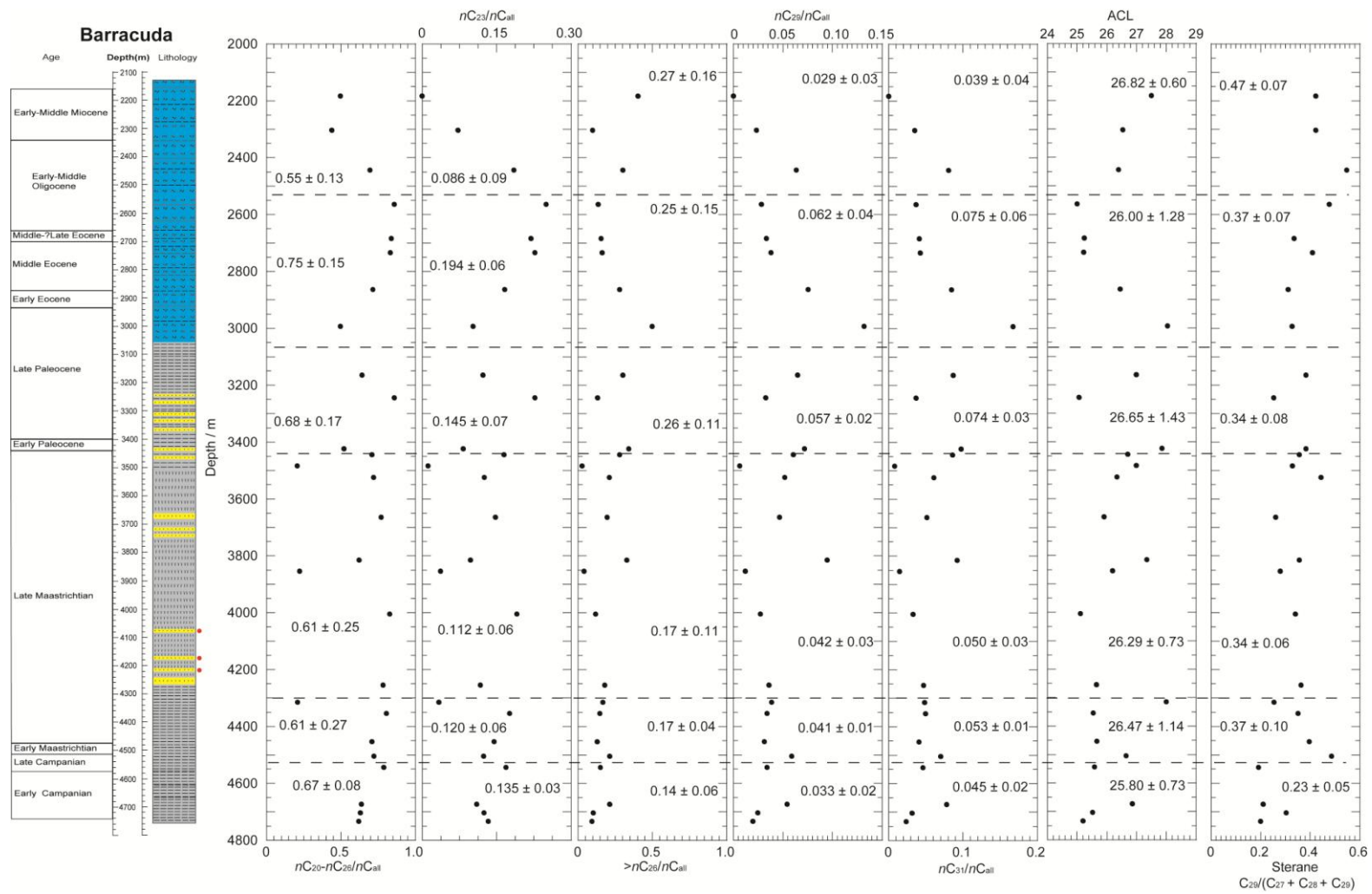


Figure 4.17: Biomarker results of the Barracuda well.

4.3 The coastal Bolgoda Lake

4.3.1 Field observations

The physical appearance of the most surface samples was generally silty clay, while few samples were sandy silty clay. The very feeble H₂S odors were emitted by some surface sediment samples. The most samples were brownish greenish black in color, while few samples were brownish black in color. The live benthic organisms, live plant materials, wood fragments and small calcareous shells were observed in some surface sediment samples.

The Bolgoda Lake has been investigated using three core samples. The sedimentary succession of the lake can be divided into two major divisions. The sedimentary facies of the lower succession is characterized by rare macrofossils and terrestrial wood fragments. However, the upper sediments consist of poorly developed, irregular, millimeter scale few laminations. Moreover, regular laminations (alternative dark and light color) generally represent cyclic changes in supplies of sediments under anoxic conditions (Berner, 1984; Gong and Hollander, 1997; Meyers, 2003; Valdés et al., 2004; Ratnayake et al., 2005). However, irregular poorly developed laminations can probably accompany with changes of clay, OM and mineral contents due to environmental and climatic fluctuations of the watershed area.

4.3.2 Bulk sedimentary organic matter

The spatial distributions of bulk organic geochemical parameters of surface sediments are shown in Figure 4.18. The computerized inverse distance weighting method of geographic information system was chosen for preparing spatial interpolation maps after successive comparison with manually drawn contours. TOC contents in

surface sediments varied from 1.31% to 14.87% with an average of 4.8%. TOC contents were relatively low (under 2.50%) in surface samples from L12, L13, L18 and L19. C/N ratios of surface sediments varied from 10.4 to 30.0. Also, C/N ratios are gradually increased towards the northern freshwater stream. C/S ratios of surface sediments varied from 0.86 to 6.55 and C/S ratios are gradually decreased towards the basin part of the study area. The vertical distribution of TOC (%), C/N ratios and C/S ratios of core samples are shown in Figure 4.19. The vertical distribution of TOC (%), C/N ratios and C/S ratios of mangrove mud core samples are shown in Figure 4.20.

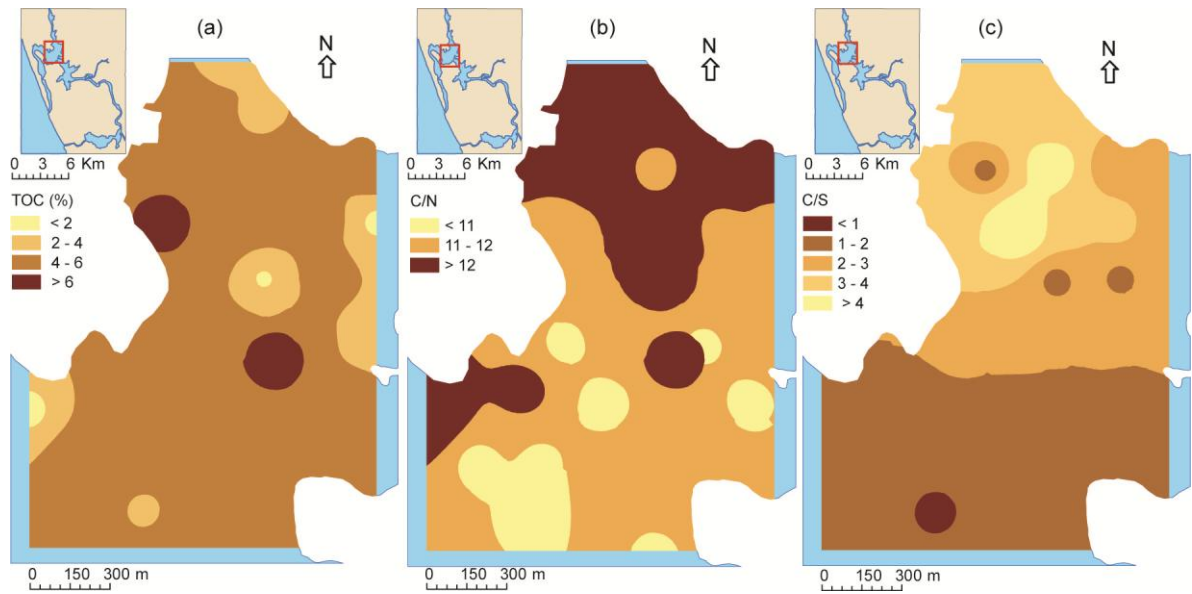


Figure 4.18: Surface distributions of TOC, C/N ratio and C/S ratio of the Bolgoda Lake surface sediments.

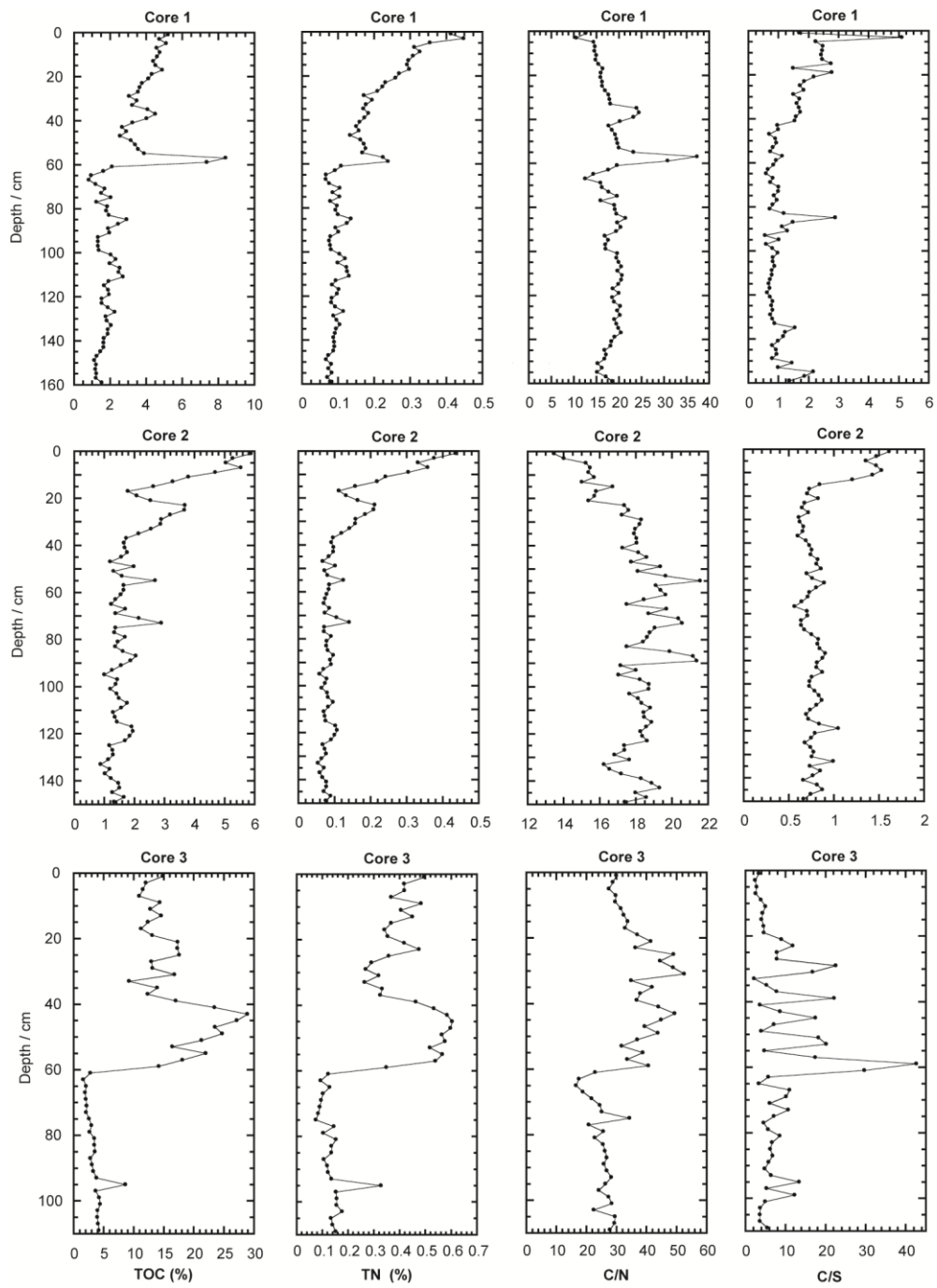


Figure 4.19: Vertical distributions of TOC, TN, C/N ratio and C/S ratio of Core 1, Core 2, and Core 3 in the Bolgoda Lake

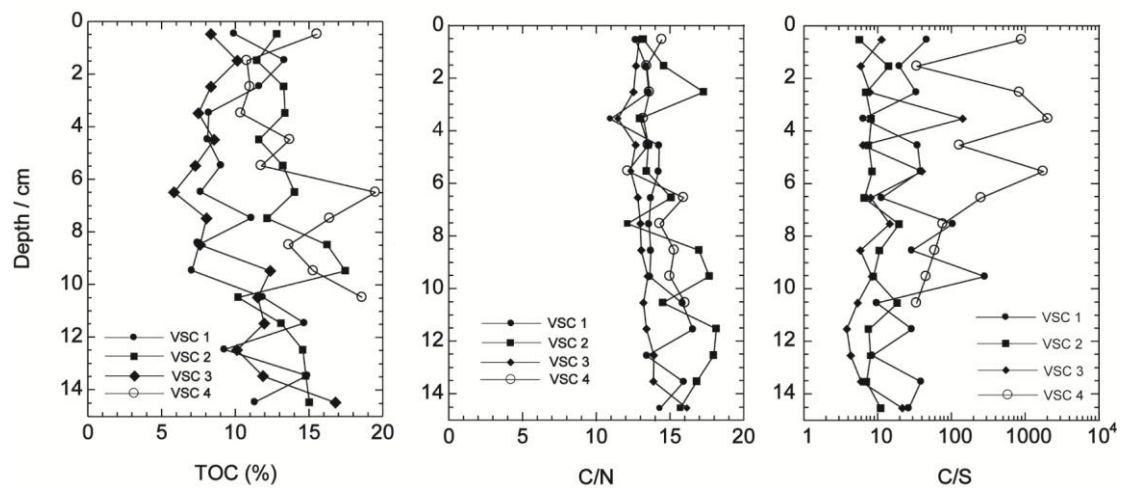


Figure 4.20: Vertical distributions of TOC, C/N ratio and C/S ratio of all very short mangrove mud core samples

4.3.3 Living organic source materials

Biological productivities of tropical coastal aquatic systems are extremely diverse due to occurrence of widely spread floras. The m/z 57 mass chromatograms of some of living OM are shown in Figure 4.21. Floating fern consists of highly overlapped bimodal pattern maximizing around n -C₂₅ and n -C₂₉ with a pronounced odd-over-even preference. Floating plant roots and leaves represent bimodal distributions maximizing around n -C₂₃, and n -C₃₁. Herbaceous terrestrial wood indicates unimodal pattern maximizing at n -C₂₅. Mangrove root, wood and leaves are represented unimodal distribution maximizing at n -C₂₃, n -C₂₃ and n -C₂₉ respectively.

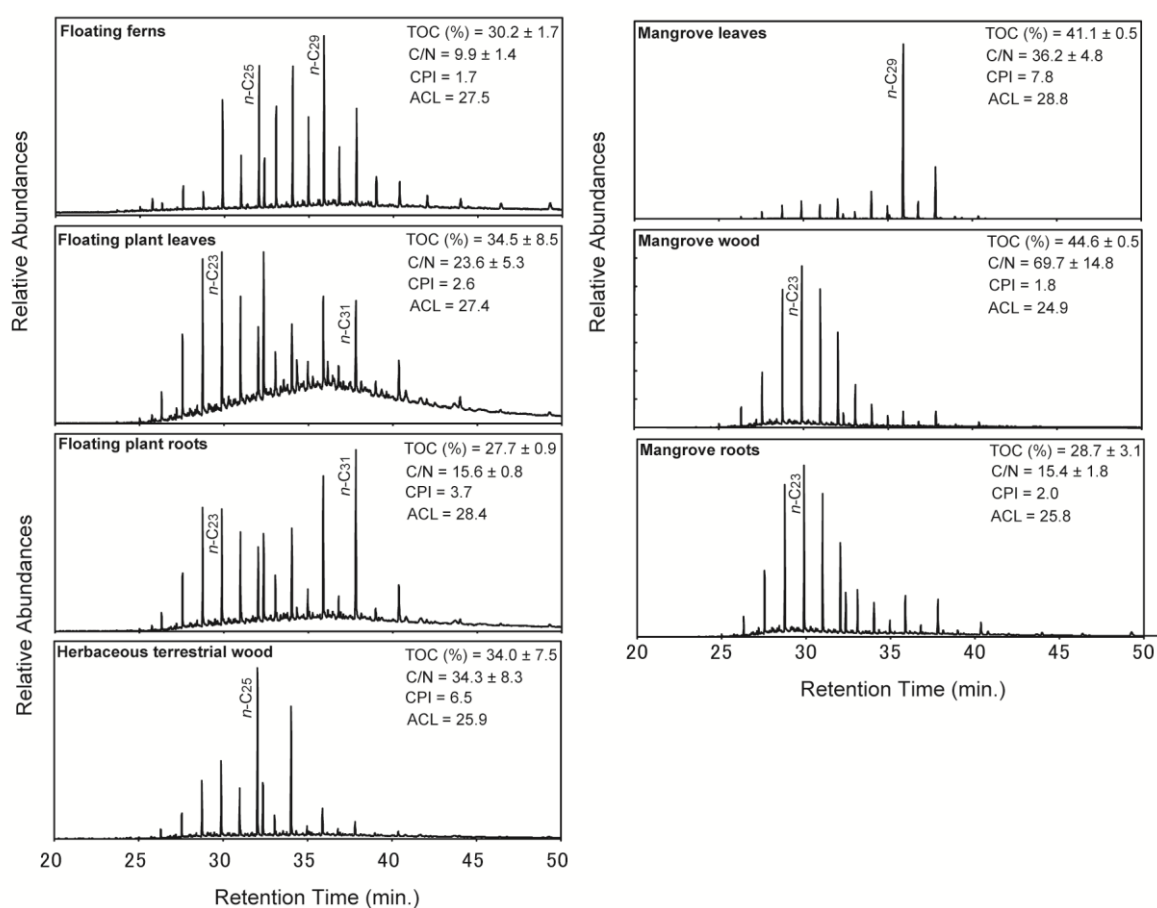


Figure 4.21: Characteristics of n -alkanes mass chromatograms for OM type in the Bolgoda Lake and its watershed area.

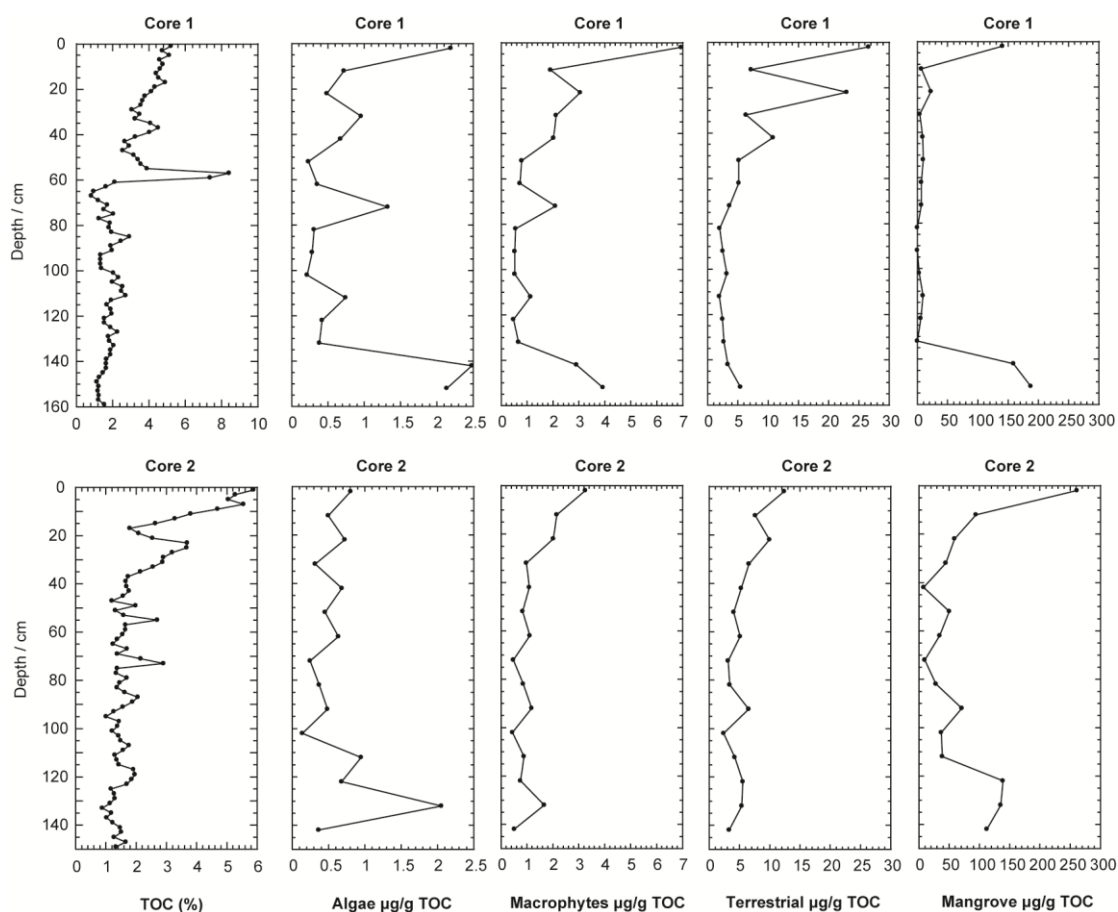


Figure 4.22: Individual concentration changes of algae ($<n-C_{21}$), floating/ herbaceous (macrophytes) plants ($n-C_{23} + n-C_{25}$), terrestrial plants ($n-C_{27} + n-C_{29} + n-C_{31} + n-C_{33}$) and mangrove (taraxerone) biomarkers in Core 1 and Core 2.

4.3.4 Molecular sedimentary organic matter

The n -alkanes biomarker results of surface sediment samples are summarized in Table 4.5. The n -alkanes fractions of surface sediment extend from $n-C_{16}$ to $n-C_{39}$. The Bolgoda Lake surface sediments were characterized by intensified $n-C_{29}$ and $n-C_{31}$ peaks and relatively higher abundance of long chain n -alkanes of $n-C_{35}$, $n-C_{37}$ and $n-C_{39}$. The average concentrations of algae, floating and herbaceous (macrophytes) plants, terrestrial plants and mangrove plants in surface sediments were $1.36 \mu\text{g/gTOC}$, $3.42 \mu\text{g/gTOC}$, $11.29 \mu\text{g/gTOC}$, $197.39 \mu\text{g/gTOC}$ respectively (Table 4.5). The individual concentration changes of algae, macrophytes, terrestrial, and mangrove biomarkers of core samples are shown in Figure 4.22. Also, characteristic $m/z = 57$ mass

chromatograms patterns of before and after major environmental change are shown in Figure 4.23. The biomarker results of Core 1 and Core 2 are shown in Figure 4.24 and results of mangrove mud core samples are summarized in Table 4.6. The mangrove mud core samples display relatively lower amount of algae (mean = 0.95 $\mu\text{g/gTOC}$) and macrophytes (mean = 2.49 $\mu\text{g/gTOC}$) respectively, than surface sediments. However, terrestrial (mean = 11.99 $\mu\text{g/gTOC}$) and mangrove (mean = 281.97 $\mu\text{g/gTOC}$) concentrations of mangrove mud core samples are higher than surface sediment samples. Also, taraxerone (friedoolean) compounds, urasane and amyrene were recognized as significant terrestrial biomarkers in the study area.

A variety of aromatic compounds were identified in majority of surface sediment samples (Table 4.7). Fluoranthene (Fla), Pyrene (Py), Benzo[a]anthracene (BaAn) and Benzofluoranthene (Bflas) are dominated PAHs in surface sediment samples. Fla, Py, BaAn and Bflas concentrations of surface sediment samples ranged from (0.00-0.89 $\mu\text{g/gTOC}$), (0.00-0.85 $\mu\text{g/gTOC}$), (0.00-0.10 $\mu\text{g/gTOC}$) and (0.00-0.28 $\mu\text{g/gTOC}$) respectively. Next, distributions of PAHs are abundance in upper most lithofacies of the core samples. Fla and Py are abundance in mangrove mud core samples (Table 4.7). Fla and Py concentrations of mangrove mud core samples ranged from (0.00-0.07 $\mu\text{g/gTOC}$) and (0.00-0.07 $\mu\text{g/gTOC}$) respectively.

The triterpanes biomarker results of surface sediments and mangrove mud cores are summarized in Table 4.8 and Table 4.9 respectively. The vertical distributions of triterpanes biomarker proxies of core samples are shown in Figure 4.25.

4.3.5 ^{14}C age dating

Results of accelerated mass spectrometry ^{14}C analysis are shown in Table 4.10.

Table 4.5: The results of biomarker proxies in surface sediment samples ($P_{aq} = (C_{23}+C_{25}) / (C_{23}+C_{25}+C_{29}+C_{31})$; $CPI = 1/2[(C_{25}+C_{27}+C_{29}+C_{31}+C_{33}) / (C_{24}+C_{26}+C_{28}+C_{30}+C_{32}) + (C_{25}+C_{27}+C_{29}+C_{31}+C_{33}) / (C_{26}+C_{28}+C_{30}+C_{32}+C_{34})]$; $ACL = (23 * C_{23} + 25 * C_{25} + 27 * C_{27} + 29 * C_{29} + 31 * C_{31} + 33 * C_{33}) / (C_{23} + C_{25} + C_{27} + C_{29} + C_{31} + C_{33})$)

Sample	<i>n</i> -alkanes proxies			Concentration ($\mu\text{g/g TOC}$)			
	P_{aq}	CPI	ACL	Algae	Macrophytes	Terrestrial	Mangrove
L 1	0.34	2.86	28.88	2.21	5.70	20.27	339.58
L 2	0.37	2.79	28.73	2.24	4.43	13.64	6.39
L 3	0.32	2.81	29.12	0.88	2.20	8.48	16.81
L 4	0.38	2.99	28.67	0.95	3.02	9.47	187.66
L 5	0.28	2.94	29.35	0.74	2.98	14.48	316.70
L 6	0.33	2.94	28.76	1.01	2.39	8.63	207.95
L 7	0.35	2.87	28.89	2.38	5.27	18.38	387.88
L 8	0.30	3.09	29.24	2.23	4.16	17.60	6.45
L 9	0.31	2.86	29.06	1.00	2.92	11.97	71.86
L 13	0.39	2.66	28.76	1.48	3.20	9.30	116.11
L 14	0.33	2.91	29.01	0.87	2.84	10.65	511.86
L 15	0.47	2.89	28.14	1.92	4.11	8.83	11.09
L 17	0.35	2.90	28.90	1.51	4.33	14.93	27.04
L 19	0.57	2.59	27.66	2.79	5.72	8.38	42.44
L 21	0.44	3.01	28.32	0.78	2.67	6.44	10.64
L 23	0.30	3.33	29.10	0.73	2.66	11.19	133.92
L 24	0.38	3.55	28.68	1.09	3.36	9.93	398.59
L 25	0.28	3.54	29.39	0.69	2.56	12.28	496.48
L 27	0.41	3.10	28.47	0.43	1.78	4.68	134.69
L 28	0.37	3.00	28.85	2.03	3.95	12.45	716.44
L 29	0.35	3.14	28.88	0.63	1.54	5.11	4.64

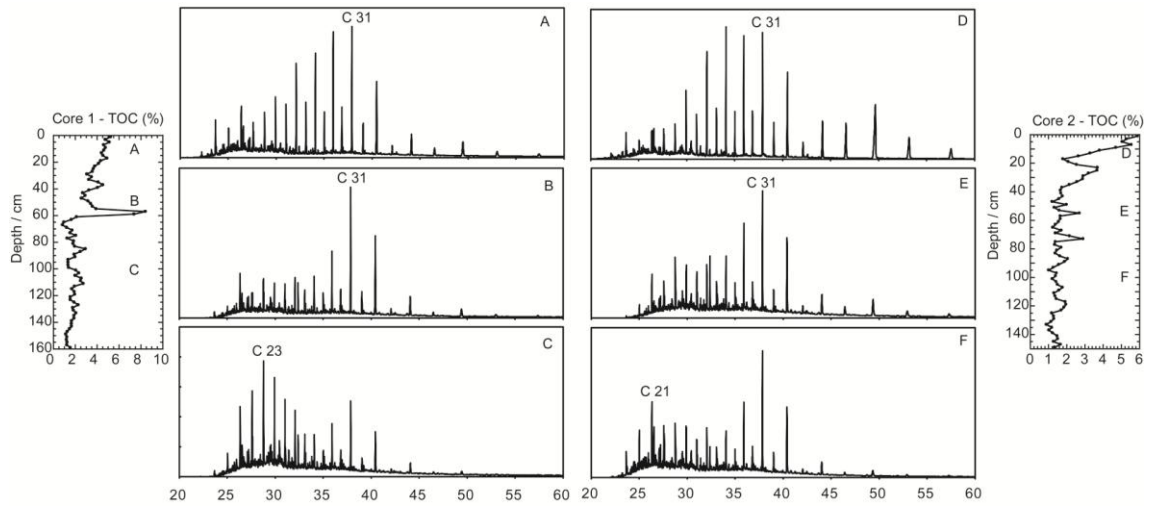


Figure 4.23: Characteristic mass chromatograms patterns of before and after major environmental change.

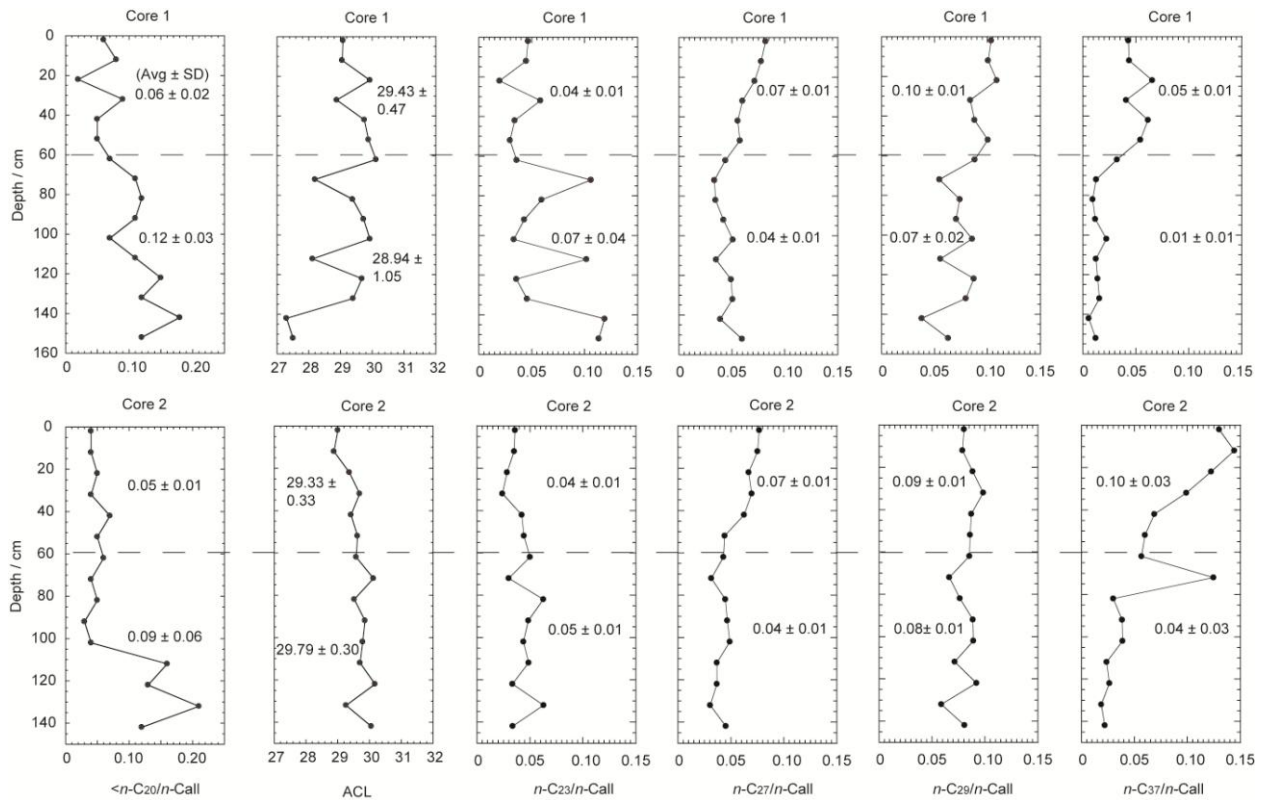


Figure 4.24: The characteristics of molecular proxies in Core 1 and Core 2.

Table 4.6: The results of biomarker proxies in mangrove mud core samples

Sample	<i>n</i> -alkanes proxies			Concentration ($\mu\text{g/g}$ TOC)			
	Paq	CPI	ACL	Algae	Macrophytes	Terrestrial	Mangrove
VSC 1(0-2cm)	0.25	6.63	29.84	1.08	3.02	18.02	417.73
VSC 1 (6-8cm)	0.25	6.84	29.70	1.24	4.34	25.24	177.66
VSC 1 (13-15cm)	0.35	5.64	29.41	0.56	1.88	6.93	777.39
VSC 2 (0-2cm)	0.23	5.75	29.89	1.30	3.32	20.19	733.82
VSC 2 (6-8cm)	0.30	4.15	29.03	0.99	3.20	12.66	682.16
VSC 2 (13-15cm)	0.25	3.98	29.33	0.80	2.00	9.85	65.51
VSC 3 (0-2cm)	0.37	3.28	28.57	0.91	1.43	4.17	39.10
VSC 3 (6-8cm)	0.36	3.76	28.70	1.60	2.53	8.30	68.41
VSC 3 (13-15cm)	0.25	4.01	29.17	0.26	0.75	3.75	86.85
VSC 4 (0-2cm)	0.21	4.58	29.40	0.98	2.01	11.67	51.01
VSC 4 (6-8cm)	0.32	5.77	28.66	0.71	2.86	11.11	2.02

Table 4.7: The average concentration and proxies of PAHs in sedimentary units (n.d., not detected)

Sample	Fla	Py	BaAn	Bfla	BePy	Fla/Py	Fla/(Fla + Py)
Core 1	52.91	65.89	8.37	107.97	25.17	0.80	0.45
Core 2	37.04	32.42	14.46	67.03	36.16	1.25	0.55
VSC 1	46.56	44.82	n.d.	n.d.	n.d.	1.03	0.51
VSC 2	45.21	42.97	n.d.	n.d.	n.d.	1.06	0.51
VSC 3	29.74	27.94	n.d.	n.d.	n.d.	1.08	0.52
VSC 4	46.50	45.15	n.d.	n.d.	n.d.	1.03	0.51
Surface sediments	67.39	70.69	12.33	40.84	n.d.	1.02	0.50

Table 4.8: Distribution of representative triterpanes biomarkers in m/z 191 mass chromatograms of surface sediments from the Bolgoda Lake

Sample	C ₃₁ -22S ng/gTOC	C ₃₁ -22R ng/gTOC	Total hopane ng/gTOC	C ₃₁ hopane (22S/22R)	22S/(22S + 22R) for C ₃₁	Ts/ (Ts + Tm)
L 1	377.78	799.56	2550.24	0.47	0.32	0.23
L 2	292.22	723.72	2008.11	0.40	0.29	0.20
L 3	95.83	201.68	561.46	0.48	0.32	0.16
L 4	220.01	632.12	1590.14	0.35	0.26	0.16
L 5	177.53	452.97	1238.47	0.39	0.28	0.19
L 6	255.91	509.89	1689.45	0.50	0.33	0.21
L 7	538.02	1059.97	3470.65	0.51	0.34	0.24
L 8	298.06	635.32	1916.95	0.47	0.32	0.21
L 9	201.98	553.24	1452.65	0.37	0.27	0.16
L 13	109.46	387.19	889.10	0.28	0.22	0.16
L 14	179.70	431.66	1214.44	0.42	0.29	0.20
L 15	285.72	776.77	2004.13	0.37	0.27	0.15
L 17	196.31	526.08	1387.99	0.37	0.27	0.14
L 19	100.27	275.25	681.99	0.36	0.27	0.18
L 21	149.97	476.53	1094.83	0.31	0.24	0.14
L 23	108.32	333.21	801.15	0.33	0.25	0.14
L 24	77.96	224.52	566.71	0.35	0.26	0.14
L 25	77.65	255.23	615.79	0.30	0.23	0.13
L 27	88.34	269.22	636.81	0.33	0.25	0.14
L 28	134.33	454.10	1028.01	0.30	0.23	0.13
L 29	82.45	306.23	666.52	0.27	0.21	0.14

Table 4.9: Distribution of representative triterpanes biomarkers in m/z 191 mass chromatograms of mangrove mud core samples

Sample	C ₃₁ -22S ng/gTOC	C ₃₁ -22R ng/gTOC	Total hopane ng/gTOC	C ₃₁ hopane (22S/22R)	22S/(22S + 22R) for C ₃₁	Ts/(Ts + Tm)
VSC 1 (0-2cm)	116.71	121.63	673.14	0.96	0.49	0.41
VSC 1 (6-8cm)	150.23	124.02	805.88	1.21	0.55	0.51
VSC 1 (13-15cm)	69.98	82.57	411.78	0.85	0.46	0.31
VSC 2 (0-2cm)	192.44	191.58	1041.04	1.00	0.50	0.41
VSC 2 (6-8cm)	183.06	207.08	1093.31	0.88	0.47	0.35
VSC 2 (13-15cm)	55.19	66.62	283.98	0.83	0.45	0.27
VSC 3 (0-2cm)	92.00	86.86	518.51	1.06	0.51	0.45
VSC 3 (6-8cm)	152.54	154.29	882.90	0.99	0.50	0.50
VSC 3 (13-15cm)	74.96	72.09	403.85	1.04	0.51	0.39
VSC 4 (0-2cm)	139.02	119.86	787.39	1.16	0.54	0.54
VSC 4 (6-8cm)	108.83	77.32	538.33	1.41	0.58	0.66

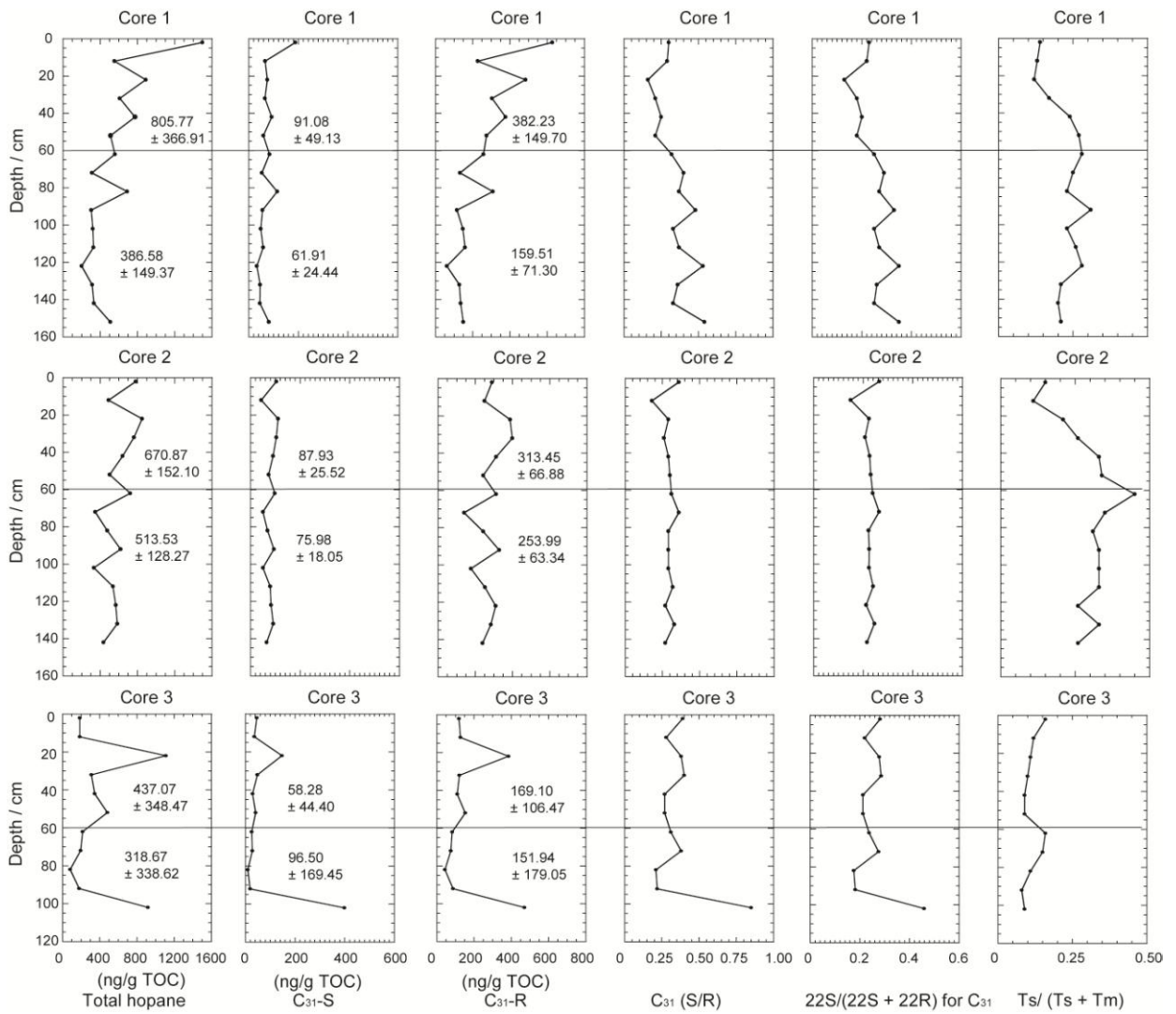


Figure 4.25: Depth profiles showing the distribution of (a) total hopane^a, (b) C₃₁ hopane – 22S isomer, (c) C₃₁ hopane – 22R isomers concentrations, (d) C₃₁ hopane (22S/22R) ratio, (e) C₃₁ hopane 22S/(22S + 22R) ratio and (f) Ts/(Ts + Tm) ratio in core samples. Total hopane^a = C₂₉ hopane + C₃₀ hopane + C₃₁ hopane 22S isomer + C₃₁ hopane 22R isomer

Table 4.10: Results of ^{14}C radiometric dating and $\delta^{13}\text{C}$ stable isotopes analyses

Reference No.	Core No.	Depth (cm)	Type	$\delta^{13}\text{C}$ (‰)	Measured ^{14}C BP	Conventional ^{14}C BP	Calibrate age BP $\pm 2\sigma$	Method	Treatment	Sedimentation rate (mm/y)
Beta-363068	1	16	Organic sediments	-26.8	1150 ± 30	1120 ± 30	1070-960	AMS	acid washes	0.14
Beta- 344058	1	52	Mollusk shell	-2.4	2280 ± 30	2650 ± 30	2360-2290	AMS	acid etch	0.20
Beta- 336902	1	60	Wood	-26.4	6560 ± 40	6540 ± 40	7510-7420	AMS	acid/alkali/acid	0.09
Beta-359581	1	154	Organic sediment	-23.9	13060 ± 50	13080 ± 50	16220-15490	AMS	acid washes	0.12
Beta- 344059	2	60	Mollusk shell	-2.7	2260 ± 30	2630 ± 30	2340-2280	AMS	acid etch	0.23
Beta- 336903	2	66	Wood	-28.2	3240 ± 30	3190 ± 30	3460-3360	AMS	acid/alkali/acid	0.21
Beta- 336904	3	44	Wood	-27.4	6880 ± 30	6840 ± 30	7700-7620	AMS	acid/alkali/acid	0.06

DISCUSSION

5.1 The onshore sedimentary basins

5.1.1 Thermal maturity

The 20S/(20S + 20R) ratio of the C₂₉ 5 α (H), 14 α (H), 17 α (H)-sterane is one of the most reliable maturity indicator due to less dependent on source variability. This ratio indicates the oil generative window from the value of 0.25 (Farrimond et al., 1998) and the equilibrium value of 0.52-0.55 (Waseda and Nishita, 1998; Farhaduzzaman et al., 2012). The 22S/(22S + 22R) ratio in the C₃₁ to C₃₅ 17 α hopanes is also an important maturity indicator. However, the 22S/(22S + 22R) ratios of C₃₁ hopanes are often affected by co-elution of a C₃₀ neohopane generated during biodegradation (Subroto et al., 1991) and release of sulfurized hopanoids from kerogen (Köster et al., 1997). The hopane 22S/(22S + 22R) ratio is more sensitive in lower maturity stage than the sterane 20S/(20S + 20R) ratio, and the hopane ratio has the equilibrium value of about 0.6 (Farrimond et al., 1998; Sawada, 2006; Pan et al., 2008). Figure 5.1 for the cross plots of C₃₁ hopanes 22S/(22S + 22R) ratios (0.46-0.62) to C₂₉ sterane 20S/(20S + 20R) ratios (0.15-0.56) shows good correlation between them ($Y = 0.40X + 0.40$, $r = 0.949$ and $n = 12$). This result indicates that biodegradation and sulfurized hopanoids were low levels. Low content of unresolved complex mixture (UCM) in Figure 4.1 expect for Aruwakkalu Red Earth and very low sulfur contents in Table 4.1 are consistent with the result in Figure 5.1. Aruwakkalu Red Earth with higher UCM (Figure 4.1) has abnormally high ratio of C₃₁ hopanes 22S/(22S + 22R) in Figure 5.1.

Therefore, Figure 5.1 revealed that all Andigama samples are thermally immature and the Tabbowa sediments and Aruwakkalu limestone are moderately matured in the oil generation main stage. It suggests that the Jurassic Tabbowa Basin in the northern part of study area could subside deeper than the Jurassic Andigama Basin in the southern part and/or effects of reworking ancient OM were influenced in the Tabbowa fluvial system.

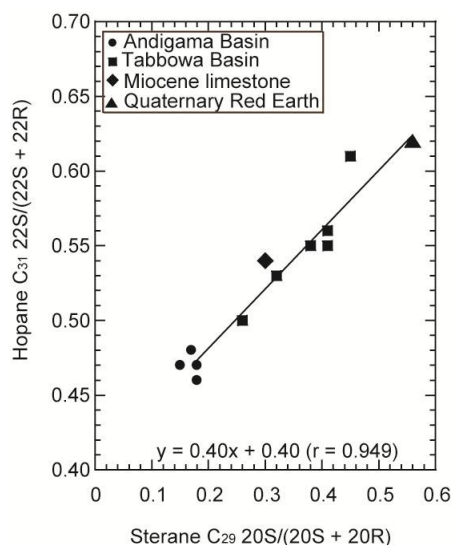


Figure 5.1: Relationship between hopane C₃₁ 22S/(22S + 22R) and sterane C₂₉ 20S/(20S+20R).

5.1.2 Origin of organic matter

The *n*-alkanes are omnipresent in geological samples and are derived from certain biotic sources (Eglinton and Hamilton, 1967; Meyers, 1997; Jeng, 2006). The Andigama samples reveal that mixing of plankton/algae and microorganism (*n*C₁₆-C₁₉) and vascular plants (*n*C₂₀-C₃₅) (Figure 4.1). The Andigama mudstones comprise a large proportion of middle chain length *n*-alkanes (*n*C₂₁-C₂₅). Bog-forming (swamp) vegetations are enhanced by middle chain length homologues (Ficken et al., 2000; Nott et al., 2000; Pancost et al., 2002; Bingham et al., 2010). In addition, TS values are very low (<0.001%) in the Andigama samples. Therefore, in this study, the Andigama mudstones could be sufficiently reflected by the development of freshwater lacustrine to swamp environments. The *n*C₁₆-C₁₉ alkanes are relatively low in the sandy mudstone sample (Figure 4.1(d)) possibly suggesting a lack of preservation in relatively high-energy depositional settings in the shallow basin estimated by the low maturity samples. On the other hand, the steranes in the Andigama samples are enriched in C₂₉ and somewhat depleted in C₂₈ and C₂₇ (Figure 5.2, Table 4.2). The C₂₉ steranes derive primarily from terrestrial higher plants (e.g., Meyers, 1997; Zhu et al., 2012), and C₂₇ and C₂₈ steranes derive from algae in lacustrine and marine environments (Volkman,

2003; Piedad-Sánchez et al., 2004). The relative distributions of C₂₇-C₂₈-C₂₉ steranes (Figure 5.2) indicate that OM in the Andigama sediments originated mainly from influx of land plant material.

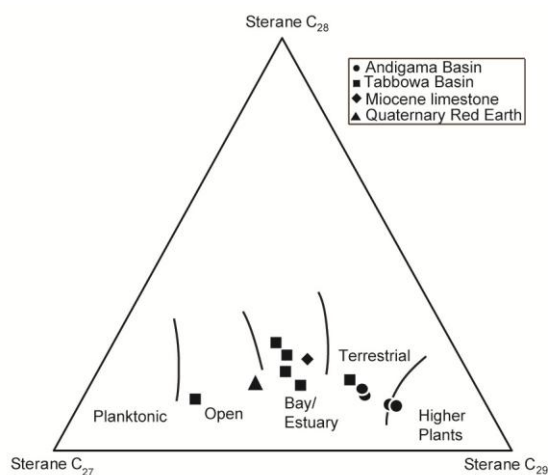


Figure 5.2: Ternary diagram of C₂₇-C₂₈-C₂₉ steranes showing OM sources and depositional environments (Huang and Meinschein, 1979).

These results are also supported by the data of C/N ratio. C/N ratios have been widely investigated to evaluate sources of bulk OM in sediments (Meyers and Ishiwatari, 1993; Meyers, 1997; Sampei and Matsumoto, 2001). Elevated C/N values of the Andigama mudstones (Table 4.1) indicate the large proportions of terrestrial OM. However, abnormally low C/N ratio (2.9) of sandy mudstone (Table 4.1) should be interpreted as the effect of inorganic NH₄⁺ absorbed by the clay (Müller, 1977). According to the effect of inorganic nitrogen, the C/N ratio becomes abnormally low in organic carbon poor sediments (Sampei and Matsumoto, 2001; Hossain et al., 2009).

As for the Tabbowa sandy sediments, *n*-alkanes compositions are dominated by lighter *n*C₁₆-C₂₁ alkanes (Figure 4.1(g-1)). The algae indicator (<C₂₀/*n*C_{all} alkanes) implies that the Tabbowa beds are predominant in algal sources compared to the Andigama beds (Table 4.2). In addition, waxy *n*-alkanes (*n*-C₂₉, *n*-C₃₁, and *n*-C₃₃) of terrestrial OM are significantly deposited and preserved in all stratigraphic units in the Tabbowa profile (Figure 4.1(g-1)). The C₂₇-C₂₈-C₂₉ steranes also show that the Tabbowa sediments are mainly derived from aquatic organism with a significant amount of

terrestrial higher plants (Figures 4.1(g-l) and 5.2). Aruwakkalu limestone and Red Earth are also abundant in planktonic OM. This is not conflict with C/N ratios. The Tabbowa beds and the Miocene limestone record very low C/N values (Table 4.1).

Incidentally, the $Ts/(Ts + Tm)$ ratios [Ts : 17 α (H)-22, 29, 30-trisnorhopane, Tm : 18 α (H)-22, 29, 30-trisnorhopane] and CPI values change according to both maturity and source variation (Waseda and Nishita, 1998; Inaba et al., 2001; Sawada, 2006). Figure 5.3(a) suggests that abundant input of terrestrial OM to shallow Andigama Basin and input of planktonic OM to deep Tabbowa Basin could occur respectively. Abundant low molecular n -alkanes ($<n-C_{20}$: Figure 4.1(g-l)) with a significant higher n -alkanes ($>n-C_{29}$: Figure 4.1(g-l)) and higher CPIs (Figure 5.3(b)) in the Tabbowa Basin suggest that nutrients for the production of planktonic OM could be from land area accompanied by terrestrial OM.

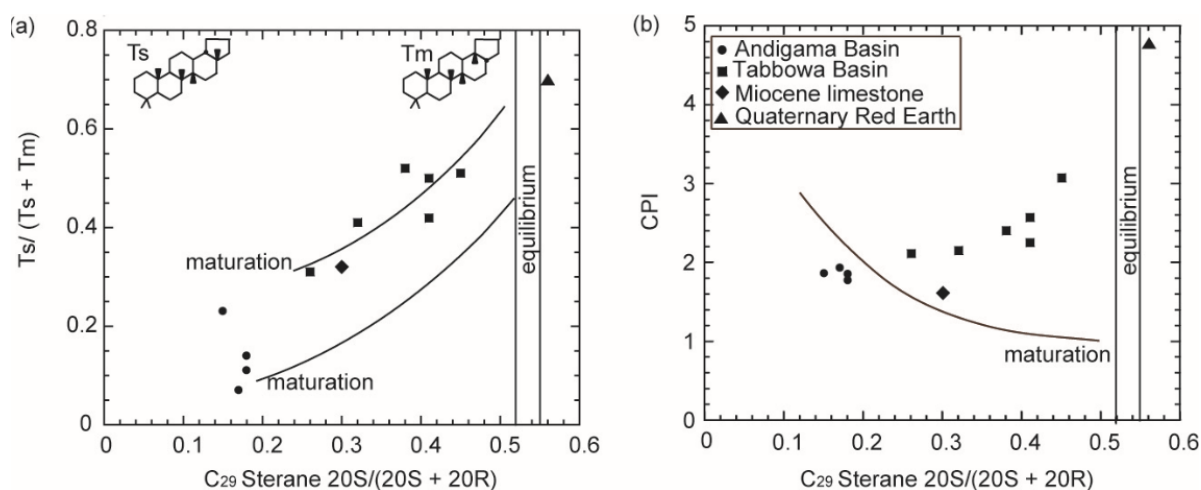


Figure 5.3: (a) $Ts/(Ts + Tm)$ ratio versus $20S/(20S + 20R)$ of C_{29} sterane and (b) CPI versus $20S/(20S + 20R)$ of C_{29} sterane for onshore sediments. Maturation trend lines (a) are from Waseda and Nishita (1998).

In contrast, remote ocean areas and arid terrestrial environments may receive terrestrial OM mainly from aeolian transport (Ratnayake et al., 2005). In this study, the highest CPI (Figure 5.3(b)) and long ACL (average chain length: Jeng, 2006) in the Quaternary Red Earth (Table 4.2) can probably indicate deposition of degraded ancient terrestrial OM under the prominent aeolian process. Specifically, the Red Earth

paleosols at Aruwakkalu indicate intense biodegradation (Figures 4.1(f) and 5.3(a)). As a result, some of the informative features of OM type may be lost.

5.1.3 Depositional environment

The TS are very low (less than the detection limit of <0.001%) even in the OM rich Andigama mudstone (Table 4.1). Low TS may suggest the freshwater or oxic seawater deposition (Berner, 1984; Berner and Raiswell, 1984). The very low TS with high TOC could be interpreted as swamp/lake in the freshwater environment (Berner, 1984). The $C_{27}/(C_{27} + C_{29})$ values of 20R steranes vs. Pr/Ph (pristane/phytane) values (2.1-3.0) of the Andigama sediments indicate that the terrestrial OM was buried under oxic conditions (Figure 5.4).

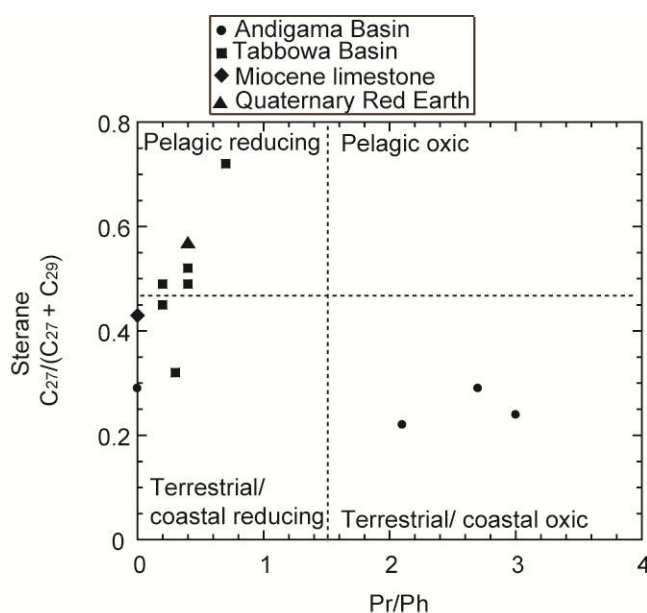


Figure 5.4: Relationship between $C_{27}/(C_{27} + C_{29})$ sterane and Pr/Ph ratio showing OM sources and depositional conditions (Waseda and Nishita, 1998; Sawada, 2006).

The lower Pr/Ph values of the Tabbowa sediments (0.2-0.7, Figure 5.4) may be affected by reducing conditions in algae/photosynthesis bacteria dominant sediments (Haven et al., 1987). Angular to sub-angular granitic sandy grains of the Tabbowa sediments can be reflected in the adjacent moderately low relief upland. The sedimentary facies with sandy grains and very low TS (%) distribution suggest fluvial

freshwater deposition. Climate and depositional environment could influence the nature of the lithic fill in this succession, and similarly in the Jurassic Gondwana sediments of India (Dutta, 2002). The sequential sedimentary developments and correlation to the Indian Gondwana lithofacies (Facies C in Figure 2.1(d)) can probably suggest that warm semi-arid climate over geological time of the Tabbowa succession.

The slightly higher content of UCM in the Tabbowa beds (Figure 4.1(g-l)) is possibly indicative of the relatively higher biodegradation compared to the Andigama samples. The UCM contents of the Aruwakkalu samples (Figure 4.1(e, f)) are appreciably greater than those in the Jurassic sediments, indicating higher activity of bacteria.

5.1.4 PAHs distribution in the Andigama mudstones

The Andigama mudstones are dominated by Ret. Sim and Pery are secondarily/thirdly abundant, and a minor peak of Cad, P, Fla, Py, BaAn, Chry, Bfla, BePy, BaPy, InPy and BghiP occur (Figures 4.3 and 4.4; Table 4.3). Ret is recognized as vascular plants marker represented by gymnosperm conifers (Jiang et al., 1998; Grice et al., 2007; Ei Mon Han et al., 2014). Sim is considered as main precursors of tri-aromatic Ret during diagenetic alteration (Yunker and Macdonald, 2003) and/or combustion of wood materials (Yunker et al., 2011). Therefore, these features imply that Ret and Sim abundances in this basin (Figures 4.3 and 4.4; Table 4.3) were controlled by gymnosperm OM such as conifer resins. In addition, Cad is another vascular plant marker that can be a diagenetic product of the cyclic sesquiterpenoidal hydrocarbons (Otto et al., 2002; Simoneit, 2005) and is detected in both angiosperm and gymnosperm coals for example in the Central Myanmar Basin (Ei Mon Han et al., 2014). However, the first unequivocal worldwide evidences of angiosperm records are from the Early Cretaceous (Friis et al., 2006). Also, oleanane type angiosperms biomarker could not be detected in the analyzed samples suggesting that flowering plants had not yet evolved in the eastern Gondwanaland during the Jurassic (e.g., Aarssen et al., 2000). Therefore, in this study, low abundance of Cad compared to Ret and Sim can also be the indicator for gymnosperm plant resins.

In contrast, Pery can be recognized as third abundance in non-alkylated PAHs from

the Andigama Basin. Previous papers indicated that precursors of Pery can be fungi (Jiang et al., 2000), wood-degrading fungi (Suzuki et al., 2010; Marynowski et al., 2013), terrestrial sources (Stout and Emsbo-Mattingly, 2008) and depositional conditions (Silliman et al., 1998). A diagenetic product of Pery is predominantly observed in humid terrestrial OM rich (peat, coal and swamp) environments (Aizenshtat, 1973; Stout and Emsbo-Mattingly, 2008). Therefore, in this basin, Pery can be derived from wood-degrading fungi under the temperate humid climatic conditions.

The Andigama samples are also composed of a well-established combustion derive PAHs such as Fla, Py, BaAn, Chry + Tpn, Bflas, BePy, BaPy, InPy and BghiP (Figures 4.3 and 4.4). The 5-ring BePy, InPy and BghiP PAHs can probably indicate high-temperature crown fire (O'Malley et al., 1997; Denis et al., 2012). Also, 4-ring Py, BaAn, Chry + Tpn and Bflas can probably indicate medium temperature ground fire (Jiang et al., 1998). According to Scott (2000), smaller living plants such as swamp vegetation, soil humus and peat provide fuel for ground fire, whereas abundant productions of living trees provide fuel for activated wild fire. In the Andigama samples, the 4-ring PAHs are more abundant than the 5-ring ones (Figure 4.4). Therefore, swamp vegetation and peat OM could be more abundant than trees OM in the Andigama Basin. The Tabbowa sediments, the Aruwakkalu limestone and Red Earth sediments did not contain such PAHs.

5.1.5 Alkylated phenanthrenes in the Andigama mudstones

Methylated aromatic isomers have been investigated in term of maturity parameters (Radke and Welte, 1983; Sampei et al., 1994; Chakhmakhchev and Suzuki, 1995), source indicators (Killops, 1991; Budzinski et al., 1995; Hossain et al., 2013) and secondary alteration processes such as biodegradation (Ahmed et al., 1999; Huang et al., 2004) of sedimentary rocks and petroleum. The MP mass fragments are characterized by predominant 1-MP with 9-MP isomers compared to 2-MP and 3-MP isomers (Figure 4.5). 1-MP is originally predominant in terrestrial OM (Type-III kerogen) rich sediments (Budzinski et al., 1995; Maslen et al., 2011) and 9-MP is highly resistant to biodegradation (Ahmed et al., 1999; Huang et al., 2004). Further, Hossain et al. (2013) reported predominant 1-MP and 9-MP possibly originated from coniferous

gymnosperms and pteridophyte plants in the Permian Gondwana coals and coaly shale in Bangladesh. In contrast, 2-MP and 3-MP are paramount in Type-I and Type-II kerogen respectively (Radke et al., 1986). Therefore, in this study, predominant 1MP isomer in the immature Andigama sediments can probably indicate less biodegradable gymnosperm OM.

Abundance of the 1, 7-DMP isomer is remarkably high compared to other DMP isomers (Figure 4.5). The DMP is more resistant to biodegradation than P and the MP isomers (Huang et al., 2004). Armstroff et al. (2006) and Fabiańska et al. (2013) showed that 1, 7-DMP can probably originate from the pimarane type diterpenoids due to decomposition of Ret. Hossain et al. (2013) and Ei Mon Han et al. (2014) reported that 1, 7-DMP possibly originated from gymnosperm resin in Gondwana coal and coaly shale. This is consistent with the paleontological reports that gymnosperms/pteridophytes fossils were observed in the Jurassic mudstone and siltstone beds in Sri Lanka (Cooray, 1984; Edirisooriya and Dharmagunawardhane, 2013).

The relative abundances of 1, 2, 7- + 1, 2, 9-TMP isomers are enhanced compared to the other TMP isomers (Figure 4.5). The $\alpha\beta\beta$ -substituted 1, 3, 6- + 1, 3, 10- + 2, 6, 10-TMP, 1, 2, 7- + 1, 2, 9-TMP and 1, 2, 8-TMP isomers can be identified as terrestrial markers in most of low maturity and less-biodegraded samples (Budzinski et al., 1995). Therefore, in this study, the high amount of 1, 2, 7- + 1, 2, 9-TMP is also consistent with a terrestrial gymnosperm origin.

5.2 The offshore Mannar Basin

5.2.1 Stratigraphy and lithology

5.2.1.1 Sandstones

The lowermost Early Campanian sediments of the Dorado North well consist of thick sandstone (Figure 4.6). These sandstone beds formed under the influence of fluvial activities as increasing river runoff can carry clastics to the structurally higher flank of the basin. Therefore, the Dorado North well may probably indicate somewhat shallower environments in the basin. Interbedded sandstones of the Late Maastrichtian porous volcanogenic sediments of the Barracuda well could represent petroleum reservoir quality lithology.

Sandstones of the Early- to Late Paleocene ranged from poor to moderate sorting and fine- to medium-grained sands. After the Late Paleocene, the relative percentages of sand in the argillaceous marl/ marlstone are remarkably low, suggesting that poor reservoir quality lithology (Figures 4.6 and 4.7 (a, c, d)).

5.2.1.2 Interbedded red mudstones

The depth and extend of the red color thin mudstone layers cannot be precisely determined using the cutting samples (Table 4.4 and Figure 4.6). However, biostratigraphic and sedimentological studies of the Upper Cretaceous oceanic red beds have been widely reported in paleoceanographic reconstructions elsewhere (e.g., Hu et al., 2005; Wang et al., 2011). Amorphous organic matter poor red color mudstones appear to be diagnostic of oxic pelagic sediments (Figure 4.7(b)). Therefore, red mudstone of the basin can probably represent (1) intercalation of little productive marine sediments under oxic conditions in the aftermath of organic-rich mudstones, or (2) reworked continental red beds by erosion and transportation to marine environments. Hu et al. (2005) observed that at least hemi-global distribution of oceanic red mudstones are predominant of the Cretaceous, although some are as younger as Early Cenozoic.

5.2.1.3 Black mudstones

The uppermost Early Campanian black mudstones of the both wells (in different thickness) show deposition of organic rich sediments during the rift transition stage of the basin (Figure 4.6). The predominant thicknesses in the Barracuda well reveal that deeper part of the basin was subjected to low-energy reducing condition, whereas the structural higher flank of the basin (the Dorado North well) was subjected to high-energy conditions during the Late Cretaceous (Table 4.4). This depositional trend can be observed up to Late Paleocene sedimentary succession of the basin. According to optical data, the relatively high intensity of the mixed amorphous organic matter indicates preservation of planktonic remains and plant resins under the reducing environments (Figure 4.7(e)). Also, black fine-scaled laminations (ca. 1-5 mm in thick gray/ black color banding) are dominant in typical form the Late Paleocene sedimentary

sequences of the both wells (Table 4.4 and Figure 4.7(a, d)). These laminations can probably represent cyclic changes in supplies of OM under oxygen-poor to anoxic conditions (e.g., Valdés et al., 2004). The Middle Oligocene to Middle Miocene sediments sometimes contain black carbon particles about 0.1-0.3 mm in diameter, possibly suggesting seasonal forest/ terrestrial fire events of the watershed area (e.g., Jia et al., 2003; Harris, 2006). Also, lithostratigraphic interpretations of the two wells indicate somewhat discontinuous and changeable depositional sequences across the basin.

5.2.1.4 Volcanogenic sediments

The Barracuda well penetrated thick volcanogenic fine tuffaceous sediments, suggesting the several periods of volcanism during the Late Maastrichtian due to the breakup of Madagascar/ Seychelles from India (Storey et al., 1995; Torsvik et al., 1998). In this marine basin, mafic to intermediate low viscosity lava could probably spread in a wider area. Also Keller et al. (2008) and Tantawy et al. (2009) described the effects of the Late Maastrichtian volcanism of the Indian Ocean, at Ninetyeast Ridge Deep Sea Drilling Project Sites 216 and 217, Wharton Basin Site 212 and Krishna-Godavari Basin. Activated local tectonics sometimes could be accompanied by volcanic activities of the area. Vonhof and Smit (1997) data suggest that a rapid outflow of more than 1×10^6 km³ of basaltic lava of the Indian region. Also, thermal history of the area indicates that significant heat flows during the Late Cretaceous to underlie Early Cretaceous synrift sediments.

5.2.1.5 Calcareous mudstone-argillaceous marlstone boundary

Calcareous mudstone probably indicates deposition of calcite by coccolithophores and foraminifera in the marine (Ridgwell and Zeebe, 2005). In contrast, tectonic movement, Cenozoic orogeny and development of shallow marine carbonate platform over the Asian paleo-oceanic basins have been widely discussed (e.g., France-Lanord and Derry, 1997; Zachos et al., 2001). The Mannar Basin is characterized by development of marlstone from the Late Paleocene and also this facies change probably correlated with the onshore Tertiary limestone beds of Sri Lanka (Figure 2.1). Further,

development of the carbonate platform is primarily related to movement of Indian Plate into warmer northern latitudes. However, increment of carbonate accumulation can be caused by weathering of broad uplifted regional mountain plateau (France-Lanord and Derry, 1997; Zachos et al., 2001). Based on the burial history model as discussed below, the Mannar Basin underwent continuous subsidence and Eocene to Miocene argillaceous marl/ marlstone can probably deposit under deepwater marine conditions.

5.2.1.6 Turbidites

The Paleocene sediments of the Dorado North well consist of mainly arenaceous sediments compared to the Barracuda well (Figure 4.6). The Paleocene mudstone and interbedded sandstone can probably represent increased clastics from land and development of deepwater turbidites systems due to sea-level changes or sediment gravity flows. The adjacent Cauvery Basin suggests regional uplift, which changes the depositional environments from upper bathyal and neritic conditions in the Late Cretaceous to sub-littoral and sub-areal conditions in the Paleocene (Shaw, 2002). The Paleocene to Early Eocene sediments of the shallow water Mannar Basin contained abundant of foraminifers such as *Subbotina triloculinoides*, *S. wilcoxensis*, *Planorotalites compressa*, *Morozovella aragonensis*, *M. formosa* and *Acarinina pentacamerata*, suggesting the upper to lower bathyal conditions (Rao et al., 2010).

5.2.2 History of sedimentation rates

The history of sedimentation rates were evaluated using the present mudstone thicknesses of the sedimentary columns (Figure 4.8). Sedimentation rates in term of mud components respond to major controlling factors in paleogeography (tectonics), paleoceanography and paleoclimate.

Mud sedimentation rates of the Dorado North well during the Campanian, Maastrichtian and Paleocene are 8 m/Ma, 22 m/Ma and 9 m/Ma, and the Barracuda well recorded values are 18 m/Ma, 49 m/Ma and 27 m/Ma, respectively (Figure 4.8). Sand dominant facies over the structurally higher flank (the Dorado North well) of the basin reflected the prominent fluvial influence during the Campanian to Paleocene. In this period, mud dominant facies over the structurally lower flank (the Barracuda well) of

the basin reflected the prominent marine influence (Figure 4.6). However, igneous activities may have caused significantly to increase the Maastrichtian sedimentation rate in the Barracuda well mainly be due to location in close to igneous source in the region (Figure 4.8). Also, rapid subsidence can act as an acceleration proxy for sinks of sediments in the Barracuda well during the Maastrichtian. Further, overall accumulation rates show somewhat a bell curve distribution from the Campanian to Paleocene (Figure 4.8).

Sedimentation rates were lowest in the Eocene (13 m/Ma) during timing of the collision between Indian and Asian plates. The Barracuda well recorded relatively higher sedimentation rates than the Dorado North well throughout the whole sedimentary succession except for the Eocene (Figure 4.8). Similarly, the lowest sedimentation rates over the basins of the Indian subcontinent were recorded during the Eocene due to the collision between Indian and Asian plates (ca. 50 Ma) and/ or weak ocean circulation (Davies et al., 1995; Goldner et al., 2014).

Sedimentation rates increased during the Oligocene (average = 27 m/Ma) and Miocene (average = 26 m/Ma). These changes can be probably correlated with accumulation of weathered soils and sediments from uplifted mountain and/ or changes of oceanic circulation/ upwelling of the region (Davies et al., 1995; Métiévier et al., 1999; Goldner et al., 2014). In contrast, Rao et al. (2010) identified hiatuses and/ or erosional unconformities using biostratigraphic studies in the shallow water Mannar Basin. The major boundaries were recorded close to Early Eocene, Middle Eocene, Late Eocene, Early Oligocene and Middle Miocene. Consequently, real mass accumulation rates may be somewhat higher than the calculated values of the Oligocene and Miocene (Figure 4.8). Similarly, rising of clastic/ terrestrial sedimentation rates of surrounding basins probably started from the Oligocene (Métiévier et al., 1999) or Neogene (Davies et al., 1995; Harris, 2006).

In summary, however, all epoch sediments from the Santonian to Miocene are recognized in the exploration wells, and changing patterns in sedimentation rates with age are similar in the both wells. Therefore, in this study, influence of unconformity/ hiatus can be negligible for general discussion in the sedimentation rates for the rifted basin. Mud sedimentation rate is about double in the Barracuda well than in the Dorado

North well during the Campanian to Paleocene (Figure 4.8). However, mud accumulation is approximately equal both in the Barracuda and the Dorado North wells during the Eocene (14 m/Ma and 12 m/Ma), Oligocene (25 m/Ma and 29 m/Ma) and Miocene (25 m/Ma and 27 m/Ma), respectively. It suggests that mud sedimentation rates of the Dorado North well show considerable accretion from the Eocene (Figure 4.8). Sedimentary facies as described above and sedimentation rates seem to change apparently from the Eocene. These shifts have been interpreted as a sign of climatic change and continuous subsidence of the basin as shown in standard burial history model (Figure 4.10). Ali and Aitchison (2008) and Chatterjee et al. (2013) suggest that Sri Lanka and Southern India was subjected to an arid climate during the Late Cretaceous and Paleocene whereas; the Eocene recorded tropical conditions. The enhanced source weathering under a warm and humid climate in tropical marine basins may have been sensitive to argillaceous sediments, burial of organic matter and to consume of atmospheric CO₂ (France-Lanord and Derry, 1997; Ridgwell and Zeebe, 2005).

5.2.3 Burial history

The different types of sedimentary basins have varying tectonic subsidence and uplift curves. Rift-type basins tend to have concave-up curve with the subsidence fast early on/after rifting and then slow later on (Watts et al., 1982; Watts and Thorne, 1984). The burial history curve of standard tectonic subsidence always records the lowest value in subsidence of any sedimentary basins (Figure 4.10). In this study, thicknesses of erosional unconformities and/ or hiatuses cannot be estimated using only sedimentary facies. However, the influence of uplifted height and an eroded thickness could be small as discussed above on sedimentation rates. The positions of minor hiatus were correlated as stated above based on mainly the previous interpretations (e.g., Rao, 2001; Shaw, 2002; Rao et al., 2010).

In this burial model, concave-up curve represents rapid tectonic subsidence at the rift transition stage from the Late Cretaceous (average = 41 m/Ma) to Paleocene (average = 25 m/Ma). In particular, the rifting and drifting of Madagascar/ Seychelles from India may cause drastically to increase the Late Cretaceous subsidence rates of the

Barracuda well. Also, model reveals that tectonic subsidence rate is more prominent in the deeper part (the Barracuda well) of the basin (Figure 4.9). This rapid subsidence gradually decreased during the Eocene (average = 16 m/Ma) probably due to collision between Indian and Asian plates. The average subsidence rates of Oligocene and Miocene are 17 and 19 m/Ma, respectively (Figure 4.9). Therefore, the changes in subsidence rates from Eocene to Miocene can be reflected a passive margin deposition. In contrast, tectonic subsidence curves of the adjacent Cauvery Basin show similarity to our interpretation (Chari et al., 1995). However, detail models of thermal history and timing of petroleum/ natural gas generation based on data of biomarker and vitrinite reflectance will be published elsewhere.

5.2.4 Sedimentary organic matter

5.2.4.1 Variations of carbonate deposition

The both core samples of the Mannar Basin recorded carbonate accumulation throughout the whole sedimentary succession (Figure 4.11). The accumulation and preservation of carbonate particles in marine sediments are controlled by number of factors mainly precipitation of calcite by coccolithophores/ foraminifera and results in higher $p\text{CO}_2$ at the surface, and weathering of carbonate and silicate rocks (e.g., Berner et al., 1983; Arthur et al., 1985; Volk, 1989; Ridgwell and Zeebe, 2005). In this study, carbonate content rich (approximately $\text{CaCO}_3 > 15\%$) strata were recorded from the Early Campanian to Late Maastrichtian sections in the Dorado North (from 3010 m to 3300 m, $\text{CaCO}_3 = 24.72\% \pm 9.39$) and the Barracuda (from 4270 m to 4741 m, $\text{CaCO}_3 = 32.50\% \pm 9.42$) wells (Figure 4.11). Consequently, the Late Cretaceous carbonate accumulation can be probably coincident with the effects of taxonomic diversification of calcareous plankton and precipitation of CaCO_3 under high $p\text{CO}_2$ (ca. 2500 ppm) level (Boss and Wilkinson, 1991; Kent and Muttoni, 2008). The higher CaCO_3 deposition in the deeper part of the basin can indicate minor effect of reworking calcareous rocks from terrestrial landmass. Changes of oceanic chemistry may cause to reduce carbonate deposition during the end of the Late Maastrichtian (Figure 4.11).

The K-Pg mass extinction event is characterized by sharp reduction of carbonate productivity for several hundred years (Caldeira and Rampino, 1993). It is difficult to

identify exact K-Pg mass extinction event in part due to lowering sample resolution, rock sloughing from above, or may be due to lost circulation and pulverization. The reductions of carbonate accumulation in both wells may indicate alteration of the open-ocean ecosystem during the Late Maastrichtian. This period is characterized by extinction of about 85% of plankton foraminifera and calcareous nannofossils in marine ecosystem (Zachos et al., 1989; D'Hondt et al., 1998). The reduction of carbonate accumulation along with TOC cannot be interpreted to increase rate of dissolution due to acidification of the ocean. Therefore, it may have resulted from a decrease in aquatic productivity and minor effects of reduction of erosional continental landmass. Keller et al. (2008) and Tantawy et al. (2009) described the characterization of biotic stress and/or major contributor to the mass extinction of planktonic foraminifera and calcareous nannofossils are regionally controlled by the Late Maastrichtian volcanism of the Indian Ocean, at Ninetyeast Ridge DSDP Sites 216 and 217, Wharton Basin Site 212 and Krishna-Godavari Basin.

The carbonate deposition is relatively low in the Dorado North (average = 9.89 ± 4.80) and Barracuda (average = 11.13 ± 6.14) wells during the Early Paleocene to Late Paleocene sediments. After the Late Paleocene, carbonate depositions were drastically increased in the both wells. The development of CaCO_3 platform from the Late Paleocene (close to the Paleocene-Eocene boundary) is primarily related to transition from arid climate into warm and humid tropical climate (movement of Indian plate into northwards warmer latitudes). In contrast, many researchers identified the Paleocene-Eocene boundary as a period of dissolution of carbonate in marine sediments deposited below several thousand meter water depth due to alter oceanic chemistry, principally by lowering the pH of seawater (Bains et al., 1999; Zachos et al., 2005; 2008). However, north east part of the Mannar Basin may not be undergone such a drastically dissolution process during the Late Paleocene-Eocene boundary.

Weathering of rocks has been said to be the main cause of the increments of carbonate platform during the Late Cenozoic sediments in and around Indian plate (France-Lanord and Derry, 1997; Métévier et al., 1999; Zachos et al., 2001). The carbonate accumulation is more prominent (approximately $\text{CaCO}_3 > 25\%$) in the deeper Barracuda well (from 2139 to 3060 m, average = $40.2\% \pm 12.1$) compared to the

shallower Dorado North well (from 2205 m to 2580 m, average = 29.3% \pm 11.4). The structural higher flank of the basin (the Dorado North) could be identified as more sensitive to terrestrial climatic changes of Sri Lankan landmass. However, the Barracuda well could be more sensitive to regional marine changes and climatic changes of Indian landmass. Consequently, increased chemical weathering rates of uplifted the rocks (e.g., Eastern Ghats) have been suggested as a cause for the increment of carbonate content in deeper part of the basin. Development of Asian monsoon (e.g., northeast monsoon) may have been caused by strengthened carbonate accumulation in the basin may be due to combined rapid physical denudation with chemical weathering. Therefore, CaCO₃ deposition in this basin correlate with Cenozoic global cooling and the initiation of the Antarctic ice sheets in the present glaciated Earth.

5.2.4.2 Variations of organic matter delivery

TOC contents are relatively low in the lower most Early Campanian sediments of the Dorado North well (from 3320 to 3580 m, average = 0.45 \pm 0.22) and the Early-Late Campanian sediments of the Barracuda well (from 4540 to 4741 m, average = 0.97 \pm 0.23) (Figure 4.12). In this section, the Dorado North well consists of sand dominant sediments in turbidities (Figure 4.6). Therefore, TOC variation can probably indicate effects of physical properties of sediments. The Early Campanian to Late Maastrichtian sediments (3060-3320 m) of the Dorado North (average = 1.64 \pm 0.57) and the Late Campanian to Late Maastrichtian sediments (4270-4540 m) of the Barracuda (average = 1.34 \pm 0.36) sequences are considered to be OM rich beds of the basin. The Late Cretaceous organic carbon accumulation somewhat correlate with carbonate deposition in this basin. However, in this study, higher carbonate deposition was recorded in the Barracuda well compared to the Dorado North well (Figure 4.11). The prominent organic carbon rich beds of the Dorado North well may probably indicate accumulation of terrestrial OM affecting the drainage of the watershed area as discussed in below section. Therefore, the Late Cretaceous OM rich beds can probably indicate significant tectonic event of the region during rift-transition stage of the basin.

TOC values are generally low in the lower Paleocene sediments of the Mannar Basin (Figure 4.12). In this sequence, the Dorado North well (2580-3010 m) recorded

lower TOC values (average = 0.44 ± 0.17) compared to the Barracuda well (3060-3440 m, average = 1.07 ± 0.39). Facies analysis reveals that Barracuda well consists of less amount of arenaceous sediments compared to the Dorado North well. Consequently, the higher TOC values in the deeper Barracuda well can probably indicate physical properties of sediments and/ or regional characteristics of oceanic currents.

Although carbonate accumulation is significantly developed in the Eocene and Oligocene passive margin sediments, organic carbon accumulation is relatively low in the both wells. The lower TOC values recorded from the Late Paleocene to the Late Eocene sediments (2205-2580 m) in the shallower Dorado North well (average = 0.56 ± 0.21) compared to the Late Paleocene to the Early-Middle Oligocene sediments (2520-3060 m) in the deeper Barracuda well (average = 0.74 ± 0.41). The lower amount of organic carbon accumulation can probably associate with a weaker Asian monsoon precipitation of the watershed area.

However, TOC content gradually increased from the Middle Oligocene sediments in the Barracuda well. Sedimentary facies analysis reveals that OM rich Middle Oligocene to Miocene bed consists of black carbon and laminations, suggesting seasonal events of the watershed area. The Middle Oligocene to Miocene (ca. 380 m thick) sedimentary sequence indicates a significant amount of OMs preservation (average = 2.51 ± 1.20). Organic carbon burial in the Mannar Basin shows that regional climatic changes could be started from the Middle Oligocene. The present relief and configuration of the south Asia has approximately began in the Oligocene followed by large-scale vertical motion (Molnar and Tapponnier, 1975). Consequently, Asian monsoon systems can probably develop from the Middle Oligocene in this region. The rising of clastic sedimentation rates of surrounding basins probably started from the Oligocene (Métiver et al., 1999) or Neogene (Davies et al., 1995). However, some researchers expected it to start at the onset of the India-Asia collision due to maintain significant topography prior to the collision (Murphy et al., 1997) that is not consistence and reliable with the Mannar Basin due to long distance from river mouths of the Ganges-Brahmaputra Rivers.

5.2.4.3 Variations of organic matter type delivery

C/N ratios reveal that algae have dominated OM input to the lower most Early Campanian sediments in the Dorado North well (average = 9.02 ± 4.81). However, Early-Late Campanian sediments in the Barracuda well indicate algae and terrestrial OMs mixed sources (average = 15.13 ± 4.68). The m/z 57 mass chromatograms of the Early-Late Campanian sediments in the Barracuda well consist of n -C₁₉ dominant bimodal peaks maximizing around n -C₂₂/ n -C₂₃ and n -C₃₁ (Figure 4.15 (a)). Middle chain length (n -C₂₃, and n -C₂₅) n -alkane homologues are enhanced by bog-forming (swamp) vegetations (Ficken et al., 2000; Nott et al., 2000; Pancost et al., 2002; Bingham et al., 2010). Also, abundance of n -C₃₁ indicates the occurrence of grasses (graminoids), floating plants, and shrub type herbaceous vegetation (non-woody) in swamps (Zhou et al., 2005; Castañeda et al., 2009; Zheng et al., 2011). Therefore, terrestrial swamp OMs are relatively predominant in the Barracuda well (average C₂₀-C₂₆/ n -C_{all} = 0.67 ± 0.08) may be due regional characteristic of the oceanic currents (Figure 4.12).

The C/N ratios of organic carbon rich the Early Campanian to Late Maastrichtian sediments (3060-3320 m) of the Dorado North (average = 27.13 ± 12.44) and the Late Campanian to Late Maastrichtian sediments (4270-4540 m) of the Barracuda (average = 20.36 ± 7.64) wells can probably indicate accumulation of terrestrial OM from higher plants suggesting that gas prone Type-III/II kerogen. The n -alkane compositions of these samples indicate a significant amount of middle-chain (n -C₂₁ to n -C₂₅) and long-chain (n -C₂₇ to n -C₃₁) wax probably from coastal swamp and terrestrial vascular plants (Figure 4.15 (b)). TOC (%) increment along with C/N ratio can probably accompany with regional subsidence and erosion of continental land mass and a sudden influx of coastal terrigenous sediments into the Mannar Basin. Also, it is followed by increment of $>n$ -C₂₆/ n -C_{all} (average = 0.17 ± 0.04), ACL (average = 26.47 ± 1.14), and sterane C₂₉/ $(C_{27} + C_{28} + C_{29})$ (average = 0.37 ± 0.10) compared to lower Campanian sedimentary sequences ($>n$ -C₂₆/ n -C_{all} average = 0.14 ± 0.06 , ACL average = 25.80 ± 0.73 , and sterane C₂₉/ $(C_{27} + C_{28} + C_{29})$ average = 0.23 ± 0.05) in the Barracuda well. Our results reveal that terrestrial OMs are prominently received from Sri Lankan landmass during the Late Cretaceous. Similarly, the Late Cretaceous subsidence and accompany erosion was apparently greater in the adjacent Cauvery Basin (Shaw, 2002). The volcanogenic

sediments of the Barracuda well indicate deposition of a significant amount of terrestrial OMs (16.64 ± 6.70) probably from surrounding coastal environments (Figure 4.15 (c)). However, terrestrial OM rich beds could end up with microorganism rich organic source materials (Figure 4.15 (d)), suggesting that a significant amount of plankton foraminifera and calcareous nannofossils extinction followed by Late Maastrichtian volcanisms or contamination of drilling mud and oil.

The Paleocene sequence of the Dorado North well (2580-3010 m, average C/N = 6.94 ± 3.05) contains algae dominated OM whereas, the Barracuda (3060-3440 m, average C/N = 15.75 ± 3.19) contains algae and terrestrial mixed OMs. Also, the Late Paleocene sediments of the Barracuda well were characterized by intensifying middle chain length n -C₂₃ n -alkane peak with a significant amount of high molecular weight ($>n$ -C₂₆) n -alkanes from surrounding coastal landmasses (Figure 4.15 (e)). Spatial changes in distribution of terrestrial OM type and physical properties of sediments may cause to increase organic carbon burial in the deeper Barracuda well as discussed in above section (Figure 4.12).

Algae dominated OMs were recorded in argillaceous marl/ marlstone sediments from the Late Paleocene to Late Eocene section in the Dorado North well (2205-2580 m, average = 9.24 ± 4.84). Similarly, the Late Paleocene to the Early-Middle Oligocene argillaceous marl/ marlstone sediments (2520-3060 m) of the Barracuda well indicate algae OM with some terrestrial contribution (average = 13.78 ± 10.0). However, n -alkanes distributions in the Barracuda well indicate a significant amount of higher plant (n -C₂₀ <) wax (Figure 4.15 (f)) from terrestrial sediments (C_{20} - C_{26}/nC_{all} average = 0.75 ± 0.15 , $>n$ -C₂₆/ n -C_{all} average = 0.25 ± 0.15 , ACL average = 26.00 ± 1.28 , and sterane C₂₉/ (C₂₇ + C₂₈ + C₂₉ average = 0.37 ± 0.07). This inconsistency pattern can probably indicate misleading of C/N ratio due to absorption of inorganic nitrogen in marine sediments.

In this study, a considerable amount of samples recorded abnormally low C/N ratio (<4) may be due to absorption of inorganic nitrogen (NH₄⁺) by clay (Müller, 1977; Sampei and Matsumoto, 2001). The inorganic nitrogen absorption was more prominent in the Early Campanian, the Early Paleocene and the Eocene sediments of the Dorado North well, the Middle Eocene to Early Oligocene sediments in the Barracuda well

(Figure 4.12). Also, TN (%) values drastically increased without TOC (%) increments in the Early Campanian sediments of the Dorado North well and the Middle Eocene to Early Oligocene sediments in the Barracuda well (Figure 4.12). Therefore, it can clearly indicate inorganic nitrogen enrichment rather than nutrient enhancement of the basin. In this study, abnormally low C/N values (<4) were removed to calculate average and standard deviations of each strata.

In contrast, terrestrial OM distribution significantly increased from the Middle Oligocene to Early Miocene (2139-2520 m) sedimentary succession of the Barracuda well (average = 23.45 ± 15.02). Also, m/z 57 mass chromatograms clearly indicate higher plant wax ($n\text{-C}_{20}$ <) dominant n -alkanes in the Early-Middle Miocene sediments (Figure 4.15 (g)). In later, the Early-Middle Miocene sediments in the Barracuda well consist of a significant amount of long-chain n -alkanes ($> n\text{-C}_{26}$) suggesting that deposition of relatively long distance transported ancient OMs (Figure 4.15 (h)). Consequently, our results can be somewhat agreed with previous interpretations of changes of atmospheric mass and energy patterns since Early-Middle Miocene series elsewhere (e.g., Quade et al., 1989; Dettman et al., 2001; Zhisheng et al., 2001; Guo et al., 2002; Clift et al., 2002; Jia et al., 2003; Gupta et al., 2004; Harris, 2006).

5.2.4.4 Depositional environments

C/S ratios reveal that the lower most Early Campanian samples probably represent oxygen poor condition with cyclic freshwater influence in the Dorado North (average = 5.81 ± 3.88) and Barracuda (average = 6.38 ± 4.93) wells. However, similar sequence of the deeper Barracuda well indicates relatively oxygen rich condition compared to the shallower Dorado North well may be due to strong oceanic currents or effects of the OM type as discussed below. C/S ratios of organic carbon rich the Early Campanian to Late Maastrichtian sediments (3060-3320 m) of the Dorado North (average = 10.80 ± 7.76) and the Late Campanian to Late Maastrichtian sediments (4270-4540 m) of the Barracuda (average = 9.15 ± 3.22) wells can probably experience marine dominated environment, with a cyclic fresh water input. The relatively higher C/S ratios compared to the lower section may indicate a lower activity of sulfate reducing bacteria in terrestrial OM rich sediments (e.g., Berner, 1984; Gong and Hollander, 1997; Sampei et

al., 1997). In this sequence, the Barracuda and the Dorado North sediments can probably represent bathyal to upper bathyal and upper bathyal respectively.

The Early-Late Paleocene values, ranging from ca. 10 to less than 100, show a wide cyclic fluctuation, implying an oxic environment with a cyclic freshwater influence may be due to significant regional uplift, and physical properties (sand dominant) of sediments. Similarly, biostratigraphic evidence of the adjacent Cauvery Basin experienced significant regional uplift during the Paleocene, indicating that a changes from upper bathyal and neritic in the Late Cretaceous to sub-littoral and sub-areal depositional conditions in the Paleocene (Shaw, 2002). In detail, wide variations in C/S ratios of the Paleocene sequence of the Dorado North (2580-3010 m, average = 32.07 ± 20.21) and the Barracuda (3060-3440 m, average 16.21 ± 20.14) wells can probably indicate sporadic mixing of freshwater and marine influx. However, in this section, the deeper Barracuda well may vulnerable to develop relatively oxygen-poor environment. The Barracuda and the Dorado North wells can probably represent upper bathyal and upper bathyal to neritic (?) depositional settings, respectively. Consequently, depositional changes in the Early-Late Paleocene sequence can be probably accompanied with relative sea-level regressions since that time.

However, C/S ratios are low from the Late Paleocene to Late Eocene sediments of the Dorado North well (2205-2580 m, average = 1.97 ± 1.13) and the Late Paleocene to the Early-Middle Oligocene sediments of the Barracuda well (2520-3060 m, average = 6.83 ± 12.24) implying marine environment in the bathyal setting. The developments of lamination (alternative dark and light color) generally represent cyclic changes in supplies of sediments under anoxic conditions (Gong and Hollander, 1997; Meyers, 2003; Valdés et al., 2004). However, relatively higher C/S ratios in this section can be interpreted probably due to (1) relatively strong regional oceanic currents (open marine condition) in the deeper part of the basin and/or (2) effects of OM types. C/S ratios of the OM rich Middle Oligocene to Early Miocene sediments of the Barracuda well (average = 5.98 ± 4.96) probably represent marine setting influenced by periodic freshwater inundation. In this study, pristane and phytane concentrations were low in the most of samples to allow calculation of reducing conditions in sediments.

5.2.5 Thermal maturity

5.2.5.1 Sterane distribution

The vertical distribution of sterane C_{29} 20S/ (20S + 20R) in the Dorado North and Barracuda wells are summarized in Figure 5.5. The C_{29} 5 α (H), 14 α (H), 17 α (H)-sterane epimers can be identified as consistent maturity indicator due to less depend on OM type (Farrimond et al., 1998; Waseda and Nishita, 1998; Farhaduzzaman et al., 2012). The lower most Early Campanian sediments of the Dorado North well (from 3320 to 3580 m, average = 0.25 ± 0.08) show relatively lower maturity compared to the Early-Late Campanian sediments of the Barracuda well (from 4540 to 4741 m, average = 0.48 ± 0.06) (Figure 5.5). Similarly, the Early Campanian to Late Maastrichtian OM rich sediments (3060-3320 m) of the Dorado North (average = 0.24 ± 0.05) indicate relatively lower maturity compared to the Late Campanian to Late Maastrichtian sediments (4270-4540 m) of the Barracuda (average = 0.39 ± 0.12). Therefore, higher maturity was observed in the deeper part of the basin (the Barracuda well) during the Late Cretaceous (Figure 5.5). Also, the calculated values of 0.54-0.56 in the Barracuda samples (3850-3860 m, 4310-4320 m, and 4730-4741 m) fall within equilibrium range of thermal maturity for oil/gas generation. The Mannar Basin records both intrusive and extrusive igneous rocks, whereas a prominent extrusive volcanic layer exists at the top of the Late Cretaceous horizon of the Barracuda well (Figure 4.6). The pre-flood volcanic and post-flood volcanic sequences were not affected by in a narrow margin (in the Dorado North well) of the eastern boundary of the basin. In this study, sterane C_{29} 20S/ (20S + 20R) and C_{31} hopane 22S/ (22S + 22R) values (See section 5.2.5.2) are not drastically increased (average = 0.38 ± 0.07) in the volcanogenic sediments of the Barracuda well. Consequently, the igneous activity can cause to increase maturity partially in the Late Cretaceous sediments of the Barracuda well.

Thermal maturity are relatively low in this the lower Paleocene sediments (average = 0.35 ± 0.08), Early-Middle Oligocene (average = 0.33 ± 0.16) and Middle Oligocene to Miocene (average = 0.33 ± 0.05) sediments of the Barracuda well (Figure 5.5). Also, the increment of maturity with depth in the Barracuda well can indicate normal diagenetic evolution. However, in the Dorado North well, maturity values are apparently high in the Paleocene (average = 0.36 ± 0.04) and Eocene (average = $0.37 \pm$

0.12) sediments compared to the Late Cretaceous sediments (Figure 5.5). Anomalous variations can probably indicate deposition of recycled OM_s from Sri Lankan landmass after the collision of Asian-Indian plates during the Eocene.

5.2.5.2 Hopane distribution

The C₃₁ to C₃₅ hopane 22S/(22S + 22R) ratio can be identified as another maturity indicator under the lower maturity stage (Farrimond et al., 1998; Sawada, 2006; Pan et al., 2008). However, hopane distributions highly depend on the OM type (Waseda and Nishita, 1998; Pan et al., 2008). The lower most Early Campanian sediments of the Dorado North well (from 3320 to 3580 m, average = 0.58 ± 0.06) indicate relatively higher maturity compared to the Early-Late Campanian sediments of the Barracuda well (from 4540 to 4741 m, average = 0.52 ± 0.07) (Figure 5.5). However, this trend is opposed to the sterane distribution in this sequence may be due to effects of OM type. The Early Campanian to Late Maastrichtian terrestrial OM rich sediments (3060-3320 m) of the Dorado North (average = 0.50 ± 0.05) indicate relatively lower maturity compared to the Late Campanian to Late Maastrichtian sediments (4270-4540 m) of the Barracuda (average = 0.53 ± 0.04). The variation of C₃₁ hopanes 22S/(22S + 22R) ratios are consistent with the C₂₉ sterane 20S/(20S + 20R) distribution in this sedimentary succession.

Hopane isomers show relatively high values in the lower Paleocene sediments of the Dorado North well (average = 0.53 ± 0.04) compared to the Barracuda well (average = 0.49 ± 0.04). It can probably indicate deposition of reworking OM_s in turbidities sediments in the Dorado North well (Figure 4.6). The deeper Barracuda well consists of relatively higher maturity in the Late Paleocene to Early-Middle Oligocene sediments (average = 0.48 ± 0.08) compared to the shallower the Late Paleocene to Late Eocene sediments (average = 0.43 ± 0.07) of the Dorado North well (Figure 5.5). Therefore, hopane accuracy is diminished in the Dorado North well where the OM has been reworked by erosion in different sedimentary sequences.

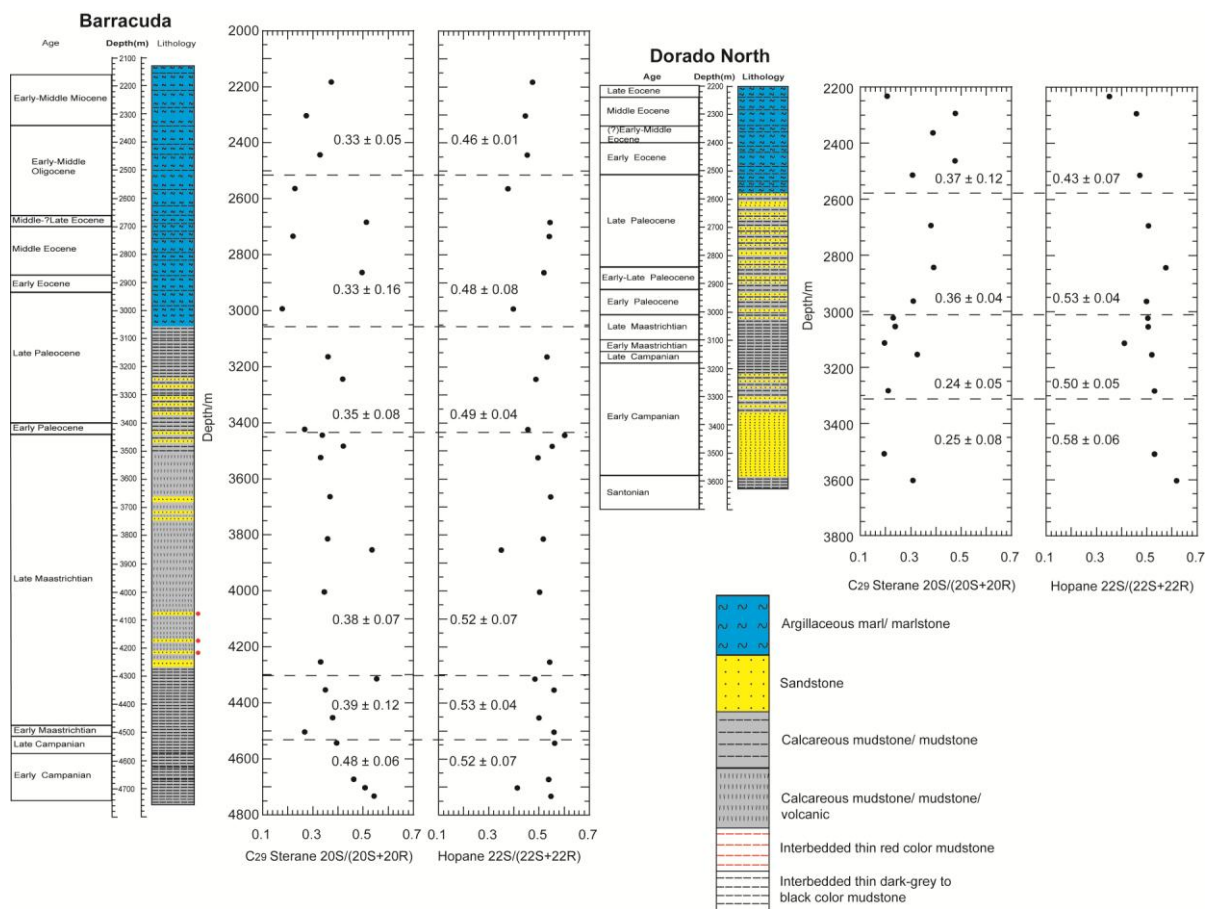


Figure 5.5: Vertical distributions of hopane $C_{31} 22S/(22S + 22R)$ and sterane $C_{29} 20S/(20S + 20R)$ ratios in the Dorado North and Barracuda wells

5.2.5.3 Prediction of paleogeothermal regime

The author considered measured maturity (biomarker) values, estimated model parameters and tectonic evolution in order to discuss average characteristics of paleothermal history in this frontier exploration basin. In particular, the estimations showed that the lowest geothermal gradient ($23^{\circ}\text{C}/\text{km}$) reach the early mature stage in much greater depths (Figure 5.6 (a)). Therefore, a significant heat should be supplied from igneous sources (instantaneous) or paleogeothermal gradient should be higher than this value.

On the other hand, the highest geothermal gradient ($70^{\circ}\text{C}/\text{km}$) indicates that wet

gas window (temperature about 150-230°C) can probably appear in the upper most Late Maastrichtian sedimentary succession (depth range from ca. 3.5 to 4.2 km) of the Barracuda well (Figure 5.6 (b)). However, the distribution of geothermal gradient and maturity in the sedimentary successions varied not only with depth and age but also with duration of thermal events and paleoclimate during the basin subsidence (Tissot et al., 1980; Welte and Yukler, 1981; Pepper and Corvi, 1995; Palumbo et al., 1999). The oil or gas window in the sedimentary successions can be significantly influenced by surface temperature when the particular basins were subjected to igneous activity, continental drift and orogeny process (Barker, 2000). The Late Cretaceous sediments could burial in shallow depth during the rift transition age (Ratnayake et al., 2014) and atmospheric paleotemperature over the Indian plate was higher than present (Kent and Muttoni, 2008; Chatterjee et al., 2013) suggesting that high heat flow characteristics to the underlie sediments. Also, it is clearly demonstrated that the steady-state geothermal (constant or time-independent geotherm) values provide a systematic overestimation for oil/gas window (maturity) by the end of the sedimentary events (e.g., Palumbo et al., 1999). Therefore, the gas generative window can be appeared in relatively shallow depths without considering the instantaneous heat supplies during the Late Cretaceous. Consequently, the upper most geothermal gradient has overestimated for the potential gas deposit in the Barracuda well. These interpretations are also supported by measured lower maturity in the shallow burial the Jurassic sediments of the adjacent offshore Andigama Basin.

In fact, stretching and thinning of the crust result in increasing the heat flux (thermal anomaly) in sedimentary basins during the rift transition stage (McKenzie, 1978; Tissot et al., 1987; Pepper and Corvi, 1995). Also, rift systems in worldwide sedimentary basins indicate a significant high heat flow histories (Johnson, 2004). In this rifted basin, the burial history diagram indicates major subsidence and highest sedimentation rates during the Late Cretaceous (Ratnayake et al., 2014). The major subsidence and highest sedimentation rates can generally represent prolonged thermal subsidence for the rifted sedimentary basins (Allen and Allen, 1990; Palumbo et al., 1999). Thus, the standard rifting heat flow can be recognized as the most compatible with the present observations of this frontier basin (Figure 5.6 (c)). Therefore, the

standard rift heat flow characteristics were used to develop kinetic models of the Mannar Basin.

5.2.5.4 Kinetic model of the Mannar Basin

Kinetic models evaluate timing of oil and gas generation in each potential source rock beds. It can be experimentally used to test present observations with respect to geological ideas or hypotheses during the basin development (e.g., Tissot et al., 1987; Pepper and Corvi, 1995; Pepper and Dodd, 1995). Kinetic of kerogen provide an empirical relationship of the amount and composition of oil/ gas generation. Figure 5.7 (a) indicate that the Late Cretaceous sediments (4260-4470 m) of the Barracuda well mainly produce in-situ gas. The in-situ gas generation of the Late Cretaceous sediments was begun during the Early Eocene and it reached peak generation ca. 20 Ma ago (Figure 5.7 (a)). However, the transformation ratio is relatively low for the in-situ oil generation in these sediments. Again, the rifting thermal history of the kinetic model provides results in agreement with the observed gas deposit (4067-4206 m) in the Late Cretaceous sediments of the Barracuda well. The Tertiary sediments (2700-2870 m) in the Barracuda well indicate poor oil or gas generation (Figure 5.7 (a)). In the Dorado North well, in-situ oil/gas generation was started during the Early Oligocene for the Late Cretaceous sediments (3180-3350 m). However, it does not show any significant cumulative hydrocarbon generation (Figure 5.7 (b)). Similarly, the Tertiary sediments of the Dorado North well (2580-2840 m) indicate weak in-situ oil/ gas generation.

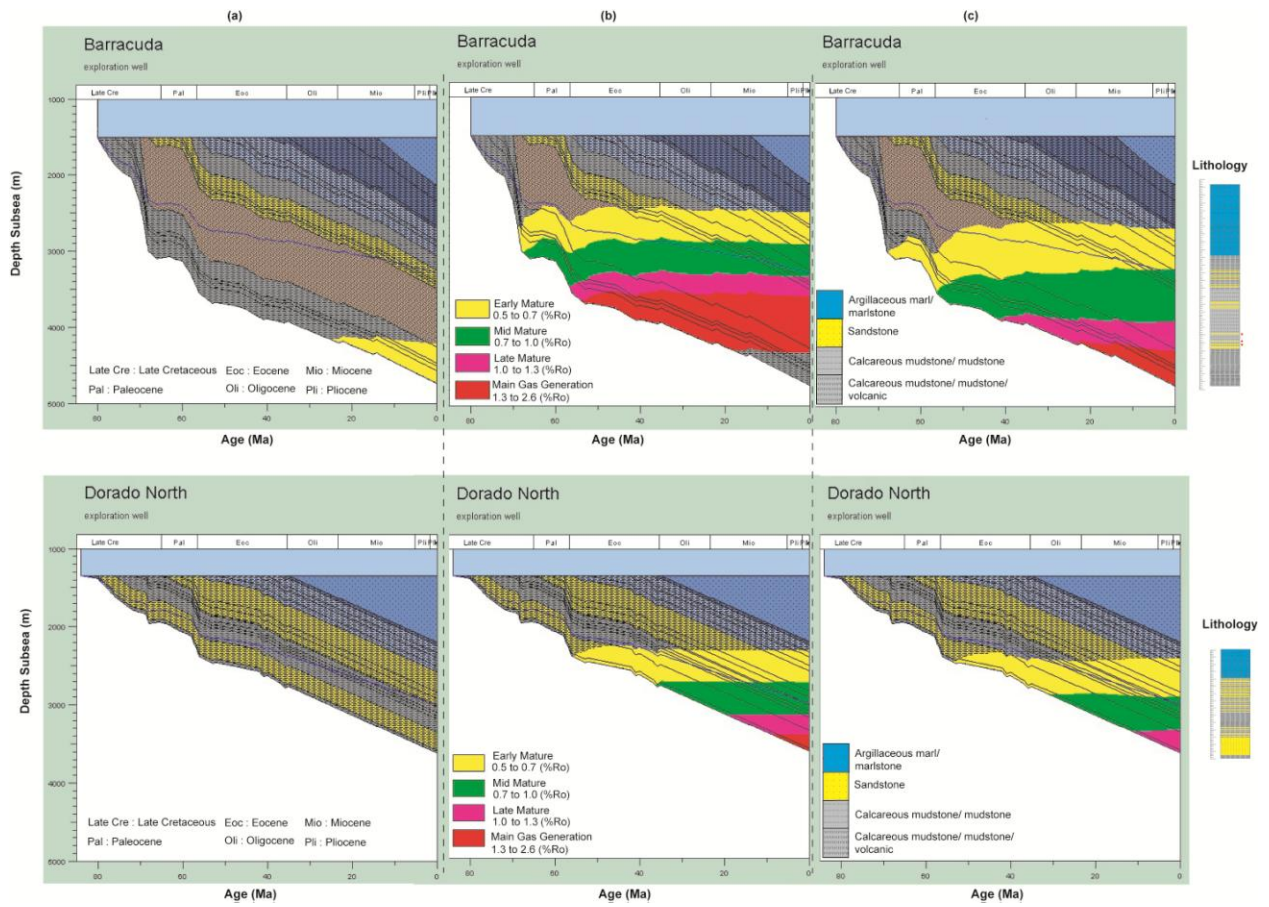


Figure 5.6: Maturity models based on constant paleogeothermal gradients of (a) 23°C/km, (b) 70°C/km, and (c) standard rifting heat flow for the Dorado North and Barracuda exploration wells.

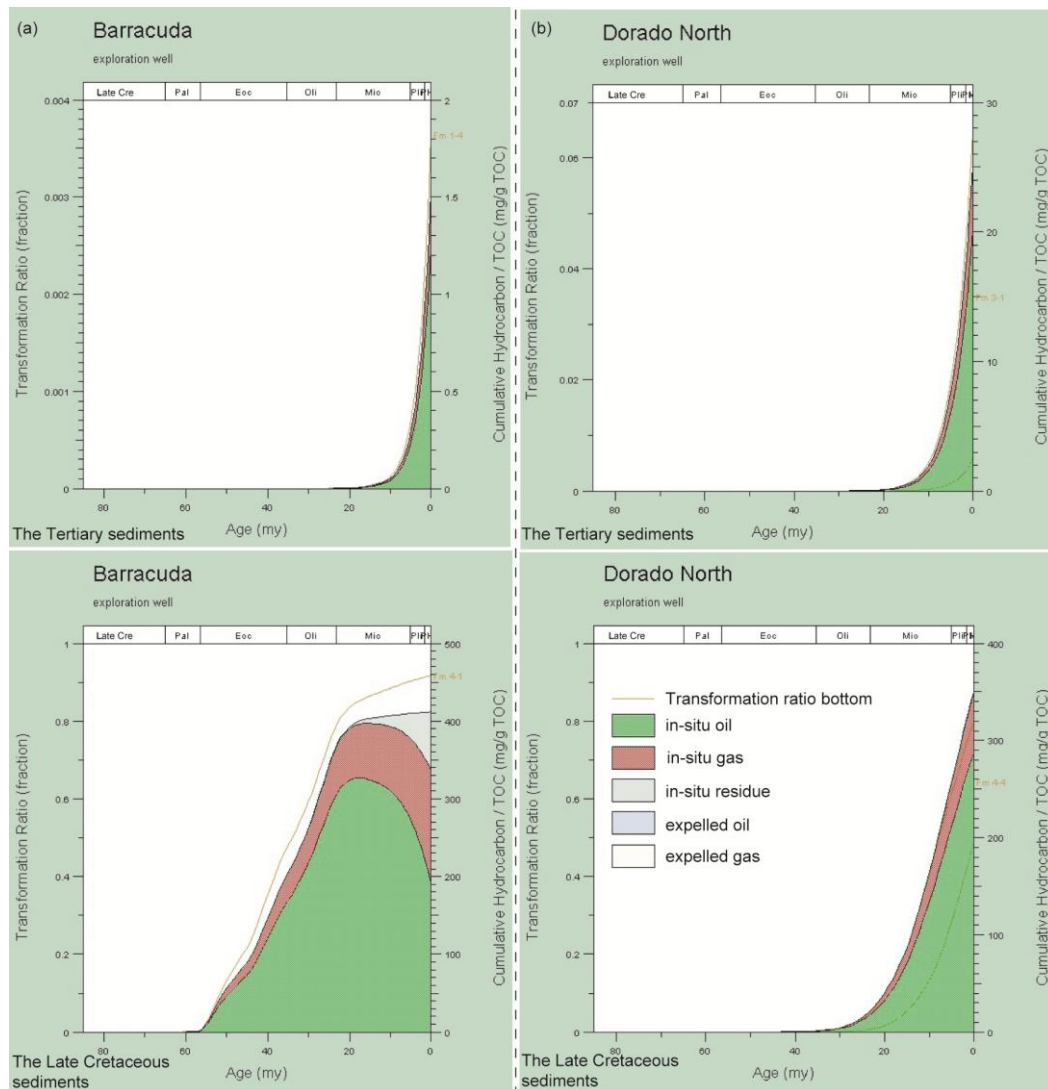


Figure 5.7: Kinetic models based on standard rifting heat flow for (a) the Barracuda and (a) the Dorado North exploration wells.

5.2.6 Paleoenvironment and paleoclimate

The author concluded that four major chronozones can be recognized in the Mannar Basin based on sedimentary facies, OM quantity/ type and depositional changes.

The lower most period (chronozone 1: the Early Campanian sediments of the Dorado North well and the Early-Late Campanian sediments of the Barracuda well) consist of organic carbon depleted (average TOC (%) of Dorado North = 0.45% and Barracuda = 0.97%) algae dominant OMs with some amount of terrestrial OMs

(average C/N of Dorado North = 9.02 and Barracuda = 15.13) were deposited under oxygen-poor depositional environments (average C/S of Dorado North = 5.81 and Barracuda = 6.38). The lower TOC values in the Dorado North well indicate poor OM preservation in sand dominant sediments. In this period, the Mannar Basin was situated in the southern subtropical arid and temperate climate belt. However, the western part of the Indian subcontinent was wetter (average mean annual precipitation = 20 cm/month) than the eastern part (6 cm/month) during the Early Campanian (Chatterjee et al., 2013). Therefore, it is consistent with relatively higher TOC and C/N ratios in the deeper Barracuda well that could be more sensitive to regional marine changes.

The chronozone 2 (The Early Campanian to Late Maastrichtian sediments of the Dorado North and the Late Campanian to Late Maastrichtian sediments of the Barracuda) record organic carbon enhanced (average TOC (%) of Dorado North = 1.64(%) and Barracuda = 1.34(%)), terrestrial OMs rich (average C/N of Dorado North = 27.13 and Barracuda = 20.36, average sterane $C_{29}/(C_{27} + C_{28} + C_{29})$ of Dorado North = 0.42 and Barracuda = 0.37) sediments were deposited in marine depositional environment, with a cyclic fresh water input (average C/S of Dorado North = 10.80 and Barracuda = 9.15). Several smaller continental blocks such as Laxmi Ridge-Seychelles (~70 Ma) and Seychelles (~65 Ma) were separated from the Indian plate during the Late Maastrichtian (Chatterjee et al., 2013). The tectonic changes were followed by deposition of terrestrial OM rich source rock beds. Although the Mannar Basin is located in the subtropical arid climatic zone, perhaps the regional mean annual temperature ranged between 17 °C and 26 °C during this time (Scotese et al., 2011). Also, the Late Cretaceous global climate was warmer than the present climate. In this period, the Indian plate became smaller and smaller, and resided as an island continent in the Southern Hemisphere. Previous investigations and this study indicate that paleoceanic basins in the Indian plate were characterized by thick carbonate sediments during the Late Cretaceous. Carbonate-rich pelagic sediments of this region were resulted in a high pCO_2 level in warmer climatic conditions during the Late Cretaceous (Kent and Muttoni, 2008).

The chronozone 2a sub-category is characterized by deposition of volcanogenic sediments due to several episodes of Deccan-Reunion basalt volcanisms at the top of the

Late Maastrichtian. The chronozone 2a indicates relatively higher TOC values (average = 0.84 ± 0.38) under the higher mud sedimentation rate (average = 49 m/Ma). Previous investigations shown that high sedimentation rates ($> ca. 40$ m/Ma) decrease TOC content due to clastic dilution (e.g., Ibach, 1982; Berner, 1982, Silliman et al., 1996; Sampei et al., 1997; Hossain et al., 2009). Therefore, higher TOC values of the Late Maastrichtian volcanogenic sediments indicate higher primary productivity and preservation of terrestrial OMs under warmer climatic conditions.

In the chronozone 3a (the Early-Late Paleocene sediments of the Dorado North and the Barracuda wells) records OM poor (average TOC (%) of Dorado North = 0.44 and Barracuda = 1.07) algae dominant OMs with some amount of terrestrial OMs (average C/N of Dorado North = 6.94 and Barracuda = 15.75) were deposited under oxic depositional environments (average C/S of Dorado North = 32.07 and Barracuda = 16.21). It can probably represent relative sea-level regression during the Paleocene. Also, the continuous terrestrial erosion can be formed turbidities under equatorial humid climatic conditions. In contrast to present day, the Paleocene was characterized by noticeably higher concentrations of greenhouse gases, and a much warmer global temperature (Pearson and Palmer, 2000; Zachos et al., 2001, 2008; Moran et al., 2006). Also the Earth experienced short term extreme global warming events such as the Late Paleocene Thermal Maximum (LPTM) around 55 million years ago near the Paleocene/Eocene boundary (Fricke et al., 1998; Bains et al., 1999; Zachos et al., 2001, 2005; Lourens et al., 2005; Weijers et al., 2007). In this period, the Mannar Basin was characterized by development of carbonate rich pelagic sediments under tropical conditions.

OM concentration (average TOC (%) of Dorado North = 0.56 and Barracuda = 0.74) and type (average C/N of Dorado North = 9.24 and Barracuda = 13.78) remain almost constant during the chronozone 3b (from the Late Paleocene to Late Eocene sediments in the Dorado North well and the Late Paleocene to the Early-Middle Oligocene argillaceous marl/ marlstone sediments in the Barracuda well). However, in this period, depositional environment was changed to oxygen-poor marine condition (average C/S of Dorado North = 1.97 and Barracuda = 6.83). The continuous decline of the $p\text{CO}_2$ from the atmosphere started a cooling trend over Eocene to Oligocene

(Zachos et al., 2001). Also, the study area experienced weaker monsoon precipitation during this period.

The chronozone 4 was recorded in the Middle Oligocene to Miocene sedimentary succession of the Barracuda well. In this section, organic carbon enhanced (average TOC (%) = 2.51), terrestrial OMs (average C/N = 23.45, average sterane $C_{29}/(C_{27} + C_{28} + C_{29}) = 0.47$) were deposited under marine depositional environment (average C/S = 5.98). The Mannar Basin was close to its present day configuration during the Middle Oligocene (~30 Ma). The Indian subcontinent provides a source of heating in the lower atmosphere during the summer, which creates a vast, low-pressure system over the continent. In contrast, the northern hemisphere creates a high-pressure system during the winter. Therefore, the mountains act as a barrier and changing the Asian (southwest and northeast) monsoon precipitation (Ramstein et al., 1997; Harris, 2006). Therefore, OM rich beds, lamination and back carbon can probably indicate development of Asian monsoon system since the Middle Oligocene. Also, the terrestrial OM dominant mass chromatograms (Figure 4.15 (h)) can probably suggest the intensification of monsoon since the Middle- to Late Miocene.

5.3 The coastal Bolgoda Lake

5.3.1 Present lake environments

5.3.1.1 Variations of organic matter delivery

TOC(%) is a fundamental proxy for understanding the abundance of OM in sediments (Meyers, 2003; Zhou et al., 2005). The relative distributions of TOC integrate the initial production, delivery routes, depositional process and amount of preservation (Silliman et al., 1996; Meyers, 2003). Therefore, it is strongly influenced by climate and local environment (Meyers and Takemura, 1997; Zhou et al., 2005). Surface sediments are rich in OM (Figure 4.18 (a)), containing up to 14.87% of TOC with an average of 4.8%. TOC content is relatively low (under 2.50%) in sandy muddy clay sediments. It implies that physical properties of sediments control OM distribution and preservations (Meyers, 2003). Modern clay rich sediments of the lake can be recognized as significant washbasin for organic carbon. Also, the lake sediments can act as filter and trap for natural and anthropogenic materials from land to the ocean.

5.3.1.2 *Origin of organic matter in surface sediments*

Bulk and molecular indicators have been widely investigated to determine sources of OM type (Meyers and Ishiwatari, 1993; Sampei and Matsumoto, 2001). The C/N ratios of surface sediments (range from 10.4 to 30.0, mean = 12.5) indicate algae and terrestrial OM mixed sediments. Also, biological origins can be principally distinguished by differences in the chain lengths of *n*-alkanes molecular suites (Eglinton and Hamilton, 1967; Meyers and Ishiwatari, 1993; Silliman et al., 1996; Meyers, 1997; Xie et al., 2003; Zhang et al., 2004; Zhou et al., 2005). The distributions of *n*-alkanes (from C₁₆ to C₃₉) imply that surface sediments mix with algae, aquatic plants and terrigenous OM. Paq, CPI and ACL proxies are strongly supported for the presence of higher plant materials in modern lake sediments (Table 4.5). Also, *n*-alkanes from higher plants have strong odd-over-even predominance and give high CPI values (>5), whereas *n*-alkanes from algae give low CPI values (≈ 1) (Zhou et al., 2005; Xiao et al., 2008).

5.3.1.3 *Depositional environments of the surface sediments*

The degree of preservation of OM can be significantly controlled by characteristics of depositional environments. Sulfur and organic carbon relationships have been widely investigated to understand oxic/anoxic depositional conditions (Berner, 1984; Berner and Raiswell, 1984; Berner, 1985; Sampei et al., 1997). C/S ratios of surface sediments indicate oxygen-poor bottom conditions while oxygen-poor environment is more predominant in the southern basin part of the study area (Figure 4.18 (c)). Less freshwater mixing and comparatively higher depths may vulnerable for developing oxygen-poor stagnant environment. Also, accumulation of nutrients have increased the productivity of algae and submerged plants, and deposition of OM usually made the oxygen poor bottom water (Silliman et al., 1996; Sampei et al., 1997; Ver et al., 1999; Ratnayake et al., 2005). Berner (1982) demonstrated that the C/S ratio of wide variety of modern anoxic terrigenous mud is 2.8 ± 0.8 . Likewise, the mean C/S ratio of Bolgoda Lake surface sediments is 2.4 ± 1.2 . It may indicate development of stagnant lake bottom environment in modern lake sediments.

5.3.1.4 Mangrove mud cores

Mangrove mud cores represent characteristic habitat of intertidal zone of river-dominated tropical coastal margin. Mangrove swamps indicate great accumulations (TOC range from 5.86% to 19.53%) of OM (Figure 4.20 (a)). Similarly, Lallier-Verges et al. (1998) shown that living root-biomass contributes to TOC contents (varied from 5% to 30%) up to 60 cm in depth range of Guadeloupe, French West Indies mangrove swamps. Also, it can be identified as a general feature of mangrove mud to have great potential of OM preservation and carbon storage. Mangrove swamps can act as an important sinks of carbon in mangrove plants (Twilley et al., 1992; Lallier-Verges et al., 1998). World Resource Institute has been estimated that global distribution of mangrove is about $24 \times 10^4 \text{ km}^2$ and about 50% of world distributions of mangroves exist within 0° to 10° north and south latitude belts (Twilley et al., 1992). In contrast, mangrove swamps are more sensitive to record environmental and climate changes. TOC contents are gradually increased with depths in all mangrove mud cores (Figure 4.20(a)). The increment of TOC contents with depth is opposed to the normal diagenetic evolution, which may indicate increment of soil destabilizations and releasing of soil OM to the lake due to increment of Southwest Monsoon (Anderson et al., 2002; Wang et al., 2012) after the Little Ice Age (Bradley and Jones, 1993; Mann, 2002).

C/N ratios and biomarker proxies of mangrove mud cores reveal a fairly constant OM type. Also, C/N values are gradually increased with depths (Figure 4.20(b)) that indicate differential decomposition of OM. The partial degradation of OM during the microbial reworking can selectively reduce protein rich components and thereby raise C/N ratios (Meyers and Ishiwatari, 1993; Meyers, 1997; Lallier-Verges et al., 1998). The C/N ratios of mangrove mud core samples imply that mangrove roots are dominant OM type in mangrove swamps. Since C/N ratios of the sediments (around 15) are equal to the C/N ratio of living root of mangrove (15.4 ± 1.8 ; Figure 4.21). Also, molecular source indicates reveal fairly constant OM type distributions in all mangrove mud core samples (Table 4.6). Higher CPI values (<4) signify great association of higher plants wax.

Mangrove mud core (range from $2 \mu\text{g/g TOC}$ to $777 \mu\text{g/g TOC}$, average = $282 \mu\text{g/g}$

TOC \pm 310 in Table 1.4.5) and surface sediments (range from 4.6 $\mu\text{g/g}$ TOC to 716 $\mu\text{g/g}$ TOC, average = 197 $\mu\text{g/g}$ TOC \pm 208 in Table 4.5) represent significant accumulations of pentacyclic taraxerone compounds probably from mangrove plants. Taraxerone biomarker can be identified as a paleogeography, paleoecological and chemotaxonomical biomarker in tropical mangrove dominant coastal regions elsewhere (e.g., Killops and Frewin, 1994; Versteegh et al., 2004; Koch et al., 2005, 2011; Jaffé et al., 2006; Grosjean et al., 2007; Volkman et al., 2007).

C/S ratios of mangrove mud cores show wide variations and it probably reflects sporadic mixing of freshwater and marine influx along the stream. However, overall C/S ratios represent oxic depositional condition. Also, the most distant mangrove mud core from the Bolgoda Lake (VSC 4) consists of very high C/S values owing to entirely freshwater depositional condition.

5.3.2 Environmental and climatic changes from middle Holocene

5.3.2.1 Age and sedimentation rates

Average sedimentation rates from ^{14}C dating of 7 samples are calculated to be 0.14, 0.20, 0.09, 0.12, 0.23, 0.21 and 0.06 mm/ year respectively. In this study, age dating of undamaged shells elaborates higher sedimentation rates compared to bulk sediments and some wood fragments (Table 4.10). Anomalously old ages of bulk sediments (1120 yr B.P. in depth 16 cm and 13080 yr B.P. in 154 cm of Core 1, Table 4.10) correspond to a mixing of disseminated pre-existing and new carbon (e.g., Eglinton et al., 1997; Dickens et al., 2004). Similarly, reworking of terrigenous woods (6540 yr B.P. in 60 cm of Core 1 and 6840 yr B.P. in 44 cm of Core 2, Table 4.10) often enhanced the actual age. Therefore, heterogeneous ages of bulk sediments and some wood fragments can be substantially higher than the actual sediment age.

In contrast, ancient suspended OM can remain in marine water from bottom deep sea sediment by upwelling. Additionally to avoid misleading age data, marine reservoir corrections were also considered based on the literatures. According to Southon et al. (2002), three bivalve samples from the Museum National d'Histoire Naturelle, Paris and one gastropod sample from US National Museum of Natural History, Smithsonian Institution in Washington, DC were used to measure marine reservoir ages from Sri

Lanka. These bivalve and gastropod shells were approximately collected from close to the Bolgoda Lake. The average reservoir age of these samples was 127 years (Southon et al., 2002). In this study, marine reservoir effect may not significantly influence for the anomalously old ages. Therefore, the ancient OM could be mainly received from the terrestrial environment.

The age data that exist in the Bolgoda Lake shows considerably low sedimentation rates compared to typical brackish lakes elsewhere. The evolution of the Bolgoda Basin was recognized as a part of the inter-connected much larger adjacent river systems (Wickramagamage, 2011). Sea-level changes may have caused to arrange semi-closed fluvial dominant estuary as discussed in below sections. Sedimentation rates of the Bolgoda Lake probably correlate with the river dominant coastal water body. This study area is interpreted to have been arranged in low-sinuosity braided fluvial systems flanked by vegetated/ mangrove overbank and swampy floodplain areas. The sediments of the pseudo-Bolgoda Lake are thought to have been deposited in a prominent fluvial setting along with coastal settings, particularly tidal flats and lagoonal environments.

5.3.2.2 Changes in organic matter contents

The history of OM distributions of the Bolgoda Lake can be divided into two major divisions that are quasi-steady state (from 7.5 ky B.P. to 2.5 ky B.P.) and non-steady state (after 2.5 ky B.P.). The increments of TOC evidence the major environmental change after the mid-Holocene sea-level highstands (Figure 4.19). In detail, the upper sediments (from 62 cm in Core 1, from 56 cm in Core 2 and from 60 cm in Core 3) are rich in OM compare to the bottom sediments (Figure 4.19). In contrast, geographical, morphological and biogeochemical factors are significantly controlled accumulations of OM in aquatic systems (Dean and Gorham, 1998; Ver et al., 1999; Boyd et al., 2006). TOC contents of the Core 3 indicate the highest values (Figure 4.19) may be due to deposition of highly to completely decompose degraded submerged aquatic plants.

5.3.2.3 Changes in origin of organic matter type

C/N values are relatively high in the upper 0-60 cm part of Core 1 and Core 3 (after 2.5 ky B.P.) with peaks at 40 cm and 60 cm in depth, and TOC contents are high in the

same part (Figure 4.19). This suggests that land plants and/or floating plants/ferns contribute as a dominant source in the sediments after 2.5 ky B.P. C/N ratios of the upper 0-20 cm (after 1 ky B.P.) of the core samples show slightly lower values than in the lower part (Figure 4.19). The compilation of above results indicates that both algae and terrestrial plants with reworking wood fragments increased after the environmental change until recent time (Figure 4.19). Aquatic primary productivity typically increases with nutrient supply from river water (Silliman et al., 1996; Meyers and Takemura, 1997; Meyers, 1997). TN values probably reflect greater supplies of fertile soil nutrients to the lake after 2.5 kyr B.P. In contrast, carbon isotopes values ($\delta^{13}\text{C}$) of the plant fragments (Table 4.10) represent a typical C_3 plants (e.g., Bender, 1971; Huang et al., 2001). From the late Holocene, the major environmental change has occurred, and reworking of soil probably increased. The site around Core 3 is situated at the central part of the Bolgoda Lake and might be a specific to deposition of land plants and contamination of highly decomposed submerged aquatic plants (Figure 4.19). Local lake morphology is significantly controlled by current and selective accumulations of sediments. In contrast, relative abundance of land plants and algae are almost constant throughout the Core 2 obtained from the river mouth (Figure 4.19).

The *n*-alkanes from algae ($n\text{-C}_{20}/n\text{-C}_{\text{all}}$) and indicator of aquatic macrophytes ($n\text{-C}_{23}/n\text{-C}_{\text{all}}$) imply that the relative abundance of algae and aquatic macrophytes gradually decreased compared to the total *n*-alkanes distribution (Figure 4.24). The long *n*-alkanes more than $n\text{-C}_{27}$ increased drastically after the environmental change (Figure 4.24). The long chain *n*-alkanes are generally from leaves/roots coated by wax layers. The *n*-alkanes are useful for reconstructions of paleoenvironments (Smolenska and Kuiper, 1977; Bulder et al., 1989; Maffei et al., 1993; Hoffmann et al., 2013). Sachse et al. (2006) reported that broadleaf tree leaves contained longer chain *n*-alkanes in the warmer/dryer regions than the same species in colder/wetter regions. The ratios of $n\text{-C}_{29}/n\text{-C}_{\text{all}}$ and $n\text{-C}_{37}/n\text{-C}_{\text{all}}$ gradually increased in the upper part compared to the lower succession may be, consequently, due to warm or dry climate. Higher plants are sensitive to climatic changes (Heimann and Reichstein, 2008) and increased in relative abundance of biosynthesize longer chain *n*-alkanes under warm climatic condition (Xie et al., 2003; Zhou et al., 2005; Xiao et al., 2008). Higher plants grown in warm climate

are characterized by dominant $n\text{-C}_{29}$ and $n\text{-C}_{31}$ alkanes (e.g., Ficken et al., 2000; Nott et al., 2000; Schwark et al., 2002; Castañeda et al., 2009). In this study, the $n\text{-C}_{31}$ n -alkane distribution of modern sediments can mainly represent the source material from floating plant species (Figure 4.24) and other swamp vegetation such as herbaceous plants and grasses (Zhou et al., 2005; Xiao et al., 2008; Castañeda et al., 2009; Zheng et al., 2011). In contrast, individual concentrations of algae, floating/ herbaceous plants and terrestrial plants drastically increased (approximately double) after the major environmental change under the warm/dry climate (Figure 4.22). Therefore, it may probably reflect greater supply of fertile soil nutrient and reworking terrestrial OM from the transgressive deposit over the watershed area.

Mangrove distributions have been widely applied to reconstruct environmental and sea-level changes elsewhere (e.g., Behling et al., 2001; Versteegh et al., 2004; Engelhart et al., 2007). The taraxerone distribution is predominant in the lowermost part of core samples (6.5-7.5 ky B.P.) suggesting that a wide distribution of mangrove vegetation in this area may be due to seawater invasion. Because the two of the most important factors required for the survival of mangroves are salinity and substrate (Kumaran et al., 2005), and are enhanced by initial saline water invasion in the study area.

5.3.2.4 *Changes in depositional environments*

C/S ratios are relatively low in the lower sedimentary columns that imply oxygen-poor depositional environment. C/S ratios slightly increased in Core 1 and Core 2 after the major environmental change (< 60 cm) and these increasing trends is prominent in Core 1 (Figure 4.19). Furthermore, the upper most sedimentary columns with higher C/S ratios (<~15 cm) represent a relatively low H_2S production environment (Figure 4.19). Results suggest a low activity of sulfate reducing bacteria probably due to land plant rich OM, which is not healthy foods for desulfovibrio, or decreasing salinity after the environmental change. Similarly, the higher C/S values of Core 3 probably indicate the lack of degradation by sulfate-reducing bacteria, which are abundantly distributed in higher plant wax. However, according to Didyk et al. (1978), high values of TOC (> 10%) and TS (> 1%) in Core 3 (Figure 4.19) indicate anoxic sedimentation conditions. In contrast, depositional settings of the study area may have been arranged as a semi-

closed and separate fluvial dominant estuary after the major environmental change followed by sea-level changes.

It is widely believed that the early Holocene eustatic sea-level was lower than present level and eustatic sea-level rise during the early to middle Holocene (e.g., Fleming et al., 1998; Woodroffe and Horton, 2005; Bird et al., 2007; Kench et al., 2013). Available preliminary sea-level curve of Sri Lanka indicates a non-uniform rise up to ca. 7 m/ky (Katupotha, 1994). Many of former basins of coastal lowlands have gradually been filled in fine silt, clay and sand from the middle Holocene (Cooray, 1984; Weerakkody, 1992; Katupotha, 1994). Interestingly, the data of the irrigation department of Sri Lanka reveal that adjacent Kalu-Ganga River flows below the sea-level about 37 km from the present mouth (Wickramagamage, 2011). It may provide strong evidence to have formed waterlogged swamp/ wetland morphological features in tropical southwest coast of Sri Lanka. Natural waterlogged swamps are characterized by limiting oxygen availability and abundant of sulfate reducing anaerobic bacteria elsewhere (e.g., Koch et al., 1990).

5.3.2.5 PAHs as artificial marker

Higher concentrations of PAHs in surface sediments, the uppermost part of Cores 1 and 2 and mangrove mud cores may indicate anthropogenic activities in the watershed area. Fla, Py, BaAn, Bflas and BePy are generally considered to be combustion-derived PAHs (Jiang et al., 1998; Yunker et al., 2002, 2011; Yunker and Macdonald, 2003; Grimalt et al., 2004; Grice et al., 2007), and Fla, Py and BaAn are also produced by catagenetic modification of petroleum and matured kerogen (Baumard et al., 1998; Yunker et al., 2002; Yan et al., 2006). Fla/Py and Fla/ (Fla + Py) ratios in the Cores 1 and 2 (Table 4.7) can be used as indicators to distinguish between PAHs of combustion and petroleum origins (Baumard et al., 1998; Yunker and Macdonald, 2003; Hossain et al., 2013). Values of Fla/Py (0.80-1.48) and Fla/ (Fla + Py) (0.45-0.60) suggest overlap of wood combustion and petroleum OM. Almost all of Fla, Py and BaAn are detected within the top 0-14 cm in the Cores 1 and 2 (0-ca.500 yr B.P.) showing that wild fire and petroleum pollution have prominently increased by mankind activities in the watershed area of the Bolgoda Lake. The weak correlation were found between Bflas

with Fla ($r = 0.04$) and Py ($r = 0.06$) suggesting that almost Fla and Py were from origin of petroleum pollution by recently increased mankind activity. Relatively weak correlations between BaAn with Fla ($r = 0.42$) and Py ($r = 0.42$) were probably due to solubilization or degradation during transportation of OM in strongly exposed to sunlight (e.g., Yunker et al., 2002; Stout and Emsbo-Mattingly, 2008).

5.3.3 The Holocene sea-level changes and coastal landforms evolution

Sri Lanka can be considered as a tectonically stable far field site to recognize the eustatic sea-level fluctuations since the Last Glacial Maximum (LGM). Melting of the ice caps led to an increase the eustatic sea-level from below 125 ± 5 m to the present level since the LGM (Fairbanks, 1989; Fleming et al., 1998). Eustatic sea-level changes can be characterized by several non-uniform rises (rapid melt water pluses). About 3-5 m of water has been added to the ocean ca. 7 ky B.P. due to melting of high latitude/altitude ice sheets of the Northern Hemisphere, coupled with a significant contribution of the Antarctic ice sheets (Nakada and Lambeck, 1988; Yokoyama et al., 2000). Complex and rapid eustatic mid-Holocene sea-level changes are evidence in the different part of the world including the Indian Ocean and Sri Lanka (Table 5.1). The reconstructed sea-level histories from different coastal sectors reveal a broad similarity across the west to southeastern coast of Sri Lanka.

Sea-level changes can be recognized as the main triggering factor for the major environmental change. The mid-Holocene highstands may cause to change geomorphology of the study area from part of the bay of larger paleoriver system (before the major environmental change, from ca. 7.5 ky B.P. to ca. 2.5 ky B.P.) to semi-closed and separate fluvial dominant estuary of local streams (after the major environmental changes, ca. 2.5 ky B.P.). The $\delta^{13}\text{C}$ values of mollusk shells (-2.4‰ and -2.7‰ , Table 1.4.9) from the upper sedimentary succession of the Bolgoda Lake are lower than those living in the open sea ($+2.6\text{‰}$) (Lécuyer et al., 2004). The author applied empirical formula proposed by Sampei et al. (2005) to estimate the paleosalinity of the Bolgoda Lake. The paleosalinity of the lake was ca. 21-22 PSU in after 2.3 ky B.P. Consequently, it is confirmed that development of present brackish environment after the sea-level fall along this coast.

Similarly, previous investigations (Katupotha, 1988, 1994; Weerakkody, 1988, 1992) clearly demonstrate that geomorphological evolution of coastal landforms based on available radiometric dating, geomorphological and geological evidences in western to southern terrain of Sri Lanka. In summary, the former drainage basins were submerged, and beach ridges/ headlands were created during the mid-Holocene transgression. Later, these bays became lagoons (e.g., Negombo Lagoon, Kalametiya-Lunama Lagoons, and Koholankala Lagoon), lakes (e.g., Mundal Lake) and swamps (e.g., Muthurajawela swamp) due to the low stands of sea-level during the late Holocene.

Table 5.1: Summary of the Holocene sea-level data in the Indian Ocean (n.d.: not determined, cal yr B.P.: calibrated age year before present, yr B.P.: age year before present, ^a: end of rapid rise, ^b: review of previous radiometric dating-mainly ¹⁴C age dating).

References	Time of mid-Holocene highstand	Height or rate of highstand	Falling to present sea-level	Analytical methods	Sample types	Locations
Banerjee (1993)	6000 yr B.P.	n.d	2500 yr B.P.	¹⁴ C dating	Peat/ geological observation	south India
Banerjee (2000)	7300 cal yr B.P.	3 m	2500 cal yr B.P.	U/Th dating	Corals and shell beds	east coast of India
Bird et al. (2007)	7400 cal yr B.P.	3-5 m	n.d	¹⁴ C dating	Wood, coral, shell	Singapore
Camoin et al. (1997)	7500 yr B.P. ^a	7 mm/ yr	2000 yr B.P.	U/Th dating	Corals	Mauritius, Réunion and Mayotte
Camoin et al. (2004)	7500 yr B.P. ^a	6 mm/ yr	2500 yr B.P.	U/Th dating	Corals	Mauritius, Réunion, Mayotte, Madagascar, Seychelles
Hameed et al. (2006)	9000 cal yr B.P.	n.d	1800 cal yr B.P.	¹⁴ C dating	Shell and bulk organics	south India
Hashimi et al. (1995)	7000 yr B.P.	2.50 m	2500 yr B.P.	^b	Wood, sediment, shell, limestone	western India
Islam and Tooley (1999)	7000 cal yr B.P. ^a	3.5 mm/ yr	n.d	¹⁴ C dating	Mangrove/ geological observation	Bangladesh
Katupotha (1988)	6110 yr B.P.	> 1 m	n.d	¹⁴ C dating	Coral	southwest Sri Lanka
Katupotha and Fujiwara (1988)	6170 yr B.P.	> 1 m	2330 yr B.P.	¹⁴ C dating	Corals and shell beds	southwest to south Sri Lanka
Kench et al. (2009)	4500 cal yr B.P.	0.50 m	2100 cal yr B.P.	U/Th dating	Corals	Maldives
Montaggioni and Faure (1997)	6900 yr B.P. ^a	4.3 mm/ yr	2500 yr B.P.	¹⁴ C dating	Corals	Mauritius
Ramsay (1995)	6500 yr B.P.	3.5 m	900 yr B.P.	¹⁴ C dating	Beachrocks	southern Africa
Ranasinghe et al. (2013)	7300 cal yr B.P.	0.75 m	3000 cal yr B.P.	¹⁴ C dating	Bulk organic, wood, mollusk shells	southeastern Sri Lanka
Tjia (1996)	6000 yr B.P.	5 m	1500 yr B.P.	^b	Corals and shell beds	Malaysia and Thailand Peninsula

The author compiled lithological characteristics of sedimentary cores (Figure 5.8) in Lunawa Estuary, Bolgoda Lake, Ratgama and Koggala Lagoons, Kirinda and Panama Estuaries, and Okada Lagoon (Ratnayake et al., 2005; Ranasinghe et al., 2013; Rajapaksha et al., 2014). In particular, the wet zone of Sri Lanka records mud dominant sediments (Figure 5.8(a-d)). However, the dry zone evidence a significant amount of sand dominant sediments (Figure 5.8(e-g)) compared to the wet zone of Sri Lanka. Therefore, environmental and climatic factors can play a significant role in the distribution of the Holocene sediments in coastal inland area.

In contrast, Facies correlations were done based on biological assemblages, physical, chemical and textural properties of sediments with a regional age-model. The stratigraphic columns can be mainly divided into two main facies with respect to sea-level changes (Figure 5.8). Facies 2 indicates timing of mid-Holocene highstands from ca. 7.5 ky B.P (the upper most value) to 2.5 ky B.P. (the lower most value). In particular, beach ridges and headlands were gradually formed during the Facies 2 (Weerakkody, 1992; Katupotha, 1994). Facies 1 signifies falling of sea-level to present level around ca. 2.5 ky B.P. Many of former basins have changed into semi-closed and closed coastal aquatic systems. In contrast, the upper sub-boundary of the Facies 1 (Figure 5.8) can probably indicate anthropogenic activity or an abrupt event such as tsunami or flood.

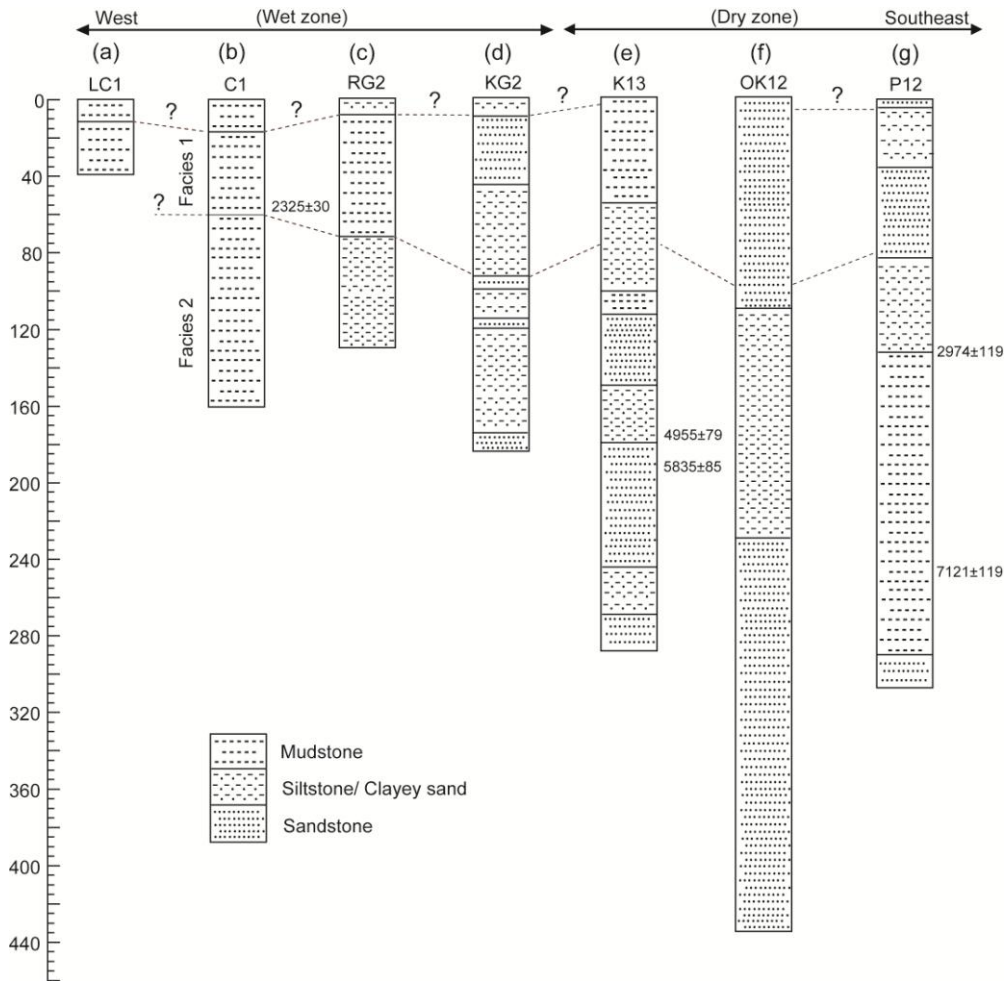


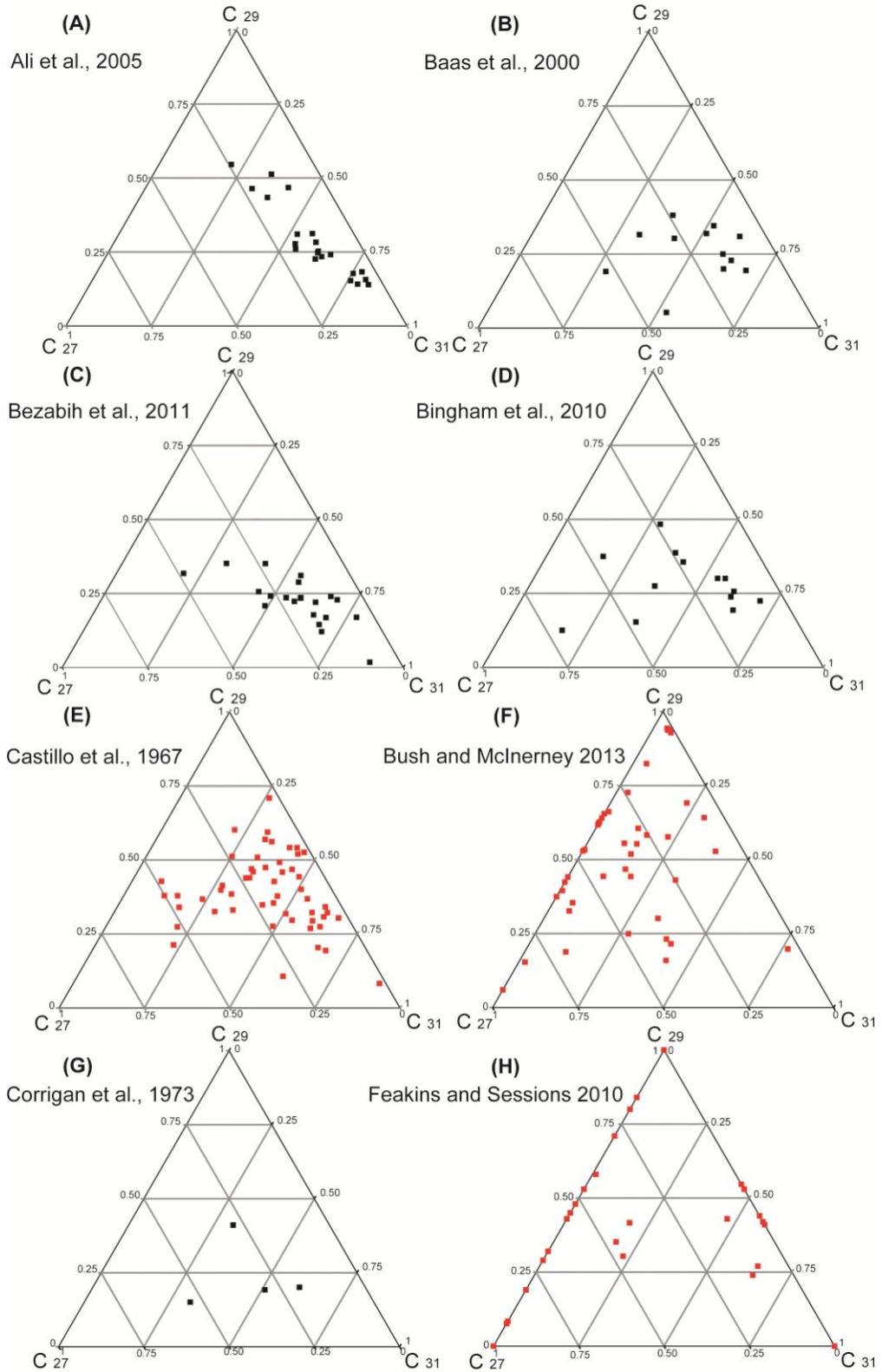
Figure 5.8: Stratigraphic correlations of representative cores in different coastal landforms on the west to southeast coast of Sri Lanka. Stratigraphic boundaries were identified using organic and inorganic geochemical proxy data and physical properties, as well as biological assemblages of sedimentary units. Correlations have been drawn in dash lines without considering the elevation differences of the cores. Ages (cal yr B.P.) are correlated using published and unpublished ^{14}C radiometric data ($n = 46$). Where, (a) Lunawa Estuary, (b) Bolgoda Lake, (c) Ratgama Lagoon, (d) Koggala Lagoon, (e) Kirinda Estuary, (f) Okanda Lagoon, and (g) Panama Estuary (after Ratnayake et al., 2005; Ranasinghe et al., 2013; Rajapaksha et al., 2014).

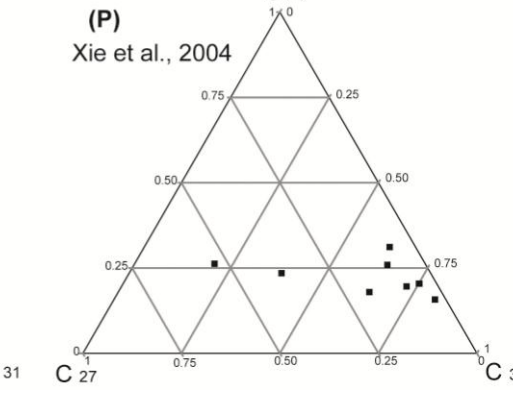
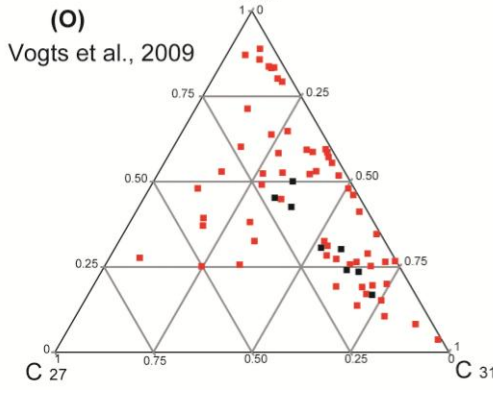
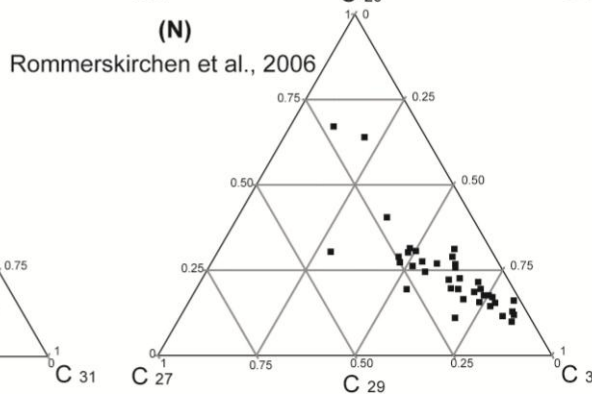
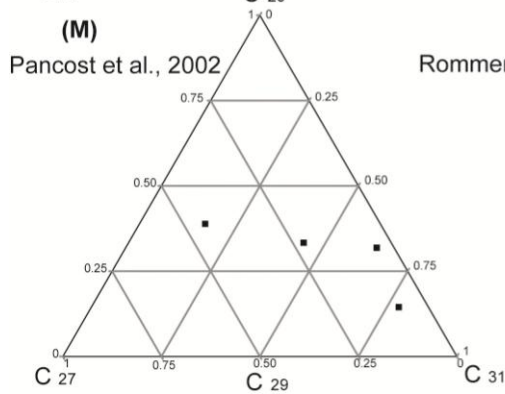
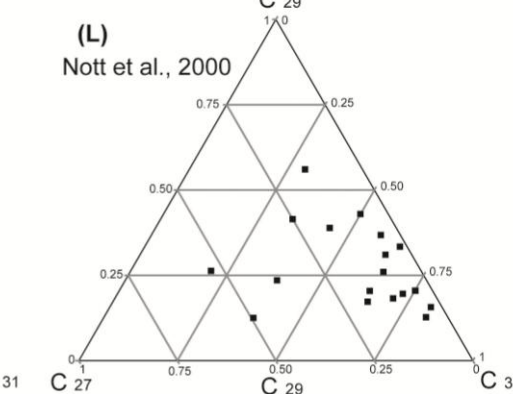
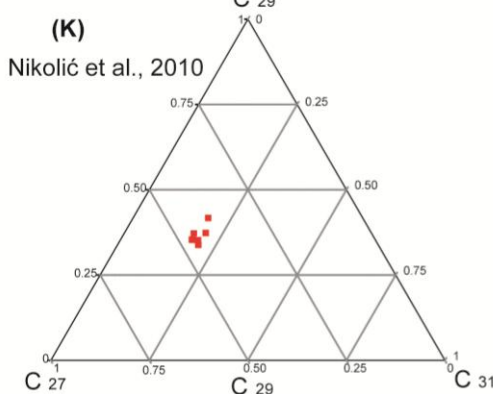
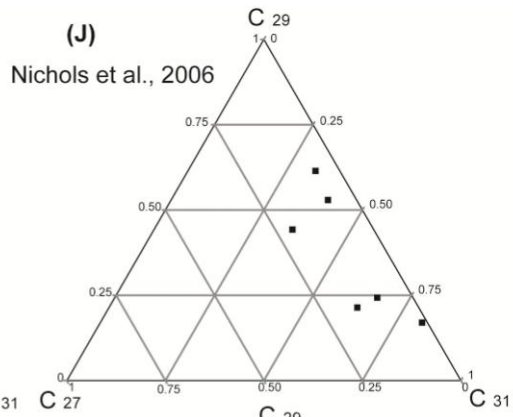
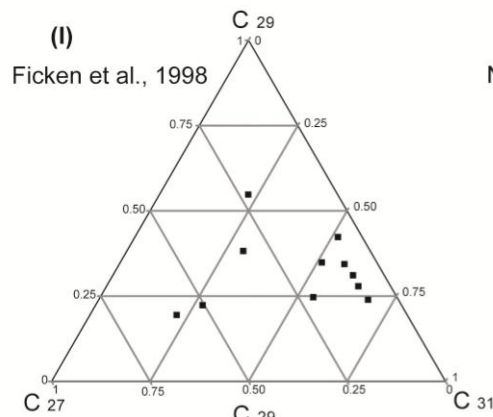
5.3.4 Paleocological and chemotaxonomical significant

The *n*-alkanes distributions have certain patterns in living OM and sediments under

the diagenesis alteration (Eglinton and Hamilton, 1967; Schwark et al., 2002; Ronkainen et al., 2013). In this study, the literature data (Castillo et al., 1967; Corrigan et al., 1973; Wannigama et al., 1981; Ficken et al., 1998; Baas et al., 2000; Nott et al., 2000; Pancost et al., 2002; Xie et al., 2004; Zhang et al., 2004b; Ali et al., 2005; Nichols et al., 2006; Rommerskirchen et al., 2006; Vogts et al., 2009; Bingham et al., 2010; Feakins and Sessions, 2010; Nikolić et al., 2010; Bezabih et al., 2011; Bush and McInerney, 2013) and new data from 386 living vegetations were initially categorized using different proxies such as angiosperm vs. gymnosperm, C₃ vs. C₄, temperate zone vs. deciduous/ evergreen and continental based separations. The variability of mid- to long-chain *n*-alkanes is complex from one another of above parameters. However, non-woody vs. woody plants can be sufficiently distinguished using the most recognizable long-chain *n*-alkanes (*n*-C₂₇, *n*-C₂₉ and *n*-C₃₁) of terrestrial OM (Figure 5.9). Therefore, changes of long-chain *n*-alkanes were used to characterize sedimentary OM in the Bolgoda Lake (Figures 5.10 and 5.11).

A ternary diagram reveals that mangrove dominant brackish sediments are enriched in *n*-C₃₁ and depleted in *n*-C₂₇ as well as a considerable amount of *n*-C₂₉ within a narrow range (Figure 5.11). The abundant of *n*-C₃₁ indicate the occurrence of grasses (graminoids), floating plants, and shrub type herbaceous vegetation (non-woody) in swamps (Zhou et al., 2005; Castañeda et al., 2009; Zheng et al., 2011). The considerable amounts of *n*-C₂₉ *n*-alkanes indicate the establishment of more diverse tropical woody plants (Ficken et al., 2000; Nott et al., 2000; Castañeda et al., 2009). Therefore, *n*-alkanes derived from herbaceous plants (grasses, floating plants) are expected to be more dispersed and survived than those from woody plants in the study area (Figure 5.11(a)).





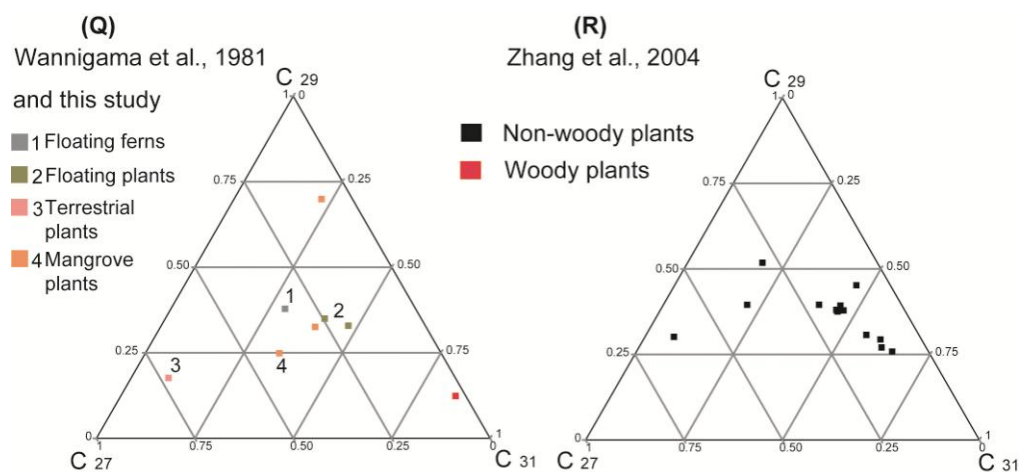


Figure 5.9: The n -C₂₇, n -C₂₉ and n -C₃₁ n -alkanes ternary diagrams of the literature data separated into woody and non-woody plants (from A to R).

In contrast, the Bolgoda Lake is characterized by (1) geomorphological and climatic changes and (2) variations of OM concentration and type in spatially and temporally in the sedimentary successions as discussed above. The variability of n -C₂₇ to n -C₃₁ n -alkanes may indicate changes in land plant input of the watershed area. The ternary diagram indicates that woody plants have dominated in the upper sedimentary successions (0-60 cm, from ~2.5 ky B.P. to the Recent) of Core 1 and Core 2 (Figure 5.10(c, d)) compared to the lower sedimentary successions (60-160 cm, from ~7.5 ky B.P. to ~2.5 ky B.P.) due to accumulation of reworking peat/ terrestrial OM after the major environmental change. In particular, accumulation of more terrestrial OM close to river mouth of the present stream may cause to increase woody plant abundance in Core 2 (Figure 5.10(d)). However, woody plant accumulation is a relatively high in the lower sedimentary succession of Core 3 (Figure 5.10(e)) may be due to nearby locations in the inner bay of larger paleoriver system (Wickramagamage, 2011). Also, submerge grasses in this location may cause to increase a non-woody plant deposition in the upper sedimentary column of Core 3 (Figure 5.10(e)). Therefore, geomorphological and climatic changes of the study area were accompanied by a shift of long-chain n -alkanes distributions in the core samples.

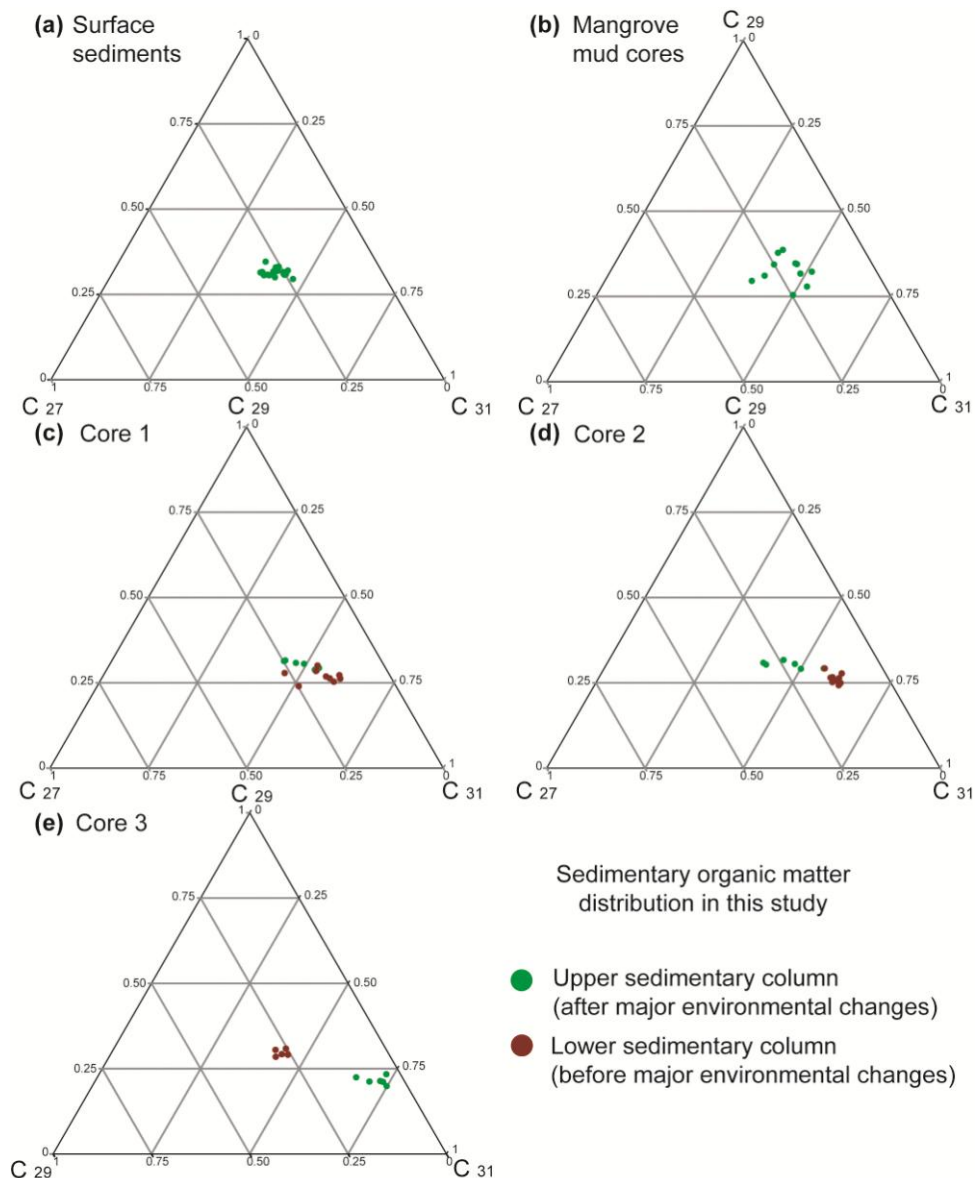


Figure 5.10: Temporal and spatial variations of n -C₂₇, n -C₂₉ and n -C₃₁ n -alkanes in (a) surface sediments, (b) mangrove mud cores, (c) Core 1, (d) Core 2 and (e) Core 3 of the Bolgoda Lake.

Similarly, the changes in the n -C₂₇ to n -C₃₁ n -alkanes distributions have been applied to differentiate changes in terrestrial plant input elsewhere (e.g., Volkman et al., 2000; Schwark et al., 2002). Therefore, our results were compared to previously published data of living and sedimentary OM (Figure 5.11(b)) in mid- to high-latitude peat bogs (Volkman et al., 2000), temperate woody angiosperms and gymnosperms

(Bush and McInerney, 2013), vegetation history in Central Europe (Schwark et al., 2002) and rainforest and savanna plants in Africa (Vogts et al., 2009, 2012).

Interestingly, the distribution of *n*-alkanes in tropical brackish sediments (this study) and mid- to high-latitude peat bogs (literature studies) are rather similar (Figure 5.11). Since tropical brackish and peat bogs communities comprise predominantly herbaceous type vegetations (e.g., graminoids), which are highly adapted to swamp type environments. Next, distributions of *n*-alkanes in tropical and sub-tropical rain forest and savanna in African habitats are a bit overlapped with our data (Figure 5.11). Tropical and sub-tropical rain forest in Africa is characterized by a large diversity of woody plants from trees, shrubs and lianas (Vogts et al., 2009, 2012). Also, savanna vegetation in Africa is distinguished by dominant grasses, shrubs species and a considerable amount of savanna tress (Vogts et al., 2009, 2012). Therefore, approximately upper section of the peat bog/ tropical brackish data in the ternary diagram was overlapped by data of herbaceous plants dominant savanna in African habitats (Figure 5.11). Although *n*-alkanes compositions depend on intra- and inter-species variability, constructive mixings of various terrestrial OM in the sedimentary successions are typically controlled by growth habitats of local environment conditions.

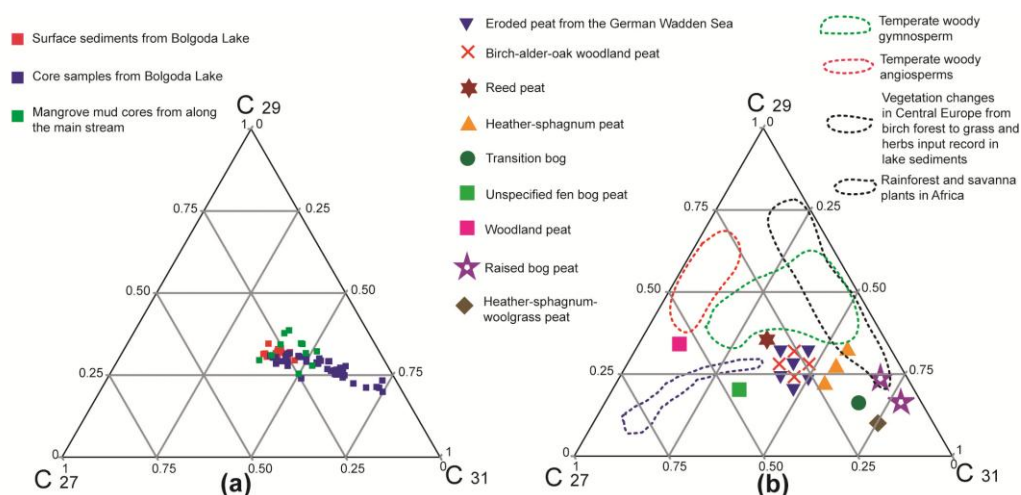


Figure 5.11: Triangular diagram showing the abundance of *n*-C₂₇, *n*-C₂₉ and *n*-C₃₁ *n*-alkanes of (a) the Bolgoda Lake sediments and (b) a comparison with literature data elsewhere (e.g., Volkman et al., 2000; Schwark et al., 2002; Vogts et al., 2009; Bush and McInerney, 2013).

5.3.5 Early stage diagenesis in the tropical brackish sediments

5.3.5.1 *Total hopane distribution in surface and mangrove sediments*

Total hopane concentration in surface sediments range from 561.46 ng/g TOC to 3470.5 ng/g TOC (average \pm standard deviation = 1336.46 ng/g TOC \pm 748.69) (Table 4.8). Total hopane concentration in mangrove mud cores range from 283.98 ng/g TOC to 1093.31 ng/g TOC (average \pm standard deviation = 676.37 ng/g TOC \pm 268.48) (Table 4.9). It may indicate the preservation of more bacterial diagenetic products (geohopanooids) in the Bolgoda Lake surface sediments compared to the sub-aerial mangrove mud cores may be due to changes of OM type and depositional environment. The Bolgoda Lake surface sediments consist of significant amount (average TOC = 4.8 \pm 2.3) of algae and terrestrial plants mixed OM (average C/N ratio = 12.5 \pm 3.4). The mangrove mud cores indicate great accumulation (average TOC = 11.8 \pm 3.2) of mangrove root-biomass (average C/N ratio = 14.2 \pm 1.6). Also, it is shown that the lake surface sediments consist of oxygen-poor brackish depositional environment (average C/S ratio = 2.4 \pm 1.2). However, sub-aerial mangrove mud cores indicate freshwater depositional condition (average C/S ratio = 129.2 \pm 383.6) with cyclic seawater invasion. It has been widely discussed that bacterial reactions depend on number of factors including mainly reactive organic compound and dissolve sulfate concentration (e.g., Berner, 1984, 1985; Berner and Raiswell, 1984). Algae OMs are favorable food for sulfate-reducing bacteria compared to lignin rich terrestrial OM (Berner, 1984; Gong and Hollander, 1997; Sampei et al., 1997). Therefore, in this study, the reactive algae OMs concentrations (regardless of its total concentration) and sulfate availability are lower for bacterial sulfate reduction in mangrove mud cores. Therefore, a significant amount of bacterial sulfate reduction can be expected in brackish water surface sediments compared to sub-aerial mangrove mud cores. In nature, this fractionation is led to the breakdown of OM to methane and carbon dioxide in the freshwater swamp ecosystems (Berner, 1985; Bridgham and Richardson, 1992; Brix et al., 2001).

5.3.5.2 *Total hopane distribution in the lake core sediments*

Total hopane distributions in core samples are shown in Figure 4.25. Total hopane concentrations decrease with depth flattens out to almost constant values in modern sediments (Figure 4.25). This pattern may probably indicate the reduction of bacterial

decomposition with increasing depth. The sediment/water interface is characterized by highly abundant microbial communities (Klump and Martens, 1989; Sun and Wakeham, 1998). In general, aerobic microorganisms exist in few centimeters below the sediment/water interface followed by penetration of dissolved oxygen from bottom water. The Bolgoda Lake is characterized by low sedimentation rates of 0.21 mm/year. Therefore, slower sedimentation rates provide sufficient time for aerobic bacterial degradation in the sediment/water interface. After that, dysaerobic or anaerobic degradation arises due to prevent of oxygen migration to deeper level of sediments. Total hopane variations in the down core profiles can probably indicate intensity of bacterial activity in sediments. However, bacterial activity depends on number of factors as discussed above.

The author considers the effect of OM type for the bacterial activity in the upper (0-60 cm) and lower (60-160 cm) sedimentary successions. Figure 5.12(a) suggests the moderate correlations between total hopane and OM type concentrations in the upper sedimentary succession. Further, it suggests the increasing trend of connection between bacterial activities and different OM types as following matter: terrestrial plants < macrophylyte plants < algae (Figure 5.12(a)). However, hopane does not show significant correlation with different OM types in the lower sedimentary succession (Figure 5.12(b)). This trend may represent the formation of more resistant geopolymers (macromolecular) after the progressive sulfate reduction in the studied samples. Also, early diagenetic reactions include structural modifications, rearrangements and stereochemical changes of biohopanoid in recent sediments (Haven et al., 1987; Innes et al., 1997; Farrimond et al., 2003).

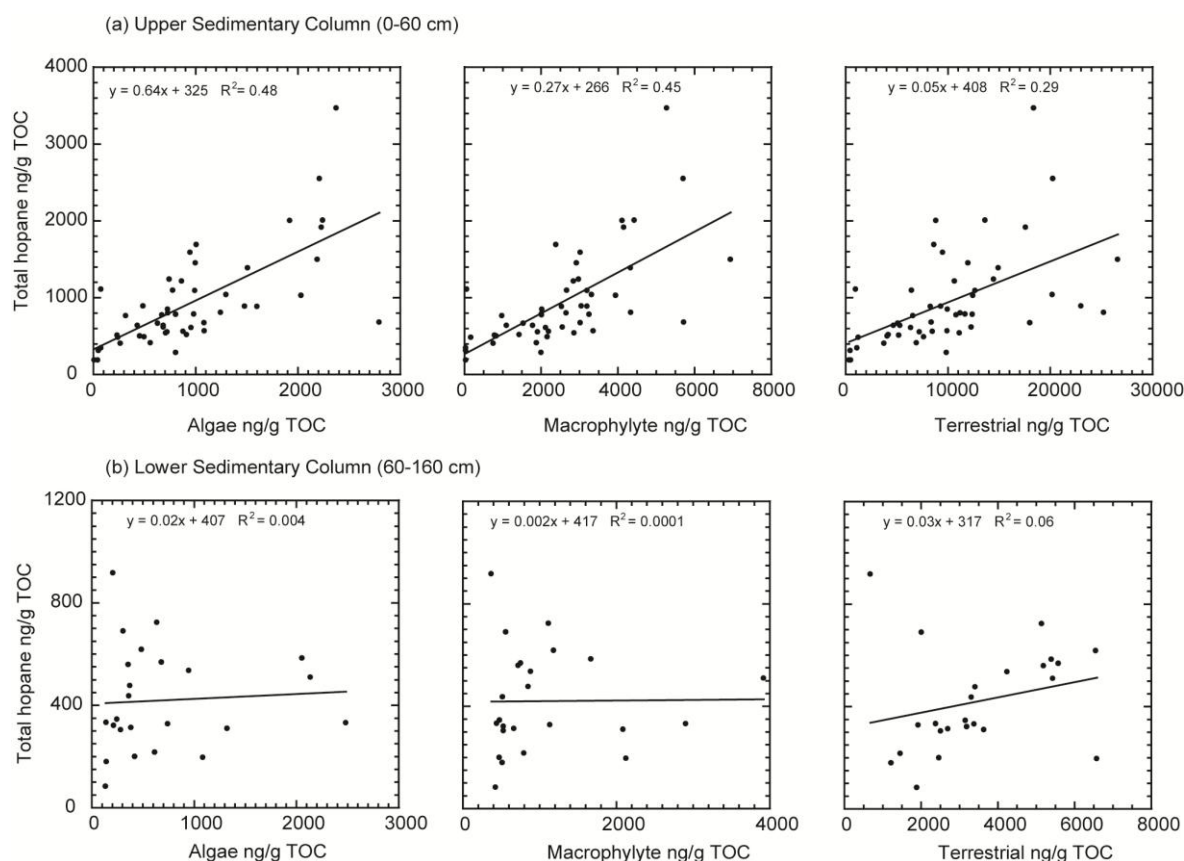


Figure 5.12: Relationship between total hopane vs. algae OMs, macrophytes OMs, and terrestrial OMs in (a) the upper sedimentary succession (0-60 cm) and (b) the lower sedimentary succession (60-160 cm) of the Bolgoda Lake system.

5.3.5.3 Effects of reworking geohopanoids in the recent sediments

The distributions of hopane are associated with the environmental factors. The significant amount of 22S C₃₁ hopane isomer was detected in modern sediments (Tables 4.8 and 4.9). The 22S ($\alpha\beta$) configuration has been predominantly detected in recent marshy peat bogs, lignite and forest soils elsewhere (e.g., Dehmer, 1995; Crossman et al., 2001; Pancost et al., 2003). Previous studies clearly indicate that early diagenetic origin of 22S ($\alpha\beta$) hopane can be formed via acid catalyzed reactions (chemical origin) in modern acidic peat bogs and forest soils (Innes et al., 1997; Pancost et al., 2003; Ishiwatari et al., 2014). In this study, the $\alpha\beta/\beta\beta$ (22S/22R) values are significantly high in the mangrove mud cores (Table 4.9) compared to the Bolgoda Lake surface sediments (Table 4.8). Therefore, C₃₁ hopane 22S/22R ratio may suggest a typical high

acidity in the mangrove dominant swamp sediments. In contrast, hopane C₃₁ 22R and 22S homologues can be frequently identified as biologically- and thermally-derived isomers respectively (Farrimond et al., 1998; Pan et al., 2008).

Thermally-derived 22S hopane in recent sediments can be used as an indicator of reworking OM, oil pollution or seepages. The upper sedimentary succession is characterized by deposition of reworking OM from the watershed area. In this study, no significant increment was observed in the concentration profile of C₃₁ 22S hopane isomer in the upper sedimentary successions (Figure 4.9). Therefore, 22S C₃₁ hopane distributions in core samples may suggest chemical origin rather than thermal origin. The author further examined the effects of reworking OM based on maturity indicating proxies under the normal thermal stress. The 22S/(22S + 22R) isomerization ratio of C₃₁ hopane is a frequently used as a maturity indicator (Farrimond et al., 1998; Pan et al., 2008). Ts [17 α (H)-22, 29, 30-trisnorhopane] and Tm [18 α (H)-22, 29, 30-trisnorhopane] variations in ratio of Ts/(Ts + Tm) can be used to understand maturity under the known OM inputs (Waseda and Nishita, 1998; Inaba et al., 2001; Sawada, 2006). The cross plot of Ts/(Ts + Tm) ratio (0.08-0.66) to C₃₁ hopane 22S/(22S + 22R) ratios (0.13-0.58) indicate relatively good correlation by $Y = 0.77X + 0.01$ ($R^2 = 0.45$, $n = 74$) (Figure 5.13). Therefore, in this study, Ts/(Ts + Tm) ratio can be used to identify reworking OM along with C₃₁ hopane 22S/(22S + 22R) ratios. These proxies do not show a significant increment in the reworking OM abundant upper sedimentary succession (Figure 5.13). Therefore, gradual increment of biologically-inherited C₃₁ 22R isomer suggests a general diagenetic trend with no significant accumulation in reworking bacterial biomarkers (geohopanoids) in the upper sedimentary succession.

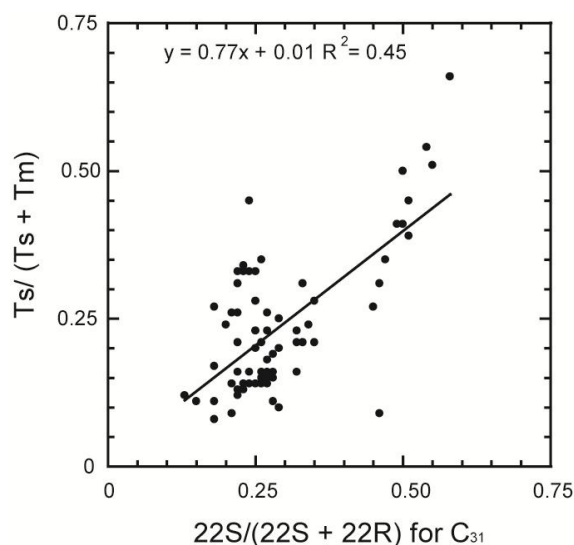


Figure 5.13: Cross plot between $Ts/(Ts + Tm)$ ratio versus C_{31} hopane $22S/(22S + 22R)$ ratio in the Bolgoda Lake system.

5.3.6 Paleoclimate and environment

In this discussion, the author concluded that the OM in the Bolgoda Lake was deposited in two major phases. In addition, two subcategories are recognized in the lower (from ~7.5 ky B.P. to ~2.5 ky B.P.) and upper sedimentary successions (from ~2.5 ky B.P. to the Recent).

In the first phase (before 7 ky B.P.), the OM originated from both algae and land/floating plants with abundant of mangrove plant material. The depositional system was the bay of larger paleoriver in the studied area. In this period, salinity has been increased following highstand of sea-level. Salinity is the most important factors required for the survival of mangroves.

According to many paleoclimatic studies, early to mid-Holocene global climate can be recognized as considerably wetter and warmer than today (Kutzbach et al., 1996; Thompson et al., 2002; Dong et al., 2010; Zheng et al., 2011) with the intensification of NHSM monsoon (Fleitmann et al., 2003; Kumaran et al., 2005). Earth's orbital variations and to solar variability played a key role in the global scale early to mid-Holocene climatic warming and it made a strong teleconnection between low-latitudes and high-latitudes fluctuations (Kutzbach et al., 1996; Fleitmann et al., 2003; Staubwasser et al., 2003; Mayewski et al., 2004). In this second phase (~7 ky B.P. to

~2.5 ky B.P.), OMs were mainly deposited in marine-terrestrial influence. In this period, organic carbon burial (average TOC (%) of Core 1 = 1.82% and Core 2 = 1.57%) and terrestrial OM accumulation (average C/N of Core 1 = 18.6 and Core 2 = 18.7) are relatively high compared to underlie period (average TOC (%) of Core 1 = 1.59% and Core 2 = 1.27% and average C/N of Core 1 = 18.1 and Core 2 = 17.7). The moderate nutrients would be achieved from soil and weathered metamorphic rocks of the Precambrian age.

The nutrient accumulation was predominant in the third phase (after major environmental change) probably due to oxygen-poor semi-closed system based on the low-stand of sea-level. The monsoon strength gradually decreased during the mid- to late-Holocene (Fleitmann et al., 2003; Staubwasser et al., 2003). This change in monsoon activity could have decreased the rainfall in the wet zone of Sri Lanka. In addition, regression of sea-level could have caused the changes of flow path of adjacent larger river systems and erosion of highstand unconsolidated sediments. Significant amount of nutrient from transgressive deposits and reworked peat bogs may reach to the Bolgoda Lake and sink in the newly formed semi-closed system.

The final phase, anthropocene, is characterized by human perturbation may be after the European settlement of Sri Lanka. PAHs distributions evidence the accumulation of both petroleum and wood combustion OM followed by industrialization and urbanization activities of the watershed area dominantly since 15th century.

5.3.7 Future environmental implications

The changes of organic carbon budget, sources of OM and depositional environments of coastal aquatic systems are closely interrelated proxies that can be used to evaluate the degree of environmental perturbation. Therefore, author would like to propose perturbation evolutionary diagram (Figure 5.14) for coastal aquatic systems that helps to understand recent environmental perturbations and aquatic evolution. The diagram indicates the lake consists of oligotrophic to mesotrophic state while northern stream remains stable non-marine freshwater conditions. Therefore, the Bolgoda Lake is acting as a biodiversity rich and relatively stable lake system though it is recorded some environmental deterioration signs. However, continuous and extreme deterioration may cause to achieve eutrophic state of the lake water in future. To date, fertilizer, sewage

discharges and land degradations can be identified as main anthropogenic factors that affecting nutrient budget of the lake. However, continues increases of nutrient from land to the lake in future may convert its from mesotrophic state to eutrophic stage, thereby the CO₂ transfer from the atmosphere to lake water would increase during the daytime owing to promote productivity in aquatic biota (Smith and Hollibaugh, 1993; Ver et al., 1999). However, extreme anthropogenic impacts and river runoff increase can be eventually responsible for the increased production of dissolved inorganic carbon and CO₂ in the lake that generally diminish the ability to act as a sink for atmospheric CO₂ (Ver et al., 1999). Finally, extreme human perturbations would potentially affect to alter phytoplankton assemblage and cause more generalized noxious blooms phenomenon of the lake water (Rabouille et al., 2001; Kemp et al., 2005).

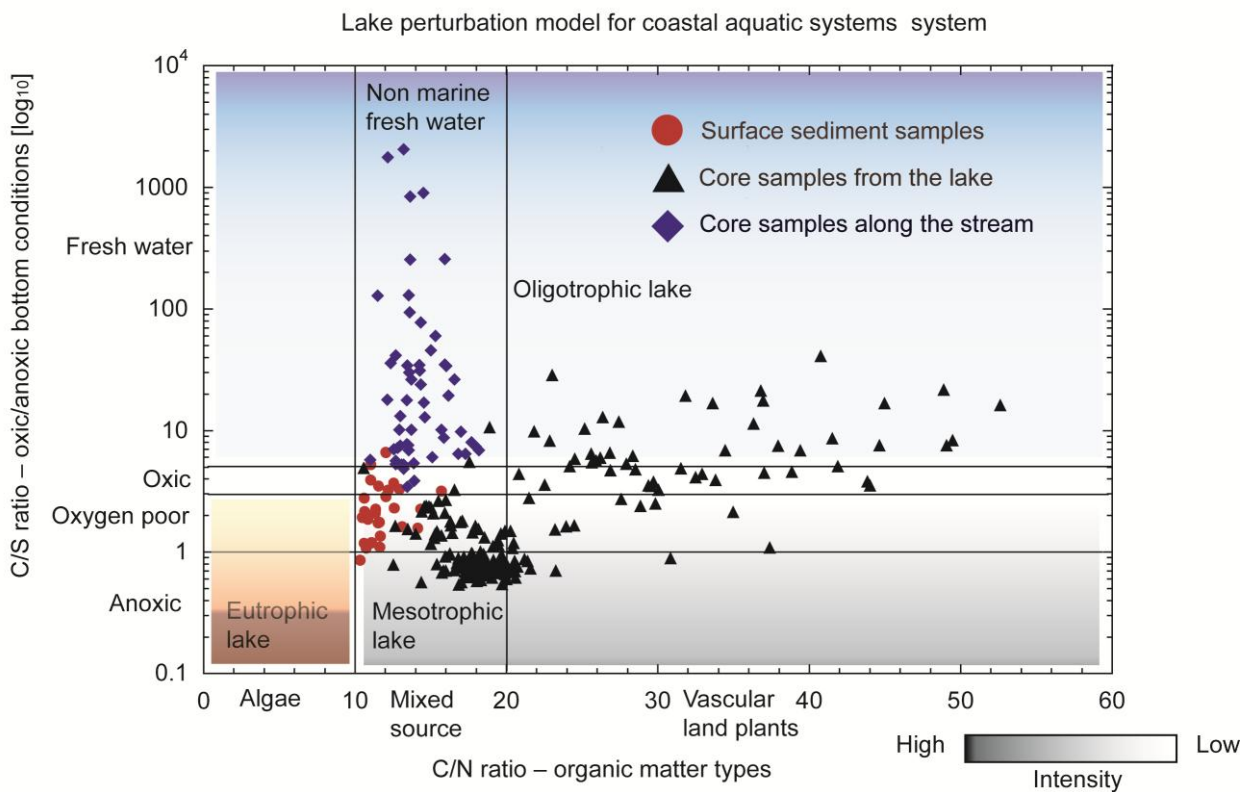


Figure 5.14: Model depicting the relation between sources of organic matter and deposition environment, and the successive stages in the evolution of environmental perturbation

CONCLUSIONS

6.1 The onshore sedimentary basins

Maturity of the Andigama mudstones are low in sterane C_{29} 20S/(20S + 20R) (0.15-0.18) and the Tabbowa sediments are high (0.26-0.45). The Aruwakkalu limestone is 0.30 in sterane C_{29} 20S/(20S + 20R), and Red Earth is over mature about 0.56 provably due to over-matured OM from weathered metamorphic rocks. All sterane C_{29} 20S/(20S + 20R) ratios (X) have an excellent correlation with the maturity parameter of hopane C_{31} 22S/(22S + 22R) ratios (Y) ($Y = 0.40X + 0.40$, $r = 0.949$, $n = 12$), suggesting that sulfurized hopanoids were low abundance. The CPI values are mainly influenced by the contribution of waxy OM but not due to maturity in this study area.

A large proportion of middle chain *n*-alkanes (nC_{21} - C_{25}), enriched C_{29} steranes and high C/N ratios (16.3-37.8) suggest swamp bog-forming origin. Very low TS (<0.001 %) with high TOC (3.05-5.10 %) and higher Pr/Ph ratios (2.1-3.0) suggest freshwater and oxic depositional environment. Abundant Ret, Sim and Pery indicate that the OM was influenced by gymnosperm with fungi in the humid climatic conditions. Predominant 1-MP with 9-MP, 1, 7-DMP and 1, 2, 7- + 1, 2, 9-TMP isomers probably indicate less biodegradable gymnosperm OM.

The Tabbowa basin was filled by sandy sediments and TOC is very low (0.04-0.17 %). However, predominant nC_{16} - C_{21} alkanes with a minor peak of waxy *n*-alkanes (n - C_{29} , n - C_{31} , and n - C_{33}), abundant C_{27} steranes and higher Ts/(Ts + Tm) ratios suggest algal origin with a significant input of terrestrial OM. The fluvial sand grains and very low TS (<0.001 %) distribution suggests lacustrine/fluvial freshwater deposition.

The Miocene limestone shows very low TOC (0.06 %) and algal origin. In the Quaternary Aruwakkalu Red Earth (TOC = 0.41 %), a high UCM, high CPI (4.78) and long average chain length (ACL = 29.9) probably indicate oxidized and/or biodegraded ancient terrestrial OM during possible aeolian process.

6.2 The offshore Mannar Basin

6.2.1 Stratigraphy and lithology

Tectonic activities have been accounted for many of the variables that control sedimentary environment, lithostratigraphy, sedimentation rates and evolutions of the basin as follows.

- (1) Lithostratigraphic columns marked thick sequences of sediments with several cycles of depositions. The Late Cretaceous to Late Paleocene lithology of the Barracuda well recorded mud dominant sediments and interbedded sandstone and volcanogenic materials whereas, the Dorado North well recorded sand dominant sediments and interbedded mudstone. It indicates that the Dorado North well was subjected to relatively high-energy and the Barracuda well was subjected to relatively low-energy depositional settings. These facies can probably represent increased clastics from land and development of deepwater turbidites systems may be due to sea-level changes or sediment gravity flows.
- (2) The Late Maastrichtian sediments of the Barracuda well are marked by thick volcanogenic sediments (ca. 820 m) overlain by calcareous mudstones (ca. 480 m).
- (3) After the Late Paleocene, sedimentary facies drastically changed from calcareous mudstone to argillaceous marl/ marlstone in the both wells. These sedimentary successions were recorded in minor to trace amount of sand.
- (4) The whole sedimentary successions can be divided into two chronozones based on sedimentation rates that are (1) Campanian to Paleocene and (2) Eocene to Miocene. The mud sedimentation rates of the Dorado North well during the Campanian, Maastrichtian and Paleocene are 8 m/Ma, 22 m/Ma and 9 m/Ma, and also in the Barracuda well recorded values are 18 m/Ma, 49 m/Ma and 27 m/Ma respectively. Consequently, significant mud accumulations (more than double) were observed in the Barracuda well during the Campanian to Paleocene. However, mud accumulation is approximately equal in the Dorado North and Barracuda exploration wells during the Eocene (14 m/Ma and 12 m/Ma), Oligocene (25 m/Ma and 29 m/Ma) and Miocene (25 m/Ma and 27 m/Ma) respectively. This considerable shift has been possibly interpreted as changes of arid climate (during the Late Cretaceous and Paleocene) into warm and humid tropical climate (from the Eocene to Miocene) and/ or continuous subsidence of the basin. Therefore, the structural higher flank of the basin (the

Dorado North well) could be more sensitive to regional terrestrial climatic changes and the basin subsidence during the first chronozone. However, in this period, deeper part of the basin (the Barracuda well) is more sensitive to regional marine changes and tectonic process such as igneous activity.

- (5) The highest sedimentation rate of the Mannar Basin was recorded in the Barracuda well during the Maastrichtian. It may be associated with igneous activities of the region. The lowest sedimentation rates of the Barracuda well indicate timing of the collision between Indian and Asian plates during the Eocene.
- (6) Sedimentation rates increased after uplifting of the region during the Oligocene and Miocene. However, unconformities may somewhat decrease the absolute sedimentation rates of the basin.
- (7) Burial history by 1D modeling of the Mannar Basin indicates the rapid subsidence from the Late Cretaceous to the Paleocene during the rift transition stage. Subsidence rate decreased during the Eocene followed by collision between Indian and Asian plates.

6.2.2 Geochemical evaluations

- (1) CaCO_3 rich ($\text{CaCO}_3 > 15\%$) the Late Cretaceous (the Early Campanian to Late Maastrichtian) pelagic sediments could indicate high-productive stages under high $p\text{CO}_2$ level in warm climatic conditions. The Deccan-Reunion basalt (Reunion plume, ~65 Ma) could be acted as a significant contributor to the mass extinction of coccolithophores/ foraminifera indicating that reduction of CaCO_3 and TOC (%) at the Late Maastrichtian sediments. The development of CaCO_3 (approximately $\text{CaCO}_3 > 25\%$) platform since the Late Paleocene could be primarily related to the movement of Indian Plate into northward warmer latitudes (climate transition to tropical conditions). The increment of weathering rates of uplifted the rocks have been suggested as a cause for the gradually increment of carbonate content, OM burial in the basin. Also, it is clearly correlated with Cenozoic global cooling towards the present glaciated Earth.
- (2) The physical properties of sediments significantly controlled organic carbon preservation in the Early-Late Campanian and lower Paleocene sediments of the

Mannar Basin. The separation of Laxmi Ridge-Seychelles (~70 Ma) and Seychelles (~65 Ma) from the Indian plate could be accompanied deposition of organic carbon rich beds during the Late Cretaceous due to changes of drainage in the watershed area. The presence of seasonal monsoon climate has strongly influenced the deposition of organic carbon rich beds since the Middle Oligocene. Therefore, three potential source rock beds were recognized based on TOC (%) values as follows: (1) Early Campanian to Late Maastrichtian sediments of the Dorado North well (thickness ca. 260 m and average TOC = 1.64 ± 0.57), (2) Late Campanian to Late Maastrichtian sediments of the Barracuda well (thickness ca. 270 m and average TOC = 1.34 ± 0.36), and (3) Middle Oligocene to Early Miocene sediments of the Barracuda well (thickness ca. 380 m and average TOC = 2.51 ± 1.20).

- (3) C/N ratios and *m/z* 57 mass chromatograms revealed that algae and swamp (non-woody herbaceous) vegetations dominant sedimentary OMs were deposited in organic carbon poor the lower most Late Cretaceous sediments. The Late Cretaceous organic carbon rich beds could be accompanied with deposition of terrestrial OMs mainly from Sri Lanka landmass (average C/N ratio of Dorado North = 27.13 ± 12.44 and Barracuda = 20.36 ± 7.64). In this succession, molecular constituents of sedimentary OM indicate that land-plant epicuticular waxes (*n*C₂₁-*n*C₃₁) have been important geolipids (gas prone Type-III/II kerogen) to the sediments. The Paleocene sedimentary successions were dominated by algae with some amount of terrestrial components (average C/N ratio of Dorado North = 6.94 ± 3.05 and Barracuda = 15.75 ± 3.19). The distributions of *n*-alkanes (C₂₀-C₂₆/*n*C_{all} average = 0.75 ± 0.15 , >C₂₆/*n*C_{all} average = 0.25 ± 0.15 , ACL average = 26.00 ± 1.28) and sterane (C₂₉ / (C₂₇ + C₂₈ + C₂₉ average = 0.37 ± 0.07) were characterized by terrestrial OMs in inorganic nitrogen rich argillaceous marl/ marlstone from the Late Paleocene to Early Oligocene sediments in the Barracuda well. A significant enhancement of C/N ratio, long-chain *n*-alkanes (> *n*C₂₆) and TOC (%) appear to record increment of seasonal monsoon climate since Early-Middle Miocene.
- (4) C/S values (average of Dorado North = 5.81 ± 3.88 and Barracuda = 6.38 ± 4.93) could indicate oxygen poor depositional environments in organic carbon

poor the lower most Late Cretaceous sediments. The relatively higher C/S ratios (average of Dorado North = 10.80 ± 7.76 and Barracuda = 9.15 ± 3.22) of organic carbon rich sediments indicated that microbial activity were depleted in terrestrial OMs rich sediments. The variations of sedimentary facies and C/S ratios (average of Dorado North = 32.07 ± 20.21 and Barracuda = 16.21 ± 20.14) implied oxic depositional environments during the Early-Late Paleocene due to regression of relative sea-level in this region. The Mannar Basin was characterized by oxygen poor anoxic marine depositional settings from the Late Paleocene. However, C/S ratios of terrestrial OM rich Middle Oligocene to Early Miocene sediments could indicate less sulfate reduction due to effects of OM type.

- (5) Sterane C₂₉ 20S/ (20S + 20R) values suggested relatively higher maturity in the deeper Barracuda well compared to shallower Dorado North well during the Late Cretaceous. Sterane isomers ratios were not significantly enhanced in the sedimentary OMs from the volcanogenic sediments suggesting that partial support to kitchen source. Sterane isomerisation values (0.54-0.56) of the Barracuda samples (3850-3860 m, 4310-4320 m, and 4730-4741 m) reached thermally equilibrium. Sterane C₂₉ 20S/(20S + 20R) values were relatively low in the Paleogene and Neogene sediments of the Barracuda well indicating that decrease in temperature and age of the rocks. However, different trend in the Dorado North well could indicate reworking OMs from Sri Lankan landmass. Also, C₃₁ hopane 22S/(22S + 22R) ratios became misleading maturity indicator in this study due to complexity of OM type and deposition of reworking sediments.

6.3 The coastal Bolgoda Lake

The Bolgoda Lake surface sediments are characterized by OM rich (TOC, 1.3-14.9%), terrestrial and algae mixed (C/N ratio, 10.4-30.0), oxygen poor to anoxic sediments (C/S ratio, 0.9-6.6). The *n*-alkane (Paq, ACL, CPI), oleanane, taraxerone compositions suggest deposition of a significant amount of higher plant wax. The Bolgoda Lake system can be recognized as low-sinuosity braided fluvial system flanked by mangrove dominant swamps along with coastal settings. The interpretation of surface sediments and cores in terms of the position of various organic facies may be

affected by depositional sequences. The lithological successions of Core 1 exhibit intermediate changes in organic geochemical proxies of the Bolgoda Lake.

It is demonstrated that the environment and climate of the Bolgoda Lake watershed area have changed during the last ~7.5 ky B.P. The increment of algae ($n\text{-C}_{20}$) and mangrove (pentacyclic taraxerone) biomarkers are believed to represent a gradual increase in the seawater invasion. The early and mid-Holocene warmer and wetter climatic conditions prevailed to increase a relative proportion of organic carbon burial (average TOC (%) of Core 1 = 1.82% and Core 2 = 1.57%) and accumulation of terrigenous OM (average C/N of Core 1 = 18.60 and Core 2 = 18.72) under the oxygen-poor to anoxic depositional environments in the bay of paleoriver system. Beach rocks/headland barriers were gradually formed owing to rise in eustatic sea-level from the last glacial maximum. The enhancement of algae productivity, TOC (%) and accumulation of terrestrial/ peat fragments in the core samples represented the beginning level of the major environmental change after the mid-Holocene highstands (~2.5 kyr B.P.). During the above mentioned period (from ~7.5 ky B.P. to ~2.5 kyr B.P.), the former drainage basin was submerged and flow path of former larger river was changed. Fluvial dominant brackish lake/ estuary of local streams were formed after the sea-level regression along this coast. The major environmental change is mainly controlled by enrichment of nutrients in the aquatic system even though, under the influence of late-Holocene reduction of monsoon precipitation over the south Asia (e.g., Staubwasser et al., 2003). Similarly, the increment of $n\text{-C}_{29}/n\text{-C}_{\text{all}}$ and $n\text{-C}_{37}/n\text{-C}_{\text{all}}$ ratios could indicate climatic transition from wetter to warmer/dryer conditions since middle Holocene. The greater delivery of nutrients to the lake water can be associated with reworking of transgressive deposits during the late-Holocene. Consequently, individual concentrations of algae, floating/ herbaceous (macrophytes) plants and terrestrial plants were gradually increased in the upper sediment succession of the Bolgoda Lake. In this study, $n\text{-C}_{31}$ n -alkane can be mainly representative of floating plant species with some significant contributions of emergent macrophytes, grass and herbaceous type vegetation in tropical brackish wetlands. PAHs compositions (Fla/Py ratios, 0.80-1.48 and Fla/ (Fla + Py) ratios, 0.45-0.60) reveal that contamination of petroleum and wood combustion OM. Occurrences of Bfla (4-ring) and BePy (5-ring) suggest moderate (>350°C) to high temperature (800-900°C) combustion derived PAHs to the uppermost

anthropogenic lake sediments and mangrove dominant intertidal brackish mud flats since European settlement (15th century).

Sediments of tropical mangrove swamps constitute a large sink of organic carbon when compared to carbon burial in oligotrophic or mesotrophic lakes. The slight increments of TOC with depths in all mangrove mud cores may indicate releasing of soil OM due to the recent increment of NHSM (Anderson et al., 2002; Wang et al., 2012) after the Little Ice Age (Bradley and Jones, 1993; Mann, 2002). In contrast, pentacyclic taraxerone (friedoolean) biomarkers can be used as reconstructions of paleoecological, paleogeographical characteristics such as distribution of mangrove vegetations, tropical/ sub-tropical coastal margins and sea-level changes.

The Bolgoda Lake sediments are increased in n -C₃₁ and n -C₂₉ are significantly abundant within a narrow range. It may suggest that n -alkanes derived from herbaceous plants (grasses, floating plants, shrub type vegetation) are expected to be more dispersed and survived than those from woody terrestrial plants in swamp ecosystems. The compilations of the literature data and new analysis presented here demonstrated that sedimentary OM in tropical brackish and mid- to high-latitude peat bogs produces unique n -alkanes patterns. Therefore, n -alkanes compositions have influenced by environmental factors may be due to metabolic modification or alterations to environmental/ climatic adaptation, possibly in addition to genetic factors. The power of biomarkers for chemotaxonomic purposes can be significantly enhanced by using a combination of several different compounds. Consequently, visualized n -C₂₇, n -C₂₉, and n -C₃₁ n -alkanes distributions in the ternary diagram and mangrove biomarkers (pentacyclic taraxerone) can provide suitable guidelines to reconstruct paleoecological and chemotaxonomical significance of brackish environment in the tropical and sub-tropical regions.

The significant amounts of hopane in the brackish Bolgoda Lake surface sediment (1336.46 ng/g TOC \pm 748.69) indicate prominent bacterial sulfate reduction compared to freshwater sub-areal mangrove sediments (676.37 ng/g TOC \pm 268.48) followed by reactive algae OM type and sulfate availability. Hopane distributions are moderately controlled by OM type in the upper sedimentary succession. However, OM type may not significantly important in the lower sedimentary succession may be due to formations of geohopanoids (macromolecular) during early diagenesis. The variation of

C₃₁ hopane 22S/22R ratio may indicate acidity of soils in the tropical mangrove dominant swamp. The C₃₁ hopane 22S isomer specifies almost constant distribution throughout the whole sedimentary succession suggesting that chemical origin. Hopane distribution in Bologoda Lake is characterized by normal diagenetic evolution rather than preservation of ancient bacterial biomarkers in the upper sedimentary succession.

6.4 General overview

Organic geochemical study on the Jurassic to Quaternary sediments reveals several stages of environmental and climatic transitions in onshore and offshore sedimentary basins of western, Sri Lanka (Figure 6.1). Also, bulk and molecular source indicators evidence that organic carbon burial shows significant correlations with terrestrial OM depositions under wide environmental and climatic variations (Figure 6.2 and 6.3). In detail, sedimentary environments in western Sri Lanka consist of different (1) depositional conditions (onshore, coastal and offshore), (2) geological time (from the Jurassic to Recent), (3) geographical regions (from middle latitude in southern hemisphere to equatorial northern hemisphere), and (4) climatic conditions (warm temperate, arid and tropical). Also, organic carbon preservations can be controlled by number of physical, bio- and geo-chemical factors such as early diagenesis/ microbial alterations, aquatic primary productivity and grain size.

However, changes in the terrestrial biological productivity/ accumulation create variations in the amount of organic carbon burial in these sedimentary basins of Sri Lanka. Also, terrestrial OMs have been microbially reworked before deposition of sedimentary basins and its most durable component survive to become part of the sedimentary record. Therefore, organic carbon burial in sedimentary environments is important to assessing OM sources, for reconstructing environmental and climatic characteristics, and for identifying changes in the availability of nutrients.

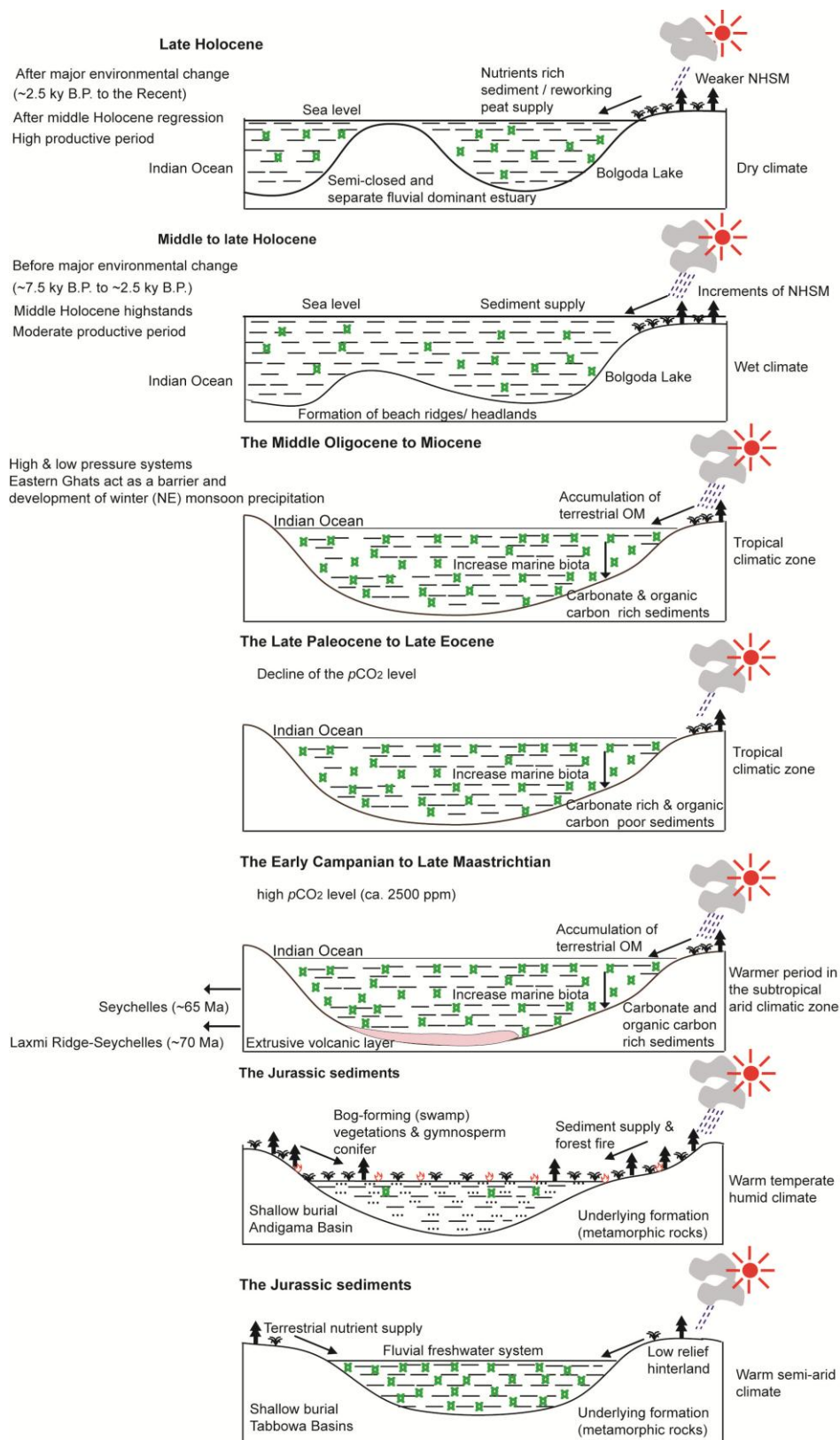


Figure 6.1: Schematic cross-sections for paleoenvironmental and paleoclimate in onshore and offshore sedimentary basins, western Sri Lanka.

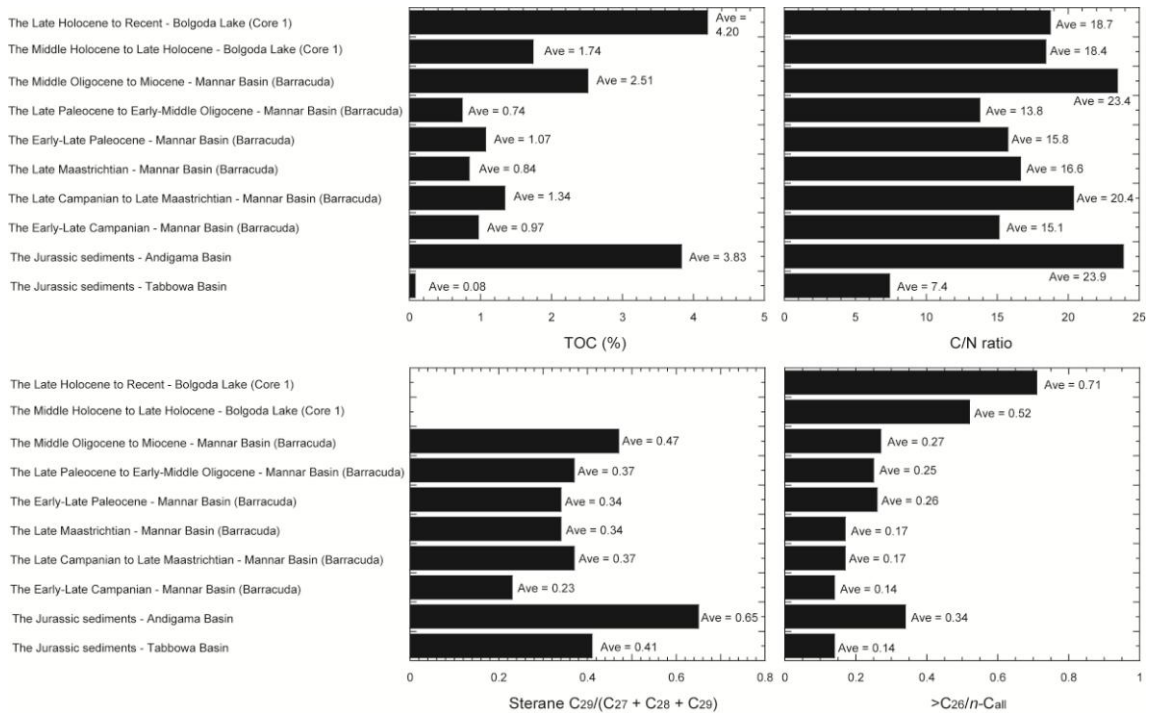


Figure 6.2: Distributions of TOC and bulk and molecular organic source indicators in all sedimentary basins.

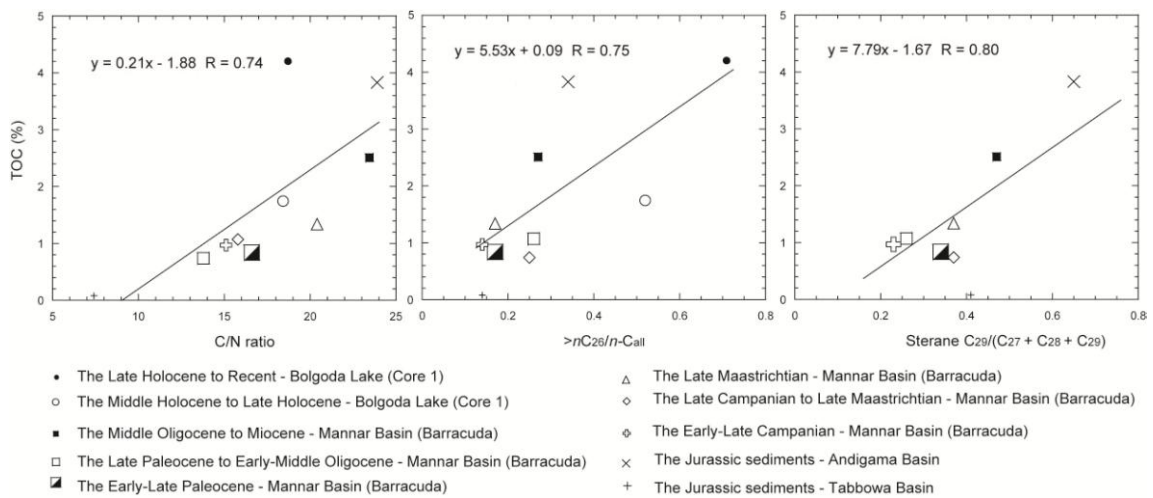


Figure 6.2: Correlations of TOC and bulk and molecular organic source indicators in all sedimentary basins.

References

- Aarssen, B.G.K.V., Alexander, R., Kagi, R.I., 2000. Higher plant biomarkers reflected palaeovegetation changes during Jurassic times. *Geochimica et Cosmochimica Acta* 64, 1417-1424.
- Acharyya, S.K., 2000. Break up of Australia – India – Madagascar block, opening of the Indian Ocean and Continental Accretion in Southeast Asia with special reference to the characteristics of the peri-Indian collision zones. *Gondwana Research* 3(4), 425-443.
- Ahmed, M., Smith, J.W., George, S.C., 1999. Effects of biodegradation on Australian Permian coals. *Organic Geochemistry* 30, 1311-1322.
- Aizenshtat, Z., 1973. Perylene and its geochemical significance. *Geochimica et Cosmochimica Acta* 37, 559-567.
- Ali, H.A.M., Mayes, R.W., Hector, B.L., Orskov, E.R., 2005. Assessment of *n*-alkanes, long-chain fatty alcohols and long-chain fatty acids as diet composition markers: The concentrations of these compounds in rangeland species from Sudan. *Animal Feed Science and Technology* 121, 257-271.
- Ali, J.R., Aitchison, J.C., 2008. Gondwana to Asia: plate tectonics, paleogeography and the biological connectivity of the Indian sub-continent from the Middle Jurassic through latest Eocene (166-35 Ma). *Earth-Science Reviews* 88, 145-166.
- Anderson, D.M., Overpeck, J.T., Gupta, A.K., 2002. Increase in the Asian southwest monsoon during the past four centuries. *Science* 297, 596-599.
- Armstroff, A., Wilkes, H., Schwarzbauer, J., Littke, R., Horsfield, B., 2006. Aromatic hydrocarbon biomarkers in terrestrial organic matter of Devonian to Permian age. *Palaeogeography, Palaeoclimatology, Palaeoecology* 240, 253-274.
- Arthur, M.A., Dean, W.E., Schlanger, S.O., 1985. Variations in the global carbon cycle during the Cretaceous related to climate, volcanism, and changes in atmospheric CO₂. *Geophysical Monograph Series* 32, 504-529.
- Baas, M., Pancost, R., Geel, B.V., Damsté, J.S.S., 2000. A comparative study of lipids in *Sphagnum* species. *Organic Geochemistry* 31, 535-541.
- Bains, S., Corfield, R.M., Norris, R.D., 1999. Mechanisms of climate weathering at the end of the Paleocene. *Science* 285, 724-727.

- Bandaranayake, W.M., 2002. Bioactivities, bioactive compounds and chemical constituents of mangrove plants. *Wetlands Ecology and Management* 10, 421-452.
- Banerjee, P.K., 1993. Imprints of late quaternary climatic and sea level changes on East and South Indian coast. *Geo-Marine Letters* 13, 56-60.
- Banerjee, P.K., 2000. Holocene and Late Pleistocene relative sea level fluctuations along the east coast of India. *Marine Geology* 167, 243-260.
- Baumard, P., Budzinski, H., Garrigues, P., 1998. Polycyclic aromatic hydrocarbons in sediments and mussels of the western Mediterranean Sea. *Environmental Toxicology and Chemistry* 17, 765-776.
- Behling, H., Cohen, M.C.L., Lara, R.J., 2001. Studies on Holocene mangrove ecosystem dynamics of the Braganca Peninsula in north-eastern Para, Brazil. *Palaeogeography, Palaeoclimatology, Palaeoecology* 167, 225-242.
- Bender, 1971. Variations in the $^{13}\text{C}/^{12}\text{C}$ ratios of plants in relation to the pathway of photosynthetic carbon dioxide fixation. *Phytochemistry* 10, 1239-1244.
- Berner, R.A., 1982. Burial of organic carbon and pyrite sulfur in the modern ocean: its geochemical and environmental significance. *American Journal of Science* 282, 451-473.
- Berner, R.A., 1984. Sedimentary pyrite formation: an update. *Geochimica et Cosmochimica Acta* 48, 605-615.
- Berner, R.A., 1985. Sulphate reduction, organic matter decomposition and pyrite formation. *Phil. Trans. R. Soc. Lond A* 315, 25-38.
- Berner, R.A., 1989. Biogeochemical cycles of carbon and sulfur and their effect on atmospheric oxygen over Phanerozoic time. *Palaeogeography, Palaeoclimatology, Palaeoecology* 75, 97-122.
- Berner, R.A., Raiswell, R., 1984. C/S method for distinguishing freshwater from marine sedimentary rocks. *Geology* 12, 365-368.
- Bertrand, S., Sterken, M., Vargas-Ramirez, L., Batist, M.D., Vyverman, W., Lepoint, G., Fagel, N., 2010. Bulk organic geochemistry of sediments from Puyehue Lake and its watershed (Chile, 40°S): implications for paleoenvironmental reconstructions. *Palaeogeography, Palaeoclimatology, Palaeoecology* 294, 56-71.
- Bezabih, M., Pellikaan, W.F., Tolera, A., Hendriks, W.H., 2011. Evaluation of *n*-alkanes and their carbon isotope enrichments ($\delta^{13}\text{C}$) as diet composition markers.

Animal 5, 57-66.

- Bingham, E.M., McClymont, E.L., Välliranta, M., Mauquoy, D., Roberts, Z., Chambers, F.M., Pancost, R.D., Evershed, R.P., 2010. Conservative composition of *n*-alkane biomarkers in *Sphagnum* species: implications for palaeoclimate reconstruction in ombrotrophic peat bogs. *Organic Geochemistry* 41, 214-220.
- Bird, M.I., Fifield, L.K., Teh, T.S., Chang, C.H., Shirlaw, N., Lambeck, K., 2007. An inflection in the rate of early mid-Holocene eustatic sea-level rise: a new sea-level curve from Singapore. *Estuarine, Coastal and Shelf Science* 71, 523-536.
- Boss, S.K., Wilkinson, B.H., 1991. Planktogenic/eustatic control on cratonic/oceanic carbonate accumulation. *The Journal of Geology* 99, 497-513.
- Bourdon, S., Laggoun-Défarge, F., Disnar, J., Maman, O., Guillet, B., Derenne, S., Largeau, C., 2000. Organic matter sources and early diagenetic degradation in a tropical peat marsh (Tritrivakely, Madagascar). Implications for environmental reconstruction during the Sub-Atlantic. *Organic Geochemistry* 31, 421-438.
- Boyd, R., Dalrymple, R.W., Zaitlin, B.A., 2006. Estuarine and incised-valley facies models. *SEPM Special Publication* 84, 171-235.
- Bradley, R.S., Jones, P.D., 1993. 'Little Ice Age' summer temperature variations: their nature and relevance to recent global warming trends. *The Holocene* 3(4), 367-376.
- Bridgham, S.D., Richardson, C.J., 1992. Mechanisms controlling soil respiration (CO₂ and CH₄) in southern peatlands. *Soil Biology and Biochemistry* 24, 1089-1099.
- Brix, H., Sorrell, B.K., Lorenzen, B., 2001. Are *Phragmites*-dominated wetlands a net source or net sink of greenhouse gases?. *Aquatic Botany* 69, 313-324.
- Budzinski, H., Garrigues, P.H., Connan, J., Devillers, J., Domine, D., Radke, M., Oudin, J.L., 1995. Alkylated phenanthrene distributions as maturity and origin indicators in crude oils and rock extracts. *Geochimica et Cosmochimica Acta* 59, 2043-2056.
- Bugge, T., Elvebakk, G., Fanavoll, S., Mangerud, G., Smelror, M., Weiss, H.M., Gjelberg, J., Kristensen, S. E., Nilsen, K., 2002. Shallow stratigraphic drilling applied in hydrocarbon exploration of the Nordkapp Basin, Barents Sea. *Marine and Petroleum Geology* 19, 13-37.
- Bush, R.T., McInerney, F.A., 2013. Leaf wax *n*-alkane distributions in and across modern plants: implications for paleoecology and chemotaxonomy. *Geochimica et*

- Cosmochimica Acta 117, 161-179.
- Caldeira, K., Rampino, M.R., 1993. Aftermath of the end-Cretaceous mass extinction: possible biogeochemical stabilization of the carbon cycle and climate. *Paleoceanography* 8(4), 515-525.
- Camoin, G.F., Montaggioni, L.F., Braithwaite, C.J.R., 2004. Late glacial to post glacial sea levels in the Western Indian Ocean. *Marine Geology* 2004, 119-146.
- Carr, A.S., Boom, A., Grimes, H.L., Chase, B.M., Meadows, M.E., Harris, A., 2014. Leaf wax *n*-alkane distributions in arid zone South African flora: Environmental controls, chemotaxonomy and palaeoecological implications. *Organic Geochemistry* 67, 72-84.
- Castañeda, I.S., Werne, J.P., Johnson, T.C., Filley, T.R., 2009. Late Quaternary vegetation history of southeast Africa: the molecular isotopic record from Lake Malawi. *Palaeogeography, Palaeoclimatology, Palaeoecology* 275, 100-112.
- Castillo, J.B.D., Brooks, C.J.W., Cambie, R.C., Eglinton, G., Hamilton, R.J., Pellitt, P., 1967. The taxonomic distribution of some hydrocarbons in gymnosperms. *Phytochemistry* 6, 391-398.
- Cenki, B., Kriegsman, L.M., 2005. Tectonics of the Neoproterozoic southern granulite terrain, South India. *Precambrian Research* 138, 37-56.
- Chakhmakhchev, A., Suzuki, N., 1995. Aromatic sulfur compounds as maturity indicators for petroleum from the Buzuluk depression, Russia. *Organic Geochemistry* 23, 617-625.
- Chari, M.V.N., Sahu, J.N., Banerjee, B., Zutshi, P.L., Chandra, K., 1995. Evolution of the Cauvery basin, India from subsidence modelling. *Marine and Petroleum Geology* 12(6), 667-675.
- Chatterjee, S., Goswami, A., Scotese, C.R., 2013. The longest voyage: Tectonic, magmatic, and paleoclimatic evolution of the Indian plate during its northward flight from Gondwana to Asia. *Gondwana Research* 23, 238-267.
- Clift, P.D., 2006. Controls on the erosion of Cenozoic Asia and the flux of clastic sediment to the Ocean. *Earth and Planetary Science Letters* 241, 571-580.
- Cooray, P.G., 1984. An introduction to the Geology of Sri Lanka. 2nd revised edition, Ceylon National Museum Publication, Colombo, pp. 135-169.
- Cooray, P.G., 1994. The Precambrian of Sri Lanka: a historical review. *Precambrian*

- Research, 66: 3-18.
- Corrigan, D., Kloos, C., O'Connor, C.S., Timoney, R.F., 1973. Alkanes from four species of *Sphagnum* moss. *Phytochemistry* 12, 213-214.
- Cranwell, P.A., 1990. Paleolimnological studies using sequential lipid extraction from recent lacustrine sediment: recognition of source organisms from biomarkers. *Hydrobiologia* 214, 293-303.
- Crossman, Z.M., McNamara, N., Parekh, N., Ineson, P., Evershed, R.P., 2001. A new method for identifying the origins of simple and complex hopanoids in sedimentary materials using stable isotope labeling with $^{13}\text{CH}_4$ and compound specific stable isotope analyses. *Organic Geochemistry* 32, 359-364.
- Crowley, T.J., 2002. Cycles, cycles everywhere. *Science* 295, 1473-1474.
- Curiale, J.A., Bromley, B.W., 1996. Migration induced compositional changes in oils and condensates of a single field. *Organic Geochemistry* 24 (12), 1097-1113.
- D'Hondt, S., Donaghay, P., Zachos, J.C., Luttenberg, D., Lindinger, M., 1998. Organic carbon fluxes and ecological recovery from the Cretaceous-Tertiary mass extinction. *Science* 282, 276-279.
- Davies, T.A., Kidd, R.B., Ramsay, S.T.S., 1995. A time-slice approach to the history of Cenozoic sedimentation in the Indian Ocean. *Sedimentary Geology* 96, 157-179.
- Dean, W.E., Gorham, E., 1998. Magnitude and significance of carbon burial in lakes, reservoirs, and peat lands. *Geology* 26, 535-538.
- Dehmer, J., 1995. Petrological and organic geochemical investigation of recent peats with known environments of deposition. *International Journal of Coal Geology* 28, 111-138.
- Denis, E.H., Toney, J.L., Tarozo, R., Anderson, R.S., Roach, L.D., Huang, Y., 2012. Polycyclic aromatic hydrocarbons (PAHs) in lake sediments record historic fire events: validation using HPLC-fluorescence detection. *Organic Geochemistry* 45, 7-17.
- Desa, M., Ramana, M.V., Ramprasad, T., 2006. Seafloor spreading magnetic anomalies south off Sri Lanka. *Marine Geology* 229, 227-240.
- Dettman, D.L., Kohn, M.J., Quade, J., Ryerson, F.J., Ojha, T.P., Hamidullah, S., 2001. Seasonal stable isotope evidence for a strong Asian monsoon throughout the past 10.7 m.y.. *Geology* 29(1), 31-34.

- Dickens, A.F., Gélinas, Y., Masiello, C.A., Wakeham, S., Hedges, J.I., 2004. Reburial of fossil organic carbon in marine sediments. *Nature* 427, 336-339.
- Dissanayake, C.B., Chandrajith, R., 1999. Sri Lanka-Madagascar Gondwana linkage: evidence for a Pan-African mineral belt. *The Journal of Geology* 107, 223-235.
- Dissanayake, C.B., Senaratne, A., Gunatilaka, L.A.A., 1982. Organic geochemical studies of the Muthurajawela peat deposit of Sri Lanka. *Organic Geochemistry* 4, 19-26.
- Dong, H., Jiang, H., Yu, B., Liu, X., Zhang, C., 2010. Impacts of environmental change and human activity on microbial ecosystems on the Tibetan Plateau, NW China. *GSA Today* 20, 4-10.
- Dutta, P., 2002. Gondwana lithostratigraphy of Peninsular India. *Gondwana Research* 5, 540-553.
- Dypvik, H., Riber, L., Burca, F., Rütger, D., Jargvoll, D., Nagy, J., Jochmann, M., 2011. The Paleocene-Eocene thermal maximum (PETM) in Svalbard – clay mineral and geochemical signals. *Palaeogeography, Palaeoclimatology, Palaeoecology* 302, 156-169.
- Edirisooriya, G., Dharmagunawardhane, H.A., 2013. Plant insect-interactions in Jurassic fossil flora from Sri Lanka. *International Journal of Scientific and Research Publications* 3 (1), 1-13.
- Eglinton, G., Hamilton, R.J., 1967. Leaf epicuticular waxes. *Science* 156, 1322-1335.
- Eglinton, T.I., Benitez-Nelson, B.C., Pearson, A., McNichol, A.P., Bauer, J.E., Druffel, E.R.M., 1997. Variability in radiocarbon ages of individual organic compounds from marine sediments. *Science* 277, 796-799.
- Ei Mon Han, Sampei, Y., Roser, B., 2014. Upper Eocene coal and coaly shale in the Central Myanmar Basin: origin of organic matter and the effect of weathering. *Geochemical Journal* 48, 1-17.
- Engelhart, S.E., Horton, B.P., Roberts, D.H., Bryant, C.L., Corbett, D.R., 2007. Mangrove pollen of Indonesia and its suitability as a sea-level indicator. *Marine Geology* 242, 65-81.
- Ercegovac, M., Kostić, A., 2006. Organic facies and palynofacies: nomenclature, classification and applicability for petroleum source rock evaluation. *International Journal of Coal Geology* 68, 70-78.

- Fabiańska, M.J., Stanislaw, R., Ćmiel, S.R., Misz-Kennan, M., 2013. Biomarkers and aromatic hydrocarbons in bituminous coals of Upper Silesian Coal Basin: Example from 405 coal seam of the Zaleskie Beds (Poland). *International Journal of Coal Geology* 107, 96-111.
- Farhaduzzaman, Md., Abdullah, W.H., Islam, Md.A., 2012. Depositional environment and hydrocarbon source potential of the Permian Gondwana coals from the Barapukuria Basin, Northwest Bangladesh. *International Journal of Coal Geology* 90-91, 162-179.
- Farrimond, P., Love, G.D., Bishop, A.N., Innes, H.E., Watson, D.F., Snape, C.E., 2003. Evidence for the rapid incorporation of hopanoids into kerogen. *Geochimica et Cosmochimica Acta* 67, 1383-1394.
- Farrimond, P., Taylor, A., Telnaes, N., 1998. Biomarker maturity parameters: the role of generation and thermal degradation. *Organic Geochemistry* 29, 1181-1197.
- Feakins, S.J., Sessions, A.L., 2010. Controls on the D/H ratios of plant leaf waxes in an arid ecosystem. *Geochimica et Cosmochimica Acta* 74, 2128-2141.
- Ficken, K.J., Barber, K.E., Eglinton, G., 1998. Lipid biomarker, $\delta^{13}\text{C}$ and plant macrofossil stratigraphy of a Scottish montane peat bog over the last two millennia. *Organic Geochemistry* 28, 217-237.
- Ficken, K.J., Li, B., Swain, D.L., Eglinton, G., 2000. An *n*-alkane proxy for the sediment input of submerged/ floating freshwater aquatic macrophytes. *Organic Geochemistry* 31, 745-749.
- Finkelstein, D.B., Pratt, L.M., Curtin, T.M., Brassell, S.C., 2005. Wildfires and seasonal aridity recorded in Lake Cretaceous strata from south-eastern Arizona, USA. *Sedimentology* 52, 587-599.
- Fleitmann, D., Burns, S.J., Mudelsee, M., Neff, U., Kramers, J., Mangini, A., Matter, A., 2003. Holocene forcing of the Indian monsoon recorded in a stalagmite from southern Oman. *Science* 300, 1737-1739.
- Fleming, K., Johnston, P., Zwart, D., Yokoyama, Y., Lambeck, K., Chappell, J., 1998. Refining the eustatic sea-level curve since the Last Glacial Maximum using far- and intermediate-field sites. *Earth and Planetary Science Letters* 163, 327-342.
- France-Lanord, C., Derry, L.A., 1997. Organic carbon burial forcing of the carbon cycle from Himalayan erosion. *Nature* 390, 65-67.

- Fricke, H.C., Clyde, W.C., O'Neil, J.R., Gingerich, P.D., 1998. Evidence for rapid climate change in North America during the latest Paleocene thermal maximum: oxygen isotope compositions of biogenic phosphate from the Bighorn Basin (Wyoming). *Earth and Planetary Science Letters* 160, 193-208.
- Friis, E.M., Pedersen, K.R., Crane, P.R., 2006. Cretaceous angiosperm flowers: Innovation and evolution in plant reproduction. *Palaeogeography, Palaeoclimatology, Palaeoecology* 232, 251-293.
- Frysjnger, G.S., Gaines, R.B., Xu, L., Reddy, C.M., 2003. Resolving the unresolved complex mixture in petroleum-contaminated sediments. *Environmental Science Technology* 37, 1653-1662.
- Gaina, C., Müller, R.D., Brown, B., Ishihara, T., Ivanov, S., 2007. Breakup and early spreading between India and Antarctica. *Geophysical Journal International* 170, 151-169.
- Gao, X., Chen, S., Xie, X., Long, A., Ma, F., 2007. Non-aromatic hydrocarbons in surface sediments near the Pearl River estuary in the South China Sea. *Environmental Pollution* 148, 40-47.
- Goldner, A., Herold, N., Huber, M., 2014. Antarctic glaciations caused ocean circulation changes at the Eocene-Oligocene transition. *Nature* 511, 574-577.
- Gong, C., Hollander, D.J., 1997. Differential contribution of bacteria to sedimentary organic matter in oxic and anoxic environments, Santa Monica Basin, California. *Organic Geochemistry* 26, 545-563.
- Grice, K., Alexander, R., Kagi, R.I., 2000. Diamondoid hydrocarbon ratios as indicator of biodegradation in Australian crude oils. *Organic geochemistry* 31, 67-73.
- Grice, K., Nabbefeld, B., Maslen, E., 2007. Source and significance of selected polycyclic aromatic hydrocarbons in sediments (Hovea-3 well, Perth Basin, Western Australia) spanning the Permian-Triassic boundary. *Organic Geochemistry* 38, 1795-1803.
- Grimalt, J.O., Drooge, B.L.V., Ribes, A., Fernández, P., Appleby, P., 2004. Polycyclic aromatic hydrocarbon composition in soils and sediments of high altitude lakes. *Environmental Pollution* 131, 13-24.
- Grosjean, E., Logan, G.A., Rollet, N., Ryan, G.J., Glenn, K., 2007. Geochemistry of shallow tropical marine sediments from the Arafura Sea, Australia. *Organic*

- Geochemistry 38, 1953-1971.
- GSMB, 1996. Colombo-Ratnapura 1:100,000 geological sheet (provisional series), Colombo, Geological Surveys and Mines Bureau, Sri Lanka.
- Guo, Z.T., Ruddiman, W.F., Hao, Q.Z., Wu, H.B., Qiao, Y.S., Zhu, R.X., Peng, S.Z., Wei, J.J., Yuan, B.Y., Liu, T.S., 2002. Onset of Asian desertification by 22 Myr ago inferred from loess deposits in China. *Nature* 416, 159-163.
- Gupta, A.K., Singh, R.K., Joseph, S., Thomas, E., 2004. Indian Ocean high-productivity event (10-8 Ma): linked to global cooling or to the initiation of the Indian monsoons?. *Geology* 32(9), 753-756.
- Hakimi, M.H., Abdullah, W.H., Shalaby, M.R., 2010. Source rock characterization and oil generating potential of the Jurassic Madbi Formation, onshore East Shabowah oilfields, Republic of Yemen. *Organic Geochemistry* 41, 513-521.
- Hameed, A., Achyuthan, H., Sekhar, B., 2006. Radiocarbon dates and Holocene sea-level change along the Cuddalore and Odinur Coast, Tamil Nadu. *Research Communications* 91 (3), 362-367.
- Harding, I.C., Charles, A.J., Marshall, J.E.A., Pälike, H., Roberts, A.P., Wilson, P.A., Jarvis, E., Thorne, R., Morris, E., Moremon, R., Pearce, R.B., Akbari, S., 2011. Sea-level and salinity fluctuations during the Paleocene-Eocene thermal maximum in Arctic Spitsbergen. *Earth and Planetary Science Letters* 303, 97-107.
- Harris, N., 2006. The elevation history of the Tibetan Plateau and its implications for the Asian monsoon. *Palaeogeography, Palaeoclimatology, Palaeoecology* 241, 4-15.
- Harris, N.B.W., Bartlett, J.M., Santosh, M., 1996. Neodymium isotope constraints on the tectonic evolution of East Gondwana. *Journal of Southeast Asian Earth Sciences* 14, 119-125.
- Hashimi, N.H., Nigam, R., Nair, R.R., Rajagopalan, G., 1995. Holocene sea level fluctuations on western Indian continental margin: an update. *Journal Geological Society of India* 46, 157-162.
- Haven, H.L.T., Leeuw, J.W.D., Rullkötter, J., Damsté, J.S.S., 1987. Restricted utility of the pristane/phytane ratio as a palaeoenvironmental indicator. *Nature* 330, 641-643.
- Heimann, M., Reichstein, M., 2008. Terrestrial ecosystem carbon dynamics and climate feedbacks. *Nature* 451, 289-292.
- Hoffmann, B., Kahmen, A., Cernusak, L.A., Arndt, S.K., Sachse, D., 2013. Abundance

- and distribution of leaf wax *n*-alkanes in leaves of Acacia and Eucalyptus trees along a strong humidity gradient in northern Australia. *Organic Geochemistry* 62, 62-67.
- Hossain, H.M.Z., Sampei, Y., Hossain, Q.H., Roser, B.P., Islam, M.S.U., 2013a. Characterization of alkyl phenanthrene distributions in Permian Gondwana coals and coaly shales from the Barapukuria Basin, NW Bangladesh. *Researches in Organic Geochemistry* 29, 17-28.
- Hossain, H.M.Z., Sampei, Y., Roser, B.P., 2009. Characterization of organic matter and depositional environment of Tertiary mudstones from the Sylhet Basin, Bangladesh. *Organic Geochemistry* 40, 743-754.
- Hossain, H.M.Z., Sampei, Y., Roser, B.P., 2013b. Polycyclic aromatic hydrocarbons (PAHs) in late Eocene to early Pleistocene mudstones of the Sylhet succession, NE Bengal Basin, Bangladesh: Implications for source and paleoclimate conditions during Himalayan uplift. *Organic Geochemistry* 56, 25-39.
- Hu, X., Jansa, L., Wang, C., Sarti, M., Bak, K., Wagreich, M., Michaik, J., Soták, J., 2005. Upper cretaceous oceanic red beds (CORBs) in the Tethys: occurrences, lithofacies, age and environments. *Cretaceous Research* 26, 3-20.
- Huang, H., Bowler, B.F.J., Oldenburg, T.B.P., Larter, S.R., 2004. The effect of biodegradation on polycyclic aromatic hydrocarbons in reservoir oils from the Liaohe basin, NE China. *Organic Geochemistry* 35, 1619-1634.
- Huang, W.Y., Meinschein, W.G., 1979. Sterols as ecological indicators. *Geochimica et Cosmochimica Acta* 43, 739-745.
- Huang, Y., Street-Perrott, F.A., Metcalfe, S.E., Brenner, M., Moreland, M., Freeman, K.H., 2001. Climate change as the dominant control on glacial-interglacial variations in C₃ and C₄ plant abundance. *Science* 293, 1647-1651.
- Ibach, L.E.J., 1982. Relationship between sedimentation rate and total organic carbon content in ancient marine sediments. *American Association of Petroleum Geologists Bulletin* 66, 170-188.
- Inaba, T., Suzuki, N., Hirai, A., Sekiguchi, K., Watanabe, T., 2001. Source rock lithology prediction based on oil diacholestane abundance in the siliceous-clastic Akita sedimentary basin, Japan. *Organic Geochemistry* 32, 877-890.
- Inagaki, F., Nunoura, T., Nakagawa, S., Teske, A., Lever, M., Lauer, A., Suzuki, M., Takai, K., Delwiche, M., Colwell, F.S., Nealson, K.H., Horikoshi, K., D'Hondt, S.,

- Jørgensen, B.B., 2006. Biogeographical distribution and diversity of microbes in methane hydrate-bearing deep marine sediments on the Pacific Ocean margin. *PNAS* 103, 2815-2820.
- Innes, H.E., Bishop, A.N., Head, I.M., Farrimond, P., 1997. Preservation and diagenesis of hopanoids in Recent lacustrine sediments of Priest Pot, England. *Organic Geochemistry* 26, 565-576.
- Ishiwatari, R., Uemura, H., Yamamoto, S., 2014. Hopanoid hydrocarbons and perylene in Lake Biwa (Japan) sediments: Environmental control on their abundance and molecular composition. *Organic Geochemistry* 76, 194-203.
- Islam, M.S., Tooley, M.J., 1999. Coastal and sea-level changes during the Holocene in Bangladesh. *Quaternary International* 55, 61-75.
- Jaffé, R., Rushdi, A.I., Medeiros, P.M., Simoneit, B.R.T., 2006. Natural product biomarkers as indicators of sources and transport of sedimentary organic matter in a subtropical river. *Chemosphere* 64, 1870-1884.
- Jandl, R., Lindner, M., Vesterdal, L., Bauwens, B., Baritz, R., Hagedorn, F., Johnson, D.W., Minkinen, K., Byrne, 2007. How strongly can forest management influence soil carbon sequestration?. *Geoderma* 137, 253-268.
- Jayatissa, L.P., Dahdouh-Guebas, F., Koedam, N., 2002. A review of the floral composition and distribution of mangrove in Sri Lanka. *Botanical Journal of the Linnean Society* 138, 29-43.
- Jeng, W.L., 2006. Higher plant *n*-alkane average chain length as an indicator of petrogenic hydrocarbon contamination in marine sediments. *Marine Chemistry* 102, 242-251.
- Jia, G., Peng, P., Zhao, Q., Jian, Z., 2003. Changes in terrestrial ecosystem since 30Ma in East Asia: Stable isotope evidence from black carbon in the South China Sea. *Geology* 31, 1093-1096.
- Jiang, C., Alexander, R., Kagi, R.I., Murray, A.P., 1998. Polycyclic aromatic hydrocarbons in ancient sediments and their relationships to palaeoclimate. *Organic Geochemistry* 29, 1721-1735.
- Jiang, C., Alexander, R., Kagi, R.I., Murray, A.P., 2000. Origin of perylene in ancient sediments and its geological significance. *Organic Geochemistry* 31, 1545-1559.
- Jones, D.M., Douglas, A.G., Parkes, R.J., Taylor, J., Giger, W., Schaffner, C., 1983.

- The recognition of biodegraded petroleum-derived aromatic hydrocarbons in recent marine sediments. *Marine Pollution Bulletin* 14 (3), 103-108.
- Kaiho, K., Kajiwara, Y., Tazaki, K., Ueshima, M., Takeda, N., Kawahata, H., Arinobu, T., Ishiwatari, R., Hirai, A., Lamolda, M.A., 1999. Oceanic primary productivity and dissolved oxygen levels at the Cretaceous/Tertiary boundary: their decrease, subsequent warming, and recovery. *Paleoceanography* 14(4), 511-524.
- Katupotha, J., 1988. Evolution of coastal landforms in the western part of Sri Lanka. *Geographical Sciences* 43(1), 18-36.
- Katupotha, J., 1994. Quaternary research in Sri Lanka. *Journal of the Geological Society of Sri Lanka* 5, 141-152.
- Katupotha, J., Fujiwara, K., 1988. Holocene sea level change on the southwest and south coasts of Sri Lanka. *Palaeogeography, Palaeoclimatology, Palaeoecology* 68, 189-203.
- Katz, M.B., 2000. Sri Lanka – India intraplate tectonics – Precambrian to Present. *Gondwana Research* 3, 3-5.
- Keller, G., Adatte, T., Gardin, S., Bartolini, A., Bajpai, S., 2008. Main Deccan volcanism phase ends near the K-T boundary: evidence from the Krishna-Godavari Basin, SE India. *Earth and Planetary Science Letters* 268, 293-311.
- Kemp, W.M., Boynton, W.R., Adolf, J.E., Boesch, D.F., Boicourt, W.C., Brush, G., Cornwell, J.C., Fisher, T.R., Glibert, P.M., Hagy, J.D., Haring, L.W., Houde, E.D., Kimmel, D.G., Miller, W.D., Newell, R.I.E., Roman, M.R., Smith, E.M., Stevenson, J.C., 2005. Eutrophication of Chesapeake Bay: historical trends and ecological interactions, *Marine Ecology Progress Series* 303, 1-29.
- Kench, P.S., Smithers, S.G., McLean, R.F., Nichol, S.L., 2009. Holocene reef growth in the Maldives: evidence of a mid-Holocene sea-level highstand in the central Indian Ocean. *Geology* 37, 455-458.
- Kent, D.V., Muttoni, G., 2008. Equatorial convergence of India and early Cenozoic climate trends. *PNAS* 105, 16065-16070.
- Kent, R.W., Pringle, M.S., Müller, D., Saunders, A.D., Ghose, N.C., 2002. ⁴⁰Ar/³⁹Ar Geochronology of the Rajmahal Basalts, India, and their relationship to the Kerguelen Plateau. *Journal of Petrology* 43, 1141-1153.
- Killops, S.D., Frewin, N.L., 1994. Triterpenoid diagenesis and cuticular preservation.

- Organic Geochemistry 21, 1193-1209.
- Koch, B.P., Filho, P.W.M.S., Behling, H., Cohen, M.C.L., Kattner, G., Rullkötter, J., Scholz-Böttcher, B., Lara, R.J., 2011. Triterpenols in mangrove sediments as a proxy for organic matter derived from the red mangrove (*Rhizophora mangle*). *Organic Geochemistry* 42, 62-73.
- Koch, B.P., Harder, J., Lara, R.J., Kattner, G., 2005. The effect of selective microbial degradation on the composition of mangrove derived pentacyclic triterpenols in surface sediments. *Organic Geochemistry* 36, 273-285.
- Köster, J., van Kaam-Peters, H.M.E., Koopmans, M.P., de Leeuw, J.W., Damsté, J.S.S., 1997. Sulphurisation of homohopanooids: Effects on carbon number distribution, speciation and 22S/22R epimer ratios. *Geochimica et Cosmochimica Acta* 61, 2431-2452.
- Krauss, K.W., Cahoon, D.R., Allen, J.A., Ewel, K.C., Lynch, J.C., Cormier, N., 2010. Surface elevation change and susceptibility of different mangrove zones to sea-level rise on Pacific high islands of Micronesia. *Ecosystems* 13, 129-143.
- Kumaran, K.P.N., Nair, K.M., Shindikar, M., Limaye, R.B., Padmalal, D., 2005. Stratigraphical and palynological appraisal of the Late Quaternary mangrove deposits of the west coast of India. *Quaternary Research* 64, 418-431.
- Kutzbach, J., Bonan, G., Foley, J., Harrison, S.P., 1996. Vegetation and soil feedbacks on the response of the African monsoon to orbital forcing in the early to middle Holocene. *Nature* 384, 623-626.
- Lallier-Verges, E., Perrussel, B.P., Disnar, J.R., Baltzer, F., 1998. Relationships between environmental conditions and the diagenetic evolution of organic matter derived from higher plants in a modern mangrove swamp system (Guadeloupe, French West Indies). *Organic Geochemistry* 29, 1663-1686.
- Lécuyer, C., Reynard, B., Martineau, F., 2004. Stable isotope fractionation between mollusc shells and marine water from Martinique Island. *Chemical Geology* 213, 293-305.
- Levenson, A.I., 1970. *Geology of Petroleum*, W.H. Freeman and Cooperation.
- Lipp, J.S., Morono, Y., Inagaki, F., Hinrichs, K., 2008. Significant contribution of Archaea to extant biomass in marine subsurface sediments. *Nature* 454, 991-994.
- Lourens, L.J., Sluijs, A., Kroon, D., Zachos, J.C., Thomas, E., Röhl, U., Bowles, J.,

- Raffi, I., 2005. Astronomical pacing of late Palaeocene to early Eocene global warming events. *Nature* 435, 1083-1086.
- Maccougall, J.D., 1988. Seawater strontium isotopes, acid rain, and the Cretaceous-Tertiary boundary. *Science* 239, 485-487.
- Mann, M.E., 2002. Little Ice Age. *The Earth System: physical and chemical dimensions of global environmental change* 1, 504-509.
- Marynowski, L., Smolarek, J., Bechtel, A., Philippe, M., Kurkiewicz, S., Simoneit, B.R.T., 2013. Perylene as an indicator of conifer fossil wood degradation by wood-degrading fungi. *Organic Geochemistry* 59, 143-151.
- Marynowski, L., Wyszomirski, P., 2008. Organic geochemical evidences of early-diagenetic oxidation of the terrestrial organic matter during the Triassic arid and semi arid climatic conditions. *Applied Geochemistry* 23, 2612-2618.
- Maslen, E., Grice, K., Métayer, P.L., Dawson, D., Edwards, D., 2011. Stable carbon isotopic compositions of individual aromatic hydrocarbons as source and age indicators in oils from western Australian basins. *Organic Geochemistry* 42, 387-398.
- Mayewski, P.A., Rohling, E.E., Stager, J.C., Karlén, W., Maasch, K.A., Meeker, L.D., Meyerson, E.A., Gasse, F., Kreveld, S.V., Holmgren, K., Lee-Thorp, J., Rosqvist, G., Rack, F., Staubwasser, M., Schneider, R.R., Steig, E.J., 2004. Holocene climate variability. *Quaternary Research* 62, 243-255.
- Métivier, F., Gaudemer, Y., Tapponnier, P., Klein, M., 1999. Mass accumulation rates in Asia during the Cenozoic. *Geophysical Journal International* 137, 280-318.
- Meyers, P.A., 1997. Organic geochemical proxies of paleoceanographic, paleolimnologic, and paleoclimatic processes. *Organic Geochemistry* 27, 213-250.
- Meyers, P.A., 2003. Applications of organic geochemistry to paleolimnological reconstructions: a summary of examples from the Laurentian Great Lakes. *Organic Geochemistry* 34, 261-289.
- Meyers, P.A., Bourbonniere, R.A., Takeuchi, N., 1980. Hydrocarbons and fatty acids in two cores of Lake Huron sediments. *Geochimica et Cosmochimica Acta* 44, 1215-1221.
- Meyers, P.A., Ishiwatari, R., 1993. Lacustrine organic geochemistry—an overview of indicators of organic matter sources and diagenesis in lake sediments. *Organic*

- Geochemistry 20, 867-900.
- Meyers, P.A., Takemura, K., 1997. Quaternary changes in delivery and accumulation of organic matter in sediments of Lake Biwa, Japan. *Journal of Paleolimnology* 21, 345-372.
- Molnar, P., England, P., 1990. Late Cenozoic uplift of mountain ranges and global climate change: chicken or egg?. *Nature* 346, 29-34.
- Molnar, P., Pardo-Casas, F., Stock, J., 1988. The Cenozoic and Late Cretaceous evolution of the Indian Ocean Basin: uncertainties in the reconstructed positions of the India, Africa and Antarctic plates. *Basin Research* 1, 23-40.
- Molnar, P., Tapponnier, P., 1975. Cenozoic tectonics of Asia: effects of a continental collision. *Science* 189, 419-426.
- Montaggioni, L.F., Faure, G., 1997. Response of reef coral communities to sea-level rise: a Holocene model from Mauritius (Western Indian Ocean). *Sedimentology* 44, 1053-1070.
- Moran, K., Backman, J., Brinkhuis, H., Clemens, S.C., Cronin, T., Dickens, G.R., Eynaud, F., Gattacceca, J., Jakobsson, M., Jordan, R.W., Kaminski, M., King, J., Koc, N., Krylov, A., Martinez, N., Matthiessen, J., McInroy, D., Moore, T.C., Onodera, J., O'Regan, M., Pälike, H., Rea, B., Rio, D., Sakamoto, T., Smith, D.C., Stein, R., John, K.S., Suto, I., Suzuki, N., Takahashi, K., Watanabe, M., Yamamoto, M., Farrell, J., Frank, M., Kubik, P., Jokat, W., Kristoffersen, Y., 2006. The Cenozoic palaeoenvironment of the Arctic Ocean. *Nature* 441, 601-605.
- Mügler, I., Sachse, D., Werner, M., Xu, B., Wu, G., Yao, T., Gleixner, G., 2008. Effect of lake evaporation on δD values of lacustrine *n*-alkanes: a comparison of Nam Co (Tibetan Plateau) and Holzmaar (Germany). *Organic Geochemistry* 39, 711-729.
- Müller, P.J., 1977. C/N ratios in Pacific deep-sea sediments: effect of inorganic ammonium and organic nitrogen compounds sorbed by clays. *Geochimica et Cosmochimica Acta* 41, 765-776.
- Murphy, M.A., Yin, A., Harrison, T.M., Dürr, S.B., Chen, Z., Ryerson, F.J., Kidd, W.S.F., Wang, X., Zhou, X., 1997. Did the Indo-Asian collision along create the Tibetan Plateau?. *Geology* 25, 719-722.
- Nakada, M., Lambeck, K., 1988. The melting history of the late Pleistocene Antarctic ice sheet. *Nature* 333, 36-40.

- Nakamura, H., Sawada, K., and Takahashi, M., 2010. Aliphatic and aromatic terpenoid biomarkers in Cretaceous and Paleogene angiosperm fossils from Japan. *Organic Geochemistry* 41, 975-980.
- Nichols, J.E., Booth, R.K., Jackson, S.T., Pendall, E.G., Huang, Y., 2006. Paleohydrologic reconstruction based on *n*-alkane distributions in ombrotrophic peat. *Organic Geochemistry* 37, 1505-1513.
- Nikolić, B., Tešević, V., Đorđević, I., Jarđranin, M., Todosijević, M., Bojović, S., Marin, P.D., 2010. *n*-Alkanes in the needle waxes of *Pinus heldreichii* var. *pančići*. *Journal of the Serbian Chemical Society* 75, 1337-1346.
- Nittrouer, C.A., Brunskill, G.J., Figueiredo, A.G., 1995. Importance of tropical coastal environments. *Geo-Marine Letters* 15, 121-126.
- Nott, C.J., Xie, S., Avsejs, L.A., Maddy, D., Chambers, F.M., Evershed, R.P., 2000. *n*-Alkane distributions in ombrotrophic mires as indicators of vegetation change related to climatic variation. *Organic Geochemistry* 31, 231-235.
- O'Brien, S.R., Mayewski, P.A., Meeker, L.D., Meese, D.A., Twickler, M.S., Whitlow, S.I., 1995. Complexity of Holocene climate as reconstructed from a Greenland ice core. *Science* 270, 1962-1964.
- Otto, A., Simoneit, B.R.T., Rember, W.C., 2005. Conifer and angiosperm biomarkers in clay sediments and fossil plants from the Miocene Clarkia Formation, Idaho, USA. *Organic Geochemistry* 36, 907-922.
- Otto, A., Simoneit, B.R.T., Wilde, V., Kunzmann, L., Püttmann, W., 2002. Terpenoid composition of three fossil resins from Cretaceous and Tertiary conifers. *Review of Palaeobotany and Palynology* 120, 203-215.
- Pälike, H., Norris, R.D., Herrle, J.O., Wilson, P.A., Coxall, H.K., Lear, C.H., Shackleton, N.J., Tripathi, A.K., Wade, B.S., 2006. The heartbeat of the Oligocene climate system. *Science* 314, 1894-1898.
- Pan, C., Peng, D., Zhang, M., Yu, L., Sheng, G., Fu, J., 2008. Distribution and isomerization of C₃₁-C₃₅ homohopanes and C₂₉ steranes in Oligocene saline lacustrine sediments from Qaidam Basin, Northwest China. *Organic Geochemistry* 39, 646-657.
- Pancost, R.D., Baas, M., Geel, B.V., Damsté, J.S.S., 2003. Response of an ombrotrophic bog to a regional climate event revealed by macrofossil, molecular

- and carbon isotopic data. *The Holocene* 13, 921-932.
- Pearson, P.N., Palmer, M.R., 2000. Atmospheric carbon dioxide concentrations over the past 60 million years. *Nature* 406, 695-699.
- Petersen, H.I., Sherwood, N., Mathiesen, A., Fyhn, M.B.W., Dau, N.T., Russell, N., Bojesen-Koefoed, J.A., Nielsen, L.H., 2009. Application of integrated vitrinite reflectance and FAMM analyses for thermal maturity assessment of the northeastern Malay Basin, offshore Vietnam: Implications for petroleum prospectivity evaluation. *Marine and Petroleum Geology* 26, 319-332.
- Piedad-Sánchez, N., Suárez-Ruiz, I., Martínez, L., Izart, A., Elie, M., Keravis, D., 2004. Organic petrology and geochemistry of the Carboniferous coal seams from the Central Austrian Coal Basin (NW Spain). *International Journal of Coal Geology* 57, 211-242.
- Powell, C.M., Roots, S.R., Veevers, J.J., 1988. Pre-breakup continental extension in east Gondwanaland and the early opening of the eastern Indian Ocean. *Tectonophysics* 155, 261-283.
- Qiang, C., Jiaren, Y., Wei, W., Wanzhing, S., Chunfeg, C., 2009. Preliminary prediction and evaluation on source rock in low exploration basin – a case study from the northeast depression, South Yellow Sea Basin, East China. *Journal of Earth Science* 20, 836-847.
- Quade, J., Cerling, T.E., Bowman, J.R., 1989. Development of Asian monsoon revealed by marked ecological shift during the latest Miocene in northern Pakistan. *Nature* 342, 163-166.
- Rabouille, C., Mackenzie, F.T., Ver, L.M., 2001. Influence of the human perturbation on carbon, nitrogen, and oxygen biogeochemical cycles in the global coastal ocean. *Geochimica et Cosmochimica Acta* 65, 3615-3641.
- Radhakrishna, T., Mathew, J., 1996. Late Precambrian (850-800 Ma) palaeomagnetic pole for the south Indian shield from the Harohalli alkaline dykes: geotectonic implications for Gondwana reconstruction. *Precambrian Research* 80, 77-87.
- Radke, M., and Welte, D.H., 1983. The methylphenanthrene index (MPI): a maturity parameter based on aromatic hydrocarbons. In: Bjørøy, M. et al. (Eds.), *Advances in Organic Geochemistry 1981*. John Wiley and Sons, New York, pp. 504-512.
- Radke, M., Welte, D.H., Willsch, H., 1986. Maturity parameters based on aromatic

- hydrocarbons: Influence of the organic matter type. In: Leythaeuser D., Rullkötter J. (Eds.), *Advances in Organic Geochemistry 1985*. John Wiley and Sons, New York, pp. 51-63.
- Ralison, O.H., Borges, A.V., Dehairs, F., Middelburg, J.J., Bouillon, S., 2008. Carbon biogeochemistry of the Betsiboka estuary (north-western Madagascar). *Organic Geochemistry* 39, 1649-1658.
- Ramana, M.V., Ramprasad, T., Desa, M., 2001. Seafloor spreading magnetic anomalies in the Enderby Basin, East Antarctica, *Earth Planet Science Letter*, 191: 241-255.
- Ramsay, P.J., 1995. 9000 years of sea-level change along the southern African coastline. *Quaternary International* 31, 71-75.
- Ramstein, G., Fluteau, F., Besse, J., Joussaume, S., 1997. Effect of orogeny, plate motion and land-sea distribution on Eurasian climate change over the past 30 million years. *Nature* 386, 788-795.
- Ranasinghe, P.N., Ortiz, J.D., Moore, A.L., McAdoo, B., Wells, N., Siriwardana, C.H.E.R., Wijesundara, D.T.D.S., 2013. Mid-late Holocene coastal environmental changes in southeastern Sri Lanka: new evidence for sea-level variations in southern Bay of Bengal, *Quaternary International* 298, 20-36.
- Rao, G.N., 2001. Sedimentation, stratigraphy and petroleum potential of Krishna-Godavari Basin, East Coast of India. *AAPG Bulletin*, 85 (9): 1623-1643.
- Rao, M.V., Chidambaram, L., Bharktya, D., Janardhanan, M., 2010. Integrated analysis of Late Albian to Middle Miocene sediments in Gulf of Mannar shallow waters of the Cauvery Basin, India: a sequence stratigraphic approach. Hyderabad, 1-9.
- Ratnayake, N.P., Sampei, Y., Tokuoka, T., Suzuki, N., Ishida, H., 2005. Anthropogenic impacts recorded in the sediments of Lunawa, a small tropical estuary, Sri Lanka. *Environmental Geology* 48, 139-148.
- Ratnayake, N.P., Suzuki, N., Okada, M., Takagi, M., 2006. The variations of stable carbon isotope ratio of land plant-derived *n*-alkanes in deep-sea sediments from the Bering Sea and the North Pacific Ocean during the last 250,000 years. *Chemical Geology* 228, 197-208.
- Ridgwell, A., Zeebe, R.E., 2005. The role of the global carbonate cycle in the regulation and evolution of the Earth system. *Earth and Planetary Science Letters* 234, 299-315.

- Rohmer, M., Bouvier-Nave, P., Ourisson, G., 1984. Distribution of hopanoid triterpenes in Prokaryotes. *Journal of General Microbiology* 130, 1137-1150.
- Rommerskirchen, F., Plader, A., Eglinton, G., Chikaraishi, Y., Rullkötter, J., 2006. Chemotaxonomic significance of distribution and stable carbon isotopic composition of long-chain alkanes and alkan-1-ols in C₄ grass waxes. *Organic Geochemistry* 37, 1303-1332.
- Ronkainen, T., McClymont, E.L., Väiliranta, M., Tuittila, E.S., 2013. The *n*-alkane and sterol composition of living fen plants as a potential tool for palaeoecological studies. *Organic Geochemistry* 59, 1-9.
- Rose, K., Boswell, R., Collett, T., 2011. Mount Elbert gas hydrate stratigraphic test well, Alaska north slope: coring operations, core sedimentology, and lithostratigraphy. *Marine and Petroleum Geology* 28, 311-331.
- Sampei, Y., Matsumoto, E., 2001. C/N ratios in a sediment core from Nakaumi Lagoon, southwest, Japan. *Geochemical Journal* 35, 189-205.
- Sampei, Y., Matsumoto, E., Dettman, D.L., Tokuoka, T., Abe, O., 2005. Paleosalinity in a brackish lake during the Holocene based on stable oxygen and carbon isotopes of shell carbonate in Nakaumi Lagoon, southwest Japan. *Palaeogeography, Palaeoclimatology, Palaeoecology* 224, 352-366.
- Sampei, Y., Matsumoto, E., Kamei, T., Tokuoka, T., 1997a. Sulfur and organic carbon relationship in sediments from coastal brackish lakes in the Shimane Peninsula District, southwest, Japan. *Geochemical Journal* 31, 245-262.
- Sampei, Y., Matsumoto, E., Tokuoka, T., Inoue, D., 1997b. Changes in accumulation rate of organic carbon during the last 8000 years in sediments of Nakaumi Lagoon, Japan. *Marine Chemistry* 58, 39-50.
- Sampei, Y., Suzuki, N., Mori, K., Nakai, T., Sekiguchi, K., 1994. Methylphenanthrenes from the MITI Takada-heiya well and thermally altered Kusanagi shales by dolerite intrusion in Northeast Japan. *Geochemical Journal* 28, 317-331.
- Sawada, K., 2006. Organic facies and geochemical aspects in Neogene neritic sediments of the Takafu syncline area of central Japan: paleoenvironmental and sedimentological reconstructions. *Island Arc* 15, 517-536.
- Sawada, K., Nakamura, H., Arai, T., Tsukagoshi, M., 2013. Evaluation of paleoenvironment using terpenoid biomarkers in lignites and plant fossil from the

- Miocene Tokiguchi Porcelain Clay Formation at the Onada mine, Tajimi, central Japan. *International Journal of Coal Geology* 107, 78-89.
- Schellekens, J., Buurman, P., 2011. *n*-Alkane distributions as palaeoclimatic proxies in ombrotrophic peat: the role of decomposition and dominant vegetation. *Geoderma* 164, 112-121.
- Schwark, L., Zink, K., Lechterbeck, J., 2002. Reconstruction of postglacial to early Holocene vegetation history in terrestrial Central Europe via cuticular lipid biomarkers and pollen records from lake sediments. *Geology* 30, 463-466.
- Scotese, C.R., Illich, H., Zumberge, J., Brown, S., Moore, T., 2011. The GANDOLPH Project: Year Four Report: Paleogeographic and Paleoclimatic Controls on Hydrocarbon Source Rock Deposition, A Report on the Methods Employed, the Results of the Paleoclimate Simulations (FOAM), and Oils/Source Rock Compilation for the Oligocene (30 Ma), Cretaceous/Tertiary (70 Ma), Permian/Triassic (250 Ma), Silurian/ Devonian (400 Ma), and Cambrian/Ordovician (480 Ma), Conclusions at the End of Year Four, April 2011. GeoMark Research Ltd., Houston, Texas. 219 pp.
- Scott, A.C., 2000. The Pre-Quaternary history of fire. *Palaeogeography, Palaeoclimatology, Palaeoecology* 164, 297-345.
- Shaw, R.D., 2002. TGS-NOPEC SL01-Phase one offshore Sri Lanka seismic survey interpretation report. New South Global Pty Ltd: 1-45.
- Silliman, J.E., Meyers, P.A., Bourbonniere, R.A., 1996. Records of postglacial organic matter delivery and burial in sediments of Lake Ontario. *Organic Geochemistry* 24, 463-472.
- Silliman, J.E., Meyers, P.A., Eadie, B.J., 1998. Perylene: an indicator of alteration processes or precursor materials?. *Organic Geochemistry* 29, 1737-1744.
- Simoneit, B.R.T., 2005. A review of current applications of mass spectrometry for biomarker/molecular tracer elucidation. *Mass Spectrometry Reviews* 24, 719-765.
- Siriwardena, P.P.G.S.N., Perera, W.K.T., 1986. Topography and substratum of Bolgoda Lake. *Journal of Inland Fish* 4, 15-25.
- Smith, S.V., Hollibaugh, J.T., 1993. Coastal metabolism and the oceanic organic carbon balance. *Reviews of Geophysics* 31, 75-89.
- Southon, J., Kashgarian, M., Fontugne, M., Metivier, B., Yim, W.W.S., 2002. Marine

- reservoir correlations for the Indian Ocean and Southeast Asia. *Radiocarbon* 44 (1), 167-180.
- Sreejith, K.M., Krishna, K.S., Bansal, A.R., 2008. Structure and isostatic compensation of the Comorin Ridge, north central Indian Ocean. *Geophysical Journal International* 175, 729-741.
- Staubwasser, M., Sirocko, F., Grootes, P.M., Segl, M., 2003. Climate change at the 4.2 ka BP termination of the Indus valley civilization and Holocene south Asian monsoon variability. *Geophysical Research Letters* 30, 1-4.
- Stefanova, M., Ivanov, D., Yaneva, N., Marinov, S., Grasset, L., Amblès, A., 2008. Palaeoenvironmental assessment of Pliocene Lom lignite (Bulgaria) from bitumen analysis and preparative off line thermochemolysis. *Organic Geochemistry* 39, 1589-1605.
- Storey, M., Mahoney, J.J., Saunders, A.D., Duncan, R.A., Kelley, S.P., Coffin, M.F., 1995. Timing of hot spot-related volcanism and the breakup of Madagascar and India. *Science* 267, 852-855.
- Stout, S.A., Emsbo-Mattingly, S.D., 2008. Concentration and character of PAHs and other hydrocarbons in coals of varying rank – implication for environmental studies of soils and sediments containing particular coal. *Organic Geochemistry* 39, 801-819.
- Subrahmanyam, C., Chand, S., 2006. Evolution of the passive continental margins of India – a geophysical appraisal. *Gondwana Research* 10, 167-178.
- Subroto, E.A., Alexander, R., Kagi, R.I., 1991. 30-Norhopanes: their occurrence in sediments and crude oils. *Chemical Geology* 93, 179-192.
- Sun, M.Y., Wakeham, S.G., 1998. A study of oxic/ anoxic effects on degradation of sterols at the simulated sediment-water interface of coastal sediments. *Organic Geochemistry* 28, 773-784.
- Suzuki, N., Yessalina, S., Kikuchi, T., 2010. Probable fungal origin of perylene in Late Cretaceous to Paleogene terrestrial sedimentary rocks of northeastern Japan as indicated from stable carbon isotopes. *Organic Geochemistry* 41, 234-241.
- Szczerba, M., Rospondek, M.J., 2010. Controls on distributions of methylphenanthrenes in sedimentary rock extracts: critical evaluation of existing geochemical data from molecular modelling. *Organic Geochemistry* 41, 1297-1311.

- Tantawy, A.A.A., Keller, G., Pardo, A., 2009. Late Maastrichtian volcanism in the Indian Ocean: effects on calcareous nannofossils and planktic foraminifera. *Palaeogeography, Palaeoclimatology, Palaeoecology* 284, 63-87.
- Tantrigoda, D.A., Geekiyanage, P., 1991. An interpretation of gravity anomalies over the Andigama and Tabbowa sedimentary basins in north-west of Sri Lanka. *Journal of the National Science Council of Sri Lanka* 19 (1), 39-51.
- Taylor, K.A., Harvey, H.R., 2011. Bacterial hopanoids as tracers of organic carbon sources and processing across the western Arctic continental shelf. *Organic Geochemistry* 42, 487-497.
- Taylor, K.C., Lamorey, G.W., Doyle, G.A., Alley, R.B., Grootes, P.M., Mayewski, P.A., White, J.W.C., Barlow, L.K., 1993. The 'flickering switch' of late Pleistocene climate change. *Nature* 361, 432-436.
- Thompson, L.G., Mosley-Thompson, E., Davis, M.E., Henderson, K.A., Brecher, H.H., Zagorodnov, V.S., Mashiotta, T.A., Lin, P., Mikhaleiko, V.N., Hardy, D.R., Beer, J., 2002. Kilimanjaro ice core records: evidence of Holocene climate change in tropical Africa. *Science* 298, 589-593.
- Tjia, H.D., 1996. Sea-level changes in the tectonically stable Malay-Thai Peninsula. *Quaternary International* 31, 95-101.
- Torsvik, T.H., Tucker, R.D., Ashwal, L.D., Eide, E.A., Rakotosolof, N.A., Wit, M.J.D., 1998. Late Cretaceous magmatism in Madagascar: palaeomagnetic evidence for a stationary Marion hotspots. *Earth and Planetary Science Letters* 164, 221-232.
- Toscano, M.A., Macintyre, I.G., 2003. Correlated western Atlantic sea-level curve for the last 11,000 years based on calibrated ^{14}C dates from *Acropora palmata* framework and intertidal mangrove peat. *Coral Reefs* 22, 257-270.
- Tsunogae, T., Santosh, M., Ohyama, H., Sato, K., 2008. High-pressure and ultrahigh-temperature metamorphism at Komateri, northern Madurai Block, southern India. *Journal of Asian Earth Sciences* 33, 395-413.
- Twilley, R.R., Chen, R.H., Hargis, T., 1992. Carbon sinks in mangroves and their implications to carbon budget of tropical coastal ecosystems. *Water, Air, and Soil Pollution* 64, 265-288.
- Valdés, J., Sifeddine, A., Lallier-Verges, E., Ortlieb, L., 2004. Petrographic and geochemical study of organic matter in surficial laminated sediments from an

- upwelling system (Mejillones del Sur Bay, Northern Chile). *Organic Geochemistry* 35, 881-894.
- Vandenbroucke, M., Largeau, C., 2007. Kerogen origin, evolution and structure. *Organic Geochemistry* 38, 719-833.
- Ver, L.M.B., Mackenzie, F.T., Lerman, A., 1999. Carbon cycle in the coastal zone: effects of global perturbations and change in the past three centuries. *Chemical Geology* 159, 283-304.
- Versteegh, G.J.M., Schefuß, E., Dupont, L., Marret, F., Damste, J.S.S., Jansen, J.H.F., 2004. Taraxerol and Rhizophora pollen as proxies for tracking past mangrove ecosystems. *Geochimica et Cosmochimica Acta* 68, 411-422.
- Vogts, A., Moossen, H., Rommerskirchen, F., Rullkötter, J., 2009. Distribution patterns and stable carbon isotopic composition of alkanes and alkan-1-ols from plant waxes of African rain forest and savanna C₃ species. *Organic Geochemistry* 40, 1037-1054.
- Volk, T., 1989. Sensitivity of climate and atmospheric CO₂ to deep-ocean and shallow-ocean carbonate burial. *Nature* 337, 637-640.
- Volkman, J.K., 2003. Sterols in microorganisms. *Applied Microbiology and Biotechnology* 60, 495-506.
- Volkman, J.K., Holdsworth, D.G., Neill, G.P., Bavor Jr, H.J., 1992. Identification of natural, anthropogenic and petroleum hydrocarbons in aquatic sediments. *The Science of the Total Environment* 112, 203-219.
- Volkman, J.K., Revill, A.T., Bonham, P.I., Clementson, L.A., 2007. Sources of organic matter in sediments from the Ord River in tropical northern Australia. *Organic Geochemistry* 38, 1039-1060.
- Volkman, J.K., Rohjans, D., Rullkötter, J., Scholz-Böttcher, B.M., Liebezeit, G., 2000. Sources and diagenesis of organic matter in tidal flat sediments from the German Wadden Sea. *Continental Shelf Research* 20, 1139-1158.
- Vonhof, H.B., Smit, J., 1997. High-resolution late Maastrichtian-early Danian ocean ⁸⁷Sr/⁸⁶Sr record: implications for Cretaceous-Tertiary boundary events. *Geology* 25, 347-350.
- Wakeham, S.G., Lee, C., Hedges, J.I., Hernes, P.J., Peterson, M.L., 1997. Molecular indicators of diagenetic status in marine organic matter. *Geochimica et*

- Cosmochimica Acta 61, 5363-5369.
- Wang, B., Liu, J., Kim, H.J., Webster, P.J., Yim, S.Y., 2012. Recent change of the global monsoon precipitation (1979-2008). *Climate Dynamics* 39, 1123-1135.
- Wang, C., Hu, X., Huang, Y., Wapreisch, M., Scott, R., Hay, W., 2011. Cretaceous oceanic red beds as possible consequence of oceanic anoxic events. *Sedimentary Geology* 235, 27-37.
- Wang, C., Hu, X., Sarti, M., Scott, R.B., Li, X., 2005. Upper Cretaceous oceanic red beds in southern Tibet: a major change from anoxic to oxic, deep-sea environments. *Cretaceous Research* 26, 21-32.
- Wang, Z., Fingas, M., 1997. Developments in the analysis of petroleum hydrocarbons in oils, petroleum products and oil-spill-related environmental samples by gas chromatography. *Journal of Chromatography A* 774, 51-78.
- Wanner, H., Beer, J., Bütikofer, J., Crowley, T.J., Cubasch, U., Flückiger, J., Goosse, H., Grosjean, M., Joos, F., Kaplan, J.O., Küttel, M., Müller, S.A., Prentice, I.C., Solomina, O., Stocker, T.F., Tarasov, P., Wagner, M., Widmann, M., 2008. Mid- to Late Holocene climate change: an overview. *Quaternary Science Reviews* 27, 1791-1828.
- Wannigama, G.P., Volkman, J.K., Gillan, F.T., Nichols, P.D., Johns, R.B., 1981. A comparison of lipid components of the fresh and dead leaves and pneumatophores of the mangrove *Avicennia Marina*. *Phytochemistry* 20, 659-666.
- Waseda, A., Nishita, H., 1998. Geochemical characteristics of terrigenous- and marine-sourced oils in Hokkaido, Japan. *Organic Geochemistry* 28, 27-41.
- Watts, A.B., Karner, G.D., Steckler, M.S., 1982. Lithospheric flexure and the evolution of sedimentary basins. *Philosophical Transactions of the Royal Society of London Series A*, 305: 249-281.
- Watts, A.B., Thorne, J., 1984. Tectonics, global changes in sea level and their relationship to stratigraphical sequences at the US Atlantic continental margin. *Marine and Petroleum Geology* 1, 319-339.
- Weerakkody, U., 1988. Mid-Holocene sea level changes in Sri Lanka. *Journal of the National Science Council of Sri Lanka* 16(1), 23-37.
- Weerakkody, U., 1992. Geomorphology of the southern coastal plain. *Journal of the National Science Council of Sri Lanka* 20(2), 251-263.

- Weijers, J.W.H., Schouten, S., Sluijs, A., Brinkhuis, H., Damsté, J.S.S., 2007. Warm arctic continents during the Paleocene-Eocene thermal maximum. *Earth and Planetary Science Letters* 261, 230-238.
- Wickramagamage, P., 2011. Evolution of the Kalu Ganga – Bolgoda Ganga flood plain system, Sri Lanka. *Journal of the Geological Society of Sri Lanka* 14, 41-53.
- Woodroffe, S.A., Horton, B.P., 2005. Holocene sea-level changes in the Indo-Pacific. *Journal of Asian Earth Sciences* 25, 29-43.
- World Petroleum Resources Project, 2011. Assessment of undiscovered oil and gas resources of the Assam, Bombay, Cauvery, and Krishna-Godavari geological provinces, South Asia. United State Geological Survey, 1-4. <http://www.usgs.gov/science/cite-view.php?cite=2949>
- Xie, S., Lai, X., Yi, Y., Gu, Y., Liu, Y., Wang, X., Liu, G., Liang, B., 2003. Molecular fossils in a Pleistocene river terrace in southern China related to paleoclimate variation. *Organic Geochemistry* 34, 789-797.
- Yan, B., Abrajano, T.A., Bopp, R.F., Benedict, L.A., Chaky, D.A., Perry, E., Song, J., Keane, D.P., 2006. Combined application of $\delta^{13}\text{C}$ and molecular ratios in sediment cores for PAH source apportionment in the New York/ New Jersey harbor complex. *Organic Geochemistry* 37, 674-687.
- Yokoyama, Y., Lambeck, K., De Deckker, P., Johnston, P., Fifield, L.K., 2000. Timing of the last Glacial Maximum from observed sea level minima. *Nature* 406, 713-716.
- Yunker, M.B., Lachmuth, C.L., Cretney, W.J., Fowler, B.R., Dangerfield, N., White, L., Ross, P.S., 2011. Biota – sediments partitioning of aluminium smelter related PAHs and pulp mill related diterpenes by intertidal clams at Kitimat, British Columbia. *Marine Environmental Research* 72, 105-126.
- Yunker, M.B., Macdonald, R.W., 2003. Alkane and PAH depositional history, sources and fluxes in sediments from the Fraser River Basin and Strait of Georgia, Canada. *Organic Geochemistry* 34, 1429-1454.
- Yunker, M.B., Macdonald, R.W., Vingarzan, R., Mitchell, R.H., Goyette, D., Sylvestre, S., 2002. PAHs in the Fraser River basin: a critical appraisal of PAH ratio as indicators of PAH source and composition. *Organic Geochemistry* 33, 489-515.
- Zachos, J., Pagani, M., Sloan, L., Thomas, E., Billups, K., 2001. Trends, rhythms, and aberrations in global climate 65 Ma to present. *Science* 292, 686-693.

- Zachos, J.C., Arthur, M.A., Dean, W.E., 1989. Geochemical evidence for suppression of pelagic marine productivity at the Cretaceous/Tertiary boundary. *Nature* 337, 61-64.
- Zachos, J.C., Dickens, G.R., Zeebe, R.E., 2008. Early Cenozoic perspective on greenhouse warming and carbon-cycle dynamics. *Nature* 451, 279-283.
- Zachos, J.C., Röhl, U., Schellenberg, S.A., Sluijs, A., Hodell, D.A., Kelly, D.C., Thomas, E., Nicolo, M., Raffi, I., Lourens, L.J., McCarren, H., Kroon, D., 2005. Rapid acidification of the ocean during the Paleocene-Eocene thermal maximum. *Science* 308, 1611-1615.
- Zhang, Z., Zhao, M., Yang, X., Wang, S., Jiang, X., Oldfield, F., Eglinton, G., 2004. A hydrocarbon biomarker record for the last 40 kyr of plant input to Lake Heping, southwestern China. *Organic Geochemistry* 35, 595-613.
- Zheng, Y., Zhou, W., Liu, X., Zhang, C.L., 2011. *n*-Alkan-2-one distributions in a northern eastern China peat core spanning the last 16 kyr. *Organic Geochemistry* 42, 25-30.
- Zhisheng, An., Kutzbach, J.E., Prell, W.L., Porter, S.C., 2001. Evolution of Asian monsoons and phased uplift of the Himalaya-Tibetan plateau since Late Miocene times. *Nature* 411, 62-66.
- Zhou, W., Xie, S., Meyers, P.A., Zheng, Y., 2005. Reconstruction of late glacial and Holocene climate evolution in southern China from geolipids and pollen in the Dingnan peat sequence. *Organic Geochemistry* 36, 1272-1284.
- Zhu, Y., Li, Y., Zhou, J., Gu, S., 2012. Geochemical characteristics of Tertiary coal-bearing source rocks in Xihu depression, East China Sea basin. *Marine and Petroleum Geology* 35, 154-165.
- Zong, Y., 2004. Mid-Holocene sea-level highstand along the Southeast Coast of China. *Quaternary International* 117, 55-67.

Appendix



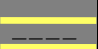


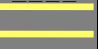
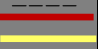

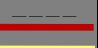
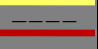
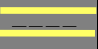
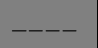
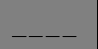



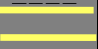

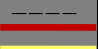
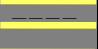


Core description – Dorado North exploration well

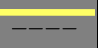




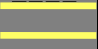
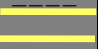
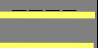
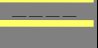





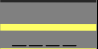

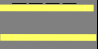

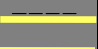



Location: Mannar Basin

Water depth: 1346.4 m

Age	Depth / m	Lithology		Remarks
Late Eocene	2200 – 2210	Marlstone	~ ~	Interbedded with thin black color mudstone
	2210 – 2220	Marlstone	~ ~	Interbedded with thin black color mudstone
	2220 – 2230	Marlstone	~ ~	Interbedded with thin black color mudstone
	2230 – 2240	Marlstone	~ ~	Interbedded with thin black color mudstone
Middle Eocene	2240 – 2250	Marlstone	~ ~	Interbedded with thin black color mudstone
	2250 – 2260	Marlstone	~ ~	Interbedded with thin black color mudstone
	2260 – 2270	Marlstone	~ ~	Interbedded with thin black color mudstone
	2270 – 2280	Marlstone	~ ~	Interbedded with thin black color mudstone
	2280 – 2290	Marlstone	~ ~	Interbedded with thin black color mudstone
	2290 – 2300	Marlstone	~ ~	Interbedded with thin black color mudstone
	2300 – 2310	Argillaceous marl/ marlstone	~ ~	Interbedded with thin black color mudstone
	2310 – 2320	Argillaceous marl/ marlstone	~ ~	Interbedded with thin black color mudstone
	2320 – 2330	Argillaceous marl/ marlstone	~ ~	Interbedded with thin black color mudstone
	2330 – 2340	Argillaceous marl/ marlstone	~ ~	Interbedded with thin black color mudstone, pebble present
(?) Early-Middle Eocene	2340 – 2350	Argillaceous marl/ marlstone	~ ~	Interbedded with thin black color mudstone
	2350 – 2360	Argillaceous marl/ marlstone	~ ~	Interbedded with thin red color mudstone
	2360 – 2370	Argillaceous marl/ marlstone	~ ~	Interbedded with thin black color mudstone
	2370 – 2380	Argillaceous marl/ marlstone	~ ~	Interbedded with thin red color mudstone

	2380 – 2390	Argillaceous marl/ marlstone		Interbedded with thin red color mudstone
	2390 – 2400	Argillaceous marl/ marlstone		Interbedded with thin red color mudstone, abundance distribution
Early Eocene	2400 – 2410	Argillaceous marl/ marlstone		Interbedded with thin red color mudstone, abundance distribution
	2410 – 2420	Argillaceous marl/ marlstone		Interbedded with thin red color mudstone
	2420 – 2430	Argillaceous marl/ marlstone		Interbedded with thin red color mudstone
	2430 – 2440	Argillaceous marl/ marlstone		Interbedded with thin black color & red color mudstone
	2440 – 2450	Argillaceous marl/ marlstone		Interbedded with thin black color & red color mudstone
	2450 – 2460	Argillaceous marl/ marlstone		Interbedded with thin black color & red color mudstone
	2460 – 2470	Argillaceous marl/ marlstone		Interbedded with thin black color & red color mudstone
	2470 – 2480	Argillaceous marl/ marlstone		Interbedded with thin black color & red color mudstone
	2480 – 2490	Argillaceous marl/ marlstone		Interbedded with thin black color & red color mudstone
	2490 – 2500	Argillaceous marl/ marlstone		Interbedded with thin black color & red color mudstone
	2500 – 2510	Argillaceous marl/ marlstone		Interbedded with thin black & red color mudstone & sandstone (minor)
	Late Paleocene	2510 – 2520	Argillaceous marl/ marlstone	
2520 – 2530		Argillaceous marl/ marlstone		Interbedded with thin black & red color mudstone & sandstone (minor)
2530 – 2540		Argillaceous marl/ marlstone		Interbedded with thin black & red color mudstone & sandstone (minor)
2540 – 2550		Argillaceous marl/ marlstone		Interbedded with thin black & red color mudstone & sandstone (minor)
2550 – 2560		Argillaceous marl/ marlstone		Interbedded with thin black & red color mudstone & sandstone (minor)
2560 – 2570		Argillaceous marl/ marlstone		Interbedded with thin black & red color mudstone & sandstone (minor)
2570 – 2580		Argillaceous marl/ marlstone		Interbedded with thin black & red color mudstone & sandstone (minor)

Late Paleocene	2580 – 2590	Slightly calcareous mudstone/ mudstone		With interbedded sandstone (~ 10%)
	2590 – 2600	Slightly calcareous mudstone/ mudstone		With interbedded sandstone (~ 10%)
	2600 – 2610	Slightly calcareous mudstone/ mudstone		With interbedded sandstone (~ 10%)
	2610 – 2620	Slightly calcareous mudstone/ mudstone		With interbedded sandstone (~ 10%)
	2620 – 2630	Slightly calcareous mudstone/ mudstone		With interbedded sandstone (~ 10%)
	2630 – 2640	Slightly calcareous mudstone/ mudstone		With interbedded sandstone (~ 40%) and minor oceanic red beds
	2640 – 2650	Slightly calcareous mudstone/ mudstone		With interbedded sandstone (~ 40%) and minor oceanic red beds
	2650 – 2660	Slightly calcareous mudstone/ mudstone		With interbedded sandstone (~ 40%) and minor oceanic red beds
	2660 – 2670	Slightly calcareous mudstone/ mudstone		With interbedded sandstone (~ 40%) and minor oceanic red beds
	2670 – 2680	Slightly calcareous mudstone/ mudstone		With interbedded sandstone (~ 40%)
	2680 – 2690	Slightly calcareous mudstone/ mudstone		
	2690 – 2700	Slightly calcareous mudstone/ mudstone		
	2700 – 2710	Slightly calcareous mudstone/ mudstone		With interbedded sandstone (~ 30%)
	2710 – 2720	Slightly calcareous mudstone/ mudstone		With interbedded sandstone (~ 30%)
	2720 – 2730	Slightly calcareous mudstone/ mudstone		With interbedded sandstone (~ 30%)
	2730 – 2740	Slightly calcareous mudstone/ mudstone		With interbedded sandstone and minor oceanic red beds (~ 30%)
	2740 – 2750	Slightly calcareous mudstone/ mudstone		With interbedded sandstone and minor oceanic red beds (~ 30%)
	2750 – 2760	Slightly calcareous mudstone/ mudstone		With interbedded sandstone (~ 30%)
	2760 – 2770	Slightly calcareous mudstone/ mudstone		With interbedded sandstone (~ 40%)
	2770 – 2780	Slightly calcareous mudstone/ mudstone		With interbedded sandstone (~ 40%)
2780 – 2790	Slightly calcareous mudstone/ mudstone		With interbedded sandstone and minor amount of peat or coal fragment (?)	
2790 – 2800	Slightly calcareous mudstone/ mudstone		With interbedded sandstone (~ 40%)	

	2800 – 2810	Slightly calcareous mudstone/ mudstone		With interbedded sandstone (~ 40%)
	2810 – 2820	Slightly calcareous mudstone/ mudstone		With interbedded sandstone (~ 40%)
	2820 – 2830	Slightly calcareous mudstone/ mudstone		With interbedded sandstone (~ 40%)
	2830 – 2840	Slightly calcareous mudstone/ mudstone		With interbedded sandstone (~ 40%)
Early-Late Paleocene	2840 – 2850	Slightly calcareous mudstone/ mudstone		With interbedded sandstone (~ 40%)
	2850 – 2860	Slightly calcareous mudstone/ mudstone		With interbedded sandstone (~ 40%)
	2860 – 2870	Slightly calcareous mudstone/ mudstone		With interbedded sandstone (~ 40%)
	2870 – 2880	Slightly calcareous mudstone/ mudstone		With interbedded sandstone (~ 40%)
	2880 – 2890	Slightly calcareous mudstone/ mudstone		With interbedded sandstone (~ 40%)
	2890 – 2900	Slightly calcareous mudstone/ mudstone		With interbedded sandstone (~ 40%)
	2900 – 2910	Slightly calcareous mudstone/ mudstone		With interbedded sandstone (~ 40%)
	2910 – 2920	Slightly calcareous mudstone/ mudstone		With interbedded sandstone and minor amount of peat or coal fragment (?)
Early Paleocene	2920 – 2930	Slightly calcareous mudstone/ mudstone		With interbedded sandstone and minor amount of peat or coal fragment (?)
	2930 – 2940	Slightly calcareous mudstone/ mudstone		With interbedded sandstone (~ 30%)
	2940 – 2950	Slightly calcareous mudstone/ mudstone		With interbedded sandstone and minor amount of peat or coal fragment (?)
	2950 – 2960	Slightly calcareous mudstone/ mudstone		With interbedded sandstone and minor oceanic red beds (~ 30%)
	2960 – 2970	Slightly calcareous mudstone/ mudstone		With interbedded sandstone (~ 30%)
	2970 – 2980	Slightly calcareous mudstone/ mudstone		With interbedded sandstone (~ 30%)
	2980 – 2990	Slightly calcareous mudstone/ mudstone		With interbedded sandstone and minor amount of peat or coal fragment (?)
	2990 – 3000	Slightly calcareous mudstone/ mudstone		With interbedded sandstone (~ 30%)
	3000 – 3010	Slightly calcareous mudstone/ mudstone		With interbedded sandstone (~ 30%)
	3010 – 3020	Slightly calcareous mudstone/ mudstone		With interbedded sandstone (~ 30%)

Late Maastrichtian	3020 – 3030	Slightly calcareous mudstone/ mudstone		With interbedded sandstone and minor oceanic red beds (~ 30%)
	3030 – 3040	Calcareous black color mudstone		
	3040 – 3050	Calcareous black color mudstone		
	3050 – 3060	Calcareous black color mudstone		
	3060 – 3070	Calcareous black color mudstone		
	3070 – 3080	Calcareous black color mudstone		
	3080 – 3090	Calcareous black color mudstone		
	3090 – 3100	Calcareous black color mudstone		
Early Maastrichtian	3100 – 3110	Calcareous black color mudstone		
	3110 – 3120	Calcareous black color mudstone		
	3120 – 3130	Calcareous black color mudstone		
	3130 – 3140	Calcareous black color mudstone		
Late Campanian	3140 – 3150	Calcareous black color mudstone		
	3150 – 3160	Calcareous black color mudstone		
	3160 – 3170	Calcareous black color mudstone		
	3170 – 3180	Calcareous black color mudstone		
Early Campanian	3180 – 3190	Calcareous black color mudstone		
	3190 – 3200	Calcareous black color mudstone		
	3200 – 3210	Calcareous black color mudstone		
	3210 – 3220	Slightly calcareous mudstone/ mudstone		With interbedded sandstone (~ 20%)
	3220 – 3230	Slightly calcareous mudstone/ mudstone		With interbedded sandstone (~ 20%)
	3230 – 3240	Slightly calcareous mudstone/ mudstone		With interbedded sandstone and minor oceanic red beds (?) (~ 30%)

Early Campanian	3240 – 3250	Slightly calcareous mudstone/ mudstone		With interbedded sandstone and minor oceanic red beds (?) (~ 30%)
	3250 – 3260	Slightly calcareous mudstone/ mudstone		With interbedded sandstone and minor oceanic red beds (?) rounded quartz grains
	3260 – 3270	Slightly calcareous mudstone/ mudstone		With interbedded sandstone and minor oceanic red beds (?) (~ 30%)
	3270 – 3280	Calcareous black color mudstone		
	3280 – 3290	Calcareous black color mudstone		
	3290 – 3300	Calcareous black color mudstone		
	3300 – 3310	Slightly calcareous mudstone/ mudstone		With interbedded sandstone (~ 20%)
	3310 – 3320	Slightly calcareous mudstone/ mudstone		With interbedded sandstone (~ 20%)
	3320 – 3330	Slightly calcareous mudstone/ mudstone		With interbedded sandstone (~ 20%)
	3330 – 3340	Slightly calcareous mudstone/ mudstone		With interbedded sandstone (~ 20%)
	3340 – 3350	Slightly calcareous mudstone/ mudstone		With interbedded sandstone (~ 20%)
	3350 – 3360	Sandy calcareous mudstone	Rounded to sub angular sand particles (~ 50%)
	3360 – 3370	Sandy calcareous mudstone	Rounded to sub angular sand particles (~ 50%)
	3370 – 3380	Sandy calcareous mudstone	Rounded to sub angular sand particles (~ 50%)
	3380 – 3390	Sandy calcareous mudstone	Rounded to sub angular sand particles (~ 50%)
	3390 – 3400	Sandy calcareous mudstone	Rounded to sub angular sand particles (~ 50%)
	3400 – 3410	Sandy calcareous mudstone	Rounded to sub angular sand particles (~ 50%)
	3410 – 3420	Sandy calcareous mudstone	Rounded to sub angular sand particles (~ 50%)
	3420 – 3430	Sandy calcareous mudstone	Rounded to sub angular sand particles (~ 50%)
	3430 – 3440	Sandy calcareous mudstone	Rounded to sub angular sand particles (~ 50%)
3440 – 3450	Sandy calcareous mudstone	Rounded to sub angular sand particles (~ 50%)	
3450 – 3460	Sandy calcareous mudstone	Rounded to sub angular sand particles (~ 50%)	

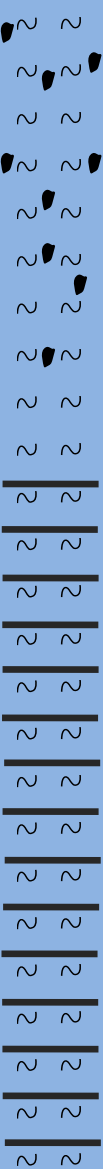
	3460 – 3470	Sandy calcareous mudstone	Rounded to sub angular sand particles (~ 50%)
	3470 – 3480	Sandy calcareous mudstone	Rounded to sub angular sand particles (~ 50%)
	3480 – 3490	Sandy calcareous mudstone	Rounded to sub angular sand particles (~ 50%)
	3490 – 3500	Sandy calcareous mudstone	Rounded to sub angular sand particles (~ 50%)
	3500 – 3510	Sandy calcareous mudstone	Rounded to sub angular sand particles (~ 50%)
	3510 – 3520	Sandy calcareous mudstone	Rounded to sub angular sand particles (~ 50%)
	3520 – 3530	Sandy calcareous mudstone	Rounded to sub angular sand particles (~ 50%)
	3530 – 3540	Sandy calcareous mudstone	Rounded to sub angular sand particles (~ 50%)
	3540 – 3550	Sandy calcareous mudstone	Rounded to sub angular sand particles (~ 50%)
	3550 – 3560	Sandy calcareous mudstone	Rounded to sub angular sand particles (~ 50%)
	3560 – 3570	Sandy calcareous mudstone	Rounded to sub angular sand particles (~ 50%)
	3570 – 3580	Sandy calcareous mudstone	Rounded to sub angular sand particles (~ 50%)
Santonian	3580 – 3590	Calcareous black color mudstone	-----	
	3590 – 3600	Calcareous black color mudstone	-----	
	3600 – 3610	Calcareous black color mudstone	-----	
	3610 – 3622	Calcareous black color mudstone	-----	

Core description – Barracuda exploration well


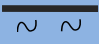



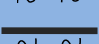
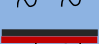
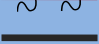
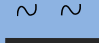

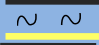
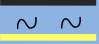
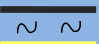
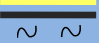

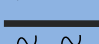
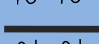
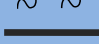

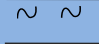
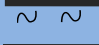
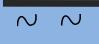
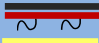
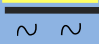
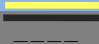
Location: Mannar Basin

Water depth: 1509 m

Age	Depth / m	Lithology		Remarks
Early–Middle Miocene	2139 – 2150	Marlstone with black carbon	~ ~	
	2150 – 2160	Marlstone with black carbon	~ ~	
	2160 – 2170	Marlstone with black carbon	~ ~	
	2170 – 2180	Marlstone with black carbon	~ ~	
	2180 – 2190	Marlstone with black carbon	~ ~	
	2190 – 2200	Marlstone with black carbon	~ ~	
	2200 – 2210	Marlstone with black carbon	~ ~	
	2210 – 2220	Marlstone with black carbon	~ ~	
	2220 – 2230	Marlstone with black carbon	~ ~	
	2230 – 2240	Marlstone with black carbon	~ ~	
	2240 – 2250	Marlstone with black carbon	~ ~	
	2250 – 2260	Marlstone with black carbon	~ ~	
	2260 – 2270	Marlstone with black carbon	~ ~	
	2270 – 2280	Marlstone with black carbon	~ ~	
	2280 – 2290	Marlstone with black carbon	~ ~	
	2290 – 2300	Marlstone with black carbon	~ ~	
	2300 – 2310	Marlstone with black carbon	~ ~	
	2310 – 2320	Marlstone with black carbon	~ ~	
2320 – 2330	Marlstone with black carbon	~ ~		
2330 – 2340	Marlstone with black carbon	~ ~		

Early–Middle Oligocene	2340 – 2350	Marlstone with black carbon		
	2350 – 2360	Marlstone with black carbon		
	2360 – 2370	Marlstone with black carbon		
	2370 – 2380	Marlstone with black carbon		
	2380 – 2390	Marlstone with black carbon		
	2390 – 2400	Marlstone with black carbon		
	2400 – 2410	Marlstone with black carbon		
	2410 – 2420	Marlstone with black carbon		
	2420 – 2430	Marlstone		
	2430 – 2440	Marlstone		
	2440 – 2450	Marlstone		Interbedded with thin black color mudstone
	2450 – 2460	Marlstone		Interbedded with thin black color mudstone
	2460 – 2470	Marlstone		Interbedded with thin black color mudstone
	2470 – 2480	Marlstone		Interbedded with thin black color mudstone
	2480 – 2490	Marlstone		Interbedded with thin black color mudstone
	2490 – 2500	Marlstone		Interbedded with thin black color mudstone
	2500 – 2510	Marlstone		Interbedded with thin black color mudstone
	2510 – 2520	Marlstone		Interbedded with thin black color mudstone
	2520 – 2530	Marlstone		Interbedded with thin black color mudstone
	2530 – 2540	Marlstone		Interbedded with thin black color mudstone
	2540 – 2550	Marlstone		Interbedded with thin black color mudstone
	2550 – 2560	Marlstone		Interbedded with thin black color mudstone
2560 – 2570	Marlstone		Interbedded with thin black color mudstone	
2570 – 2580	Marlstone		Interbedded with thin black color mudstone	
2580 – 2590	Marlstone		Interbedded with thin black color mudstone	

	2590 – 2600	Marlstone	~ ~	Interbedded with thin black color mudstone
	2600 – 2610	Marlstone	~ ~	Interbedded with thin black color mudstone
	2610 – 2620	Marlstone	~ ~	Interbedded with thin black color mudstone
	2620 – 2630	Marlstone	~ ~	Interbedded with thin black color mudstone
	2630 – 2640	Marlstone	~ ~	Interbedded with thin black color mudstone
	2640 – 2650	Marlstone	~ ~	Interbedded with thin black color mudstone
	2650 – 2660	Marlstone	~ ~	Interbedded with thin black color mudstone
Middle-(?) Late Eocene	2660 – 2670	Marlstone	~ ~	Interbedded with thin red color mudstone
	2670 – 2680	Marlstone	~ ~	Interbedded with thin red color mudstone
	2680 – 2690	Marlstone	~ ~	Interbedded with thin red color mudstone
	2690 – 2700	Marlstone	~ ~	Interbedded with thin red color mudstone
Middle Eocene	2700 – 2710	Marlstone	~ ~	Interbedded with thin red color mudstone
	2710 – 2720	Marlstone	~ ~	Interbedded with thin red color mudstone
	2720 – 2730	Marlstone	~ ~	Interbedded with very thin red color mudstone
	2730 – 2740	Marlstone	~ ~	Interbedded with very thin black color mudstone
	2740 – 2750	Marlstone	~ ~	Interbedded with very thin black color mudstone
	2750 – 2760	Marlstone	~ ~	Interbedded with thin black color mudstone, rounded quartz grains (minor)
	2760 – 2770	Marlstone	~ ~	Interbedded with thin black color mudstone, rounded quartz grains (minor)
	2770 – 2780	Marlstone	~ ~	Interbedded with thin red color mudstone, rounded quartz grains (minor)
	2780 – 2790	Marlstone	~ ~	Interbedded with thin black color mudstone, rounded quartz grains (minor)
	2790 – 2800	Marlstone	~ ~	Interbedded with thin black color mudstone, rounded quartz grains (minor)
	2800 – 2810	Argillaceous marl/ marlstone	~ ~	Interbedded with thin black color mudstone, rounded quartz grains (minor)
	2810 – 2820	Argillaceous marl/ marlstone	~ ~	Interbedded with thin black color mudstone, rounded quartz grains (minor)
	2820 – 2830	Argillaceous marl/ marlstone	~ ~	Interbedded with thin black color mudstone, rounded quartz grains (minor)
	2830 – 2840	Argillaceous marl/ marlstone	~ ~	Interbedded with thin black color mudstone, rounded quartz grains (minor)

	2840 – 2850	Argillaceous marl/ marlstone		Interbedded with thin black color & red color mudstone, rounded quartz grains
	2850 – 2860	Argillaceous marl/ marlstone		Interbedded with thin black color mudstone, rounded quartz grains (minor)
	2860 – 2870	Argillaceous marl/ marlstone		Interbedded with thin black color mudstone, rounded quartz grains (minor)
Early Eocene	2870 – 2880	Argillaceous marl/ marlstone		Interbedded with thin black color mudstone, rounded quartz grains (minor)
	2880 – 2890	Argillaceous marl/ marlstone		Interbedded with thin black color & red color mudstone
	2890 – 2900	Argillaceous marl/ marlstone		Interbedded with thin black color mudstone, rounded quartz grains (minor)
	2900 – 2910	Argillaceous marl/ marlstone		Interbedded with thin black color & red color mudstone
	2910 – 2920	Argillaceous marl/ marlstone		Interbedded with thin black color mudstone
	2920 – 2930	Argillaceous marl/ marlstone		Interbedded with thin black color mudstone,
Late Paleocene	2930 – 2940	Argillaceous marl/ marlstone		Interbedded with thin black color mudstone, and sandstone (~ 15%)
	2940 – 2950	Argillaceous marl/ marlstone		Interbedded with thin black color mudstone, and sandstone (~ 15%)
	2950 – 2960	Argillaceous marl/ marlstone		Interbedded with thin black color mudstone, and sandstone (~ 15%)
	2960 – 2970	Argillaceous marl/ marlstone		Interbedded with thin black color mudstone, and sandstone (~ 15%)
	2970 – 2980	Argillaceous marl/ marlstone		Interbedded with thin black color mudstone
	2980 – 2990	Argillaceous marl/ marlstone		Interbedded with thin black color mudstone
	2990 – 3000	Argillaceous marl/ marlstone		Interbedded with thin black color mudstone
	3000 – 3010	Argillaceous marl/ marlstone		Interbedded with thin black color mudstone
	3010 – 3020	Argillaceous marl/ marlstone		Interbedded with thin black color mudstone
	3020 – 3030	Argillaceous marl/ marlstone		
	3030 – 3040	Argillaceous marl/ marlstone		
	3040 – 3050	Argillaceous marl/ marlstone		Interbedded with thin black & red color mudstone, sandstone
	3050 – 3060	Argillaceous marl/ marlstone		sandstone
	3060 – 3070	Slightly calcareous mudstone/ mudstone		Interbedded with thin black color mudstone and sandstone (~ 20%)
	3070 – 3080	Slightly calcareous mudstone/ mudstone		Interbedded with thin black color mudstone and sandstone (~ 20%)
3080 – 3090	Slightly calcareous mudstone/ mudstone		Interbedded with thin black color mudstone and sandstone (~ 20%)	

Late Paleocene	3090 – 3100	Slightly calcareous mudstone/ mudstone		Interbedded with thin black color mudstone and sandstone (~ 20%)
	3100 – 3110	Slightly calcareous mudstone/ mudstone		Interbedded with thin black color mudstone and sandstone (~ 20%)
	3110 – 3120	Slightly calcareous mudstone/ mudstone		Interbedded with thin black color mudstone and sandstone (~ 20%)
	3120 – 3130	Slightly calcareous mudstone/ mudstone		Interbedded with thin black color mudstone
	3130 – 3140	Slightly calcareous mudstone/ mudstone		Interbedded with thin black color mudstone
	3140 – 3150	Slightly calcareous mudstone/ mudstone		Interbedded with thin black color mudstone
	3150 – 3160	Slightly calcareous mudstone/ mudstone		Interbedded with thin black color mudstone
	3160 – 3170	Slightly calcareous mudstone/ mudstone		Interbedded with thin black color mudstone
	3170 – 3180	Slightly calcareous mudstone/ mudstone		Interbedded with thin black color mudstone
	3180 – 3190	Slightly calcareous mudstone/ mudstone		Interbedded with thin black color mudstone
	3190 – 3200	Slightly calcareous mudstone/ mudstone		Interbedded with thin black color mudstone
	3200 – 3210	Slightly calcareous mudstone/ mudstone		
	3210 – 3220	Slightly calcareous mudstone/ mudstone		
	3220 – 3230	Slightly calcareous mudstone/ mudstone		
	3230 – 3240	Slightly calcareous mudstone/ mudstone		
	3240 – 3250	Slightly calcareous mudstone/ mudstone		
	3250 – 3260	Slightly calcareous mudstone/ mudstone		Interbedded with minor sandstone (~ 30%)
	3260 – 3270	Slightly calcareous mudstone/ mudstone		
	3270 – 3280	Slightly calcareous mudstone/ mudstone		
	3280 – 3290	Slightly calcareous mudstone/ mudstone		Interbedded with minor sandstone (~ 30%)
	3290 – 3300	Slightly calcareous mudstone/ mudstone		
	3300 – 3310	Slightly calcareous mudstone/ mudstone		Interbedded with minor sandstone (~ 30%)
	3310 – 3320	Slightly calcareous mudstone/ mudstone		Interbedded with minor sandstone (~ 30%)
3320 – 3330	Slightly calcareous mudstone/ mudstone		Interbedded with minor sandstone (~ 30%)	
3330 – 3340	Slightly calcareous mudstone/ mudstone		Interbedded with minor sandstone (~ 30%)	

	3340 – 3350	Slightly calcareous mudstone/ mudstone		Interbedded with minor sandstone (~ 30%)
	3350 – 3360	Slightly calcareous mudstone/ mudstone		
	3360 – 3370	Slightly calcareous mudstone/ mudstone		
	3370 – 3380	Slightly calcareous mudstone/ mudstone		
	3380 – 3390	Slightly calcareous mudstone/ mudstone		Interbedded with sandstone (~ 40%)
	3390 – 3400	Slightly calcareous mudstone/ mudstone		Interbedded with minor sandstone (~ 40%)
Early Paleocene	3400 – 3410	Slightly calcareous mudstone/ mudstone		Interbedded with minor sandstone (~ 30%)
	3410 – 3420	Slightly calcareous mudstone/ mudstone		Interbedded with minor sandstone (~ 30%)
	3420 – 3430	Slightly calcareous mudstone/ mudstone		Interbedded with minor sandstone (~ 30%)
	3430 – 3440	Slightly calcareous mudstone/ mudstone		Interbedded with minor sandstone (~ 30%)
Late Maastrichtian	3440 – 3450	Slightly calcareous mudstone/ mudstone		Interbedded with minor sandstone
	3450 – 3460	Slightly calcareous mudstone/ mudstone		Interbedded with minor sandstone
	3460 – 3470	Slightly calcareous mudstone/ mudstone		Interbedded with sandstone
	3470 – 3480	Slightly calcareous mudstone/ mudstone		
	3480 – 3490	Slightly calcareous mudstone/ mudstone		
	3490 – 3500	Slightly calcareous mudstone/ mudstone		
	3500 – 3510	Slightly calcareous mudstone/ mudstone		Interbedded with minor volcanic
	3510 – 3520	Slightly calcareous mudstone/ mudstone		Interbedded with minor volcanic
	3520 – 3530	Slightly calcareous mudstone/ mudstone		Interbedded with minor volcanic
	3530 – 3540	Slightly calcareous mudstone/ mudstone		Interbedded with minor volcanic
	3540 – 3550	Slightly calcareous mudstone/ mudstone		Interbedded with minor volcanic
	3550 – 3560	Slightly calcareous mudstone/ mudstone		Interbedded with minor volcanic
	3560 – 3570	Slightly calcareous mudstone/ mudstone		Interbedded with minor volcanic
	3570 – 3580	Slightly calcareous mudstone/ mudstone		Interbedded with minor volcanic
3580 – 3590	Slightly calcareous mudstone/ mudstone		Interbedded with minor volcanic	

Late Maastrichtian	3590 – 3600	Slightly calcareous mudstone/ mudstone		Interbedded with minor volcanic
	3600 – 3610	Slightly calcareous mudstone/ mudstone		Interbedded with minor volcanic
	3610 – 3620	Slightly calcareous mudstone/ mudstone		Interbedded with minor volcanic & sandstone (~ 10%)
	3620 – 3630	Slightly calcareous mudstone/ mudstone		Interbedded with minor volcanic & sandstone (~ 10%)
	3630 – 3640	Slightly calcareous mudstone/ mudstone		Interbedded with minor volcanic & sandstone (~ 10%)
	3640 – 3650	Slightly calcareous mudstone/ mudstone		Interbedded with minor volcanic & sandstone (~ 10%)
	3650 – 3660	Slightly calcareous mudstone/ mudstone		Interbedded with minor volcanic
	3660 – 3670	Slightly calcareous mudstone/ mudstone		Interbedded with minor volcanic
	3670 – 3680	Slightly calcareous mudstone/ mudstone		Interbedded with minor volcanic
	3680 – 3690	Slightly calcareous mudstone/ mudstone/ volcanic		
	3690 – 3700	Slightly calcareous mudstone/ mudstone		Interbedded with volcanic
	3700 – 3710	Slightly calcareous mudstone/ mudstone		Interbedded with minor volcanic
	3710 – 3720	Slightly calcareous mudstone/ mudstone		Interbedded with minor volcanic
	3720 – 3730	Slightly calcareous mudstone/ mudstone		Interbedded with minor volcanic
	3730 – 3740	Slightly calcareous mudstone/ mudstone		Interbedded with minor volcanic & sandstone (~ 10%)
	3740 – 3750	Slightly calcareous mudstone/ mudstone		Interbedded with minor volcanic
	3750 – 3760	Slightly calcareous mudstone/ mudstone		Interbedded with minor volcanic
	3760 – 3770	Slightly calcareous mudstone/ mudstone		Interbedded with minor volcanic
	3770 – 3780	Slightly calcareous mudstone/ mudstone		Interbedded with minor volcanic
	3780 – 3790	Slightly calcareous mudstone/ mudstone		Interbedded with minor volcanic
	3790 – 3800	Slightly calcareous mudstone/ mudstone		Interbedded with minor volcanic
	3800 – 3810	Slightly calcareous mudstone/ mudstone		Interbedded with minor volcanic
	3810 – 3820	Slightly calcareous mudstone/ mudstone		
	3820 – 3830	Slightly calcareous mudstone/ mudstone		Interbedded with minor volcanic
3830 – 3840	Slightly calcareous mudstone/ mudstone		Interbedded with minor volcanic	

Late Maastrichtian	3840 – 3850	Slightly calcareous mudstone/ mudstone	-----	
	3850 – 3860	Slightly calcareous mudstone/ mudstone	
	3860 – 3870	Slightly calcareous mudstone/ mudstone	-----	
	3870 – 3880	Slightly calcareous mudstone/ mudstone	
	3880 – 3890	Slightly calcareous mudstone/ mudstone	-----	
	3890 – 3900	Slightly calcareous mudstone/ mudstone	
	3900 – 3910	Slightly calcareous mudstone/ mudstone	-----	Interbedded with minor volcanic
	3910 – 3920	Slightly calcareous mudstone/ mudstone/ volcanic	
	3920 – 3930	Slightly calcareous mudstone/ mudstone	-----	Interbedded with minor volcanic
	3930 – 3940	Slightly calcareous mudstone/ mudstone	Interbedded with minor volcanic
	3940 – 3950	Slightly calcareous mudstone/ mudstone	-----	Interbedded with minor volcanic
	3950 – 3960	Slightly calcareous mudstone/ mudstone/ volcanic	
	3960 – 3970	Slightly calcareous mudstone/ mudstone/ volcanic	-----	
	3970 – 3980	Slightly calcareous mudstone/ mudstone/ volcanic	
	3980 – 3990	Slightly calcareous mudstone/ mudstone	-----	Interbedded with minor volcanic
	3990 – 4000	Slightly calcareous mudstone/ mudstone/ volcanic	
	4000 – 4010	Slightly calcareous mudstone/ mudstone/ volcanic	-----	
	4010 – 4020	Slightly calcareous mudstone/ mudstone/ volcanic	
	4020 – 4030	Slightly calcareous mudstone/ mudstone/ volcanic	-----	
	4030 – 4040	Slightly calcareous mudstone/ mudstone/ volcanic	
	4040 – 4050	Slightly calcareous mudstone/ mudstone/ volcanic	-----	
	4050 – 4060	Slightly calcareous mudstone/ mudstone	
	4060 – 4070	Slightly calcareous mudstone/ mudstone	-----	Intra – volcanic gas sand - 1
4070 – 4080	Slightly calcareous mudstone/ mudstone		
4080 – 4090	Slightly calcareous mudstone/ mudstone	-----		

Late Maastrichtian	4090 – 4100	Slightly calcareous mudstone/ mudstone		
	4100 – 4110	Slightly calcareous mudstone/ mudstone		
	4110 – 4120	Slightly calcareous mudstone/ mudstone		
	4120 – 4130	Slightly calcareous mudstone/ mudstone		
	4130 – 4140	Slightly calcareous mudstone/ mudstone		
	4140 – 4150	Slightly calcareous mudstone/ mudstone		
	4150 – 4160	Slightly calcareous mudstone/ mudstone		
	4160 – 4170	Slightly calcareous mudstone/ mudstone		Intra – volcanic gas sand - 2
	4170 – 4180	Slightly calcareous mudstone/ mudstone		
	4180 – 4190	Slightly calcareous mudstone/ mudstone		
	4190 – 4200	Slightly calcareous mudstone/ mudstone		
	4200 – 4210	Slightly calcareous mudstone/ mudstone		Intra – volcanic gas sand - 3
	4210 – 4220	Slightly calcareous mudstone/ mudstone		
	4220 – 4230	Slightly calcareous mudstone/ mudstone		
	4230 – 4240	Slightly calcareous mudstone/ mudstone		
	4240 – 4250	Slightly calcareous mudstone/ mudstone		
	4250 – 4260	Slightly calcareous mudstone/ mudstone		
	4260 – 4270	Slightly calcareous mudstone/ mudstone		With interbedded sandstone
	4270 – 4280	Slightly calcareous mudstone/ mudstone		With interbedded sandstone
	4280 – 4290	Slightly calcareous mudstone/ mudstone		With interbedded sandstone
	4290 – 4300	Slightly calcareous mudstone/ mudstone		
	4300 – 4310	Slightly calcareous mudstone/ mudstone		
	4310 – 4320	Slightly calcareous mudstone/ mudstone		
4320 – 4330	Slightly calcareous mudstone/ mudstone			

	4330 – 4340	Slightly calcareous mudstone/ mudstone	-----	
Late Maastrichtian	4340 – 4350	Slightly calcareous mudstone/ mudstone	-----	
	4350 – 4360	Slightly calcareous mudstone/ mudstone	-----	
	4360 – 4370	Slightly calcareous mudstone/ mudstone	-----	
	4370 – 4380	Slightly calcareous mudstone/ mudstone	-----	
	4380 – 4390	Slightly calcareous mudstone/ mudstone	-----	
	4390 – 4400	Slightly calcareous mudstone/ mudstone	-----	
	4400 – 4410	Slightly calcareous mudstone/ mudstone	-----	
	4410 – 4420	Slightly calcareous mudstone/ mudstone	-----	
	4420 – 4430	Slightly calcareous mudstone/ mudstone	-----	
	4430 – 4440	Slightly calcareous mudstone/ mudstone	-----	
	4440 – 4450	Slightly calcareous mudstone/ mudstone	-----	
	4450 – 4460	Slightly calcareous mudstone/ mudstone	-----	
	4460 – 4470	Slightly calcareous mudstone/ mudstone	-----	
	Early Maastrichtian	4470 – 4480	Slightly calcareous mudstone/ mudstone	-----
4480 – 4490		Slightly calcareous mudstone/ mudstone	-----	
4490 – 4500		Slightly calcareous mudstone/ mudstone	-----	
4500 – 4510		Slightly calcareous mudstone/ mudstone	-----	
Late Campanian	4510 – 4520	Slightly calcareous mudstone/ mudstone	-----	
	4520 – 4530	Slightly calcareous mudstone/ mudstone	-----	
	4530 – 4540	Slightly calcareous mudstone/ mudstone	-----	
	4540 – 4550	Slightly calcareous mudstone/ mudstone	-----	
	4550 – 4560	Slightly calcareous mudstone/ mudstone	----- -----	Interbedded with thin red color mudstone
	4560 – 4570	Slightly calcareous mudstone/ mudstone	----- -----	Interbedded with thin red color mudstone
	4570 – 4580	Slightly calcareous mudstone/ mudstone	----- -----	Interbedded with thin red color mudstone

	4580 – 4590	Slightly calcareous mudstone/ mudstone	-----	Interbedded with thin red color mudstone
	4590 – 4600	Slightly calcareous mudstone/ mudstone	-----	Interbedded with thin red color mudstone
Early Campanian	4600 – 4610	Slightly calcareous mudstone/ mudstone	-----	Interbedded with thin red color mudstone
	4610 – 4620	Slightly calcareous mudstone/ mudstone	-----	Interbedded with thin red color mudstone
	4620 – 4630	Slightly calcareous mudstone/ mudstone	-----	Interbedded with thin red color mudstone
	4630 – 4640	Slightly calcareous mudstone/ mudstone	-----	Interbedded with thin red color mudstone
	4640 – 4650	Slightly calcareous mudstone/ mudstone	-----	Interbedded with thin red color mudstone
	4650 – 4660	Slightly calcareous mudstone/ mudstone	-----	Interbedded with thin red color mudstone
	4660 – 4670	Slightly calcareous mudstone/ mudstone	-----	
	4670 – 4680	Slightly calcareous mudstone/ mudstone	-----	
	4680 – 4690	Slightly calcareous mudstone/ mudstone	-----	
	4690 – 4700	Slightly calcareous mudstone/ mudstone	-----	
	4700 – 4710	Slightly calcareous mudstone/ mudstone	-----	
	4710 – 4720	Slightly calcareous mudstone/ mudstone	-----	
	4720 – 4730	Slightly calcareous mudstone/ mudstone	-----	
	4730 – 4741	Slightly calcareous mudstone/ mudstone	-----	

